The systemic-prime, mucosal-boost vaccine regimen for protection against respiratory viruses

Cameron Bissett
Linacre College
University of Oxford

Thesis submitted for the degree of Doctor of Philosophy
DPhil (Clinical Medicine)

Michaelmas term 2024
Word count: ~50,000 (excluding tables, figure legends, references and appendix)

Abstract

Respiratory viruses, such as influenza, respiratory syncytial virus (RSV), and SARS-CoV-2, continue to impose a significant global health burden despite the availability of licensed vaccines. While current vaccines that are generally administered via the intramuscular (IM) route are effective in preventing severe disease, they fail to elicit robust mucosal immunity needed for the prevention of viral infection and transmission. Additionally, immunological imprinting from prior exposures to influenza strains and SARS-CoV-2 variants can limit the effectiveness of the responses to updated annual booster vaccines. In this PhD, the use of the intranasal (IN) route for boosting was explored in a mouse immunisation model, with a focus on overcoming the shortcomings of IM vaccination, and inducing dual systemic and mucosal immunity. In a heterologous boosting scenario, IN-boosting of an omicron vaccine in mice that were IM-primed with wildtype vaccine exceeded IM-boosting immunogenicity by multiple mechanisms. Notably, the IN route overcame suppressive immunological imprinting, elicited robust cross-reactive memory T cell, de novo B cell and IgA and IgG responses both in the respiratory mucosa and systemically, highlighting its potential to induce sterilising immunity. In contrast, both the IM-boosting of IM-primed mice and the IN-boosting of IN-primed mice were constrained by the effects of imprinting and elicited suboptimal responses to the omicron strain, revealing a unidirectional relationship between IM and IN vaccination routes and their capacity to stimulate the systemic and/or mucosal immune compartments. IN-boosting was then tested in a homologous antigen setting using a bivalent RSV-influenza vaccine, where the dual-mode IM-IN route once again outperformed the standard IM-IM and IN-IN single-mode regimens, providing superior protection against both infection and

disease. These findings underscore the potential of mucosal vaccination strategies, particularly IM-prime followed by IN-boost, to overcome hurdles such as immunological imprinting, and enhance mucosal immunity.

Acknowledgements

This DPhil project would not be possible without the support of a number of people, to whom I extend my deepest gratitude. I would first like to thank my supervisors Professor Teresa Lambe, Dr Sandra Belij-Rammerstorfer, Dr Nick Provine, and Dr Alex Spencer, for the huge amount of support and guidance they gave me throughout this project. Tess, I want to thank you for the trust you had in me to take on this project, your belief in my abilities and judgement, and the freedom you granted me that enabled me to pursue areas of the project that I found most interesting; together these have been a great source of motivation for me. Sandra, thank you for being more than just a supervisor, but a true friend and colleague; to say you have taught me a lot is an understatement, your mentorship has left a lasting impact on both my personal and professional growth. Nick, I am sincerely grateful for your guidance; our scientific discussions and exchanges of ideas have had a profound impact on my research, helping me shape this project. And Alex, I am especially grateful for all the support you gave me during the first half of this project; you fostered many of the early ideas that have led to this completed project. I'd also like to extend a special thanks Marta Ulaszewska for the countless hours of support and training she has given me regarding mouse work; her technical expertise and strong work ethic have been inspiring.

I would especially like to thank some past members of the Emerging Pathogens group that inspired me to begin this DPhil in the first place, including Hannah Sharpe, Ciaran Gilbride and Liz Allen. Each one of you has been immensely supportive; thank you for passing down your wisdom and helping me through some of my initial large animal experiments. I am also deeply grateful for my fellow PhD colleagues Sarah Batawi, Alex

Sampson, Jack Saunders and Rebecca Makinson, with whom I was able to bounce ideas off of and troubleshoot problems with; you guys have made this DPhil journey much less intimidating. To Sarah, thank you for all the laughs and company on late lab days. Alex, I'd like to specifically thank you for setting up the pseudoneutralisation assay which was critical for my project. And Jack and Becks, thank you for all the favours you've done for me, and for uplifting the overall mood of the lab.

I'd like to extend thanks to some of the post-docs that shared their expertise throughout my DPhil, including Danny Wright, Leila Godfrey and Susan Morris. Sue, I'd specifically like to thank you for sharing your molecular biology expertise and for constructing many of the vaccines that I used and were integral to this project; both you and Reshma held my hand through the early days of my Masters' project that led me to continue on with this DPhil.

I'd like to thank Claire and the VVCF staff for their assistance in viral vector production, as well as the FGF staff who have supported my animal work. Additionally, I would like to thank those who I have collaborated with that have kindly contributed to the work I present in this thesis, including Lyn Yong, who performed the S1pr2 mouse experiments, and John Tregoning and his colleagues who performed the virus challenge studies.

Lastly, I would like to thank my parents, my partner João and my friend Ben, for their continued support throughout these past years; they were an integral part of this journey and stood by me through all the highs and lows.

Table of contents

List of figures

List of tables

List of abbreviations

Abs	Antibodies
ARI	Acute respiratory tract infection
ACE-2	Angiotensin converting enzyme-2
ACK	Ammonium-Chloride-Potassium lysing buffer
Ad	Adenovirus
Ag	Antigen
ALRI	Acute lower respiratory infection
APC	Antigen-presenting cell
AP	Alkaline phosphatase
AUC	Area under the curve
BAC	Bacterial artificial chromosome
BAL(F)	Brocho-alveolar lavage (fluid)
BCR	B cell receptor
B_{RM}	Tissue-resident memory B cell
ChAdOx	Chimpanzee adenovirus Oxford
COVID-19	Coronavirus-19
DC	Dendritic cell
DNA	Deoxyribonucleic acid
ELISA	Enzyme-linked immunosorbent assay
ELISpot	Enzyme-linked immunospot assay
EU	ELISA units
ERD	Enhanced respiratory disease
FCS	Fetal calf serum
FI-RSV	Formalin-inactivated RSV
FcR	Fc receptor
GISAID	the Global Initiative on Sharing Avian Influenza Data
GFP	Green fluorescent protein
HA	Hemagglutinin
HAI	Hemagglutinin inhibition assay
HEK	Human embryonic kidney
ICS	Intracellular staining
IFNγ	Interferon gamma
IgG/A/M	Immunoglobulin G/A/M
IL	Interleukin
IM	Intramuscular
IN	Intranasal
INN	International Nonproprietary Name
IP	Intraperitoneal or intrapulmonary
IU	Infectious unit
IV	Intravenous
LAIV	Live attenuated influenza vaccine
LHS	Lung homogenate supernatant
MALT	Mucosa-associated lymphoid tissue
MBC	Memory B cell
MHC	Major histocompatibility complex

MVA	Modified vaccinia Ankara
M1	Matrix protein 1
NA	Neuraminidase
NAb	Neutralising antibody
NALT	Nasal-associated lymphoid tissue
NC	Nucleocapsid
NHP	Non-human primate
NP	Nucleoprotein
OD	Optical density
PB	Plasmablast
PC	Plasma cell
PBS	Phosphate-buffered saline
pNPP	P-Nitrophenyl phosphate
QIV	Quadrivalent influenza vaccine
RSV	Respiratory syncytial virus
RSVF	Respiratory syncytial virus fusion protein
RT	Room temperature
SARS	Severe acute respiratory syndrome
T_{CM}	Central memory T cell
TCR	T cell receptor
$T_{EFF/EM}$	Effector/effector memory T cell
TMPRSS2	Transmembrane protease, serine 2
TNF	Tumor necrosis factor
TPA	Tissue plasminogen activator
T_{REG}	Regulatory T cell
T_{RM}	Tissue-resident memory T cell
URTI	Upper respiratory tract infection
LRTI	Lower respiratory tract infection
VOC	Variant of concern
WHO	World health organisation
WT	Wildtype

Statement of authorship

This thesis was written by Cameron Bissett. All experiments were completed by Cameron Bissett unless otherwise described. All data were analysed by Cameron Bissett. The following contributions are acknowledged:

- The mouse virus challenge experiments in Chapter 6 were completed by John Tregoning *et al.*; the measurements of weight change and lung viral load were completed by John Tregoning *et al*.
- Lyn Yong conducted the transgenic S1pr2 vaccination experiments and contributed to the initial data processing of the associated datasets featured in Chapter 5
- All ChAdOx1 vaccines used in this study, apart from ChAdOx1-BA.4/5 which was constructed by Cameron Bissett, were constructed by Susan Morris, Reshma Kailath and/or Elisabeth Allen. All ChAdOx1 vaccine constructs were transfected and purified by the Viral Vector Core Facility (VVCF) led by Claire Powers.
- Sandra Belij-Rammerstorfer, Marta Ulaszewska and Alex Spencer assisted in certain mouse procedures. Sandra Belij-Rammerstorfer, Marta Ulaszewska, Alex Spencer, Hannah Sharpe, Nok Ma, Elizabeth Allen assisted in the sample processing involved in certain mouse experiments.

  The following publication was written by Cameron Bissett and features data produced during the course of this thesis project:

  - Bissett, C., Belij-Rammerstorfer, S., Ulaszewska, M., Smith, H., Kailath, R., Morris, S., Powers, C., Sebastian, S., Sharpe, H.R., Allen, E.R., et al. (2024). Systemic prime mucosal boost significantly increases protective efficacy of bivalent RSV influenza viral vectored vaccine. npj Vaccines *9*, 1–14. https://doi.org/10.1038/s41541-024-00912-1.

1
Introduction

1. Introduction

1. Respiratory viruses
1.1 SARS-CoV-2 and variants
1.1.1 SARS-CoV-2 epidemiology
1.1.2 SARS-CoV-2 virus classification, encoded proteins and lifecycle
1.1.3 The emergence of SARS-CoV-2 variants
1.1.4 SARS-CoV-2 pathogenesis
1.1.5 Vaccine strategies against SARS-CoV-2
1.2 Respiratory syncytial virus (RSV)
1.2.1 RSV epidemiology and burden on global health
1.2.2 RSV classification and encoded proteins
1.2.3 RSV pathogenesis and host immune responses
1.2.4 Current therapeutic and vaccine strategies against RSV
1.3 Influenza virus
1.3.1 The burden of epidemic influenza on global health
1.3.2 Influenza virus classification and encoded proteins
1.3.3 Influenza virus pathogenesis and host immune responses
1.3.4 Influenza virus ecology and pandemic potential
1.3.5 Current vaccine strategies against influenza virus
2. The immune system and immunity to viruses
2.1 The adaptive immune system
2.2 The mucosal immune system in the nasal mucosa and the respiratory tract
2.2.1 The nasal mucosa and upper respiratory tract
2.2.2 The lower respiratory tract
2.2.3 Tissue-resident memory T and B cells in the respiratory mucosa
2.2.4 IgA in the respiratory mucosa
2.3 Immunological imprinting
2.3.1 The primary addiction model of immunological imprinting
2.3.2 The antigenic seniority model of immunological imprinting
2.3.3 Measuring immunological imprinting
3. Vaccines and vaccine strategies
3.1 “Next-generation” vaccines
3.1.1 Viral vector vaccines and the ChAdOx1 platform technology
3.1.1.1 The immune response following adenoviral vector vaccination
3.1.1.2 Anti-vector immunity
3.2 Routes of vaccination and vaccine strategies

1. Respiratory viruses

Respiratory viruses are a major contributor to disease in humans, inflicting an immense burden on global health and the global economy[1]. Respiratory viruses enter the human airways where they are able to infect the respiratory tract (RTI), leading to a wide spectrum of disease. They can spread through populations in pandemic, epidemic or endemic forms, transmitting human-to-human, and affecting people across all demographics. However, younger (e.g., infants) and older individuals are often at greater risk of severe infection-derived disease[2]. Among the plethora of respiratory viruses that infect humans, respiratory syncytial virus (RSV), SARS-CoV-2 and influenza are particularly impactful on global health.

1.1 SARS-CoV-2 and variants

1.1.1 SARS-CoV-2 epidemiology

Since the emergence of severe acute respiratory syndrome-2 (SARS-CoV-2) virus at the end of 2019, more than 776 million cases of coronavirus 19 disease (COVID-19), and over 7 million COVID-19-related deaths have been reported by the world health organisation (WHO)[3]. SARS-CoV-19 has also resulted in more than 400 million cases of post-acute COVID sequelae or "long COVID", with an associated $1 trillion annual burden on the global economy[4]. COVID-19 is now widely considered an endemic rather than pandemic disease as a result of the widespread immunity gained through global vaccination campaigns, and the immunity gained through natural infection. The virus has persisted in the human population since its emergence as a result of its recurrent mutation, that has enabled (partial) immune evasion, in combination with the waning of population immunity. Nevertheless, the recent waves of infection of certain mutated variants, as well as

observed “spikes” in cases in the colder months of temperate climates, have also been interpreted as epidemics.

1.1.2 SARS-CoV-2 virus classification, encoded proteins and lifecycle

SARS-CoV-2 is a virus within the family *Coronaviridiae*, genus *Betacoronavirus,* subgenus *Sarbecovirus* and species *Betacoronavirus pandemicum.* SARS-CoV-2 is a spherical, lipid bilayer-enveloped virus that contains a positive-sense, single-stranded RNA genome[5]. The genome encodes 16 non-structural proteins (NSP1-16), four structural proteins (spike (S), envelope (E), membrane (M) and nucleocapsid (N)), as well as nine accessory proteins[5,6]. An encoded RNA-dependent RNA polymerase (RdRp) mediates viral replication and the transcription of genes, and is encoded by the *nsp12* gene[7].

The spike glycoprotein is a homotrimer abundantly distributed on the outer virion envelope and initiates the viral lifecycle by binding to the angiotensin-converting enzyme 2 (ACE-2) on host cells, and mediating the subsequent membrane fusion events. A variety of host cell types express ACE-2; within the respiratory tract where SARS-CoV-2 primarily infects, these include goblet cells and ciliated epithelial cells, as well as type II alveolar epithelial cells (AT2) deeper in the lungs[8]. ACE-2 is also highly expressed on enterocytes of the digestive tract, and is expressed in a variety of non-mucosal tissues including cardiomyocytes and even neurons[8].

The spike protein has two main domains that need to be cleaved apart by host serine proteases (normally within the host cell) at the S1/S2 polybasic furin-recognition cleavage site, in order to prime the protein for ACE-2-binding: the S1 domain, which contains the receptor-binding domain (RBD), and the S2 domain, which is involved in membrane fusion[9,10]. Following the binding of receptor-binding motif (RBM) within the

RBD (that is in the RBM-exposing “up” conformation) to ACE-2, an additional site “S2’” is exposed that is downstream of the S1/S2 cleavage site and proximal to the fusion peptide (FP)[11,12]. The S2’ site is then cleaved by host proteases, typically transmembrane protease serine 2 (TMPRSS2) (membrane fusion pathway) or cathepsin L (within the endolysosome, when the virus enters via the alternative endosomal pathway)[11,12]. S2’ cleavage removes the S1 subunit and triggers a cascade of conformational changes that stabilise S2 into an elongated trimer, and prompt the release and insertion of the FP into the host cell membrane, resulting in the formation of a fusion pore[12]. Upon membrane fusion, the viral genome is released into the host cytoplasm and translation of the genome by host ribosomes is commenced[9]. The RdRp of SARS-CoV-2 is encoded by the *nsp12* gene[13].

The M protein is another membrane protein that is involved in the assembly and morphogenesis of SARS-CoV-2; it is able to associate with the N protein during viral assembly before viral budding, which allows the packaging of the viral genome into the virion[14]. The exact functions of the E membrane protein are not known; it is a viroporin and can shuttle cations in a pH-dependent manner across the endoplasmic reticulum Golgi intermediate (ERGIC) membrane[15]. It is suggested that E may create a more alkaline environment such as to prevent premature spike activation during virus assembly[15]. N is the final structural protein, it binds and packages the RNA viral genome[16].

Finally, the non-structural proteins (NSP and accessory) carry out a number of functions, including immunomodulatory roles such as IFN antagonism, as well as mediating and regulating RNA replication[17].

1.1.3 The emergence of SARS-CoV-2 variants

SARS-CoV-2 variants of concern (VOC) began appearing roughly a year after the emergence of SARS-CoV-2, as a result of the increasing selection pressures of host immunity (including NAbs and the anti-viral innate response) and the use of anti-viral drugs[18]. The SARS-CoV-2 genome is constantly mutating as a result of genome replication errors introduced by the RdRp, despite the presence of the NSP14 replication proofreading protein; a small fraction of the error-derived mutations may be advantageous (gain-of-function)[18], hence selected for, such as those that lead to immune evasion, increased virulence, infectivity, transmissibility, and/or viral replication[19]. The spike protein is a particular hotspot for mutations as the antigen is used in most vaccines and the majority of NAbs target it (roughly 90% of serum NAb were shown to target the spike RBD in individuals who gained immunity through natural SARS-CoV-2 infection) (Figure 1.1)[18].

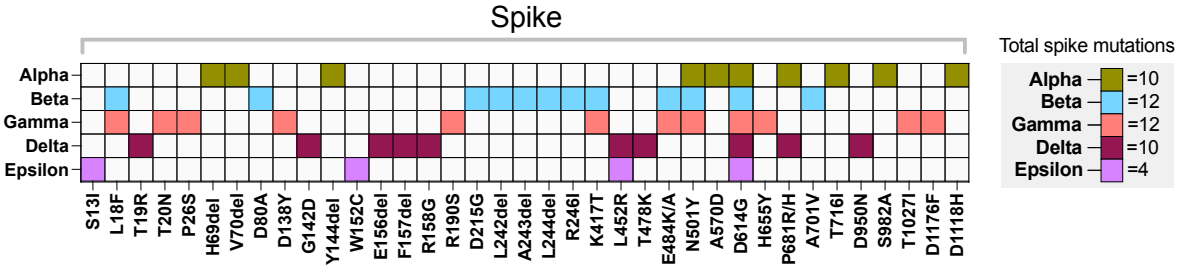

Figure 1.1: Key spike mutations in ancestral SARS-CoV-2 variants

Mutation profile is derived from the GISAID COVID-19 EpiCoV™ sequence repository database (www.GISAID.org). N.B. the exact/representative mutations for each subvariant will vary from source to source.

Advantageous mutations were detected shortly after SARS-CoV-2 began infecting humans and continued to appear at a constant, modest rate of roughly 2 amino acid substitutions per month (from the period of December 2019 to October 2020)[18]. The D614G amino acid change was one of the initial mutations within the spike protein that became prevalent in April 2020 onwards and has been shown to augment the infectivity

and transmissibility of the virus[18,20]. In late 2020 the mutation rate markedly accelerated with the emergence of the Alpha (7 spike-specific substitutions, 3 deletions), Beta (9 spike-specific substitutions, 3 deletions) and Gamma (12 spike-specific mutations) VOCs (Figure 1.1 and Table 1.1)[20–24]. Notable mutations detected in these variants included the N501Y, E484K/Q and K417N/T mutations within the RBD, which were shown to mediate immune escape and/or increase the transmissibility of virus through enhancing ACE-2 receptor binding[21,24–26]. Although the K417N mutation results in the evasion of NAb, it has also been shown to reduce the efficiency of RBD-ACE-2-binding as a result of the loss of the K417 salt bridge; this mutation is commonly paired with N501Y and/or E484K, which together "re-set" the binding efficiency and counteract the negative impact of K417N[22]. The co-occurrence of these three mutations highlights the delicate balance between the selection of advantageous, immune-evading mutations and preservation of the necessary physiochemical interactions needed for virus infection[22].

Table 1.1: Notable mutations of selected ancestral SARS-CoV-2 variants (pre-omicron)[23]

Variant	Emergence	Key/notable mutations	Effect
Alpha (α)	September 2020	N501Y	Enhances infectivity and transmissibility; increases affinity to ACE-2[24]
		D614G	Enhances infectivity and virion stability; shift towards RBD "up" conformation for ACE-2 binding[20,27]
		P681H	Confers level of resistance to IFN-β; reduces dependence on endosomal cathepsins[28]
Beta (β)	September 2020	K417N	NAb resistance[21]
		E484K	Increases binding of RBD-ACE-2; introduces additional hydrogen bond between RBD and ACE-2[22]; NAb resistance[29]
		N501Y	Enhances infectivity and transmissibility; increases affinity to ACE-2[24]

		D614G	Enhances infectivity and virion stability; shift towards RBD "up" conformation for ACE-2 binding[20,27]
Gamma (γ)	December 2020	K417T	NAb resistance[30]
		E484K	Increases binding of RBD-ACE-2; introduces additional hydrogen bond between RBD and ACE-2[22]; NAb resistance[29]
		N501Y	Enhances infectivity and transmissibility; increases affinity to ACE-2[24]
		D614G	Enhances infectivity and virion stability; shift towards RBD "up" conformation for ACE-2 binding[20,27]
Delta (δ)	December 2020	L452R	Enhances infectivity and transmissibility;
		T478K	Enhances infectivity[21]
		D614G	Enhances infectivity and virion stability; shift towards RBD "up" conformation for ACE-2 binding[20,27]
		P681R	Enhances infectivity; increases cleavability of S into S1/S2[31]
Epsilon (ε)	September 2020	L452R	NAb resistance; enhances infectivity and transmissibility[21]
		D614G	Enhances infectivity and virion stability; shift towards "up" conformation for ACE-2 binding[20,27]

In October 2020, the Delta VOC emerged and became dominant by June 2021. The occurrence of Delta breakthrough infections in vaccinated individuals has been linked with the infectivity-increasing mutations and subsequent increased transmissibility it gained (albeit having less of an immune-evading mutation phenotype compared with Beta, for example)[32]; it was estimated to be ~63%-167% more transmissible than Alpha[33]. Delta possesses a number of spike mutations (10), including a spike furin cleavage site mutation, P681R, that enhances the cleavability of the S1/S2 site, which in turn enhances the efficiency of viral entry (Figure 1.1 and Table 1.1)[34]. Importantly, several characteristics of the Delta mutations have been linked to its augmented pathogenicity which will be touched on in the next section.

By the end of November 2021, the Omicron variant was declared a VOC, spreading rapidly and having garnered a large number of mutations (~50 total, with 33 in the spike domain alone) in its genome compared with other former variants, marking a clear antigenic shift, rather than drift from the more ancestral variants; the Omicron variant swiftly replaced Delta to become the most prevalent variant, and was dominant globally by January 2022. Omicron was shown to be immune-evading, and was more transmissible than delta (3.31-fold higher than delta)[35,36]. However, interestingly, Omicron gained certain mutations that resulted in reduced cleavability (P681H, H655Y and N679K) of the S1/S2 site compared with Delta, which altered the preferred cell entry pathway to the endosomal-dependent, rather than TMPRSS2-dependent pathway[36,37]. Contrarily, Omicron gained certain mutations that enhanced ACE-2-binding[36,37].

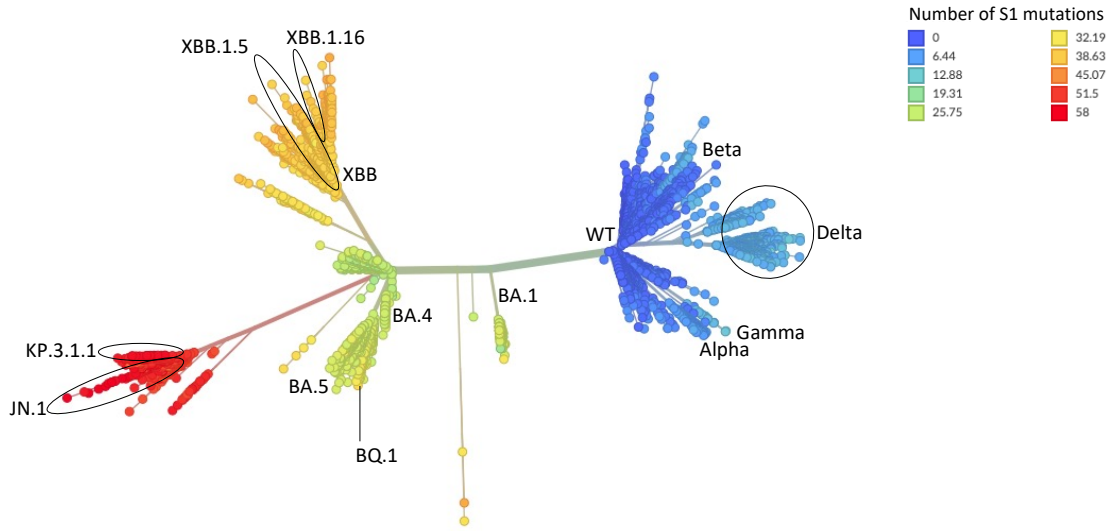

Figure 1.2: SARS-CoV-2 phylogenetic tree with selected variants from Nextstrain.org (GISAID)

The tree branch length represents nucleotide divergence (total genome mutations compared with wildtype). The colouring is related to number of mutations in the S1 domain. The dots represent strains. Diagram sourced from Nextstrain.org (GISAID); Licensed under CC-BY-4.0.

The antigenically-shifted Omicron variant is widely hypothesised to have arisen from chronically infected individuals who had suboptimal immunity that enabled the virus

to persist; the treatment of these individuals with convalescent plasma and/or antivirals provided the viral strains with further opportunity to gain resistance; these mutants then spilled out into the population via shedding and rapidly spread[38,39]. Within chronic individuals, multiple strains may arise over time that compete with each other under precise selection pressures such as antiviral treatment[38,39]. The divergence of the Omicron variant (BA.1) is illustrated through phylogenetic tree adapted from Nextstrain in Figure 1.2[40,41].

The Omicron variant continued to mutate into various subvariants with considerable antigenic diversity relative to one another (Figure 1.2 and Figure 1.3)[42,43]. Interestingly, certain subvariants are the product of recombination events between two viruses during co-infection, exemplifying an additional mechanism for the introduction of genome variation in SARS-CoV-2 (in addition to RdRp error)[44]. The XBB subvariant (which has since further mutated into XBB.1.16 and XBB.1.5) was the descendent of two BA.2 lineages, BJ.1 and BA.2.75 (BM.1.1.1), which recombined, with a breakpoint that was located within the RBD domain[44,45]. Other recombinants included the XE variant (BA.1 and BA.2) and the XF variant (BA.1 and Delta) which did not become as prevalent as the XBB lineage[46,47]. In 2024, two descendants of Omicron have shown high prevalence globally: JN.1 (~November 2023-May 2024) and KP.1.1.3 (~June 2024-October 2024)[48].

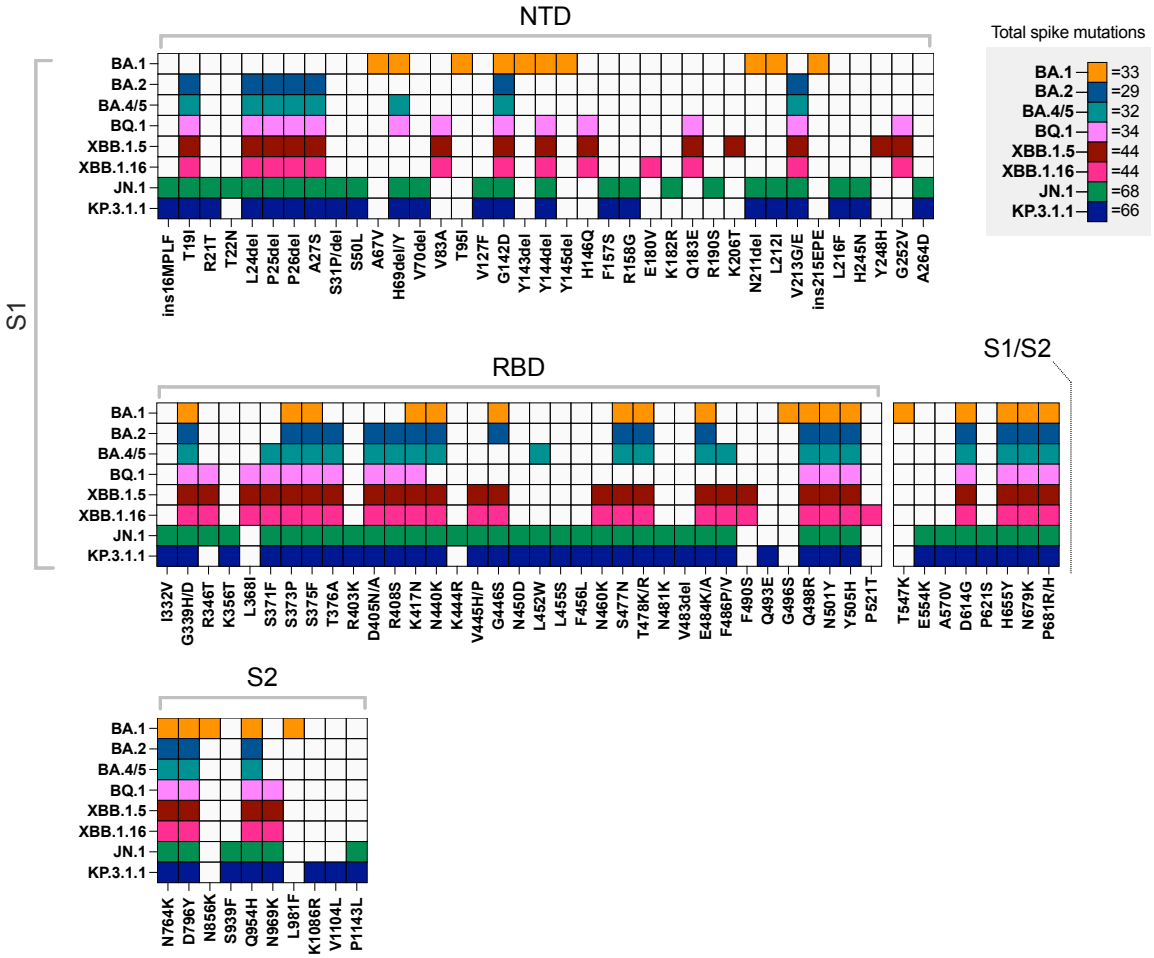

Figure 1.3: Key spike mutations in Omicron subvariants

Key spike mutations of selected Omicron subvariants derived from the GISAID COVID-19 sequence repository. N.B. the exact/representative mutations for each subvariant will vary from source to source.

1.1.4 SARS-CoV-2 pathogenesis

SARS-CoV-2 causes a wide spectrum of disease (COVID-19) in humans; the virus's pathogenicity has changed throughout the COVID-19 pandemic as a result of its extensive mutation, and the immunity gained within the population as a result of vaccination and natural infection. SARS-CoV-2 is transmitted from an infected individual via aerosol or droplets that are then inhaled, and then enter the respiratory tract; the virus initially infects the luminal ciliated cells[49]. Following roughly 4-5 days of incubation, symptoms typical of

moderate respiratory disease develop in most individuals, such as a sore throat, cough, headache, fever and myalgia, however a subset of individuals may also be asymptomatic[49].

In some cases the infection is not contained within the upper respiratory tract (URT) and the virus spreads to the lower respiratory tract (LRT) via the tracheobronchial tree or through inhalation[49]. This can lead to the development of severe disease (which typically arises a week post-symptom onset), often involving hypoxaemia, and potentially progressing to acute respiratory distress syndrome (ARDS) and severe pneumonia[49]. In such individuals, excessive inflammation and damage of the lung tissues, especially alveolar epithelia, are observed, and occasionally the disease progresses to affect other organs as a result of further dissemination of the virus[49–51]; in autopsies of deceased individuals who succumbed to severe COVID-19 infection, SARS-CoV-2 was detected in various non-respiratory tissues including the brain[52].

The primary target of SARS-CoV-2 within the LRT is the AT2 cell, which produces surfactant, however, AT1 pneumocytes, which account for more of the alveolar surface and facilitate gas exchange, may also be infected[53]. Histological analyses of the lung tissue of individuals deceased as a result of infection revealed signs of diffuse alveolar damage (DAD), including: oedema (interstitial and intra-alveolar), alveolar epithelial cell necrosis, microvascular thrombosis, capillary congestion and hyaline membrane formation (reducing oxygen exchange)[49–51]. Various human factors influence the likelihood of developing severe COVID-19; these include being of older age, male, and/or possessing comorbidities such as diabetes or chronic pulmonary disease[49]. Notably, in contrast to other respiratory viruses, SARS-CoV-2 does not tend to elicit severe disease in children; this is hypothesised to be as a result of lower expression of ACE-2 in the respiratory tract

compared with that in adults, however, various other factors have been hypothesised as well[54,55].

Due to the immunity offered through widespread vaccination and infection, as well as the improved knowledge on COVID-19, and less burdened healthcare systems, infections in individuals in more recent years have generally resulted in less severe disease compared with infections towards the beginning of the pandemic. Additionally, the pathogenicity of the more recent Omicron variants is attenuated due to certain intrinsic viral properties, especially compared with earlier variants such as Delta that elicited more severe forms of disease, despite the fact that Omicron has caused more breakthrough infections, is more infectious and has a higher affinity to ACE-2[36,55].

The abundance of mutations in the Omicron spike domain has resulted in its efficient immune evasion and ability to compromise the protective capacity of wildtype spike-based vaccines, although certain mutations around the S1/S2 cleavage site (P681H, H655Y and N679K) of the variant have been associated with the reduced cleavability of its spike protein (hence reducing the priming efficiency of spike)[36,37]. The reduced cleavability of Omicron spike is linked to its altered preference for the endosomal cell entry pathway that is TMPRSS2-independent and does not require pre-S1/S2 cleavage (priming)[37,56]. Omicron has a greater tropism towards the URT compared with Delta (which can infect both URT and LRT), which may partially explain the lessened severity associated with Omicron infection[37]; higher TMPRSS2 expression has been reported in the alveolar AT1 and AT2 pneumocytes in the LRT, compared with generally less relative TMPRSS2 expression in the URT[37]. In addition, the lessened usage of TMPRSS2 pathway has reduced the fusogenicity of Omicron; the formation of syncytia (cell-cell fusion) is associated with

increased pathogenesis and is a mechanism by which virus can infect adjacent cells without being exposed to the host's extracellular antibodies[37].

Despite the attenuated disease elicited in most vaccinated individuals by later variants, the vulnerable populations, such as immunocompromised, still remain at risk of complications. Moreover, detrimental long COVID can occur after SARS-CoV-2 infection of a diverse range of individuals irrespective of the severity of the acute phase of their infection, and exists as a major global health issue[4,57].

1.1.5 Vaccine strategies against SARS-CoV-2

Several SARS-CoV-2 vaccines were rapidly produced, trialled and employed for use globally following the emergence of SARS-CoV-2; the first COVID-19 vaccines were introduced in December 2020[58], and since then 13.64 billion doses of vaccine have been delivered globally, with an estimated 67% of the global population having received a complete primary course of COVID-19 vaccine, and 32% having received at least one booster dose[59]. The overall efficacy of these initial vaccines that used the original "wildtype" spike against COVID-19 disease was high, as demonstrated through phase 3 clinical trials (Table 1.2).

Table 1.2: Selection of SARS-CoV-2 vaccines approved for human use

Vaccine	Type	Route	Phase 3 trial efficacy results
Pfizer-BioNTech; Comirnaty; BNT162b2	mRNA; two-dose with 21-day interval for primary series, booster 5 months after recommended	IM	95% (95% CI 90.3%-97.6) effective in preventing COVID-19; 21,720 (≥16 years old) received vaccine[60]
Moderna; Spikevax; mRNA-1273	mRNA; two-dose with 28-day interval for primary series,	IM	94.1% (95% CI 89.3%-96.8%) reduction in symptomatic COVID-19;

	booster 5 months after recommended		14,134 (≥18 years old) vaccinated[61,62]
Astrazeneca-Oxford; Vaxzevria; AZD1222	Viral vector (ChAdOx1); two-dose with 4-12-weeks interval for primary series, mRNA booster 3 months after recommended	IM	74% (95% CI 54.2%-94.1%) reduction in symptomatic COVID-19; 21,632 vaccinated adults[63]
Johnson and Johnson (Janssen); Ad26.COV2.S	Viral vector (Ad26); initially recommended as single-dose, booster later recommended at least 2 months after primary series	IM	66.9% (95% CI 59.0%-73.4%) effective in preventing moderate to severe COVID-19; 19,630 (≥18 years old) vaccinated[64]
Novavax; Nuvaxovid; NVX-CoV2373	Protein subunit with matrix-M adjuvant; two-dose with 3-week interval for primary series, booster 6 months after recommended for some individuals	IM	90.4% (95% CI 82.9%-94.6%) reduction in symptomatic COVID-19; 19,714 (≥18 years old) vaccinated[65]
Sinovac; CoronaVac	Inactivated virus vaccine; two-dose with 2-4-week interval for primary series, booster 3-6 months after recommended	IM	83.5% (95% CI 65.4%-92.1%) reduction in reduction in symptomatic COVID-19; 10,214 (18-59 years old) vaccinated[66]

Nevertheless, the subsequent emergence of immune-evading variants has resulted in the compromised efficacy of the wildtype spike-based vaccines, although the immunity from these initial vaccines has generally contributed to protection against severe disease, hospitalisation and death, namely through the induction of cross-reactive immunity[67]. Nonetheless, the cross-protection against infection and disease conferred by these primary series vaccines has been shown to wane rapidly with time and with the continued drift and shift of variants, and a sizeable number of severe cases and deaths continue to occur in those that are vulnerable[67]. Additionally, the continued vaccination with wildtype spike vaccine may have negative consequences by enforcing an immunological imprint that could hamper the immune responses to newer variant; this phenomenon will be touched on later in this chapter[68–72].

Because of these limitations, updated booster strategies have been implemented which include the Omicron (subvariant) spike, and are aimed at of broadening pre-existing immunity to more current variants (Table 1.3)[73–76]. In the UK, booster vaccination is recommended for those at greatest risk; i.e. ≥75 year olds, and those aged ≥6 months with a compromised immune system[77]. Several challenges have accompanied the booster vaccine strategies, namely that the virus is evolving at a rapid rate and the updating of vaccine to match current circulating strain is a timely and costly process, and logistically challenging. Much like with influenza virus, it is difficult to ascertain the true efficacy (via clinical trial) of a booster vaccine against a quickly evolving virus, due to the incidence of mismatch. Although mismatched boosting has been proven in certain studies to generate beneficial immunity[78], other findings have highlighted the relatively fast waning of cross-protective responses induced upon mismatched booster, e.g. as evidenced in a study examining the protection of BA.1 and BA.4/5 bivalent vaccine-boosted ≥60 year-olds against XBB-related hospitalisations long term; this is likely a reflection of the high relative antigenic distance between the different omicron subvariants[79].

Additionally, the performance of these modified bivalent vaccines has varied in comparison to boosting with an original vaccine instead; it has been proposed this is due to the involvement of immunological imprinting[80–86]. The WT spike component of the omicron booster vaccine has now been omitted from more recent booster formulas, and this has been completed in hopes eliciting a more targeted response to the relevant variant; Qian Wang *et al* have suggested the wildtype component of the booster vaccine is contributing to a “deep” immunological imprint[80].

Table 1.3: Adapted SARS-CoV-2 variant booster vaccines

Booster vaccine	Type of vaccine and antigen		Route
Pfizer-BioNTech; Comirnaty	Bivalent mRNA	Original and BA.1	IM
		Original and BA.4/5	
		Original and XBB.1.5	
	Monovalent mRNA	XBB.1.5	
		KP.2 (2024-2025 formula)[76]	
Moderna; Spikevax	Bivalent mRNA	Original and BA.1	IM
		Original and BA.4/5	
	Monovalent mRNA	XBB.1.5	
		JN.1	
		KP.2 (2024-2025 formula)[75]	
Novavax; Nuvaxovid	Monovalent adjuvanted (Matrix-M) recombinant protein	XBB.1.5	IM
		JN.1 (2024-2025 formula)[74]	

To this end, the current booster strategies could benefit from further optimisation that considers factors such as immunological imprinting; enhancing the current strategies such that more durable and transmission-blocking forms of immunity are elicited would help reduce the seasonal health burden that these circulating variants now impose, particularly on the elderly and immunocompromised. The use of the mucosal route, for example, has been proposed as a more effective means of inducing immunity that controls and prevents airway infection (not solely preventing severe disease), and could be implemented in optimised boosting campaigns[87,88]; the mucosal route has been used for certain wildtype-only vaccines that were tested, and some even approved for use (around the emergence of the Delta and Omicron variants), but there remains limited, and variable

efficacy data on their protective capacity[89–91]; one particular trial will be further touched on later in this chapter[92].

1.2 Respiratory syncytial virus (RSV)

1.2.1 RSV epidemiology and burden on global health

Human respiratory syncytial virus (RSV) is a common, globally widespread virus capable of infecting all age groups. RSV is a major contributor to acute lower respiratory tract infections (LRTI) in young infants[93]. Within 2 years of age the majority of infants are infected with RSV (approximately 80%), and the resultant immunity gained from infection is typically poor and wanes quickly, hence reinfections within this timeframe are commonplace[94–96]. RSV inflicts a major global health burden; in 2019 alone, an estimated 33 million hospital admissions were attributed to RSV-elicited LRTI in children less than 5 years old[97]. It is estimated that over 100,000 deaths in <5 year olds per annum are as a result of RSV infection globally[98]. Of this estimate, more than 45,000 of the deaths are in young infants (1 month to 6 months old), thus making approximately 3.6% of all the deaths in this age bracket a result of RSV infection[98]. The majority of these deaths (97%) are in developing countries[97,98].

The elderly are also significantly affected by RSV, who are most commonly exposed to the virus via contact with children and staff in nursing care homes[99]. The disease burden of RSV infection is often overlooked in older adults; studies have observed a similar mortality rate and hospital burden in observed cohorts of elderly infected by either RSV or influenza[99,100]. An RSV infection rate of 600.7 cases per 100,000 individuals and hospitalisation rate of 157 hospitalisations per 100,000 individuals is estimated for older adults living in industrialised countries[99]. The annual hospital cost burden for RSV infection in the U.S. was estimated to be $743.9 million[99,101].

Younger, healthy adults are susceptible to RSV infection, however, clinical symptoms are often self-contained and similar to those of a common cold. The infections in such cases remain restricted to the upper airways, however, infected individuals still risk transmitting the virus to vulnerable younger and older individuals due to the highly contagious nature of the virus.

In regions with more temperate climates, the frequency of RSV infections tends to increase in the colder months, whereas in tropical regions with high precipitation, cases of RSV infection tend to coincide with the wetter seasons, however, not all climates are well defined in terms of seasonal pattern of infections[95,102,103]. The COVID-19 pandemic has significantly influenced the spread and incidences of RSV infection[104]. Cases of RSV dropped by approximately 98% at the beginning of the COVID-19 pandemic as a result of social distancing and the increased use of masks; this was then met by a surge of RSV cases as social distancing policies were relaxed and the naïve, RSV-unexposed young population encountered the virus[105,106].

1.2.2 RSV classification and encoded proteins

RSV is classed within the *Paramyoxiviridiae* family, subfamily *Pneumovirinae*, genus *Pneumovirus*[107]. RSV is an enveloped virus with a non-segmented, negative-strand RNA genome. Within the *Pneumovirus* genus, bovine RSV, ovine RSV and pneumonia virus of mice also exist[107]. The human RSV virus has two subgroups denoted A and B, that have considerably different glycoprotein G sequences that are used to classify the two subgroups (53% homologous in amino acid sequence)[107]. RSV A and RSV B tend to co-circulate each season, however, their relative prevalence may differ seasonally[108].

The RSV genome consists of 10 genes that encode for 11 proteins, with mRNA transcription mediated by an RNA-dependent RNA polymerase, composed of L, P and M2-1 proteins (Table 1.4)[107,109,110]; the RNA-dependent RNA polymerase also mediates replication of the whole virus genome and antigenome[110]. The nucleoprotein (N) associates with the virus RNA to form a helical nucleocapsid (NC) complex[111]. The RSV virion can be spherical, filamentous or asymmetrical in shape (pleomorphic), with a matrix (M) protein lattice lining the interior of the virus membrane, which is enveloped by a host cell-derived lipid bilayer[109,112]. The M2-1 viral protein is an elongation factor involved in the transcription of mRNA[113]. The M2-2 viral protein is a polymerase cofactor believed to play a role in regulating the balance between mRNA synthesis and genome RNA replication, promoting the latter process[114,115].

Table 1.4: List of human RSV proteins

Protein name (ordered by position in genome)	**Protein function**		**Amino acid sequence identity between RSV A and RSV B subgroups (%)**
NS1	Type I interferon antagonist		87
NS2	Type I interferon antagonist		92
N	Nucleoprotein	Encapsulation of viral RNA into ribonucleoprotein complex (RNP)	96
P	Phosphoprotein		91
M	Matrix protein		91
SH	Membrane proteins	Short hydrophobic protein; pentameric ion channel	76
G		Receptor attachment glycoprotein	53
F		Host cell membrane fusion protein	89
M2-1	Genome transcription and replication		92
M2-2	Genome transcription and replication		72
L	RNA-dependent RNA polymerase; large protein		93

RSV has three surface proteins, SH, G and F[112]. The small hydrophobic (SH) protein forms a pentameric ion channel that has been shown to prevent apoptosis of infected cells, however its exact biological functions are not known[116]. The G and F proteins mediate cell attachment and fusion, respectively, although the G protein is not essential for cell entry in contrast to the F protein[117]. The F protein is highly conserved between the two antigenic subgroups (89%). It is first synthesised in the producer cell as an F_0 precursor protein; the precursor possesses two furin cleavage sites that when cleaved by host furin-like proteases allow the removal of the P27 portion, which results in a monomer of F_1 (C-terminal) and F_2 (N-terminal) subunits that are joined covalently through disulphide bonds; the F_1 subunit bares various characterised epitopes that NAbs target, and it mediates virus-host membrane fusion[118]. The F_1-F_2 monomers trimerize into a functional homotrimer and are transported to the viral envelope, where they are embedded[119].

The RSV F trimer exists in two major structural states: pre- and post-fusion; the pre-fusion state RSV F trimer is metastable, meaning it can easily convert into a more stabilised post-fusion form[119]. Five antigenic sites can be found on the pre-fusion F protein: “I”, “II”, “III”, “IV” and “Ø”, a site at the apex which is a target for many potently neutralising antibodies[119,120]. The RSV pre-fusion F protein undergoes a pH-independent refolding event at the host-cell surface that involves insertion of the F_1 N terminus fusion peptide into the host membrane (pre-hairpin conformation), followed by further refolding events (hemi-fusion-to-post-fusion state) that result in the mixing of lipids and eventual membrane fusion (pore formation) allowing for subsequent infection of the host cell (release of viral RNA into the cell)[121]. The transition to the post-fusion F protein conformation state is driven through the association of the fusion peptide heptad repeats and the F_1 C terminus heptad repeats, leading to a highly stabilised six-helix bundle[121,122].

Spontaneous conversion to the post-fusion conformation can occur without host cell membrane contact, and results in the concealment of antigenic sites “III”, “V” and “Ø”[120].

The RSV G glycoprotein is also known as the virus membrane-bound host cell-attachment protein (mG), and exists as a monomer; it also exists in a soluble form (sG)[123]. RSV virus preferentially infects ciliated epithelial cells of the respiratory tract airways in a process initiated through the binding of the RSV G to the CX3CR1 cell receptor via its conserved CX3C chemokine motif[123]. RSV G and F proteins have also been shown to bind several other surface proteins, including nucleolin, epidermal growth factor (EGF), heparan sulphate proteoglycans (HSPGs) and intercellular adhesion molecule-1[124]. The RSV G protein also has immunomodulatory and immune-evading (e.g. heavy glycosylation for epitope shielding) functions in addition to its role in virus attachment to host cell; for example, the soluble form of G has been suggested to act like an antigen decoy, misdirecting immune responses[125]. Removal of the G protein does not render RSV unable to infect cells, however, attenuates the virus and lessens the efficiency of infection; this highlights the F protein’s capacity to independently facilitate infection[125].

Lastly, the two non-structural proteins (NS1 and NS2) have been associated with various immunomodulatory and immunosuppressive roles including the suppression of IFN-β induction[126]. The NS proteins are the first transcribed genes upon RSV infection, such that the suppression of innate immune response can be coordinated early in the viral life cycle[127].

1.2.3 RSV pathogenesis and host immune responses

RSV is most commonly transmitted from infected to uninfected individual via the inhalation of airborne mucus droplets derived from coughing or sneezing; typically 3 to 7

days after exposure symptoms develop, which can resemble those following a common cold; e.g., runny nose, cough and tight chest[128]. In most individuals of all ages, RSV is restricted to the upper respiratory tract only (URTI)[129]. However, in a subset of individuals (approximately one third of infant RSV cases), the URTI quickly spreads to the LRT, leading to more serious cases of bronchiolitis[129]. In very severe cases, individuals can develop interstitial pneumonia, and exhibit laboured breathing and suffer from hypoxia[129,130]. Early histopathological analyses of the lung tissue of infants that succumbed to severe RSV disease revealed that the infected cells of the lower airway epithelia (alveolar and bronchioles) were acutely damaged by infection, exhibiting an irregular, enlarged and multinucleated cellular morphology (syncytia)[130]. The sloughing of necrotic tissue into the narrow lower airway lumen is thought to contribute to the obstruction of the airways in severe cases, alongside oedema; the syncytialisation of cells, excessive cell death and retention of cellular material promote the infiltration of inflammatory cells such as neutrophils and eosinophils (eosinophilia) into the distal airways, exacerbating this airway obstruction and augmenting infection[130,131]. Cases of RSV-elicited bronchiolitis in infants have been associated with the development of childhood asthma[132].

Various factors contribute to the increased incidences of severe disease in infants and the elderly following RSV infection. It is hypothesised that the immaturity of the infant adaptive immune system (especially neonates and young infants) make this age bracket particularly vulnerable to RSV disease; the neonatal immune system is skewed against the pro-inflammatory response (tending towards a Th2-type T cell response), tends to have elevated proportions of T_{reg}s (relative to $CD4^+$ and $CD8^+$ T cells) in comparison with adults, and more generally the infant's airways are much smaller that the adult human, hence are much more easily obstructed[133]. Generally, the elderly are at greater risk of severe RSV

disease due to the effects of immunosenescence (including thymus atrophy), leading to weakened adaptive immune systems, and the increased likelihood of underlying health conditions such as chronic obstructive pulmonary disease (COPD) in their age group[102].

Several viral factors contribute to the pathogenicity of RSV; as listed in Table 1.4 and touched on in section 1.2.2. Notably, the NS1 and NS2 proteins suppress type I IFN pathways via inhibition of RIG-like receptor-I (RIG-1) and melanoma differentiation-associated protein 5 (MDA5) pathways, compromising the host anti-viral response, thus contributing to the virulence of RSV[126].

1.2.4 Current therapeutic and vaccine strategies against RSV

Efforts to develop and license an effective vaccine against RSV have spanned decades, and certain hurdles and challenges have made the process particularly difficult. Whilst natural infection-gained immunity can normally help inform of the immune correlates of protection that are needed when designing a vaccine, natural infection with RSV does not necessarily induce a quality and durable (life-long) protective response against reinfection[134]. A well-studied clinical trial in the 1960s evaluating a formalin-inactivated RSV (FI-RSV) candidate vaccine resulted in cases of vaccine-enhanced respiratory disease (ERD) in infants and children that were naturally infected with RSV after vaccination; 80% of the participants were hospitalised, and two died, following natural virus exposure[135]. The failure to mount quality, neutralising antibody responses, and the skewing to a Th2-type T cell response in the lungs, are among several suggested explanations for the observed ERD following the natural RSV infection in FI-RSV-vaccinated participants[135]. The failure of this vaccine trial heightened the cautiousness and hesitancy

around the clinical testing of other RSV candidates, however, the trial also prompted further important research on ERD, and informed of RSV vaccine design[136,137].

Considerable progress has been made in determining the best antigenic candidates for RSV vaccines, especially as a result of the innovative structure-based antigen design approach taken by McLellan et al[138]. The stabilised pre-fusion forms of RSV F protein have been shown to better induce NAbs compared with the post-fusion form RSV F (as was the predominant form in the FI-RSV vaccine), as they preserve the antigenic "Ø" site[138,139]. The stabilised pre-fusion RSV F protein is "fastened" in its conformation via several site-specific mutations, and features additional disulphide bonds[138]. The RSV F protein is an ideal antigen candidate given that its function is essential for virus's entry into cells, and that it is highly conserved between the two co-circulating RSV subgroups A and B[140].

Pre-fusion-stabilised RSV F antigen is now used in a number of vaccines that have demonstrated efficacy against RSV respiratory tract infection and/or disease, including vaccines from GSK, Pfizer and Moderna (Table 1.5)[141]. Arexvy (GSK) is FDA-approved for use in adults 60 and above and was shown to safely reduce the risk of LRTD by 83% in the vaccinated group of their phase 3 trial[142], nevertheless, the efficacy decreased by 34% in those above 80 years of age[143]. The vaccine consists of the recombinant pre-fusion RSV F (RSVPreF3; based on RSV A) protein adjuvanted with AS01E, and is administered intramuscularly[142,143]. Abrysvo (Pfizer) is another licensed recombinant vaccine recommended for use in adults 60 and above, as well as for pregnant individuals, such that their infants be protected in their early months of life via the acquisition of protective maternal antibody (maternal vaccine)[144]. The Abrysvo vaccine contains the pre-fusion-stabilised RSV A and B proteins (unadjuvanted), and following intramuscular administration in 16,308 older adults it was shown to reduce the risk of acquiring an RSV-elicited LRTD by

67% (with two or more symptoms)[144,145]. Additionally, a 51% reduction in the risk of acquiring RSV-LRTD (up to 90 days after birth), and 82% reduction in incidences of severe, medically-attended RSV-LRTD (up to 180 days after birth) were noted from the 3,495 infants born from individuals vaccinated with Abrysvo in a separate trial[144,146]. The other currently approved (FDA and European Commission) vaccine for use is mRESVIA (Moderna), an mRNA vaccine encoding the RSV prefusion F protein based on RSV A; the vaccine phase 3 clinical trial demonstrated a 84% reduction in RSV-LRTD in adults 60 or over[147,148].

Table 1.5: List of licensed RSV vaccines and associated phase III trial results

Vaccine	Target group	Type	Route	Phase 3 trial efficacy of reduction in RSV-LRTD	Long term
Arexvy; GSK	>60-year-olds	Recombinant pre-fusion-stabilised F; AS01E adjuvant	IM	Adult Respiratory Syncytial Virus-006: 82.6% (96.95% CI 57.9%-94.1%)	Second season follow-up: 66.5% (95% 55.2%-75.5%)
Abrysvo; Pfizer	Pregnant individuals 32-36 weeks gestation	Recombinant pre-fusion-stabilised F	IM	MATISSE (3570 infants from vaccinated pregnant individuals): 57.1% (99.5% CI 14.7%-79.8%); up to 90 days after birth	N/A
	>60-year-olds			RENOIR (34,284 adults >60): 88.9% (95.0% CI 53.6%-98.7%) within first RSV season after vaccination (infection with ≥3 symptoms)	Second season follow-up: 77.8% (95.0% CI 51.4%-91.1%) (infection with ≥3 symptoms)
mRESVIA (mRNA-1345); Moderna	>60-year-olds	mRNA encoding pre-fusion-stabilised F	IM	ConquerRSV (37,000 adults >60): 83.7% (95.88% CI 66.0%-92.2%); median follow-up 112 days	Vaccine displayed long term protection in 8.6-month follow-up

In addition to vaccination, passive antibody transfer of the humanised monoclonal Palivizumab is an effective prophylactic treatment against severe RSV-LRTI taken before exposure[149]. The antibody binds to the "II" site present on both the pre- and post-fusion conformations of RSV F[150]. However, there are several drawbacks to Palivizumab, mainly that it must be administered monthly to account for its short half-life (approximately 20 days), and that it is expensive; it is normally restricted for use in high-risk infants only[140]. Recent advances have seen the licensure of an improved monoclonal treatment, Nirsevimab (AstraZeneca in partnership with Sanofi) that features an extended half-life of up to 100 days (thus can cover the RSV season once administered) and alternatively targets the "Ø" site, leading to higher neutralisation potency[140,151]. Nirsevimab is a human recombinant IgG1 monoclonal antibody with the YTE amino acid substitutions in the Fc region that enhance its binding affinity to the neonatal fetal receptor (FcRn), which increases the antibody half-life[152]; in a trial where 994 infants received Nirsevimab prior to the RSV season ("MELODY"), an efficacy of 74.5% (95% CI 49.6%-87.1%) reduced risk of medically-attended RSV-LRTI was observed (up to 150 days post-injection)[152].

The licensure and implementation of these vaccines and the Nirsevimab monoclonal therapy represent a major leap forward regarding the ongoing effort to eradicate RSV-elicited disease. Nevertheless, this is only the beginning, and there are important considerations that should be made moving forward. These include the potential risk of the emergence of immune-escaping RSV mutants subsequent to the increased, more widespread use of the licensed vaccines and Nirsevimab antibody, as well questions of how durable these vaccines are and how waning vaccine immunity will impact the protection in vulnerable individuals longterm[140]. Although the aforementioned vaccines protect against (severe) LRTI, efforts should also be focused the potential of

transmission blocking vaccines; different modes of vaccination such as the mucosal route should still be considered, potentially for booster campaigns. There are mucosal RSV vaccines in the early stage of development that have been tested in humans, with promising results[153,154]. Furthermore, the distribution of these vaccines and novel treatments to low-income countries should be prioritised, with consideration of how the cost burden can be navigated[140].

1.3 Influenza virus

1.3.1 The burden of epidemic influenza on global health

Seasonal, epidemic influenza inflicts a massive burden on global health; it is estimated that annually there are roughly one billion cases of influenza, leading to 3-5 million incidences of severe disease and upwards of 650,000 deaths[155]. The largest burden is in developing countries, where 99% of the annual <5-year-old influenza-related deaths occur[155]. Similarly to RSV, influenza can infect all age groups, but younger children and the elderly are particularly vulnerable, as well as those with comorbidities, those that are pregnant, and those that are immunocompromised[155]. In addition to the health burden, influenza inflicts an enormous economic burden; in the UK alone, an estimated £644 million loss in the economy is associated with seasonal influenza[156]. Much like RSV, a reduction in influenza cases were observed during the COVID-19 pandemic, which can be attributed to the introduction social distancing measures, however, cases of influenza are now reportedly similar to the levels recorded prior to the pandemic[157].

Much like RSV, influenza epidemics occur during the colder months in places with temperate climates, whereas the seasonality is less defined or present in the subtropical and tropical regions[158]. In addition to the seasonal epidemics, there are occasional

pandemics that have occurred every 10-50 years, and result in high incidences of severe disease and high fatalities; these are explained in more detail later in this chapter.

1.3.2 Influenza virus classification and encoded proteins

Influenza viruses exist within the family *Orthomyxoviridae*, of which three genera or types, *Alphainfluenzavirus* (influenza A virus (IAV)), *Betainfluenzavirus* (influenza B virus (IVB)) and *Gammainfluenzavirus* (influenza C virus (IVC)) out of the total of five, are known to infect humans[159]. The RNA genome of the influenza virus is segmented (IAV and IBV: 8, ICV: 7) and negative-strand, and is encapsulated in a host lipid bilayer envelope[159]. All three viruses share a pleomorphic morphology; however, ICV exists in a filamentous shape more often than the influenza A and B viruses, which are more structurally similar. The IAV encodes 11 proteins, and of the 10 that are shared between IAV and IBV, there is limited sequence homology, as illustrated through the sequence alignments of two selected, representative strains (Table 1.6)[159].

Table 1.6: List of influenza A (A/Puerto Rico/8/1934 (H1N1)) proteins and homology of protein amino acid sequence with influenza B (B/Lee/1940)

Genome segment	Encoded protein	Protein function	Amino acid sequence identity between influenza A and B (%)
1	PB2	Polymerase subunit; mRNA cap recognition	38
2	PB1	Polymerase subunit; RNA elongation and endonuclease activity	61
	PB1-F2	Pro-apoptotic activity	N/A
3	PA	Polymerase subunit; protease activity	37
4	HA	Receptor binding and fusion; surface glycoprotein	28
5	NP	RNA-binding protein	38
6	NA	Sialidase activity and virus release; surface glycoprotein	35
7	M1	Matrix protein	31
	M2	Ion channel	47
8	NS1	Interferon agonist protein	<25%
	NEP/NS2	Nuclear export of RNA	26

The influenza A viruses are organised via a unique system because the hemagglutinin (HA) and neuraminidase (NA) glycoproteins within the genus are diverse in sequence identity; in addition, different combinations of the various HA and NA glycoproteins are possible as a result of the segmentation of the RNA genome[160]. Co-infection of an organism with two different influenza A viruses can result in the mixing of gene segments, leading to viral progeny with "swapped" HA and NA combinations encoded in their genome. The particular HA and NA combinations inform the IAV subtype. There are two phylogenetic groups for the HA and NA proteins denoted HA group 1 and HA group 2, and NA group 1 and NA group 2, respectively, that are organised based off of their amino acid sequences (Figure 1.4)[160]. 18 HA (H1-H18) and 11 NA (N1-N11) subtypes have been identified[161], hence 144 HA-NA combinations are theoretically possible, however only 120

have been identified naturally thus far across the wide range of host species[162]. The IBV is not divided into subtypes, but rather, lineages, of which there are two: B/Yamagata and B/Victoria[160]. The B/Yamagata lineage has not been detected since March 2020[157]. The influenza C virus does not display a similar level of genetic and antigenic diversity to that of influenza A, hence it is not organised in a similar way.

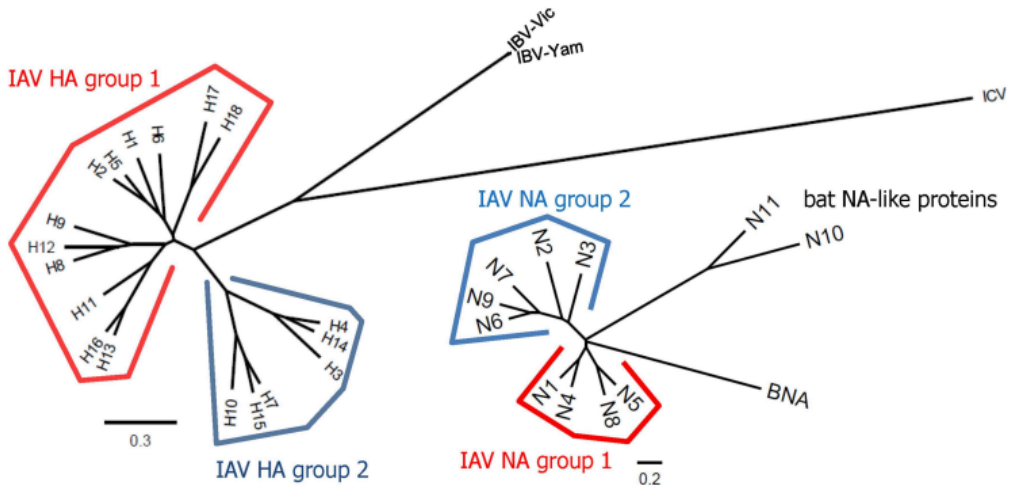

Figure 1.4: Phylogenetic tree of the HA and NA proteins of influenza A and B viruses from Yo Han Jang and Baik Lin Seong (2019)©; Licensed under CC-BY-4.0[160]

The HA and NA glycoproteins of IAV (and to a lesser extent IBV), regularly collect point mutations as a result of an error-prone RNA-dependent RNA polymerase comprised of three subunits (PB1, PB2 and PA) that lacks exonuclease proofreading ability; due to the external (host) selection pressures of vaccine- and infection-derived immunity, IAV evolves at a rapid rate[163,164]. Through minor, yet advantageous mutations that change the surface glycoproteins, IAV is able to evade pre-existing immunity derived from exposure to related antigen and "re-infect" individuals. This form of virus evolution is termed antigenic drift. Antigenic drift results in seasonal changes to the influenza A and B viruses, however IVB tends to mutate less frequently than IAV. The H3N2 and H1N1 subtypes of influenza A are

the most prevalent subtypes and tend to co-circulate in seasonal epidemics, typically together with either B/Yamagata or B/Victoria lineages.

The HA and NA surface glycoproteins have opposing functions[162]. The HA exists as a homotrimer with an immunodominant globular head domain that contains a sialic acid (SA) binding site (RBS), that binds α2-6 sialylated glycans specifically, for seasonal IAV, as well as a more conserved immunosubdominant stalk domain[162,165,166]; α2-6 SA are often the terminating branches of ciliated epithelial cell surface glycans in the URT[167,168]. Many potent NAbs target the RBS, which when bound blocks HA attachment to the SA on host cell glycans[162]. The affinity of HA to SA is relatively weak, hence virus attachment requires several HA-SA interactions that enhance the binding avidity[169]. Following host cell attachment, the virus enters the cell via endocytosis; acidification of the endosome triggers the necessary confirmational changes in HA that lead to the exposure of the hydrophobic fusion peptide, that then inserts itself into the cell membrane, resulting in the fusion of the endosome and viral membranes[170].

NA exists as a tetramer, and is understood to play an antagonistic role to that of HA, mediating the release of progeny virions that have budded from the host cell by cleaving off the terminal SAs of cell surface glycans that have associated with virion HA and are tethering the virus to the host cell[171]. Moreover, NA has been suggested to assist in viral infection by removing decoy receptors on the surface of host cells at the mucus-rich epithelial surface, where influenza initially infects[171]. The matrix 2 (M2) is the final surface protein, that functions as a proton channel that allows the influx of protons, hence acidification, of the viral endosome during the viral cell entry process[172].

The ribonucleoprotein complexes (vRNPs) within the virus consist of the nucleoprotein (NP) which aids in the packing of RNA (among other functions), the RNA

polymerase (PA, PB1 and PB2) and associated viral RNA; the drop of viral endosome pH during influenza virus entry triggers the detachment of vRNPs from matrix 1 (M1) protein that coats the inside of the virion, facilitating the release of them into the host cell[170].

Influenza viruses also encode the non-structural proteins NS1, PB1-F2 and PA-X, that are not incorporated into viral progeny, but are involved in the regulation of virus replication, transcription and also have immunomodulatory functions[173].

1.3.3 Influenza virus ecology and pandemic potential

Unlike IBV, which is typically restricted to humans and pinnipeds, IAV can infect many different non-human species, including pigs, horses, wild birds, domesticated poultry, pinnipeds and mink[164]. Wild aquatic birds are considered the main natural, stable reservoir of IAV (enzootic), incubating a variety of subtypes of the virus; significant co-infection and genetic reassortment takes place in this reservoir[164,174]. Other animals play different roles regarding the distribution and prevalence of different types of IAV. Domestic poultry for instance, may be infected with IAV via contact with wild aquatic birds, which can lead to epidemics within their species, and they can also serve as an intermediate host for the transmission of virus to humans due to the high level of contact between the two species. Pigs are an especially important intermediate reservoir as they are susceptible to co-infection with different IAV subtypes from birds and human strains[164]. This can lead to the emergence of reassorted, novel strains that could have pandemic potential via a zoonotic spill over event[164]. The lack of immunity to the potential emergent, reassorted viruses in the human population can result in a pandemic, rather than epidemic-type event. A notable spill over event was the 2009 H1N1 “swine flu” pandemic, where a reassorted strain featuring swine, human and avian segments emerged into the human population,

causing an estimated 123,000-203,000 deaths[158,175]. Other notable pandemics that arose as a result of reassortments include the 1918 H1N1 pandemic, with an estimated >50 million associated fatalities[176], the 1957 H2N2 pandemic with an estimated 1.1 million deaths[177], and the 1968 H3N2 pandemic, with an estimated 1 million deaths[158,164,178].

Highly pathogenic avian influenza viruses (HPAI), such as human-adapted H5N1, are a particular ongoing concern; H5N1 has infected an estimated 889 humans between the years 2003 and 2024, resulting in 463 deaths, hence the case fatality rate (CFR) is very high[179]. HPAI is commonly transmitted from wild birds to poultry where it can lead to deadly outbreaks (the "high pathogenicity" in the acronym HPAI is in reference to the outcome of infection in birds, not humans), and can occasionally spill into humans. Although HPAI does not tend to transmit effectively from human to human, humans infected with HPAI often succumb to severe disease. Other HPAI subtypes have circulated in poultry and infected humans, causing severe disease, including H7N9, which had originally emerged in the human population in 2013 as a low-pathogenic avian influenza virus (LPAIV), and has subsequently caused five waves of human infection[180]. H7N9 epidemics resulted in 616 deaths and 1,568 humans cases as of February 2024[180,181]. A list of HAIVs with associated human cases that have caused deaths as reported by the WHO are present in Table 1.7[182,183].

Table 1.7: List of reported AIVs with associated human cases and deaths

AIV	Reporting start date	Last case reported	Reported human cases	Reported human deaths	Case fatality rate (%)
H3N8	?	22.02.23	3	1	33
H5N1	01.01.03	11.08.24	889	463	52
H5N6	01.01.03	17.06.24	258	141	55
H7N7	01.05.03	2003	89	1	1
H7N9	01.12.15	2019	1568	616	39
H9N2	01.12.15	12.08.24	103	2	2

1.3.4 Influenza virus pathogenesis and host immune responses

The disease and symptoms elicited following influenza infection are influenced by several host and virus factors. In the majority of individuals, an infection with seasonal IAV will cause mild disease as a result of URTI; associated symptoms include rhinorrhoea, cough, sore throat, fever, headache, muscle aches and general malaise. Through histological analysis, typical, mild seasonal influenza infection was shown to result in the necrosis of the epithelial cells within the URT, and as well as infiltration of lymphocytes and APCs into the lamina propria[168]. The previous influenza infection history of the individual, age and underlying health issues will also influence the outcome of infection. For example, younger individuals were more likely to develop more severe disease following infection with the 2009 H1N1 swine flu than those born before 1950, because the latter individuals possessed cross-reactive NAbs to HA that they had developed from infection earlier in life with similar strains[168,184]. In contrast to seasonal influenza, pandemic and HPAIV strains of influenza virus can cause severe LRT disease and can be lethal[168]. Secondary bacterial co-infections are strongly associated with influenza mortality (i.e., co-pathogenesis), and can often occur following infection with pandemic influenza infection or HPAIV infection; the virus-compromised epithelial barriers encourage secondary bacterial infection[185].

Certain mutations of pandemic and HPAI strains are associated with their increased pathogenicity[186]. The increased pathogenicity of HPAIV has been linked to the preferential recognition of α2-3 sialylated glycans (by HA), as opposed to α2-6 sialylated glycans, which are located abundantly on type 2 pneumocytes situated deeper in the human lung alveoli, as well as on club cells located in the bronchioles, and alveolar macrophages (both of which have a mixture of α2-3 and α2-6 sialylated glycans); this results in an altered viral tropism

to the LRT and is associated with severe pneumonia[186]. Post-mortem analyses of HPAIV H5N1-infected individuals have reported the collection of alveolar fluid, that contains leukocytes, in the lumen, as well as necrotic alveolar epithelial cells[168,187]. The 2009 H1N1 swine flu virus had dual specificity to both α2-3 and α2-6 sialylated glycans, and was able to infect the URT and LRT[187]. Interestingly, H7-type HPAIV have shown a tropism to the conjunctiva as well[168,187]. Other factors related to the HA gene of more pathogenic strains of influenza include the presence of a multi-basic cleavage site for the cleavage of HA into H1 and H2 subunits, and mutations in the replication genes that lead to the enhancement of viral replication efficiency[186]. PB1-F2 and NS1 proteins are known virulence factors with functions that have shown to be enhanced through certain mutations[186].

1.3.5 Current vaccine strategies against influenza virus

Vaccination has been the main preventative measure against influenza virus infection for many decades; nevertheless, influenza virus still inflicts a major health burden annually, highlighting the need for improved vaccination strategies. Currently a range of vaccines are used against seasonal influenza, including inactivated influenza vaccines (IIV), LAIVs and recombinant vaccines, with varied efficacy in different age groups (as well as pregnant individuals) as demonstrated through several trials[188]. In more recent years, quadrivalent versions of the vaccines have been used such that the four main co-circulating influenza viruses could be covered: IAV H1N1 and H3N2 subtypes, as well as two IBV strains B/Yamagata and B/Victoria[188]. It is hypothesised that the B/Yamagata lineage has become extinct (onset following the COVID-19 pandemic), hence its omission from the 2024-2025 seasonal vaccine formulation will be implemented[188–191].

Several technologies are used to produce the aforementioned influenza vaccines; the traditional method for IIV production involves growing the virus in fertilised chicken eggs or cell cultures, purifying the virus and then inactivating it[188]. IIV can be chemically or physically inactivated to produce inactivated whole virion, or the viral envelop can be disrupted with surfactant to produce "split-virion"; the split-virion preparation can be further purified to only contain the HA and NA antigens, making a "subunit" vaccine[188]. The sole licensed recombinant vaccine (Flublock) is produced by expressing HA in insect cells (by transfecting cells with a baculovirus containing the selected HA gene) and purifying the antigen[188,192]. These vaccines are administered via intramuscular injection. The live-attenuated influenza vaccine (LAIV), FluMist, is produced by incubating the virus in embryonated eggs at 25°C to create a cold-adapted strain, which is then harvested and purified; the virus is then administered intranasally and will only weakly infect individuals, with infection restricted to the URT[157].

The main aim of these vaccines is to induce antibodies against the HA and NA surface glycoproteins, which are strain-specific. It is standard practise to use a hemagglutination inhibition assay (HAI) to assess the ability of vaccine to induce HA-binding NAbs[193,194]. Due to the constant drifting of seasonal influenza virus and subsequent evasion of pre-existing immunity, updates to the composition of the vaccines need to be made each season, which are based off of recommendations by the WHO; strain predictions are conducted by the WHO Global Influenza Surveillance and Response System ahead of the influenza season[188]. Unfortunately, this process is costly and is not always effective as mismatch of the predicted strain and actual circulating strain frequently occurs; the efficacy of these vaccines is highly contingent on the matching of predicted strain to actual strain[195]. For instance, the vaccine effectiveness of influenza vaccines has varied

widely season to season in the past 10 years from 10% to 60%[196]. These seasonally updated vaccines are also not designed to cover potential pandemic strains.

A plethora of next generation universal influenza vaccines (UIV) that aim to broadly protect against different influenza A and B subtypes (hetero(sub)typic protection), as well as accommodate the seasonal drift of subtypes, are currently being trialled at preclinical and clinical stage as alternatives to the current seasonal prediction-based vaccines[196–199]. Many of these vaccines deviate from the HAI-based strategies that generate effective, but narrow protection. Some of these vaccines also target other respiratory viruses, such as SARS-CoV-2[197]. One approach focusses on conserved antigens, e.g., nucleoprotein (NP) and matrix 1 (M1), with the aim of inducing memory $CD8^+$ T cell populations that are broadly reactive to different influenza subtypes[200,201]. By facilitating rapid clearance of virus within the URT, NP- and M1-specific T cells are thought to limit virus infection and lessen disease severity[201,202]. Other approaches have included a regimen that refocuses the antibody response to the less immunogenic, yet more conserved stalk domain of HA, such that broader NAb responses be induced that can bind group 1, group 2 and IBV HAs[203]. This strategy was tested in a phase I trial where differently constructed chimeric HAs (cHAs) were used that consisted of either a group 1 or 2 HA, that was combined with a different avian HA head domain; by sequentially exposing the immune system to the different cHAs with the same stalk domain and different HA head domains, the NAb response to the stalk was boosted[203].

2. The immune system and immunity to viruses

The immune system serves to protect an organism against foreign infectious pathogens. The immune system comprises of specialised cells, tissues and organs that

concertedly recognise foreign pathogen (and distinguish foreign antigen from self) and prevent and limit pathogen infection and potential disease.

2.1 The adaptive immune system

The adaptive immune system is an arm of the vertebrate immune system that allows for the formation of highly specific and long-lasting (memory) protection against pathogen infection and subsequent disease[204]. Upon encounter of virus or virus protein, the adaptive immune system generates and sustains a form of immunity that is able to specifically detect the foreign virus, and subsequently intercept the viral life cycle, through multiple mechanisms leading to viral clearance. When pathogen is encountered that the immune system has already mounted adapted immunity towards, it is able to mount a more rapid, yet specific, secondary immune response because of immune memory. The adaptive immune system is comprised of two main types of lymphocytes, B cells (generated in the bone marrow) and T cells (generated in the thymus); either lymphocyte type is capable of detecting foreign viral protein.

The main role of B cells is in generating antigen-specific antibodies. Antibodies can have multiple anti-viral functions once bound to virus antigen, including the neutralisation of virus, i.e., blocking of virus entry into host cell or the tagging of pathogen for destruction via phagocytosis by innate cells. B cells are able to recognise pathogens in a highly specific manner through the B cell receptor (BCR), an immunoglobulin that is expressed on the B cell surface[205]. During the maturation of B cells, somatic recombination of the gene segments encoding the BCR results in diverse assortment of B cells with unique variable antigen-binding BCR regions[206]. Once a BCR binds to foreign antigen either in a soluble state

or presented by APC[207], the antigen is internalised, processed, and presented on the cell surface in peptide form, bound to an MHC II molecule[205].

The T cell maturation process also involves somatic recombination events that result in a T cell population with a diverse repertoire of T cell receptors (TCR). Naïve $CD4^+$ T helper (Th) cells are primed in secondary lymphoid organs (SLO) in the T cell zone by antigen-presenting cells (APC) via specific interaction of their TCR and cognate peptide-MCH II complex[208]. Naïve $CD4^+$ T cells may differentiate into many different subsets, with this differentiation governed by many factors, including the surrounding cytokine environment[209]. The Th1 and Th2 cell subsets, which primarily secrete TNF and IFNγ, or IL-4, respectively, are associated with different types of immune response[210]. Whilst Th1 cells have been associated with macrophage activation, inflammation and cell-mediated responses to intracellular pathogens, Th2 cells have been associated with eosinophil recruitment and the promotion of humoral responses to extracellular pathogens such as helminths[210].

Once a $CD4^+$ T cell TCR with a CD4 receptor encounters the correct, cognate MHC II-peptide complex presented on an antigen-activated B cell that has entered the T cell zone of the SLO, and the respective T cell CD40 ligand and B cell CD40 surface proteins bind, cytokine signals are released from the activated T cell which eventually lead to the proliferation of the B cell[205]. These activated B cells follow two main differentiation pathways, either differentiating into extrafollicular short-lived antibody-secreting plasma cells (SLPC) (the immediate lower affinity antibody response) or long-lived memory B cells (MBC), or they proceed to seed the germinal centre (GC) reaction by rapidly dividing[207]. Plasmablasts (PB) are an intermediate, short-lived antibody-producing cell type that may differentiate into longer-lived PCs[211].

GCs develop within the B cell follicles of SLOs, where they support the generation of high affinity antibodies through a process termed affinity maturation[212]. GCs have an ordered structure: a "dark zone (DZ)" that features concentrated populations of proliferating B cells which cycle to the "light zone (LZ)" where they encounter follicular dendritic cells (FDC), which serve to present whole antigen, and a specialised T_h subset, termed follicular T helper cells (T_{FH})[212].

Within the GC DZ, GC B cells undergo extensive rates of somatic hypermutation (SHM) of the variable regions of their immunoglobulin genes; this results in a concentration of diverse B cell clones[212]. SHM results in the downregulation of DZ-retention receptor CXCR4 (which binds to CXCL12 on DZ stromal cells) and the upregulation of CXCR5, which responds to CXCL13 which is abundantly expressed within the LZ; this facilitates the migration of DZ GC B cells to the LZ[213]. Upon entering the LZ, B cell clones "compete" to bind to limited whole antigen presented by FDC; the higher the affinity of the BCR expressed on the GC B cell clone, the more likely it is able to outcompete and internalise whole antigen. B cell clones that have successfully processed antigen and have presented their MHC II-peptide complexes then additionally compete with each other to bind to a limited population of TCR-expressing cognate T_{FH}. Successful engagement of T_{FH} results in the expression of survival signals by T_{FH} which support the subsequent proliferation of high affinity B cell clones[212]. Outcompeted B cell clones that have failed to capture FDC-presented antigen, or engage T_{FH}, primarily undergo apoptosis (and are subsequently cleared by macrophages) or re-enter the DZ where they undergo further rounds of SHM (and cycle back to the LZ)[214]. Selected B cell clones of high affinity either exit the B cell follicle as long-lived antibody-secreting plasma cells (LLPC), some of which then situate in

the bone marrow, and other non-PC that exist as circulatory MBC that will rapidly differentiate into PC upon antigen reencounter[207].

Class-switch recombination (CSR) typically occurs early on during both the non-GC and GC differentiation pathways and results in the expression of antibodies by B cells of particular isotypes that have distinct functional properties. CSR involves the permanent genetic rearrangement of the constant Ig heavy chain of IgM-expressing B cells, resulting in the expression of IgG, IgA or IgE Ig isotypes; such isotypes have different structures, functions, and distributions, and can be associated with different types of immune responses (importantly, CSR does not change the variable region)[215]. The type of CSR is influenced by T helper cell subtype (as described earlier) in the T cell-dependent CSR pathway[216]; during the engagement of T_H and B cell (necessary for B cell activation), engaged T cell subtypes will express and release particular cytokines which influence the switching of B cells into particular isotypes and IgG subclasses. IgG and IgA are isotypes of particular focus in this thesis; IgG is the most prevalent antibody isotype in the blood and can be divided into subclasses that have different effector functions (mediated via their Fc region which can bind to Fc receptors (FcRs) present on innate cells) and properties; IFNγ release by Th1 cells is associated with differentiation to the IgG2a subclass (in mice), IL-4 release by Th2 cells is associated with differentiation into the IgG1 subclass (in mice), and TGF-β release is associated with class-switching to IgA, a key mucosal isotype which will be touched on later in this chapter[216].

$CD8^+$ T cells are an effector T cell that also play an important role in eliminating virus by targeting cells infected with virus and triggering their programmed cell death[217]. $CD8^+$ T cell TCRs recognise MHC I molecules that present peptide from cytosolic viral protein. Upon binding of the TCR and $CD8^+$ receptor with a cognate MHC I-peptide complex presented on

the infected cell surface, $CD8^+$ cells release granules containing perforin and granzymes; perforin facilitates the formation of pores on the target cell that allow granzyme to enter and trigger apoptosis of the cell[217]. $CD8^+$ T cells can be initially primed via cross-presentation of MHC I-peptide complex by APCs. After infections, the activated $CD8^+$ T cell population contracts in number, however a subset of memory $CD8^+$ T cells remain that can be reactivated upon reinfection to facilitate a more rapid secondary immune response. Different memory $CD8^+$ T cells exist: central memory $CD8^+$ T cells (T_{CM}) circulate between the SLO and circulatory system, and effector memory $CD8^+$ T cells (T_{EM}) circulate between the circulatory system and periphery. Additionally, tissue-resident $CD8^+$ T cells (T_{RM}) exist that remain fixed at the effector sites of initial infection in the periphery that will activate and proliferate rapidly upon viral insult.

2.2 The mucosal immune system in the nasal mucosa and the respiratory tract

The nasal mucosa and respiratory tract are in constant exposure with the external environment, hence have adapted immunological features that are functionally distinct from the wider systemic immune system; they are especially adapted for protection against airborne viruses that are inhaled and infect the mucosal surfaces. The respiratory mucosa, a barrier that lines the airways with ciliated epithelial cells and goblet cell-produced mucus, can be divided into two main regions: the URT, which contains the nasal cavities, mouth, pharynx and larynx, and the LRT, which contains the trachea, bronchi, bronchioles and alveoli within the lung[218].

The different areas of the respiratory mucosa possess certain shared characteristics. Dendritic cells (DC), a type of APC, continuously monitor and sample (immunosurveillance) for the presence of virus within the mucosal lumen via their

dendrites, and microfold (M) cells also transcellularly present antigen to the basal membrane for APC uptake[219]. Upon encountering virus antigen, presenting cells process the antigen and traffic to the proximal draining lymph nodes (LN) where they present the antigen via MHC II molecules to $CD4^+$ T cells, and cross-present antigen to $CD8^+$ T cells via MHC I molecules[218,219]. These local inductive lymphoid sites facilitate the germinal centre (GC) reaction and the generation of high-affinity antibody.

The mucus lining of the respiratory lumen which airborne viruses first come into contact with contains various immune components, such as secretory virus-neutralising antibodies (NAbs), proteases and peptides such as defensins[220,221]. The antigen-experienced respiratory mucosa also contains tissue-resident memory $CD8^+$ T cells capable of clearing virus-infected cells. Tissue-resident memory B cells (B_{RM}) also exist at mucosa effector sites and can respond to potential secondary virus insult by facilitating a rapid local antibody response[222]. The presence of these localised lymphocytes and antibodies enables much faster response to secondary viral insult; the time interval between virus entry and adaptive immune response is critical and can dictate the level of control of the spread of infection.

2.2.1 The nasal mucosa and upper respiratory tract

An important feature of the nasal mucosa is the nasal-associated lymphoid tissue (NALT), which serves as the primary inductive site of the URT in mice. In mice, the NALT consists of bilateral non-encapsulated lymphoid tissue that lies under the epithelium, posterior to the cartilaginous soft palate[219,223]. The Waldeyer's ring consisting of the tonsils and adenoids has been interpreted as the human equivalent of murine NALT[223]. The NALT is an organised tissue sharing the common features of SLOs, that is high endothelial venules

(HEV) that allow naïve B and T cell recirculation, a follicle associated epithelium (FAE) and T and B cell zones[219]. Activated T and B cells within these sites can drain to the cervical lymph nodes (CLN) which are most proximal to the nasal mucosa, enter the blood stream and subsequently home to mucosal effector sites such as the nasal lamina propria or prompt a wider systemic response[219]. The NALT serves to initiate the secretory IgA response in the mucosa, with IgA being the principal antibody isotype of the URT[219]. Immunity in the URT is critical for the prevention of spread of virus to the LRT (and potentially wider organism), which can lead to more severe disease such as pneumonia[194].

2.2.2 The lower respiratory tract

The bronchus-associated lymphoid tissue (BALT) serves as the main inductive site of the larger, central airways of the lungs (trachea, bronchi and bronchioles) in humans and mice. Unlike NALT, which is constitutive, BALT is normally only induced following pathogen exposure in healthy adult mice and humans (hence it is sometimes referred to as iBALT and defined as a tertiary lymphoid structure), but it is present in early human childhood for a short period before it begins to wane with age[224,225]. Additionally, parabronchial, hilar and paratracheal draining LNs (lung-associated LNs) are present in the lungs that associate with vessels and bronchi, draining the LRT and lung parenchyma[219]. As with the NALT, the BALT consists of organised concentrations of lymphocytes in follicular structures, as well as stromal cells and APCs, and HEV and lymph ducts that enable the circulation and draining of activated B and T cells to local effector sites at the lamina propria[219,224]. The function of the BALT and lung-associated LNs is to establish a localised adaptive response to pathogen. Much like NALT, secretory IgA can be found on the mucosal surfaces of the LRT, however,

in contrast to the URT compartment, the IgG isotype is the major Ig isotype here (that is primarily derived from the circulation).

2.2.3 Tissue-resident memory T cells and B cells in the respiratory mucosa

Lung and nasal tissue-resident memory T cells (T_{RM}) are particularly important T cell subtypes for protection against respiratory viral infection[226]. T_{RM} remain lodged in peripheral non-lymphoid effector sites without recirculating, unlike other memory T cell subsets that only transiently act in effector sites, and they are poised to reactivate at the sites of possible virus reinfection as the primary responders[227]. T_{RM} possess a defined cell phenotype and transcriptional profile[228]. CD103 expression has been especially associated with T_{RM}, hence it is a widely accepted marker when defining the cells[227]. CD103 is a subunit (α_E) of the $\alpha_E\beta_7$ integrin expressed on the T_{RM} cell surface that aids in T_{RM} retention at peripheral sites, by associating with E-cadherin expressed on epithelial cells[228,229]. TGF-β signalling has been shown to stimulate CD103 upregulation on T_{RM} cells, and along with local antigen recognition, is necessary for optimal lung T_{RM} differentiation[230]. In addition, T_{RM} constitutively express the retention and activation marker CD69, and lack expression of the LN homing marker CD62L[228,231]. Various studies have supported the existence of T_{RM}; the linking of the circulatory systems of a previously infected and uninfected mouse (parabiosis), for example, has been used to prove that the T_{RM} population derived from infection remains lodged in the tissue of the infected mouse and does not migrate into the uninfected, conjoined mouse[228]. It has become commonplace when measuring T_{RM} via flow cytometry to intravenously (IV) inject a pan-lymphocyte antibody-fluorochrome conjugate into mice prior to tissue processing, such that all circulatory lymphocytes are labelled and

excluded from the resident memory population (that can be positively stained for using CD103 and CD69 markers)[228,232,233].

Once activated, $CD8^+$ T_{RM}, especially the airway subset, can release proinflammatory cytokines such as IFNγ into the local vicinity to recruit innate cells for the execution of a local immune response[234]. In addition, the activation of $CD8^+$ T_{RM} has been suggested to increase vascular permeability in nonlymphoid tissues, enabling the influx of circulatory blood IgG into the peripheral site[235]. Interstitial $CD8^+$ T_{RM}, unlike airway $CD8^+$ T_{RM}, can be cytolytic; the interstitial $CD8^+$ T_{RM} also serve to replenish the declining airway $CD8^+$ T_{RM} pool[236]. $CD4^+$ T_{RM} have been shown to play a role in activating $CD8^+$ T_{RM}, as well as supporting local B cell activation and antibody responses at the site of infection[236]. The durability of $CD4^+$ and $CD8^+$ lung T_{RM} is unclear, as there are certain human and mouse studies that have reported a rapid decline in the measured populations in the months following infection, and others that have supported that they are maintained for months to years[228,230,237–241]. In one study, it was noted that antigen stimulation was necessarily to maintain lung $CD8^+$ T_{RM}; the waning of lung T_{RM} could be an evolutionary means of counteracting potential over-activation and inflammation within the lungs[236]. In contrast to lung T_{RM}, murine nasal T_{RM} are reportedly more persistent over time, and less reliant on local antigen recognition[230].

Lung-resident B cells (B_{RM}) have also been identified as a specialised subset of resident memory lymphocyte. Like T_{RM}, B_{RM} have been distinguished from ordinary systemic B_{EM} phenotypically, with lung B_{RM} expressing CXCR3 (which can also be expressed on $CD4^+$ T_{RM}) and lacking expression of CD62L (similarly to $CD8^+$ and $CD4^+$ T_{RM}), and have been confirmed as non-circulatory via parabiosis[231,242]. B_{RM} have especially been studied following influenza infection, where they are understood to act as a local source of

plasmablasts (via differentiation) in the lungs, poised to differentiate and act rapidly upon potential antigen re-encounter[242].

2.2.4 IgA in the respiratory mucosa

IgA is the main Ig isotype found in the upper respiratory mucosa[219]. The B cell class switching to IgA is promoted by the expression of TGF-β and IL-10 by mucosal T cells and epithelial cells[243]. In humans, IgA can be found in both a dimeric, secreted form (sIgA) within the mucosa, produced at the lamina propria, or a circulatory, monomeric form present in the blood[243]. Mouse IgA, however, only exists in a dimeric form in both the blood and mucosa. The dimers of IgA produced by the lamina propria-situated B cells are linked together by a J chain, and transmitted across the epithelial barrier by the polymeric immunoglobulin receptor (pIgR); cleavage of the dimers by proteases on the apical surface of the epithelia facilitates IgA release into the lumen[243]. IgA is capable of binding virus located in the airways and blocking it before it infects cells (neutralisation), as well as neutralise virus within infected epithelial cells (as the IgA is transported across the cell), and also to facilitate the removal of excess antigen in the lumen by binding and transporting antigen across the epithelium[243].

There are other differences to the mouse and human IgA isotypes. Human IgA has two subclasses (IgA1 and IgA2), and is able to bind FcαRI, whereas mouse IgA only exists in one form, and does not bind to FcαRI. Whereas IgA (and to a lesser extent IgG) can be produced "in situ" at inductive mucosal sites and deposited at epithelial barriers, IgG from the circulation can also be transported to the luminal epithelial side (transcytosis) via the neonatal Fc receptor (FcRn) and possibly transudation (e.g., encouraged via $CD8^+$ T_{RM} activation)[219,244]. Dimeric IgA produced systemically may also enter the mucosa via

transcytosis in mice, however, this is much less common in humans, where the IgA produced in mucosal and systemic compartments tends to remain in the respective compartment[245].

A summary illustration of the mucosal immune response is featured in Figure 1.5.

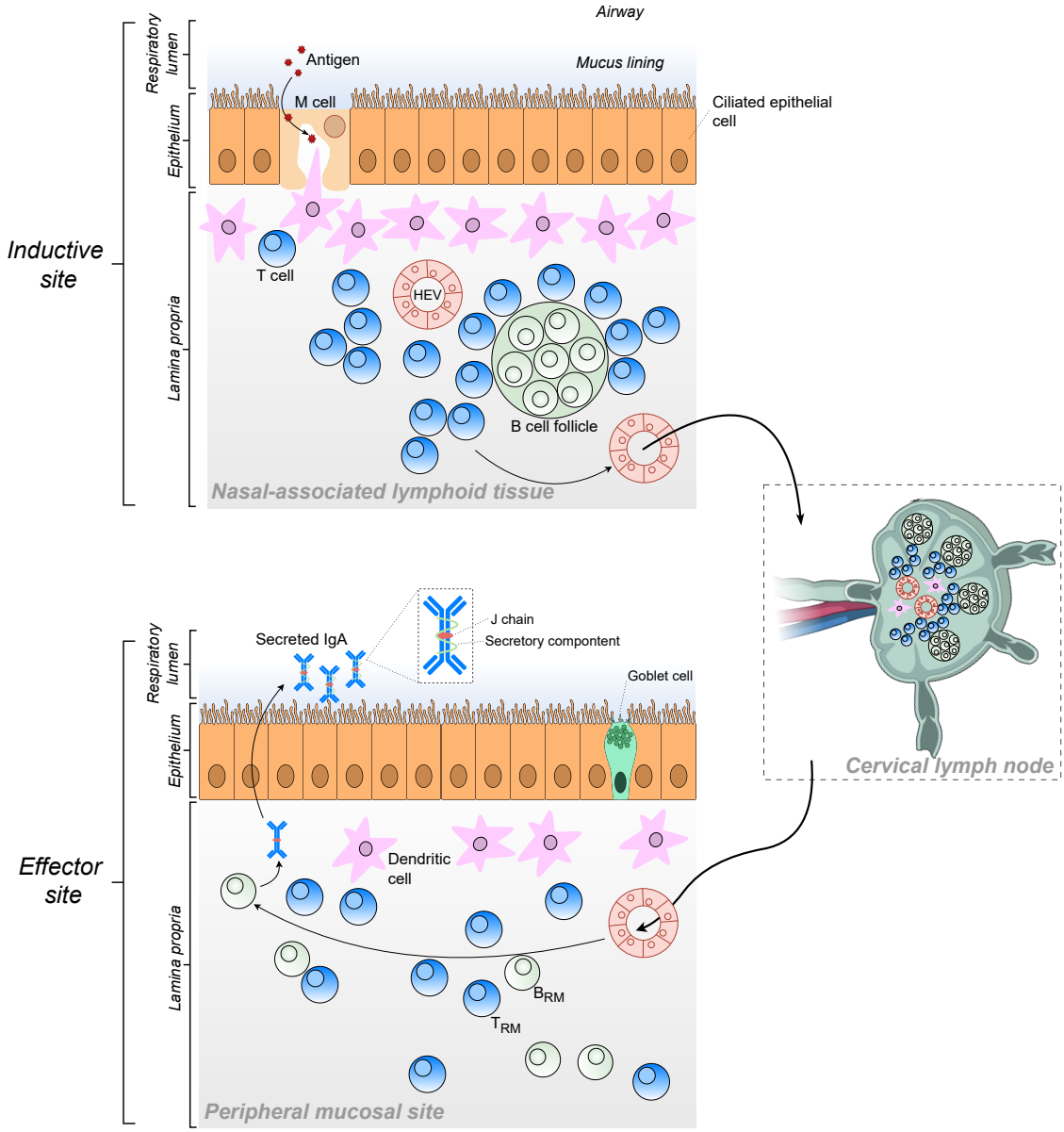

Figure 1.5: Immune response to antigen in the nasal mucosa

Diagram created independently using Principles of Mucosal Immunology, Second Edition (2020) as a reference

2.3 Immunological imprinting

Immunological imprinting is a phenomenon in which pre-existing immunity influences the latter immune response to an antigen/virus that has some level of homology to the antigen/virus that provoked the formation of the pre-existing immunity. Specifically, the concept of immunological imprinting is contingent on the fundamental ability of the adaptive immune system to establish immune memory, or in this case, an "imprint", that will be responsive to heterologous insult. This imprint must be cross-reactive in order to be influential to the latter responses to heterologous antigen/virus[246]. Hence, immunological imprinting is relevant in instances where a virus shares some level of homology to other viruses or rather, variants. Importantly, immunological imprinting should be distinguished from other phenomena such as "immune amnesia" or "immune exhaustion", where prior infection with an unrelated virus negatively influences the immune response to a completely different virus with no shared homology, as has been reported with measles infections[247]. Under the collective term of imprinting are various terms that relate to specific phenomena, models and/or measurements that may not be mutually exclusive. Importantly, in this thesis the use of adjectives such as "negative" or "detrimental" to describe the type of imprinting refer to the effect of imprinting in lowering or completely suppressing the magnitude of, or reducing the quality of, an immune response (suboptimal), in contrast to an otherwise optimal immune response. As there are various terms used in this thesis related to imprinting, a glossary of immunological imprinting terms has been created for clarity (Table 1.8), with certain mechanisms and models also illustrated in Figure 1.6.

Because immunological imprinting relies on the cross-reactivity of immune response, the degree of imprinting is a function of the antigenic distance between two

antigens[248]; that is, the more distant two antigens/viruses are from each other in identity, the less likely an immunological imprint is going to influence the latter responses to the distant, but related, antigen. Following this relationship, as modelled by Schiepers *et al*, two identical antigens of zero antigenic distance display the greatest relative level of imprinting, with increasing distance weakening the occurrence of imprinting[248].

Immunological imprinting has important implications for public health, having been observed in the context of various different viruses, including most famously influenza virus, as well as Dengue virus, and now with SARS-CoV-2[68,69,71,72,249–259]. Furthering the understanding of immunological imprinting will contribute to the optimisation of current vaccine strategy. Additionally, it is important to note that the impact immunological imprinting will have on a vaccination, disease, or infection outcome will be contingent on the specific correlates of protection for the particular pathogen of interest; as immunological imprinting is largely a B cell and antibody-related phenomenon, it's presence may not have important implications for a virus primarily protected against via T cell immunity.

Table 1.8: Glossary of immunological imprinting terms

Term	Category	Definition
Immunological imprinting; *Also referred to as **immune imprinting, antigenic imprinting***	Collective term	In this thesis, immunological imprinting is used as a broad term that encompasses the following models, phenomena and/or measurements, that are not necessarily mutually exclusive. Broadly defined, immunological imprinting is the influence of pre-existing immunity on latter responses to a heterologous antigen that possesses some level of homology to the antigen of previous exposure (in which immunity was initially developed towards).
Primary addiction; *Also referred to as **original antigenic sin (OAS), negative interference, immune interference***	Model	A model of immunological imprinting in which a pre-existing (primary) immune response prevents the formation of a de novo response to heterologous antigen, with immunity 'locked' to a primary cohort of memory B cells.
Antigenic Seniority; *Also referred to as **sequential contribution***	Model	A bias in the magnitude of immune responses to different, sequentially exposed antigens based off of the order in which they were introduced to the immune system, in a 'hierarchal' manner. Antigenic seniority is in part dependent on the frequency of restimulations or 'boosts' (via heterologous antigen exposure) a particular response has had.
Back boosting	Phenomenon; measurement	The restimulation or recall of pre-existing immune responses upon exposure to heterologous antigen.
Antigenic blunting; *Also referred to as **antigenic masking***	Phenomenon; mechanism	The 'shielding' of antigen by bound antibodies, to the detriment of potential B cell recognition (via BCR binding). Antigenic blunting lessens the immunogenicity of antigen by reducing its availability to naïve or MBC, consequently blocking B cell activation.
Antigenic clearance	Phenomenon; mechanism	The removal of antigen that is presented via vaccination or infection by innate immune cells. Clearance can be mediated in an antibody-dependent manner, whereby antibody binds to the antigen and engages innate cells via Fc-FcR interactions.

A

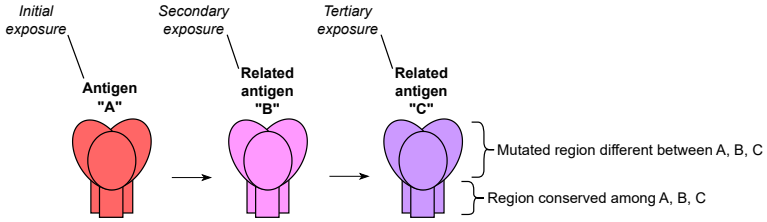
Initial exposure
Secondary exposure
Tertiary exposure
Antigen "A"
Related antigen "B"
Related antigen "C"
Mutated region different between A, B, C
Region conserved among A, B, C

B

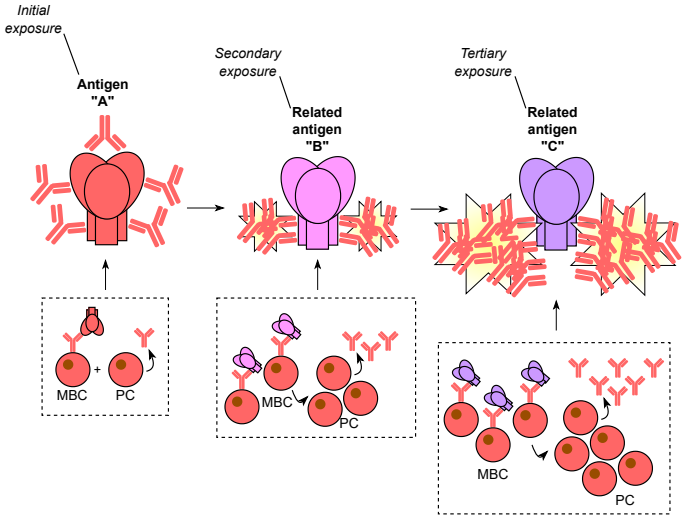
Initial exposure
Secondary exposure
Tertiary exposure
Antigen "A"
Related antigen "B"
Related antigen "C"
MBC
PC
MBC
PC
MBC
PC

C

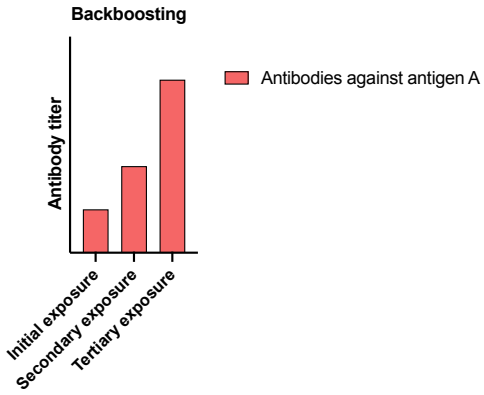
Backboosting
Antibody titer
Antibodies against antigen A
Initial exposure
Secondary exposure
Tertiary exposure

D

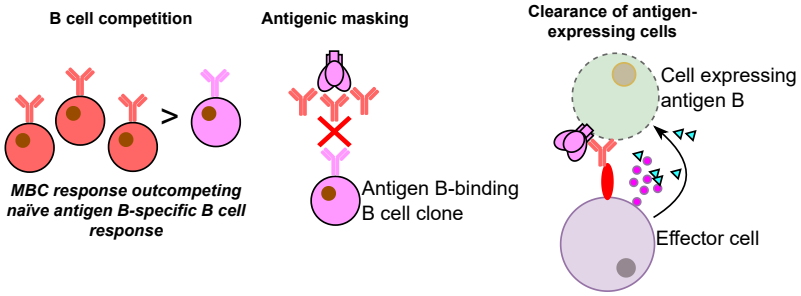
B cell competition
MBC response outcompeting naïve antigen B-specific B cell response
Antigenic masking
Antigen B-binding B cell clone
Clearance of antigen-expressing cells
Cell expressing antigen B
Effector cell

E

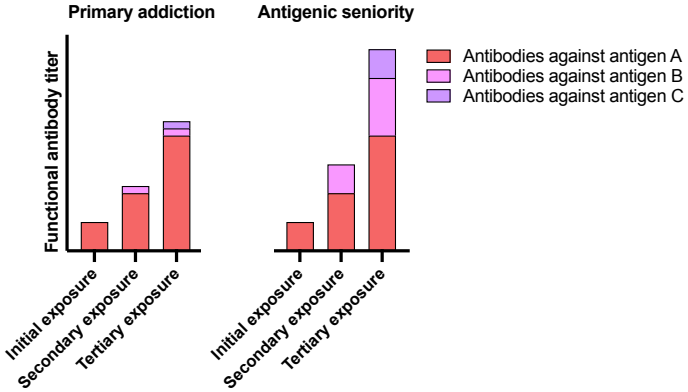
Primary addiction
Antigenic seniority
Functional antibody titer
Antibodies against antigen A
Antibodies against antigen B
Antibodies against antigen C
Initial exposure
Secondary exposure
Tertiary exposure
Initial exposure
Secondary exposure
Tertiary exposure

Figure 1.6: Back boosting and mechanisms and models of immunological imprinting

(A) Sequential exposure of an immune system to three different, but related antigens (A, B and C). The antigens have a conserved (shared) stalk region and a more mutated head region that differs between each antigenic species. (B) Back boosting of the primary cohort of B cells and subsequent antibodies that were established after initial exposure to the antigen A. Following secondary exposure to antigen B and tertiary exposure to antigen C, these primary cohort memory B cells (MBC) are restimulated and differentiate to plasma cells (PC) that produce antibody. B cell clones (and subsequent antibodies) that bind to the stalk region that is conserved between A, B and C antigens are selected for and preferentially restimulated, resulting in a "boost" of cross-reactive, stalk-binding antibodies. (C) The cumulative increase in antibodies against antigen A following exposure to B and C antigens as a result of back boosting of the initial response to antigen A. (D) Hypothetical mechanisms of the suppression of the de novo immune responses to antigen B as a result of a pre-existing inhibitory immunological imprint formed following initial antigen A exposure. From left to right: B cell competition; primary cohort MBC outcompete naïve B cell clones against antigen B and result in the perpetuation of the pre-existing anti-antigen A antibody response, antigenic masking; pre-existing, cross-reactive anti-antigen A antibodies mask antigen B and prevent its recognition by naïve B cells, preventing their activation, and antigenic clearance; pre-existing, cross-reactive anti-antigen A antibodies bind to antigen B expressed on the surface of cells and engage innate cells via Fc-FcR interactions, resulting in the cell death of the antigen expressing cell and interfering with antigen presentation. The effector cell facilitates cell destruction through the release of granzymes and perforin. (E) Two models of immunological imprinting: primary addiction involves an active suppression of the de novo response by the pre-existing imprint; functional antibody responses against antigen B and C following their exposure are not mounted, however the immune response towards antigen A is boosted (the immune response is "locked" to the primary B cell cohort). Antigenic seniority describes a hierarchy of the magnitude of immune responses towards related antigens dependent on the order of exposure of the immune system to the antigenic species. Following antigen B and C exposure, antigen A antibody responses are boosted, and de novo antibody responses to antigen B and C are mounted as well. However, the overall magnitude of antibody response is biased towards antigen A after antigen B exposure (A>B), and towards antigen A after antigen C exposure, with antigen B antibodies being at intermediate level (A>B>C).

2.3.1 The primary addiction model of immunological imprinting

Immunological imprinting can have both positive or negative outcomes; however, it is often described as a negative occurrence. Immunological imprinting was first described by Thomas Francis Jr, who termed it "original antigenic sin (OAS)", after having observed differences in the immune responses to a particular influenza strain infection between younger and older age groups that had different prior infection histories[260]. OAS is now

often referred to as primary addiction, or negative/immune interference[248,261,262]. Primary addiction can be interpreted as a model of imprinting. Critically, to be considered primary addiction, the latter de novo response to secondary antigen must be suppressed as a result of the pre-existing immune imprint formed from the initial antigen[248,253].

Upon encounter of the secondary antigen, primary addiction involves the re-activation or recall of the pre-existing or "primary" memory B cell (MBC) cohort, and the failure of naïve B cells to be activated and selected for, and thus contribute to a de novo response to the secondary antigen (hence, "addiction")[248]. Consequently, the primary antibody response is re-activated. The pre-existing immune imprint, consisting of matured, high affinity MBC, will mount a far quicker and more intense antibody response (secondary immune response) to the (conserved regions of) secondary antigen than the de novo pathway that naïve B cells will take (primary immune response), in this way, the primary MBC cohort essentially "outcompetes" the naïve B cell cohort[263,264]. This theory is supported by observations that MBC cohorts expand and restimulate the pre-existing antibody response following the encounter of conserved epitopes[263,265]. The dominant re-activated cohort of MBC will perpetuate an antibody response that is poor at neutralising the secondary virus, and the naïve responses that are more fine-tuned to the secondary antigen are simultaneously dampened.

In addition to the more circumstantial mechanism driving primary addiction, are various inhibitory mechanisms that may also contribute to the suppression of de novo responses to secondary antigen: pre-existing antibodies, as well as those produced upon restimulation of the primary MBC cohort, may mask the secondary antigen (as a result of their cross-reactivity). This may result in the blocking of presented antigen to naïve B cells, leading to inhibition of the immune responses to the novel antigen; this process has also

been previously referred to as antigenic blunting in a homologous prime-boost antigen setting[262]. The default or "locking" into the primary B cell cohort leads to the perpetuation of a cross-reactive, yet non-neutralising antibody response to the secondary antigen. The perpetuation of a cross-reactive, non-neutralising (and non-protective) response is possible in the scenario where an immune imprint encounters a drifted or shifted mutant virus that harbours mutations at epitopes that are neutralising when bound by antibody, but also conserved regions that are non-neutralising; the encountered non-neutralising, conserved regions then provoke an antibody response to this region. This scenario can occur for instance, with viruses that undergo evolutionary pressures that increase the "plasticity" of the receptor-binding domains of their surface receptor-binding proteins; other areas of the surface protein such as the stalk may be more conserved between variants, yet lack neutralising epitopes[263].

Additionally, within a vaccination context the pre-existing antibodies and antibodies generated upon a recall response may enhance the clearance of antigen encountered upon vaccination, thus reducing the de novo response to vaccine[266]. In such a scenario, pre-existing cross-reactive antibodies bind to vaccine antigen and facilitate the clearance of antigen-presenting cells via the engagement of FcR-expressing innate cells, such as NK cells[266].

The tendency of an immune response to favour pre-existing antibody responses to the detriment of the generation of novel ones to secondary antigen has been described and modelled in literature[267]. Interestingly, this has been proposed as a possible evolutionary mechanism of the immune system: the presence of antibody derived the primary exposure has an inhibitory influence on the ability of pre-existing MBC to seed secondary germinal centre reactions, thus supporting the participation of naïve B cells in

secondary GCs, in consequence, diversifying the downstream antibody pool[267]. In contrast to the more naïve-like cellular phenotype of secondary GC B cells upon the exposure to related heterologous antigen, at an antibody level, the phenotype of the recall response is described as more recall-like, and facilitated by the action of primary cohort-derived plasma cells that are stimulated upon heterologous boost[267].

2.3.2 The antigenic seniority model of immunological imprinting

Whereas the primary addiction model of immunological imprinting necessitates that the de novo responses to secondary antigen be suppressed, the antigenic seniority model of imprinting does not. In the antigenic seniority model, there is a hierarchal ordering to the levels of response elicited to sequential, related antigens exposed to the immune system. When a related antigen is exposed to the immune system, a pre-existing response is back boosted, but a de novo response is still mounted to the new antigen. However, the resultant overall level of response will be biased to the antigen of primary/earlier exposure. As such, although in the antigenic seniority model the levels of responses between exposed antigens will differ, the ability to mount a quality, neutralising response to the secondary antigen should not be compromised. Henceforth, the antigenic seniority scenario could be interpreted as a “beneficial” immune imprinting outcome.

The immune responses in the antigenic seniority model will not only be influenced by the degree of similarity between two different antigens/viruses (like in the case of the primary addiction model), but also the number of sequential exposures, as the back boosting of antigen results in a cumulative effect, in which the initial antigen exposed to the immune system is sequentially boosted each time a similar antigen/virus is then exposed to the immune system.

2.3.3 Measuring immunological imprinting

There are various approaches to measuring immunological imprinting, however it can be complicated to do so in a real-life context as humans are often exposed to multiple variants of the same virus in their lifetime; the variation in the immune histories within the human population, as well as the complexity and layers to a given human's pre-existing immunity, make ascertaining the involvement of imprinting particularly challenging. Henceforth, simpler, reductionist mouse vaccination models can be valuable for this reason.

Measurement of the impairment of an immune response to a particular antigen or virus by imprinting can be achieved by comparing the immune responses generated after priming naïve mice with the "secondary" antigen and the responses to the "secondary" antigen after it is administered as a booster in pre-exposed ("primary antigen") mice (Figure 1.7). In such an experiment however, the immunological readout should be the quantity of neutralising antibodies, or antibodies specific to the mutated regions of the antigen; otherwise, the potential baseline cross-reactivity elicited by the primary antigen, as well as the effects of back-boosting to the conserved regions that are shared between the antigens, may conflate the results.

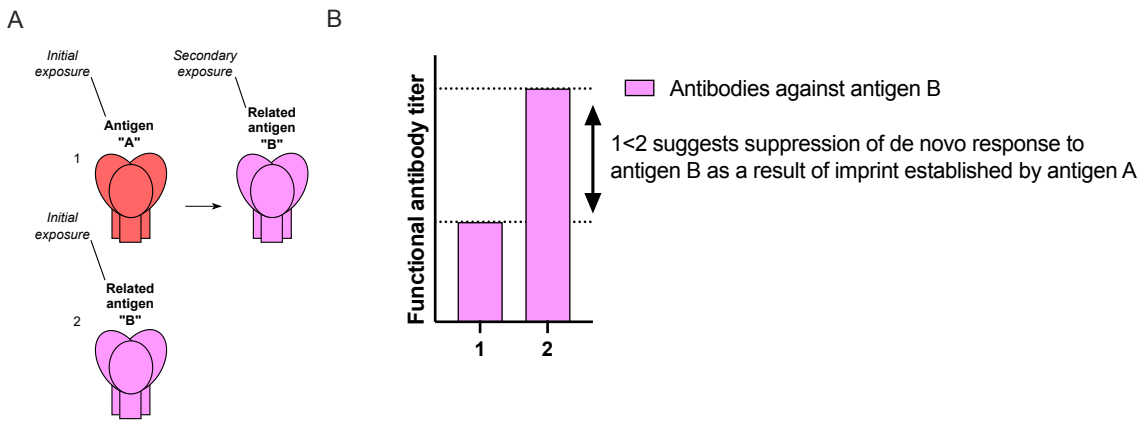

Figure 1.7: Measuring immunological imprinting by comparing a heterologous prime-boost and prime-only regimen

(A) Comparison of a regimen where mice are primed with antigen A, and then boosted with related antigen B (1) and a regimen where mice are solely primed with related antigen B (2). (B) Potential immunological imprinting outcome: the de novo functional antibody response mounted to antigen B is suboptimal when the immune system has been previously exposed to antigen A. This is indicated by the higher anti-antigen B response in the prime-only group (2) where an optimal response is measured, compared with the antigen A-prime, antigen B-boost group, where a lower response is measured.

The aforementioned scenario would not directly measure whether antibodies were derived from a de novo, or back boosted response, which would be imperative in a primary addiction-type scenario. More advanced approaches have been developed with the use of transgenic mice, where antibodies can be tagged in an inducible manner ("molecular fate-mapping"), thus allowing the direct dissection of antibody populations by ascribing them to their origin, i.e., the B cell cohort they are derived from (i.e., pre-existing response vs. de novo)[248]. In addition, cell lineage tracing mouse systems exist that can enable the labelling of B cells at specific timepoints, such as just after antigen exposure[268,269].

Indeed, by linking an antibody to the specific, punctate response it was generated from (i.e., the antigen that the immune system was exposed to), a more accurate measurement of back boosting is made, as the measurement of an increase in antibodies reactive to the prime antigen upon boost may be the result of either 1. "True/B cell" back boosting whereby MBC are restimulated and secrete more antibody, or 2. "Pseudo/antibody" back boosting whereby the heterologous boost antigen stimulates naïve B cells, but not pre-existing MBC, that then generate cross-reactive antibodies that are able to bind to the prime antigen, hence increasing the overall titres of prime antigen-binding antibodies; it is likely that both of these forms of back boosting occur

simultaneously, and that they are both contingent on the relative antigenic distance between the heterologous antigens, as well as influenced by factors such as the presence of cross-reactive T cells that would be generated following priming. If solely prime antigen-binding antibody levels were measured between prime and heterologous boost timepoints, it would be challenging to definitively discern whether the additional fraction of prime antigen-binding antibodies gained upon boost were MBC- or naïve B cell (boost) derived.

Another method that has been used to distinguish antibodies derived from either back boosted or de novo responses to boost antigen is antibody depletion/pre-absorption[253,270]. In this approach, antibodies are pre-incubated with the antigen of first exposure, such that all cross-reactive antibodies are pre-absorbed. A normal ELISA is then completed using the secondary antigen. By pre-absorbing the cross-reactive fraction of antibodies, the remaining antibodies that are specific to epitopes unique to the secondary antigen can be measured for; such antibodies are likely de novo-derived, as opposed to back boosting-derived. An advantage of the depletion assay is that it can be performed in a clinical setting on human serum samples, and not just mice.

3. Vaccines and vaccine strategies

Vaccination is one of the most effective means of preventing disease, having contributed immensely to global health. The purpose of vaccination is to safely present antigen(s) or pathogen(s) to the immune system without causing disease, and initiate an immune response that generates immune memory to the antigen(s) or pathogen(s), such that the immune system is prepared to recognise and protect against potential infection with the pathogen, or disease elicited by the pathogen. As the development of a primary

adaptive immune response to novel pathogen can take several days to weeks, vaccination mainly serves as a prophylactic measure, to be completed before potential pathogen exposure. Vaccination can also be a means of boosting pre-existing immunity developed through natural infection.

3.1 “Next-generation” vaccines

Considerable advances have been made regarding the approaches to vaccination, which have been showcased during the COVID-19 pandemic; four viral vector vaccines, two mRNA vaccines and two recombinant protein vaccines were licensed in a short timeframe. Since then, mRNA and recombinant protein vaccines have been licensed for RSV and novel influenza vaccines are currently undergoing trials. These vaccine types can be distinguished from the traditional, first-generation vaccines that include live-attenuated and inactivated types.

3.1.1 Viral vector vaccines and the ChAdOx1 platform technology

Viral vector vaccines are a “next generation”-type vaccine that exploit the natural ability of viruses to infect and deliver genetic material to a host cell. By modifying virus to carry the genetic material encoding the desired antigen(s), the virus can subsequently deliver (“vector") and facilitate host cell expression of the antigen(s) inserted into the virus and an immune response to the antigen will follow. Viral vectors are a “platform” technology, as whilst different antigen sequences can be selected and inserted into the backbone of the virus, the backbone itself remains unchanged. Complementary, cumulative safety data from previous clinical trials with vector vaccines that have the

identical backbone but a different antigenic insert to the newly constructed vector vaccine, can accelerate the developmental pipeline of the candidate vector vaccines.

Various viruses have been selected and modified for use as viral vectors, including adenoviruses, poxviruses, vesicular stomatitis virus (VSV) and vaccinia virus[271]. The chimpanzee adenovirus vector 1 (ChAdOx1) is a replication-deficient simian adenovirus vector (derived from the Y25 serotype) that has been attenuated through targeted gene deletion; the vector is able to infect host cells, however, cannot undergo its complete viral lifecycle[272]. The safety profile and immunogenicity of the ChAdOx1 platform has been well-studied for vaccines against various pathogens, including SARS-CoV-2[273–277]. IM immunisation with ChAdOx1 has been used in global vaccination schemes, and this vaccine technology can be administered safely via the mucosal IN route[92,278,279]. Additionally, it can be modified to express multiple antigenic sequences facilitating immunity to multiple pathogens through one vaccine dose (multivalency). A similar vector using the AdC68 serotype, "ChAdOx2", is also currently being used for a number of non-SARS-CoV-2 vaccines and advantageously is less affected by anti-ChAdOx1 immunity, that is now widespread due to the ChAdOx1 nCoV-19/Vaxzevria campaign[272].

3.1.1.1 The immune response following adenoviral vector vaccination

Viral vectors have adjuvant properties (self-adjuvant), expressing pathogen-associated molecular patterns (PAMPs) that activate the innate immune system, thus the vaccine does not require formulation with adjuvants[280]. Within the initial stage of vaccination with an adenovirus-based vector (<24 hours post-vaccination)[280], the vector infects local DCs, as well as muscle cells (in the case of IM vaccination) and epithelial cells (in the case of respiratory mucosal vaccination) via engaging the coxsackievirus and

adenovirus receptor (CAR) expressed on the host cell surface[281]. Upon entry into the cell, the viral DNA is transported to the host cell nucleus where it is transcribed into mRNA[280].

Certain pattern recognition receptors (PRRs) on the host cell surface and within the host cell detect the foreign vector during this period and initiate a rapid innate immune response: toll-like receptor 2 (TL2) on the host cell surface recognises the viral capsid proteins such as the hexon protein, leading to the release of pro-inflammatory cytokines and activation of the NF-kB, toll-like receptor 9 (TL9) within the endosome of infected DCs recognises the viral DNA via CpG motifs, triggering the production of IFN-α/β, and cGAS/STING and NLRP3 inflammasomes within the infected host cell cytoplasm also detect viral components leading to activation of the type I IFN and STING pathways, as well as secretion of IL-1β and IL-18, respectively[281]. The activation of such pathways and release of cytokines results in the activation of DCs leading to enhanced uptake of expressed viral antigen, as well as the recruitment of innate cells to the local site of vaccination (for the clearance of infected cell), subsequently promoting the initiation of the adaptive immune response, which begins within days of vaccination.

Once the transcribed mRNA is transported to the host cytoplasm, it is translated into protein by host machinery. The encoded antigen of viral vectors is subsequently presented to the immune system through multiple pathways: antigen expressed (thus exposed) intracellularly (within the host cell), and may be presented on the host cell surface as MHC I peptide or whole antigen (e.g., when the target antigen is a viral envelope protein with transmembrane domain), or secreted into the extracellular milieu, or disseminated within necrotic or apoptotic cellular bodies, for APC uptake[280]. Activated DCs containing the antigen drain to the lymph nodes where they then present antigen to cognate $CD4^+$ cells, cross-prime cognate $CD8^+$ T cells, and activate cognate B cells,

facilitating initiation of the adaptive immune response[280]. The period of T cell activation and proliferation begins within a week of vaccination and peaks roughly two weeks post-vaccination[281]. The antibody response can take slightly longer, at 3 to 4 weeks post-vaccination[281].

The resulting adaptive response results in immune memory which can last months to years[282]; the durability of immune response to vector is highly dependent on various factors, such as age, regimen and route of vaccination.

3.1.1.2 Anti-vector immunity

The main disadvantage to viral vectors is the potential presence of pre-existing host anti-vector immunity or its development following-viral vector vaccination (which could for instance, impact booster immunogenicity). Although both T cell and antibody anti-vector immunity can form following vector vaccination, anti-vector NAbs have greater potential in reducing vaccine potency as they can prevent the vector from infecting the host cell and delivering the transgene, thus preventing antigenic expression all together[283]. Anti-vector antibodies may also alter the vaccine efficacy by engaging innate cells via Fc-FcR interactions and subsequently destroying the vector before it is able to infect the host cell and facilitate antigenic expression[284,285].

A particular clinical study for example, has demonstrated that pre-existing adenovirus immunity, acquired for example, through infection, resulted in the reduced immunogenicity of ChAdOx1 nCoV-19 vaccine compared with when absent before vaccination[2]. Another publication hypothesised that at intervals less than 3 months between the prime and boost of ChAdOx1 nCoV-19 vaccination, anti-vector immunity negatively interferes with the vaccine regimens' potency, and alluded to the impact of dosage of the prime on immunogenicity of vaccine following boost[286].

As the primary mechanisms of anti-vector immunity that result in the reduced potency of vector vaccine are antibody-mediated, and the window of opportunity of vector suppression is presumably within the initial stages of vaccination, the quantity and location of anti-vector antibody are likely to have a strong influence on the degree to which it will dampen the immune response. The durability of anti-vector immunity overtime, and specifically the extent to which anti-vector antibodies wane with time, will have important implications regarding prime-boost strategies involving the same vector for the prime and the boost. Likewise, cross-reactive, mucosal anti-vector immunity established after adenovirus infection may have implications and impact the potency of mucosally-administered adenovirus-based vector vaccines.

The issue of anti-vector immunity can be tackled via multiple means: vectors with low associated seroprevalence among the human population can be selected for in the cases of potential pre-existing anti-vector immunity, and for booster vaccinations, different vectors can be used to express the same transgene, or the dose can be augmented[283]. Additionally, the prime-boost interval could presumably be lengthened past the peak anti-vector antibody response to allow considerable waning of antibody prior to the boost; further exploration of these approaches nonetheless, is warranted.

3.2 Routes of vaccination and vaccine strategies

3.2.1 Mucosal vaccination against respiratory viruses

Generally, vaccination via the parenteral route, such as intramuscular (IM), subcutaneous (SC) or intradermal (ID), does not elicit strong immune responses in the local respiratory mucosa, where respiratory viruses enter and initially infect[287]. Although systemic immunity derived from respiratory virus vaccines that are delivered via the

parenteral route is often associated with protection against more severe forms of disease, it is usually unable to prevent infection of the upper airways[288]. Systemic immunity provides control of wider infection by restricting the virus to the mucosa; antibodies and lymphocytes present in circulation are able to rapidly access any potential disseminated virus that enters the blood stream and prevent the infection of systemic tissues; this form of protection is particularly relevant for viruses such as SARS-CoV-2 which can infect many tissues in addition to the respiratory tract epithelium[50–52,289]. Moreover, the IM route of vaccination may provide some level of control against mucosal virus infection (particularly lower airway infection) through the mobilisation of pre-existing systemic T and B cells (via circulation) to the respiratory mucosa following infection, as well as potentially the transudation of systemic IgG into the mucosa (leading to virus neutralisation)[290]; these mechanisms of immunity typically result in the formation of resident-memory populations in the mucosa that collectively protect against future re-infections (hybrid immunity)[287]. Although the mobilisation of systemic-derived immunity to the respiratory mucosa would assist in the control of virus infection, this form of response is not typically rapid enough to control airway infection and is only engaged following substantial infection of the mucosa; the presence of pre-existing mucosal immunity alternatively, can act more rapidly as it is locally situated.

The mucosal tissues can be viewed as “immunologically restrictive” and form a distinct compartment, necessitating infection (hence direct contact with the mucosal surface) or inflammation for local T and B cell responses to be induced[291]. The benefit of localised immunity in the airways and inductive sites, as described earlier, is a more rapid response to viral insult, with the potential to control and better prevent subsequent infection. Moreover, the immune response of the respiratory mucosa is distinct from wider

systemic responses, and specifically adapted for protection against airborne viruses. By delivering vaccine to the site of natural infection, mucosal vaccination can "mimic" natural infection by introducing antigen at the relevant site and induce localised immunity.

There are several variations and approaches to mucosal vaccination, including intranasal (IN) vaccination, which typically involves spraying or dropping vaccine suspension into the nostrils[292], or aerosol vaccination (AE), in which nebulised or powder-form vaccine is inhaled; devices such as nebulisers or inhalers are needed for AE vaccination[293]. The intra-tracheal vaccination route is not commonly used for human vaccination; it is less practical to administer (more procedural) and also does not result in even distribution of vaccine within the lungs, however it can be used in animals when aerosolised vaccine cannot be used[294].

Despite the inherent advantages of mucosal vaccination, very few mucosal vaccines have been licensed for use against a respiratory virus; these include FluMist against influenza virus infection and CanSinoBIO's COVID-19 inhaled vaccine[295]. The ease of administration of nasal vaccine, paired with it being an alternative to injection for those that are needle-phobic, are two advantages over the traditional IM route; the FluMist vaccine for instance, has recently been approved by the FDA for at-home use in the autumn of 2025[296].

Certain disadvantages to the mucosal route have limited the number of mucosal vaccines currently on the market; these include practical considerations, such as the high cost in manufacturing mucosal vaccine delivery devices compared with a standard IM needle, as well as the difficulty in determining robust mucosal correlates of protection that are easy to define and measure. Other concerns with mucosal vaccines include the potential adverse effects of vaccine reactogenicity within the lung, especially when

administering mucosal vaccine in infants or when adjuvant is needed, and contrarily, that this route will be less immunogenic due to the lung tissue being more tolerogenic as it is in constant exposure with the external environment[297]. In the latter scenario, the potential requirement for adjuvants that increase the immunogenicity, and also have a good safety profile when administered mucosally, could pose a particular challenge during vaccine development[297]. Likewise, given that immune correlates such as lung T_{RM} have been shown in certain studies to wane quickly following the mucosal immune response, there is potential that mucosal vaccination would not lead to as durable protection as parenteral routes[228,230,237–241].

Certain vaccines administered mucosally in preclinical studies have been unsuccessful when brought into human trials, as illustrated for example in a 2022 study using the Astra Zeneca ChAdOx1 nCoV-19 vaccine[92]. In this particular study, several possible reasons for the lack of desired trial outcome were made; these included 1. the ChAdOx1 vector potentially having lowered tropism to the human airway epithelium compared with that in NHPs, 2. anatomical differences between humans and NHPs, where in the latter the vaccine was shown to elicit robust responses when delivered through the same MAD300 atomisation device as used in the human trial[92]. In addition, biodistribution of the vaccine was not evaluated in this study, and the use of nebulisation devices, higher doses of vaccine (much higher proportional doses were used in the NHP trial), and adjuvants were suggested as potential approaches for increasing the immunogenicity of the vaccine[92]. Interestingly, when individuals received IM vaccine prior to or after IN vaccination, the mucosal immunogenicity was superior to one or two doses of IN vaccination; these dual-mode-type IM- and IN-containing regimens are a focus of this thesis and will be touched on further[92]. This study reflected the complexity of translating a

successful preclinical mucosal vaccine candidate into humans, and how focus should be aimed at the adaptation of mucosal vaccination strategies for human application[92].

3.2.2 Prime-pull vaccination

The "prime-pull" vaccine strategy was first described by Akiko Iwasaki and Haina Sin for a vaccine regimen against genital herpes (HSV-2); the aim of the vaccine was to elicit a robust T_{RM} population at the local, peripheral site of potential infection, as previous vaccines that solely elicited circulatory memory T cell populations were not efficacious[291]. The study demonstrated that priming mice with a vaccine through the conventional IM route (prime), and then topically applying chemokines to the vagina (pull), resulted in superior protection against HSV-2-elicited disease and neuronal infection of the dorsal root ganglia[291].

Since then, the dual model prime-pull vaccination regimen has been tested in various preclinical studies where a vaccine has been used as the "pull" as opposed to a chemokine, and where the target tissue has been the respiratory mucosa, with positive outcomes[194,255,298–305]. The parenteral/systemic-prime, then respiratory mucosal-boost regimen is aimed to pull and amplify the pre-existing, prime-derived cellular immune response to the respiratory tract such that resident-memory populations and mucosal antibody are generated, and reside poised for potential viral insult. By priming systemically, robust circulatory IgG, MBC, and memory T cells responses can be generated; the mucosal boost can then both amplify the pre-existing response, and additionally "refine" the response such that it be present at the local site of potential virus infection. Hence the two modes, which elicit different types of immune responses, can have a complimentary effect when combined in a single strategy (in a homologous antigen setting).

Additionally, the dual mode strategy may offer more durable immunity than mucosal vaccination-only regimens, however, this area has not yet been readily explored. The priming of immune system systemically moreover, has been proposed as a means of preventing deleterious reactogenicity following the mucosal boost, by lessening the required dose of vaccine for the mucosal boost, or the requirement for adjuvant.

3.3 The murine vaccination model

The use of mice to assess the immunogenicity and protection conferred by vaccines and regimens is common and often one of the initial steps in the vaccine development pipeline. Mice are a convenient choice of animal for vaccine testing as they are relatively cheap, easy to care for and house, they are small and require minimal training to handle, their immune systems are well characterised, and a wealth of knowledge and immunological tools exist that can be used to analyse and dissect their immune responses[306]. There is considerable overlap between the mouse and human immune system. Moreover, mouse challenge models exist that allow the assessment of the protection conferred through vaccination.

Certain reductionist characteristics of mouse vaccination experiments are advantageous as they can allow for a particular independent variable, e.g., dose or route, to be altered within a highly controlled environment, such that a clear result be obtained. Certain strains of mice, such as BALB/c and C57BL/6, are inbred; the lack of variability between mice in groups from these strains allows for the resolution of potentially subtle, yet important differences between differently treated groups. The housing of “clean” mice in individually vented cages (IVCs) prevents the tested mice from encountering pathogen and ensures that other factors do not conflate the observed immune response.

Nevertheless, these reductionist characteristics also make the (inbred) mouse model less realistic and representative of a human population. Another disadvantage of the inbred mouse model is the lack of diversity in the MHC haplotypes expressed; the human population expresses a diverse set of MHC haplotypes, with the identity of the haplotype known to influence the immune response to antigen. To overcome the limitation of lack of variability, outbred strains such as the CD-1 strain can be used that are more genetically diverse, and better reflect the diversity expected within the human population.

Other advantages to the mouse model include the capacity of editing the murine genome and create congenic and transgenic strains, such as those that enable the inducible labelling of cell populations, and the capability of easily harvesting different tissues and fluids for the evaluation of the immune response in different compartments, in contrast to humans.

4. Thesis outline and aims

Vaccination is an effective means of preventing virus-elicited disease and reducing disease burden, and licensed vaccines against major respiratory pathogens influenza virus, SARS-CoV-2 and RSV exist. Nevertheless, there remains room for improvement of the vaccination strategies against these respiratory viruses. Notably, the use of the alternative mucosal route of vaccination shows potential in augmenting the level of protection against respiratory virus infection achieved by vaccine. This thesis hypothesises that the mucosal route for homologous and heterologous boosting provides greater benefit than the standard intramuscular route.

The principle aim of this thesis was to investigate how mucosal boosting and the systemic prime, mucosal (IN) boost (IM-IN) regimen (also termed 'prime-pull'), could be used for vaccines against RSV, influenza and SARS-CoV-2 variants. The particular aims of each experimental chapter were the following:

- Chapter 3: To model and investigate immunological imprinting within the context of SARS-CoV-2 variants
- Chapter 4: To investigate the alternative mucosal route for heterologous SARS-CoV-2 omicron booster vaccine
- Chapter 5: To dissect the immunological mechanisms driving the heterologous systemic-prime, mucosal-boost response presented in Chapter 4
- Chapter 6: To determine the immunogenicity and protective capacity of the systemic-prime, mucosal-boost regimen when applied within a homologous prime-boost context for a novel vaccine candidate targeting influenza and RSV virus

In-house constructed vaccines and the murine vaccination model were used as tools to assess the protective potential of the IM-IN regimen. Although this thesis focusses on vaccines against these three aforementioned viruses, the following work is aimed to contribute to the vaccination strategies against respiratory pathogen "X".

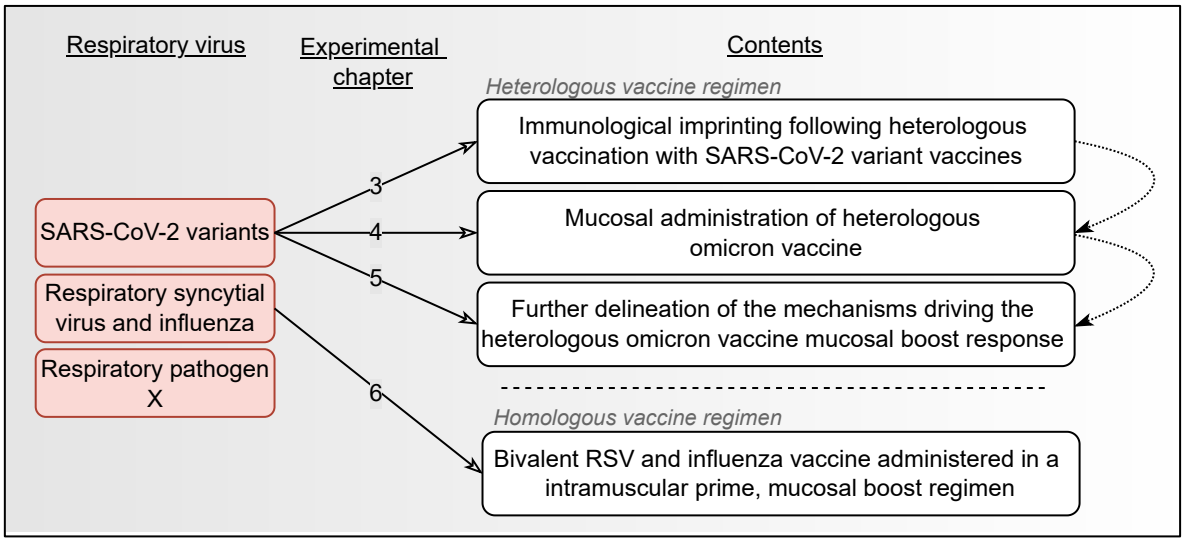

Figure 1.8: Schematic of the ordering and contents of the experimental chapters in this thesis

The first three experimental chapters (3, 4 and 5) of this thesis used "next-generation" SARS-CoV-2 variant vaccines as tools: Chapter 3 explored immunological imprinting within the context of vaccination, and in doing so, demonstrated a limitation to heterologous boosting via the IM route, a route used in current vaccine booster campaigns against influenza and SARS-CoV-2. Chapter 4 then explored the alternative mucosal route for heterologous boosting; specifically, it was investigated whether mucosal administration could 1. "Overcome" suppressive immunological imprints derived from IM-vaccination, and 2. How it could lead to an overall more immunogenic regimen and enhance respiratory mucosal immunity. Chapter 5 further explored the mechanisms underpinning the responses observed following the heterologous IN boost vaccination in Chapter 4. The final

experimental chapter (Chapter 6) explored the IM-IN regimen within a homologous regimen context: the immunogenicity and protective capacity of a bivalent RSV-influenza ChAdOx1 vaccine delivered IM-IN was evaluated.

2
Materials and methods

2. Materials and methods

1. Materials

1.1 General reagents and equipment

Table 2.1: List of reagents and equipment used in this thesis

Category	Reagent or material	Supplier	Catalogue number
ELISA and ELISpot antibodies	Alkaline phosphatase (AP)-conjugated goat anti-mouse IgG	Sigma Aldrich	A3562
	Goat Anti-Mouse IgA-AP	SouthernBiotech	1040-04
	Goat Anti-Mouse IgM-AP	SouthernBiotech	1021-04
	Goat Anti-Mouse IgG1, Human/Bovine/Horse SP ads-AP	SouthernBiotech	1071-40
	Goat Anti-Mouse IgG2a, Human/Bovine/Horse SP ads-AP	SouthernBiotech	1081-04
	Goat Anti-Mouse IgG2b, Human/Bovine/Horse SP ads-AP	SouthernBiotech	1091-04
	Goat Anti-Mouse IgG2c, Human/Bovine/Horse SP ads-AP	SouthernBiotech	1078-04
	Goat Anti-Mouse IgG3 heavy chain (Alkaline Phosphatase) preabsorbed	Abcam	ab98705
	IFN-gamma ELISpot ALP Kit: Capture mAb: AN18, Detection mAb: R4-6A2 biotinylated	Mabtech	3321-2A
Assay and culture plates	PVDF-membrane ELISpot plates	Millipore	
	6 Well Clear TC-Treated Multiple Well Plates individually wrapped sterile	Costar	3516
	96-well Nunc™MaxiSorp™ plates		
	48-well cell culture plate	Costar	
	Nunc™ FluoroNunc™/LumiNunc™ 96-Well Plates	Thermo Scientific™	
	96-well U-bottom plate	BD Biosciences	353077
Development buffers	p-Nitrophenyl Phosphate, Disodium Salt substrate	Sigma-Aldrich	
	Pierce™ diethanolamine substrate buffer	ThermoFisher Scientific	
	Elispot Colour Development Kit - AP conjugate substrate kit	BioRad	1706432
	Brightglo™	Promega	E2620
Tissue processing	Collagenase type XI	Merck Life Science Ltd	C7657
	Falcon 70um Cell Strainer For 50ml Falcon Tube	Scientific Laboratory Supplies Ltd	352350
	15 mL Falcon		
	50 mL Falcon		

	5 mL sterile syringe		
	DNAse type I	Merck Life Science Ltd	D5025
Buffers and solutions	Blocker™ Casein in PBS	Life Technologies Ltd	37528
	Formalin solution, neutral buffered, 10%	STARLAB (UK) Ltd	E1405-2141
	Perm/Wash buffer	BD Biosciences	554723
	Sterile H_2O		
	Sterile phosphate buffered saline		
	Ammonium chloride	Merck Life Science Ltd	A9434-500G
	Ehtylenediameinetetraacetic acid disodium	Merck Life Science Ltd	E7889-100ML
	Potassium bicarbonate	Merck Life Science Ltd	60339-500G
	Tryphan Blue		
	Zombie Yellow Fixable Viability Kit	Biolegend	423103
	LIVE/DEAD Fixable Near-IR Dead Cell Stain Kit	Thermo Fisher Scientific	L10119
	FuGENE-HD Transfection reagent	Promega	E2311
Recombinant proteins	SARS-CoV-2 B.1.1.529 (Omicron) spike RBD protein (His & AVI Tag), Biotinylated	Stratech Scientific Ltd	40592-V49H7-B-SIB
	SARS-CoV-2 B.1.1.529 (Omicron) spike RBD	SinoBiological	40592-V08H121
	Influenza A H1N1 (A/Puerto Rico/8/34/Mount Sinai) Matrix protein 1 / M1 Protein (His Tag)	Stratech Scientific Ltd	40010-V07E-SIB-100ug
	Influenza A H1N1 (A/Puerto Rico/8/34/Mount Sinai) Nucleoprotein / NP (I116M) Protein (ECD, His Tag)	Stratech Scientific Ltd	11675-V08B-SIB-100ug
	Influenza A H3N2 (A/Hong Kong/45/2019) Nucleoprotein / NP Protein (His Tag)	Stratech Scientific Ltd	40754-V08B-SIB-100ug
	Human respiratory syncytial virus (RSV) (A2) Fusion glycoprotein / RSV-F Protein (ECD, His Tag)	Stratech Scientific Ltd	11049-V08B-SIB
	SARS-CoV-2 B.1.1.529 (Omicron) Spike S1+S2 Protein (ECD, His Tag)	Stratech Scientific Ltd	40589-V08B33-SIB-100ug
	SARS-CoV-2 (2019-nCoV) Spike S1+S2 ECD-His Recombinant Protein	Stratech Scientific Ltd	40589-V08B1-SIB-100ug

	SARS-CoV-2 (BA.4/BA.5/BA.5.2) Spike S1+S2 trimer Protein (ECD, His Tag) (HPLC-verified)	SinoBiological	40589-V08H32
	SARS-CoV-2 XBB.1.5 (Omicron) Spike S1+S2 trimer Protein (ECD, His Tag) (HPLCverified)	SinoBiological	40589-V08H45
	SARS-CoV-2 BQ.1.1 (Omicron) Spike S1+S2 trimer Protein (ECD, His Tag) (HPLC-verified)	SinoBiological	40589-V08H41
	SARS-CoV-2 (BA.2) Spike S1+S2 trimer Protein (ECD, His Tag) (HPLC-verified)	SinoBiological	40589-V08H28
	Luminex magnetic plate washer	DiaSorin I.N.UK Ltd	CN-0269-01
	UltraComp eBeads™ Compensation Beads-100 tests	Life Technologies Ltd	01-2222-42
	ArC™ Amine Reactive Compensation Bead Kit (for use with LIVE/DEAD™ Fixable dead cell stain kits)	Life Technologies Ltd	A10346
	Neutralizing Antibody 6-Plex ProcartaPlex™ Panel kit	ThermoFisher scientific	
	Syringe 0.5mL 29Gx12.7mm Needle	Scientific Laboratory Supplies Limited	324892
	X100 BD Micro Lance 3 special cannulas	Fisher Scientific UK Ltd	10442204
	1ml Syringe, disposable, sterile	Terumo	GS572
	BD Micro-fine 0.5ml/8mm/30g Insulin Syringe	Scientific Laboratory Supplies Ltd	BD324893
	Protein Transport Inhibitor (Containing Brefeldin A)	BD Bioscience	555029
Streptavidin for B cell probe	Streptavidin, AF647 conjugate	Life Technologies Ltd	S21374
	Streptavidin, APC conjugate	Biolegend	405243
	Streptavidin, BV421 conjugate	Biolegend	405225
	Streptavidin, PE conjugate	Biolegend	405203

1.2 Flow cytometry antibodies and tetramers

Table 2.2: List of flow cytometry antibodies

	Anti-mouse flow cytometry antibodies				
	Antibody	Clone	Fluorochrome	Supplier	Catalogue number
Surface	IgD	11-26c.2a	BV650	Biolegend	405721
	IgD	11-26c.2a	BV711	Biolegend	405731
	IgM	RMM-1	PE/Cy7	Biolegend	406514
	IgM	RMM-1	BV510	Biolegend	406531
	IgM	RMM-1	BV605	Biolegend	406523
	CD62L	MEL-14	AF700	Biolegend	104426
	CD62L	95218	AF350	Bio-Techne	FAB5761U-100UG
	CD62L	MEL-14	PE/Cy7	Biolegend	104418
	CD44	IM7	PE/Cy5	Biolegend	103010
	CD44	IM7	PerCP	Biolegend	103036
	CD44	IM7	AF700	Biolegend	103026
	CD44	IM7	AF700	ThermoFisher	56-0441-82
	CD44	IM7	BV711	Biolegend	103001
	CD4	GK1.5	Spark Blue 550	Biolegend	100474
	CD4	GK1.5	BUV496	BD Biosciences	612952
	CD4	RM4-5	PerCP-Cy5.5	Biolegend	100540
	CD69	H1.2F3	BV711	Biolegend	104537
	CD69	H1.2F3	PE/Cy5	Biolegend	104510
	CD69	H1.2F3	BV711	Biolegend	104537
	CD69	H1.2F3	APC	Biolegend	104513
	CD103	2E7	BV421	Biolegend	121421
	CD103	2E7	PE/Dazzle 594	Biolegend	121430
	CD103	QA17A24	PE/Dazzle 594	Biolegend	156910
	CD103	2E7	BV605	Biolegend	121433
	CD8	53-6.7	BV570	Biolegend	100739
	CD8	53-6.7	APC-eFluor780	eBioscience	47-0081-82
	CD8	53-6.7	BUV395	BD Biosciences	563786
	CD8	53-6.7	APC-H7	BD Biosciences	560247
	CD19	6D5	Pacific Blue	Biolegend	115523
	CD19	1D3	BUV563	BD Biosciences	749028
	CD127	SB/199	BUV737	BD Biosciences	612841

	CD127	A7R34	PE/Cy5	Biolegend	135016
	CXCR5	CXCR3-173	BV605	Biolegend	126523
	CD185	L138D7	PE/Cy7	Biolegend	145516
	CD138	281-2	PE/Cy7	Biolegend	142514
	CD138	281-2	BV785	Biolegend	142534
	CD45.1	A20	BUV615	BD Biosciences	751467
	CD45.2	104	BV510	Biolegend	109838
	CD45	30-F11	AF700	Biolegend	103128
	CD80	16-10A1	AF594	Biolegend	104754
	CD73	TY/11.8	BV605	Biolegend	127215
	CD273	TY25	BUV395	BD Biosciences	565102
	GL7	GL7	FITC	Biolegend	144604
	Fas	15A7	PerCP-eFluor710	Invitrogen	46-0951-82
	NK-1.1	PK136	APC-Cy7	Biolegend	108724
	CD3	17A2	BV650	Biolegend	100229
	CD3	BB23-8E6-8C6	PerCP-Cy5.5	BD Biosciences	561478
	B220	RA3-6B2	AF700	Biolegend	103232
	CD45R	RA3-6B2	BV650	Biolegend	103241
	F4/80	BM8	APC-Cy7	Biolegend	123118
	CD16/CD32	2.4G2	N/A	BD Biosciences	553141
Intracellular	IL-2	JES6-5H4	PerCP/Cy5.5	Biolegend	503822
	IFNγ	XMG1.2	eFluor450	ThermoFisher	48-7311-82
	IL-4	11B11	PE	Biolegend	504104
	TNF	MP6-XT22	AF488	Biolegend	506313

Table 2.3: Mouse T cell tetramers

Antigen	Details	Target	Fluorochrome	Supplier
SARS-CoV-2 WT spike (539-546)	MHCI H-2K^{b} tetramer	VNFNFNGL	PE	NIH Tetramer core facility
SARS-CoV-2 WT spike (539-546)	MHCI H-2K^{b} tetramer	VNFNFNGL	BV421	NIH Tetramer core facility
RSV A F (85-93)	MHCI H-2K^{d} pentamer	KYKNAVTEL	PE	ProImmune
Influenza A (PR8) NP (147-155)	MHCI H-2K^{d} pentamer	TYQRTALV	PE	ProImmune

2. Methods

2.1 Vaccine construction

2.1.1 Construction of ChAdOx1-NP+M1-mRSV(F)-DS2

ChAdOx1-NP+M1-mRSV(F)-DS2 was constructed in-house prior to this project, by colleagues. Briefly, as described by Susan Morris, the nucleoprotein (NP) gene and Matrix protein 1 (M1) gene from influenza virus A/Panama/2007/99 (H3N2) were linked through a glycine linker and codon optimised for expression in human cells. The genes were synthesised by GeneArt Gene Synthesis (Thermo Fisher Scientific). The genes were inserted into the Gateway® attL1/2 recombination cassette of a shuttle plasmid containing a human cytomegalovirus major immediate early promoter (IE CMV), including two tetracycline operator 2 sites, and the bovine growth hormone polyadenylation signal. The separate pre-fusion-stabilised RSV-F (DS2) gene sequence was codon-optimized for expression in human cell lines and synthesised by GeneArt Gene Synthesis (Thermo Fisher Scientific). This gene was inserted into the Gateway® attL3/4 recombination cassette of a shuttle plasmid containing a human cytomegalovirus major immediate early promoter (IE CMV), also including two tetracycline operator 2 sites, and the SV40 polyadenylation signal. Bacterial artificial chromosomes (BACs) containing ChAdOx1 NP+M1-RSVF were prepared by Gateway® recombination between the ChAdOx1 destination DNA BAC vector (described in Dicks, M. D. J. *et al*) and the shuttle plasmids containing the influenza virus NP+M1 gene expression cassette and RSVF gene expression cassette using standard protocols resulting in the insertion of the influenza virus gene expression cassette at the E1 locus and RSV gene expression cassette at the E4 locus (downstream of the E4 genes and upstream of the right inverted terminal repeat)[307]. The ChAdOx1 NP+M1-RSVF adenovirus genome was excised from the BAC using unique PmeI sites flanking the adenovirus genome sequence. ChAdOx1

NP+M1-RSVF viral vectors were rescued in T-RExTM cells (Invitrogen, Cat. R71007), a derivative of HEK293 cells which constitutively express the Tet repressor protein and prevent antigen expression during virus production. The resultant virus, ChAdOx1 NP+M1-RSVF, was purified by CsCl gradient ultracentrifugation as described previously[308]. The titres were determined on T-RExTM cells using anti-hexon immunostaining assay based on the QuickTiter™ Adenovirus Titer Immunoassay kit (Cell Biolabs Inc).

2.1.2 Construction of SARS-CoV-2 variant vaccines

An accumulating "library" of monovalent ChAdOx1-based viral vector vaccines were produced in-house following the emergence of SARS-CoV-2 and the sequential emergence of its variants. In this study, all such vaccines were used, but not constructed, apart from ChAdOx1-BA.4/5. Ad-α (ChAdOx1-α), Ad-β (ChAdOx1-β), Ad-γ (ChAdOx1-γ), Ad-δ (ChAdOx1-δ) and Ad-ο (ChAdOx1-ο) were constructed in similar fashion to ChAdOx1 nCoV-19, which was abbreviated as Ad-WT in this thesis for simplicity, and formerly marketed as Vaxzevria (INN: ChAdOx1-S)[309]. In brief, the spike sequences of the variants were either sourced from GISAID or provided by Astra Zeneca and codon optimised for expression in human cells, and modified to include a tissue-type plasminogen activator (TPA) leader sequence. The sequences were then synthesised by GeneArt (Thermo Fisher Scientific). The sequences were then cloned directly into a derivative of bacterial artificial chromosome (BAC) containing the ChAdOx1 genome, as previously described by *Dicks et al*[307]; the spike ORF was cloned downstream of a long CMV promoter and upstream of a BGH polyA termination sequence. The ChAdOx1-spike genome was then excised from the BAC, and the virus rescued using T-REx™ cells (Cat: R71007, (Invitrogen)). The virus was purified by CsCl gradient ultracentrifugation[310].

2.2 Mouse procedures

Mice for the immunogenicity studies in Chapters 3, 4, 5 and 6 were used in accordance with the UK Animals (Scientific Procedures) Act (ASPA) under project license number P9804B4F1, PP2352929 or PP3430109 granted by the UK Home Office following ethical review by the University of Oxford Animal Welfare and Ethical Review Board (AWERB). Mice for infection studies in Chapter 6 were used under license PP5168779, with all work approved by the Animal Welfare and Ethical Review board at Imperial College London; studies were in accordance with the Animal Research: Reporting of in vivo Experiments (ARRIVE) guidelines. All procedures conducted were followed according to UK home office/ASPA regulations by a PIL-holder.

2.2.1 Mouse housing conditions

Animals were group housed in IVCs under SPF conditions, with constant temperature and humidity with lighting on a 12:12 (8am to 8pm) or 13:11 (7am to 8pm) light-dark cycle.

2.2.2 Mouse specifications

Mice for all experiments were 5-8 weeks old at the beginning of the experiment. CD-1® outbred mice (Charles River Laboratories) were used for the bivalent RSV and influenza vaccine immunogenicity studies. BALB/cOlaHsd (Envigo or Charles River) mice were used for all other experiments apart from the adoptive cell transfer and S1pr2 experiments, where congenic Ly5.1 (B6.SJL-PtprcaPepcb/BoyCrl; obtained through Biomedical Services (BMS) Oxford) and C57BL/6JOlaHsd (Envigo) mice, or trangenic *S1pr2-ERT2cre Ai9* mice (obtained acquired with the assistance of Prof Oliver Bannard),

respectively, were used. All mice used for experiments were female. Mice were grouped in numbers of 5-6 unless otherwise stated.

2.2.3 Mouse vaccinations

All vaccines for mouse vaccinations were diluted (when dilution necessary) with PBS to appropriate concentration in a sterile tissue-culture hood. For all ChAdOx1 and ChAdOx2 vaccinations, a standard murine dose of 10^8 infectious units per mouse was used. For vaccinations with Pfizer/BioNTech (Comirnaty) COVID-19 vaccine and Novavax (Nuvaxovid) COVID-19 vaccine, doses of 1 µg and 5 µg spike (50 µg of Matrix-M), respectively, were used. Mice were anaesthetised (short-term) using vaporised IsoFlo® for all vaccinations. All vaccinations were completed by Cameron Bissett, apart from the vaccinations completed for the S1pr2 experiment by Lyn Yong, and the vaccinations completed for the virus challenge experiments completed by John Tregoning *et al*.

2.2.3.1 Intramuscular vaccination

For intramuscular vaccinations, 50 µL of vaccine preparation was injected into the left thigh muscle, unless higher volumes of vaccine needed to be injected, in which case, both the right and left thigh muscles were injected with 50 µL of vaccine. Injections were completed on mice under a light anaesthesia using BD micro-fine 8mm 0.5 mL insulin syringes (Scientific Laboratory Supplies Limited). Exceptionally, for the S1pr2 experiments, the IM vaccinations were performed on the right thigh muscle, as opposed to the left.

2.2.3.2 Intranasal vaccination

For intranasal vaccinations, doses of vaccine were identical to those for intramuscular vaccinations, however, prepared to a total 25-30 µL volume per mouse. Whilst mice were under light anaesthesia, they were held so that their abdomens were faced upwards, and vaccine droplets were positioned above the nostrils with a P200 pipette, in such a way to ensure the active inhalation of vaccine as opposed to the forced administration into the nostril. Droplets of vaccine were presented to both nostrils of the mouse.

2.2.4 Mouse challenges with respiratory viruses

For virus challenge experiments conducted by John Tregoning *et al*, female BALB/c mice (Charles River, Polcreek) were anaesthetised using vaporised IsoFlo® and virus in a total volume of 100 µL was administered intranasally, in identical fashion to that described for the intranasal vaccinations. The following doses were used for each virus: RSV - 7.7x105 PFU RSV A2; H1N1 - 2.1x105 413 PFU A/California/7/2009; H3N2 2x105 414 PFU X31. The viruses were propagated as described by John Tregoning: RSV A2 was grown on Hep2 cells; from the 3rd passage of a plaque-purified virus isolated by Dr Hongwei Wang (Imperial). The influenza viruses were grown on MDCK cells, and were a gift from Wendy Barclay (Imperial); they were also low passage. Mice were weighed daily following infection.

2.2.5 Administration of sera or cells via peripheral tail vein injection

For the serum transfer experiments, sera from vaccinated BALB/cOlaHsd mice were collected and pooled in groups under sterile conditions. A total volume of 100 µL of serum was injected into the peripheral tail vein of each recipient BALB/cOlaHsd mouse. For the adoptive cell transfer experiment, the spleens of vaccinated Ly5.1/CD45.1^{+} congenic mice

(B6.SJL-PtprcaPepcb/BoyCrl) were harvested and processed under sterile conditions to single cell suspension as detailed previously. Splenocytes were pooled in groups, and cell concentrations determined via Countess™ 3 Automated Cell Counter. Group cell concentrations of were normalised across groups via dilution in PBS. A total of six processed donor spleens were pooled per group, with 100 μL total volume transferred via peripheral tail injection into each recipient mouse. For all peripheral tail vein injections, mice were warmed at 37°C for 10 minutes to optimally dilate the tail veins prior to injection.

2.2.6 Tamoxifen administration

Cre expression in CD57BL/6J *S1pr2*-ERT2Cre-tdTomato mice was induced by administering a single dose of 12.5 mg tamoxifen (Sigma) dissolved in corn oil at 50 mg/mL by oral gavage 14 days post-prime. Tamoxifen administration was completed by Lyn Yong.

2.2.7 Blood sampling

2.2.7.1 Peripheral tail vein bleed

To collect blood via peripheral tail vein, mice were first warmed in a heatbox at 37°C for a minimum of 10 minutes, to dilate tail veins. Mice were then positioned within a tube restrainer, and the tail vein pricked with a sterile scalpel blade. Blood was then collected via capillary action using a Microvette 200 serum (Sarstedt Ltd). A maximum 10% of total blood volume was sampled at one time, and a maximum 15% total blood sampled in a 28-day period.

2.2.7.2 Terminal cardiac bleed

Mice were anaesthetised to a deep anaesthesia using vaporised IsoFlo® for all terminal cardiac bleeds. Blood was withdrawn slowly from the heart ventricle using 1 mL

sterile syringes (Terumo) with 26G micro lance 3 special cannulas (BD) for puncture. Following exsanguination, cervical dislocations were performed. To confirm death of the mouse, the severed cervical spine was palpated and cessation of pulse confirmed.

2.2.8 Mouse euthanasia

All animals were humanely sacrificed at the end of each experiment by cervical dislocation, or via administration of 100 μL of intraperitoneal pentobarbitone (20 mg dose, Pentoject, Animalcare Ltd., UK) for the infection studies in Chapter 6 (performed by John Tregoning *et al*). To confirm death of the mouse, the severed cervical spine was palpated and cessation of pulse confirmed.

2.3 Tissue processing

2.3.1 Blood processing

After collection via peripheral tail bleed or terminal cardiac puncture, blood samples were left to clot for a minimum of 30 minutes, and then centrifuged at 4000 g to separate the top serum fraction, which was then collected and transferred to an Eppendorf tube using a pipette; samples were stored frozen at -20°C to -80°C and thawed when needed for assays.

2.3.2 Spleen harvest and processing

To access the spleens, murine abdomens were opened with scissors. Spleens were removed with the use of tweezers and scissors; any pancreatic and connective tissue associated with the organ was removed. Spleens were then placed in 1.5 mL Eppendorf tubes containing 900 μL ice-cold sterile PBS prior to processing. Spleens were then homogenised by mashing with the end of a sterile syringe. Homogenised spleen was then

filtered through a 70 μM cell strainer (Falcon) and flushed with PBS. Homogenates were then spun down at 1500 RPM for 3 minutes and supernatants discarded. Red blood cells were lysed by adding 5 mL ACK buffer to the resuspended pellets for 5 minutes. To make ACK buffer, autoclave a mixture of 8.023g NH_4Cl [0.15M] (Sigma A-4514), 1g $KHCO_3$ [10mM] (Sigma P-9144), 37.2mg Na_2EDTA (Sigma ED2SS) and 1L milli-Q water that has been adjusted to a pH to 7.2-7.4 with 1N HCl. The lysis reaction was quenched by adding 40 mL of PBS. Samples were then spun down at 1500 RPM for 3 minutes and resuspended in 5 mL of MEM media, Alpha Modifications (Sigma Aldrich), containing 10% fetal calf serum, 1% penicillin/streptomycin and 1% L-glutamine. The number of viable cells were counted with a CASY® cell counter prior to use for assays.

2.3.3 Lung harvest and processing

To remove murine lungs, an excision along the thorax was made and the chest cavity exposed. Lungs were removed with tweezers, and connective tissue and thymus removed with scissors. Lungs were then cut into small pieces with scissors in 5 mL screw top bijou containers (Sterilin™). 3 mL of a digestion mixture was then added to the lung pieces. The digestion mixture contained RPMI 1640 media, containing 1% penicillin/streptomycin, 1% L-glutamine, 100mg/mL collagenase type XI (Sigma-Aldrich) and 10mg/mL DNAse type IV. Samples were then incubated for 1 hour in digestion mixture at 37°C, shaking. Sample contents were then pushed through a 70 μM cell strainer (Falcon) and flushed with media. Samples were spun down at 1500 RPM for 3 minutes and supernatant discarded, or, the lung homogenate supernatant (LHS) was collected for the subsequent measurement of antibody responses. Red blood cells were lysed by adding 5 mL ACK buffer to the resuspended pellet for 5 minutes. The reaction was quenched by

adding 40 mL of PBS. Samples were then spun down at 1500 RPM for 3 minutes and resuspended in 1 mL of RPMI 1640 media, containing 10% fetal calf serum, 1% penicillin/streptomycin and 1% L-glutamine. The number of viable cells were counted with a CASY® cell counter prior to use for ex-vivo assays/cell staining and flow cytometry.

2.3.4 NALT collection and fluid processing

To acquire NALT fluid, the soft upper cartilaginous palates of mice were excised with a scalpel and tweezers. Palates were cleaned of blood and debris by washing with ice-cold, sterile PBS. The cleaned palates were then added to a 48-well flat-well plate, submerged in 500 µL complete RPMI (containing 10% fetal calf serum (FCS), 1% penicillin/streptomycin and 1% L-glutamine). The palates were then incubated for 3 days at 37°C in a cell culture incubator. After incubation, supernatant was removed and centrifuged at 460 g to pellet cellular debris. Supernatant was stored at -20°C until use in assays. A more detailed protocol is described by Cisney *et al*[311].

2.3.5 BALF and BAL cell collection and processing

To collect BALF, a catheter was inserted into the trachea and mouse lungs were then lavaged with a syringe once with 300 µL; tweezers were used to clamp the trachea above the catheter puncture site during lavage to prevent the up-flow of PBS. BAL fluid was then transferred to a 1.5 mL collection tube and centrifuged at 460 g for 5 mins. Supernatant was then removed and treated with protease inhibitor at a 1:100 dilution prior to freezing at -80°C. For collection of BAL cells for cellular staining, the pellets formed upon centrifugation were resuspended with 500 µL of ACK for 2 minutes, then quenched with PBS. Samples were then centrifuged at 460 g for 5 minutes, then resuspended in RPMI for flow cytometry. BAL cell collection and staining was conducted by John Tregoning *et al.*

2.3.6 Nasal washes

Nasal fluid for NWs was collected by flushing the nasal cavity with 1 mL of PBS and collecting the fluid in an Eppendorf tube. NWs were completed by John Tregoning *et al.*

2.3.7 Inguinal and cervical lymph node removal and processing

Inguinal and cervical lymph nodes were collected and added to RPMI media containing 5% fetal calf serum and 1% penicillin/streptomycin. Tissues were mechanically dissociated through 70 μM cell strainers to obtain single cell suspensions. LN removal and processing was completed by Lyn Yong.

2.4 Antibody assays

2.4.1 Standardised indirect antigen-specific isotype ELISA

96 well Nunc™MaxiSorp™ plates were separately coated with 50μL/well of 2μg/mL (for tIgG) or 5μg/mL (for IgA and IgM detection) recombinant Influenza A H1N1 (A/Puerto Rico/8/34/Mount Sinai) Nucleoprotein/NP I116M (ECD, His Tag), Influenza A H1N1 (A/Puerto Rico/8/34/Mount Sinai) Matrix protein 1 / M1 Protein (His Tag), Influenza A H3N2 (A/Hong Kong/2671/2019) Nucleoprotein / NP Protein (His Tag) Influenza A H3N2 (A/Aichi/2/1968) Matrix protein 1 / M1 Protein (His Tag) or Human respiratory syncytial virus (RSV) (A2) Fusion glycoprotein/RSV-F protein (ECD, His Tag) (all SinoBiological), overnight at 4°C for ELISAs in Chapter 6. For SARS-CoV-2 variant vaccine experiments in Chapters 3, 4 and 5, plates were separately coated with 50μL/well of 2μg/mL (for tIgG detection) or 5μg/mL (for IgA detection) recombinant SARS-CoV-2 spike variants alpha (B.1.1.7), beta (B.1.351), gamma (P.1), epsilon (B.1.429), delta (B.1.617.2), original spike with a D614G mutation (B.1) (all obtained through Astra Zeneca) or omicron spike

(B.1.1.529) (from Native Antigen) or RBD (Sinobiological) overnight at 4°C. Alternatively, for anti-ChAdOx1 IgG ELISA, the plate was coated with 50μL/well ChAdOx1 virus at a 6.42E+07 IU/mL concentration. Plates were then washed with PBS/Tween (0.05% v/v), and then blocked for 1 hour at RT with Blocker Casein in PBS (Thermo Fisher Scientific). Blocker was then tapped off, and standard positive "high-responding" serum or mucosal tissue fluid was added, along with samples at individual dilutions in casein, and other appropriate controls, all in duplicate; sample incubation was 2 hours at RT for all assays. For the measurement of anti-alpha, -beta, -gamma, -delta, -epsilon or -B.1 IgG or IgA, a cross-reactive standard curve was used that performed similarly on each antigen and allowed for the comparison of interpolated values cross-antigen (Figure 2.1); all the aforementioned antigens were derived from the same source to ensure consistency of the different IgG variant assays conducted. Plates were washed after incubation, and casein-diluted secondary antibody added to plates for incubation 1 hour RT shaking; antibodies used were alkaline phosphatase (AP)-conjugated goat anti-mouse IgG (1:5000, Sigma-Aldrich; A3562), Goat Anti-Mouse IgA-AP (1:1500, SouthernBiotech), Goat Anti-Mouse IgM-AP (1:1500, SouthernBiotech). Unbound detection antibody was washed prior to addition of 100μL/well p-Nitrophenyl Phosphate, Disodium Salt substrate (SigmaAldrich). For IgG, IgA and IgM assays, OD405nm values were interpolated off a standard curve made of positive reference sera, which was assigned arbitrary ELISA units and fitted to a 4-parameter logistic curve. Methods for interpolation and processing of OD405nm values were based off of work from Miura *et al* 2008[312].

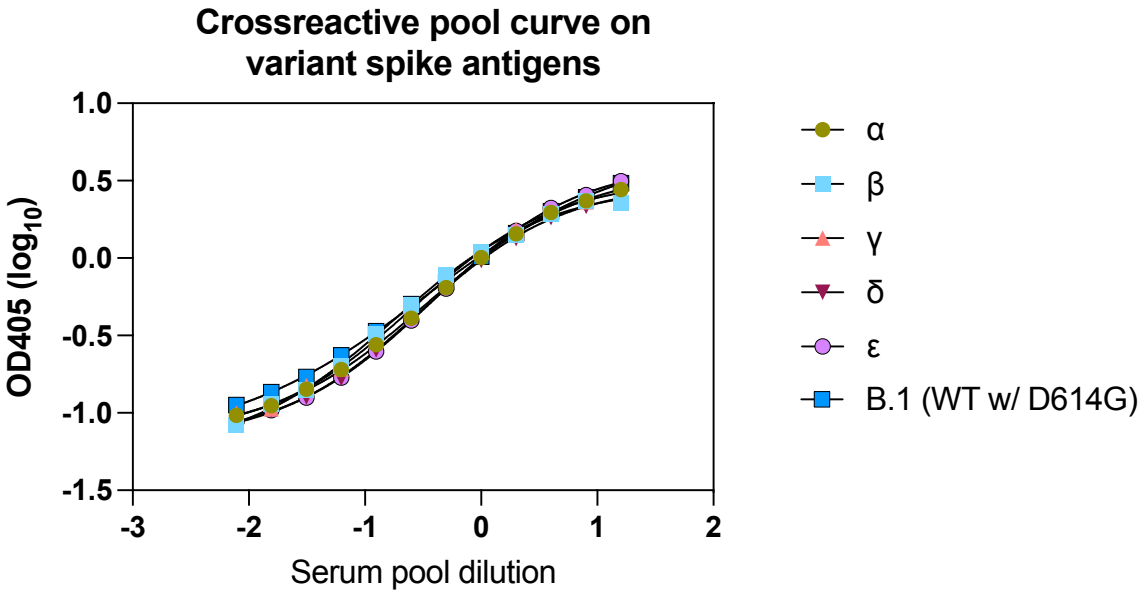

Figure 2.1: Cross-reactive standard curve for the direct comparison of antibody ELISA units reactive to different SARS-CoV-2 ancestral variant spike antigens

In order to establish an assay that could allow for the comparison of serum IgG responses to different ancestral spike antigens, a cross-reactive pool of sera was used, that comprised of equal parts of serum from mice vaccinated with homologously with Ad-α, Ad-β, Ad-γ, Ad-δ or Ad-WT.

2.4.2 WT spike IgG depletion ELISA

To measure o-RBD-specific antibodies that are non-WT spike cross-reactive, a protocol based off of that detailed by Pušnik *et al* was used[253]. In brief, the quantity of anti-o-RBD IgG in samples were first determined via indirect standardised ELISA as described above; plates were coated with 2 μg/mL SARS-CoV-2 B.1.1.529 (Omicron) spike RBD (Cat: 40592-V08H121 (SinoBiological). The subsequent, calculated EU values were used to normalise each sample to the equivalent quantity of anti-o-RBD IgG, by diluting each sample with casein. Each sample (in duplicate) was then incubated for 1 hour at 37°C (shaking) in a flat bottom 96-well non-absorbent plate with a range of different concentrations of WT spike (total volume of 100 μL/well); WT spike was titrated from 6

μg/mL to 0.008 μg/mL via 1:3 serial dilutions. A WT spike-free control was also included. After incubation, 50 μL of the mixture was transferred to a pre-o-RBD-coated (2μg/mL), pre-casein-blocked plate. A standard indirect IgG ELISA was then conducted as described above. Development of each sample curve was stopped when the WT spike-free control reached an OD_{405nm} of 1.00. Curves were plotted and area under the curve (AUC) values calculated.

2.4.3 Normalised IgG subclass ELISA

96 well Nunc™MaxiSorp™ plates were separately coated with 50μL/well of 2μg/mL recombinant Influenza A H1N1 (A/Puerto Rico/8/34/Mount Sinai) Nucleoprotein/NP I116M (ECD, His Tag) or Human respiratory syncytial virus (RSV) (A2) Fusion glycoprotein/RSV-F protein (ECD, His Tag) overnight at 4°C. Plates were then washed with PBS/Tween (0.05% v/v), and then blocked for 1 hour at RT with Blocker Casein in PBS (Thermo Fisher Scientific). To assess relative levels of IgG subclasses between samples, samples were first normalised for total IgG (EUs), such that all samples were adjusted to contain identical quantities of total IgG. Once blocker was tapped off, samples were plated in duplicate and incubated 2 hours at RT. Plates were washed after incubation, and casein-diluted secondary antibody added to plates for incubation 1 hour RT shaking; antibodies used were alkaline phosphatase (AP)-conjugated Goat Anti-Mouse IgG1, Human/Bovine/Horse SP ads-AP (1:4000, SouthernBiotech), Goat Anti-Mouse IgG2a, Human/Bovine/Horse SP ads-AP (1:4000, SouthernBiotech), Goat Anti-Mouse IgG2b, Human/Bovine/Horse SP ads-AP (1:4000, SouthernBiotech), Goat Anti-Mouse IgG2c, Human/Bovine/Horse SP ads-AP (1:4000, SouthernBiotech), Goat Anti-Mouse IgG3 heavy chain (Alkaline Phosphatase) preadsorbed (1:1000, Abcam). Unbound detection antibody

was washed prior to addition of 100µL/well developer (p-Nitrophenyl Phosphate, Disodium Salt substrate (SigmaAldrich)). Plates were read periodically upon addition of developer, and values recorded when the first of any sample reached 1.00 OD405nm, for each subclass.

2.4.4 Luminex ACE-2 competition assay

To assess the capacity antibody sera to inhibit SARS-CoV-2 variants alpha (B.1.1.7), beta (B.1.351), gamma (P.1), delta (B.1.617.2), omicron (B.1.1.529) and wildtype (WT) from binding to ACE-2, the Neutralizing Antibody 6-Plex ProcartaPlex™ Panel kit (ThermoFisher scientific) was used, with user manual instructions followed. In brief, serum samples were diluted 1:400 and NALT samples diluted 1:15 in assay buffer and incubated with washed Luminex beads coated either with recombinant alpha (B.1.1.7), beta (B.1.351), gamma (P.1), delta (B.1.617.2), wildtype (WT) and omicron (B.1.1.529) spike S1 (except for gamma, which was full spike) on a shaker at RT for 2 hours. After washing, biotinylated recombinant ACE-2 was added and plate incubated on a shaker at RT for 30 minutes. Beads were then washed, and incubated for an additional 30 minutes at RT (shaking) with streptavidin-PE. After a final wash, beads were acquired in reading buffer on a MAGPIX^{TM} Luminex machine. ACE-2 competition was represented as a percentage, with 0% competition defined as the mean fluorescence intensity of the internal plate blank; the blank sample will enable complete binding of spike to ACE-2 and generate the upper MFI limit.

To assess the ACE-2-competition capacity of omicron subvariant spike-binding antibodies, an in-house bead panel was made using the Bio-Plex Amine Coupling Kit (BioRad); in brief, each omicron subvariant spike protein (BA.1, BA.2, BA.4/5/5.1, BQ.1.1, XBB.1.5 and XBB.1.16; all Sino Biological) was coupled to a unique (fluorescently dyed)

COOH magnetic bead (BioRad). Spike proteins were buffer-exchanged prior to coupling. Coupled beads were adjusted in concentration and pooled to create a bead mixture that was then used instead of the bead mixture provided in the ProcartaPlex™ kit; the assay was completed identically to that described for the ProcartaPlex™ kit.

2.4.5 Lentivirus pseudoneutralisation assay

To assess the capacity of sera to neutralise SARS-CoV-2 variants wildtype (WT) and omicron (B.1.1.529) virus via blocking of lentiviral entry into target cells, omicron- and WT-spike encoding lentivirus were produced by Alexander Sampson as previously described[313]. Briefly, HEK293T/17 cells at 60% confluency in 6-well plates were transfected with 250ng p8.91 lentiviral packaging plasmid, 375ng pCSFLW luciferase reporter, and 50ng pcDNA3.1 expressing plasmid encoding either the wildtype or omicron spike gene. After 72 hours, the supernatant was collected and filtered using 0.45μm Millipore® syringe filters and titrated on ACE2/TMPRSS2 transfected target cells. For neutralisation assays, HEK293T/17 cells at approximately 70% confluence in T75 flasks were transfected to express ACE-2 and TMPRSS2 by the addition of 600 μL opti-MEM containing 2μg ACE-2 pCAGGS plasmid, 150 ng TMPRSS2 pCAGGS plasmid and 6.45 μL FuGENE-HD (Promega). Serum samples diluted over a two-fold dilution series from 1:100 to 1:12800 in 50 μL DMEM media (10% fetal calf serum (FCS), 1% penicillin/streptomycin and 1% L-glutamine) were incubated at 37°C for 1 hour on Thermo Scientific™ Nunc™ FluoroNunc™/LumiNunc™ 96-Well Plates with 50 μL virus ($2x10^7$ RLU/mL) (except for cell-only control). Following incubation, 50 μL of transfected target HEK293T/17 cells were added at a density of $3x10^5$ cells/mL in fresh complete DMEM media to all wells and incubated for 48 hours at 37°C, 5% CO_2. To develop plates, plates were flicked and then tapped to remove media, and then 30μL Brightglo™

(Promega) diluted 1:1 in PBS was added to each well. After 5 minutes at RT, plate luminescence was measured on a CLARIOstar Plus (BMG LABTECH) reader. The IC50 values were interpolated off of control-normalised, non-linear curve transformations for each sample, in similar method to Ferrara *et al*[314].

2.4.6 Adenovirus antibody neutralisation assay

To assess the ability of BALF samples to neutralise ChAdOx1 virus entry into host cells, ChAdOx1 virus modified to contain the secreted placental alkaline phosphatase (SEAP) reporter gene was used. In brief, $3x10^4$ GripTite 293 MSR cells (at passage below 35) were added to the wells of a 96-well tissue culture plate (Nunc), and the plate incubated for 24 hours at 37°C, such that a monolayer confluence of 80-100% be achieved the following day. For the later stage maintenance and dilution of cells, DMEM (10% FBS, 1% L-glutamine, 1% pen/strep, phenol red-free) was used, and to dissociate cells from the cell culture flask, a cell scraper was used. BALF samples were then diluted following a 1:2-fold serial dilution from neat with DMEM (0% FBS, phenol red-free) and then incubated with a fixed concentration of ChAdOx1-SEAP (prepared in DMEM (0% FBS, 1% L-glutamine, 1% pen/strep, phenol red-free)) for 1 hour at 37°C. The GripTite 293 MSR cells were then infected with the virus/sample mixture (following removal of the supernatant from the cell wells) and the plate incubated for 24 hours at 37°C. Following incubation, 50 μL of supernatant from each well was added to a black 96-well plate (with each sample serial dilution in duplicate). The chemiluminescent substrate CSPD (TROPIX phospha-light kit) was then added to wells and the plate incubated for 45 minutes at RT. The plate was then measured on a CLARIOstar Plus (BMG LABTECH) reader. The subsequent IC50 values were interpolated off of control-normalised, non-linear curve transformations for each sample

similarly to that completed for the pseudoneutralisation assay described above. The methodology was based off of an SOP written by Nick Edwards (Pandemic Sciences Institute).

2.5 Cellular assays

2.5.1 Spleen and lung IFNγ ELISpot

PVDF-membrane ELISpot plates (Millipore) were coated with 50 μL (per well) of 5μg/mL anti-mouse IFNγ (Clone: AN18, Cat: 3321-2 (Mabtech)) overnight at 4°C. Plates were then washed with PBS and then blocked by adding 100 μL complete α-MEM media and incubating for 1 hour at RT. Splenocytes and lung cells processed to single cell suspension and adjusted to a cell density of 10^7 cells/mL were added to plates. Each sample was plated in duplicate, and titrated to achieve three cell concentrations: 5E+05, 2.5E+5 and 1.25E+5 (and plated once additionally at 5E+05 for unstimulated control). Then, peptide pool was added for stimulation of the cells over 18 hours at 37°C. For the SARS-CoV-2 omicron booster vaccine experiment in Chapter 4, a peptide pool of peptides from the omicron S1 region that contain mutations was used: Supplemental Table 1. For ELISpots completed in Chapter 6, peptide pools spanning RSV F protein (5 pools) and influenza NP and M1 (4 pools) were used: Supplemental Table 8. IFNγ spots were detected with biotinylated anti-mouse IFNγ antibody (mAb R4-6A2, Cat: 3321-2 A, biotin (Mabtech), diluted to 1 μg/mL), followed by streptavidin-ALP (Cat: 3321-2 A (Mabtech), diluted to 1 μg/mL). To develop spots, AP conjugate substrate (Cat: 1706432 (Biorad)) was added. Spots were counted on an AID ELISpot reader, and data represented as spot forming units (SFUs) per million splenocytes. When multiple pools were used to span one antigen, the sum of the SFU values was presented in figures.

2.6 Lung viral load measurement

Viral load was assessed by John Tregoning *et al.* Viral load was assessed by Trizol extraction of RNA from frozen lung tissue disrupted in a TissueLyzer (Qiagen, Manchester, UK). RNA was converted into cDNA, and quantitative RT PCR was carried out on a Stratagene Mx3005p (Agilent technologies, Santa Clara, CA, USA). For influenza M gene 0.1 µM forward primer (5'AAGACAAGACCAATYCTGTCACCTCT-3'), 0.1 µM reverse primer (5'-TCTACGYTGCAGTCCYCGCT-3') and 0.2 µM probe (5'-FAM501 TYACGCTCACCGTGCCCAGTG-TAMRA-3'). M-specific RNA copy number was determined using an influenza M gene standard plasmid. For RSV L gene, 0.1µM primers 5' GAACTCAGTGTAGGTAGAATGTTTGCA-3' and 5'-TTCAGCTATCATTTTCTCTGCCAA-3' and probe 5'-6-carboxyfluorescein (FAM)-TTTGAACCTGTCTGAACAT-6-carboxytetramethylrhodamine (TAMRA)-3'. RNA copy number per mg of lung RNA was determined using an RSV L gene standard.

2.7 Cellular staining and flow cytometry

2.7.1 Surface staining

To stain cells, cells were first incubated with a mixture of LIVE/DEAD^{TM} Fixable Near-IR Dead Cell Stain Kit (1:2000; Cat: L34975 (Invitrogen^{TM})), or Zombie Yellow Fixable Viability Kit (1:2000; Cat: 423103 (Biolegend)), along with Anti-Mouse CD16/CD32 Fc block (1:25, Clone: 2.4G2, Cat: 553141 (BD Biosciences)) in a 96-well round bottom plate for 30 minutes in the dark at 4^{o}C. Cells were then washed with PBS with 0.5% Bovine Serum Albumin (BSA). An antibody cocktail was then added and the plate incubated for 30 minutes in the dark at 4^{o}C. Antibody panels for staining (resident) memory T cells in the respiratory mucosa contained certain "core" markers listed in Table 2.4. Additional markers, such as those for staining B cells, or pathogen-specific B or T cell probes, were

included to the core panel depending on the experiment. A B cell-focussed panel was used for the S1pr2 cell lineage tracing experiment (Table 2.5). Following incubation, when no intracellular staining was completed, cells were washed and resuspended in 100 μL PBS with 0.5% BSA. For experiments involving intracellular staining (completed by Cameron Bissett), or solely surface staining completed by John Tregoning *et al*, equal numbers of cells were plated for staining. For experiments solely involving the surface staining of lung cells, that were completed by Cameron Bissett, all lung cells were plated prior to staining. Cells were acquired on a SONY ID7000^{TM} Spectral Cell Analyzer or a BD LSR II Flow Cytometer.

In certain experiments where lung tissue-resident memory populations were stained for, mice were injected intravenously with 1-3 μg of anti-mouse CD45, CD3 or CD45.2 fluorochrome-conjugated antibody diluted in PBS (100 μL total volume), 5 minutes prior to cull; in such a way, the circulatory lymphocyte population was identifiable in processed lung samples and excluded from the resident population.

Flow data was analysed on FlowJo software (10.9.0). The gating strategies are presented in the Appendices: Supplemental Figure 2, Supplemental Figure 3 and Supplemental Figure 6). In experiments where concentration or frequency were used for lung and/or BAL cell readouts such as the S1pr2, virus challenge and intracellular staining experiments, the total cell count was not used as the readout on figures as a subset of cells were plated for staining, as opposed to all processed cells. When total cell counts were used as the readout for certain cell populations such as T_{RM}, in Chapters 4, 5 and 6, they were calculated after gating out dead, non-singlet and non-lymphocyte (based on size and granularity) populations, and all cells from the tissue were included in the staining well and acquired (total population), as opposed to a subset. When frequencies were used as a

readout, the population of which the frequency was calculated was detailed in the figure; all frequencies were calculated on live, singlet, lymphocyte populations. For infection studies conducted by John Tregoning *et al*, cell populations were presented in concentration (cells/mL); this was the product of the defined frequency of the cell population and the cell concentration as determined through a separate tryphan blue stain of the processed cell suspension (prior to staining).

Table 2.4: T cell (+B cell) surface staining flow cytometry panel for measuring respiratory mucosa immune responses

Antibody	Dilution	Comment
IgD	1:100	In B+T cell panel
IgM	1:100	In B+T cell panel
CD62L	1:50-1:200	Core
CD44	1:100-1:200	Core
CD4	1:100-1:200	Core
CD8	1:100	Core
CD3	1:100-1:400	Optional; When IV injection for circulatory stain completed (alternative to CD45)
CD69	1:70-1:100	Core
CD103	1:70-1:100	Core
CD11a	1:150	Optional
CD19	1:100	In B+T cell panel
CD127	1:100	Core
CXCR3 (CD183)	1:50	Core
CD138	1:50	In B+T cell panel
CD273 (PD-L2)	1:100	In B+T cell panel
CD73	1:100	In B+T cell panel
CD80	1:100	In B+T cell panel
CD45.1	1:100	Adoptive transfer experiment
CD45.2		When IV injection for circulatory stain completed (alternative to CD45)
CD45R	1:100	Optional
CD45	1-3 μg/mouse	When IV injection for circulatory stain completed
CXCR5 (CD185)		Adoptive transfer experiment
Live/dead stain	1:1000	Core
Omicron RBD B cell probe I	2:37	SARS-CoV-2 experiments

Omicron RBD B cell probe II	2:37	SARS-CoV-2 experiments
WT spike B cell probe I		SARS-CoV-2 experiments
MHC I VNFNFNGL tetramer I (SARS-CoV-2 spike)	1:500	Adoptive transfer experiment
MHC I VNFNFNGL tetramer II (SARS-CoV-2 spike)	1:500	Adoptive transfer experiment
MHC I KYKNAVTEL pentamer I (RSV A)	1:100	RSV A challenge experiment
MHC I TYQRTALV pentamer II (Influenza A)	1:100	Influenza A challenge experiments
Fc block	1:25	Core

Table 2.5: B cell surface staining flow cytometry panel for S1pr2 cell lineage tracing experiment

Antibody	Dilution
GL7	1:100
Fas	1:50
NK-1.1	1:100
F4/80	1:100
CD138	1:100
IgM	1:100
CD3	1:50
IgD	1:100
Omicron RBD B cell probe I	2:37
Omicron RBD B cell probe II	2:37
Fc block	1:25

2.7.2 Intracellular staining

When antigen-specific cytokine secretion was measured, the processed spleen or lung cells were first stimulated by incubating them with antigen peptides (at a working concentration of 2μg/mL diluted in complete α-MEM media) prior to staining, for 6 hours at 37°C. Each sample was also left unstimulated with no peptide such that the background levels of cytokine staining could be measured. After the first 2 hours of incubation, BD Golgiplug™ was added to the cells. Following incubation, and after completion of cell

surface staining as described in 2.7.1, cells were fixed with 10% neutral-buffered formalin (containing 4% paraformaldehyde) for 10 minutes in the dark at 4°C, and then permeabilised by washing with BD PERM/Wash™ buffer. The intracellular cytokine antibody cocktail (Table 2.6), diluted in BD PERM/Wash™, was then added to the cells and the cells were incubated for 30 minutes in the dark at 4°C. Cells were washed once with BD PERM/Wash™, and then twice with PBS/BSA (0.5%), and then resuspended in PBS/BSA (0.5%) for acquisition on the flow cytometer. The gating strategy used is illustrated in Supplemental Figure 6A. To calculate the frequencies of antigen-specific, cytokine-positive cells, the frequency of cytokine-positive cells when the sample was unstimulated (negative control) was first subtracted from the frequency of stimulated, cytokine-positive cells for that given sample.

Table 2.6: Intracellular cytokine antibody staining panel

Antibody	Dilution
TNF	1:100
IFNγ	1:50
IL-2	1:50
IL-4	1:50

2.7.3 B cell probe preparation

B cell probes were produced in-house by combining the streptavidin-fluorochrome conjugates with biotinylated omicron RBD (Sino Biological) in a 1:4 molar ratio, respectively, in a 1.5 mL Eppendorf tube. The mixture was incubated on ice for 30 minutes in the dark, with periodical mixing by flicking. Following incubation, the mixture was added to staining panels.

2.8 Statistical and data analyses

All statistical analyses used for the final figures presented in this thesis were performed on GraphPad Prism 9.0 and 10.0 by Cameron Bissett. Medians were used as representative values for each mouse group, unless otherwise stated. To assess if data were normally distributed, a Shapiro-Wilk test was performed. When figures contained different graphs that were treated with either parametric and non-parametric tests, a "+" symbol was used to distinguish the graphs that were treated with a non-parametric test. For the comparison of two groups, unpaired parametric t tests or non-parametric Mann-Whitney U-Tests were performed. When three or more groups were compared against each other, a parametric one-way ANOVA test or non-parametric Kruskal-Wallis test was performed. When multiple comparisons were made, parametric Tukey's or Šidáks test was performed depending on whether all groups were compared with each other, or to a specific a control group, respectively. For non-normal data a Dunn's test was used. For the multiple comparisons of paired data, Friedman tests were performed. Correlation between two given variable readouts was assessed using Pearson correlations. P values were symbolised as asterisks (* = $P<0.05$, ** = $P<0.01$, *** = $P<0.001$, **** = $P\leq0.0001$. If data was represented in log form, data was converted to log prior to statistical analyses.

3

Immunological imprinting with SARS-CoV-2 variant vaccines

3. Immunological imprinting with SARS-CoV-2 variant vaccines

1. Introduction and aims

Extensively-mutated SARS-CoV-2 variants such as omicron have evaded the immunity offered by original, wildtype (WT) spike-encoding SARS-CoV-2 vaccines and previous infection with original and earlier ancestral variant viruses, which has led to increased incidences of breakthrough infection within the global population. Nevertheless, omicron and omicron subvariant infections have generally elicited attenuated forms of COVID-19 disease compared with ancestral variants and the WT strain; this is likely in part as a result of pre-existing cross-reactive non-neutralising antibodies and T cell immunity[315,316], in addition to the intrinsic changes to the omicron virus that include the lessened usage of TMPRSS2 for host cell entry, that is linked to a greater tropism to the upper respiratory tract[37,317]. Many individuals even so, remain vulnerable to disease as a result of compromised immune systems and other comorbidities, and detrimental long COVID has also been shown to proceed even mild infections[318–321]. For this reason, there remains a need for vaccines that reduce the levels of virus infection and subsequent virus transmission, as opposed to vaccines that solely perpetuate pre-existing cross-reactive immunity.

In response to the emergence of omicron and its subvariants, updated booster vaccines based on the variant spike have been created and employed; the purpose of these boosters is to broaden immunity towards the emergent variants. Such boosters include the bivalent and monovalent mRNA vaccines from Moderna and Pfizer/BioNtech, that both contain WT and omicron (BA.1) messenger RNAs, and subunit vaccines from Novavax (Table 1.3).

The pre-existing immunity offered via WT-spike vaccination albeit linked to reduced disease severity following omicron infection[322,323], has also been linked to the impairment

of the immunogenicity of omicron booster vaccines, that are administered via the intramuscular (IM) route, via the process of immunological imprinting[80–84].

The heterogeneity of the human population's immunity to SARS-CoV-2, including their vaccination and infection history, make understanding the influence and impact of immunological imprinting on vaccination strategies challenging; this is compounded by the multifaceted nature of immunological imprinting and the lack of well-established methods of measuring it. In this chapter, the aim was to investigate and model immunological imprinting through the heterologous vaccination of mice.

Specifically, to:

- Understand how priming the immune system with a particular SARS-CoV-2 antigen influences the latter immune response following heterologous boost
- Investigate the effect original SARS-CoV-2 "WT" vaccine-derived antibodies have on the de novo responses to heterologous omicron boost vaccine

2. Results

2.1 Construction of a library of SARS-CoV-2 variant spike-encoding vaccines

As variants of the SARS-CoV-2 virus have sequentially emerged within the human population, we have accordingly constructed updated monovalent ChAdOx1-based viral vector vaccines that encode the matching sequences of the full-length variant virus spike proteins, in doing so, forming a 'library' of variant vaccines (Table 3.1). These vaccines were constructed in similar method to the original ChAdOx1 nCoV-19 vaccine; the sequence encoding the spike antigen was inserted into the ChAdOx1 backbone, replacing the E1 region. A TPA leader sequence was added to the beginning of the spike sequences to enhance antigen expression within cells.

Table 3.1: List of ChAdOx1 variant vaccines constructed in-house

Antigenic cluster	Vaccine name and abbreviation used in this project	Full-length spike sequence encoded in vaccine
Primary ancestral cluster	ChAdOx1-WT/Ad-WT, also known as ChAdOx1 nCoV-19 or ChAdOx1-S (INN), and formerly marketed as Vaxzevria	Original 'Wuhan'
	ChAdOx1-α/Ad-α	Alpha (B.1.1.7)
	ChAdOx1-β/Ad-β	Beta (B.1.351)
	ChAdOx1-γ/Ad-γ	Gamma (P.1)
	ChAdOx1-δ/Ad-δ	Delta (B.1.617.2)
	ChAdOx1-ο/Ad-ο	Omicron (B.1.1.529/BA.1)
	ChAdOx1-BA.4/5/Ad-BA.4/5*	Omicron subvariant BA.4/5
	ChAdOx1-XBB.1.5/Ad-XBB.1.5	Omicron subvariant XBB.1.5
	ChAdOx1-XBB.1.16/Ad-XBB.1.16	Omicron subvariant XBB.1.16

2.2 Immunological imprinting with SARS-CoV-2 vaccines

2.2.1 Homologous vaccination with ancestral variant (pre-omicron emergence) spike vaccines

Prior to the emergence, rapid spread, and dominance of the omicron variant and subsequence omicron subvariants, which are significantly antigenically distant to the original WT virus, earlier 'ancestral' variants, including alpha, beta, gamma and delta were prevalent and spread through the global population in waves[324]. Relative to the antigenic distance of omicron, these variants can be viewed as a 'primary ancestral cluster' with higher spike sequence homology to each other than with omicron and its subvariants.

It was specifically investigated whether immunological imprinting occurred when the immune system was successively exposed to different earlier ancestral variant spike antigens. To do this, mice were first vaccinated with the monovalent primary cluster variant vaccines following a homologous IM prime-boost regimen (Figure 3.1A and Figure 3.1B), to establish the expected baseline antibody responses developed in naïve mice, that could then be compared with the responses developed following heterologous IM regimens. The inbred BALB/c mouse strain was chosen such that subtle, yet potentially

significant differences in immune response could be detected between regimens that could otherwise be conflated by the variability expected in a small, outbred mouse experiment. Blood was sampled 4 weeks post-prime, and collected 3 weeks post-boost, for serological analysis.

The levels of IgG reactive to cognate encoded spike antigen and other primary cluster antigens were measured and compared with a negative control group of mice that were vaccinated with ChAdOx1-GFP (abbreviated Ad-GFP), which was used as it encodes an irrelevant antigen. To enable the comparison of amounts of IgG reactive to different variant spike antigens, an ELISA was conducted using a cross-reactive standard curve that performed similarly on each antigen (Figure 2.1). Instead of WT spike, the B.1 antigen was used, which contains the D614G mutation that was adopted early on during the COVID-19 pandemic. IgG against the epsilon variant spike antigen were additionally measured as this variant was temporarily a variant of interest and the antigen was available to be used.

Following the priming and boosting of mice with Ad-α, Ad-β, Ad-γ or Ad-δ, IgG reactive to the cognate antigen encoded in the respective construct were detected in mouse serum (Figure 3.1C and Figure 3.1D). High levels of cross-reactive (non-cognate) IgG were also detected following vaccination with all four vaccines after priming and boosting in contrast to the negative Ad-GFP+Ad-GFP control group; however, these levels were generally lower than those measured against cognate antigen (e.g., anti-γ IgG>anti-α/β/δ/ε/B.1 IgG following the Ad-γ regimen). The levels of IgG reactive to both cognate and non-cognate antigen established after priming increased after homologous boosting of vaccine.

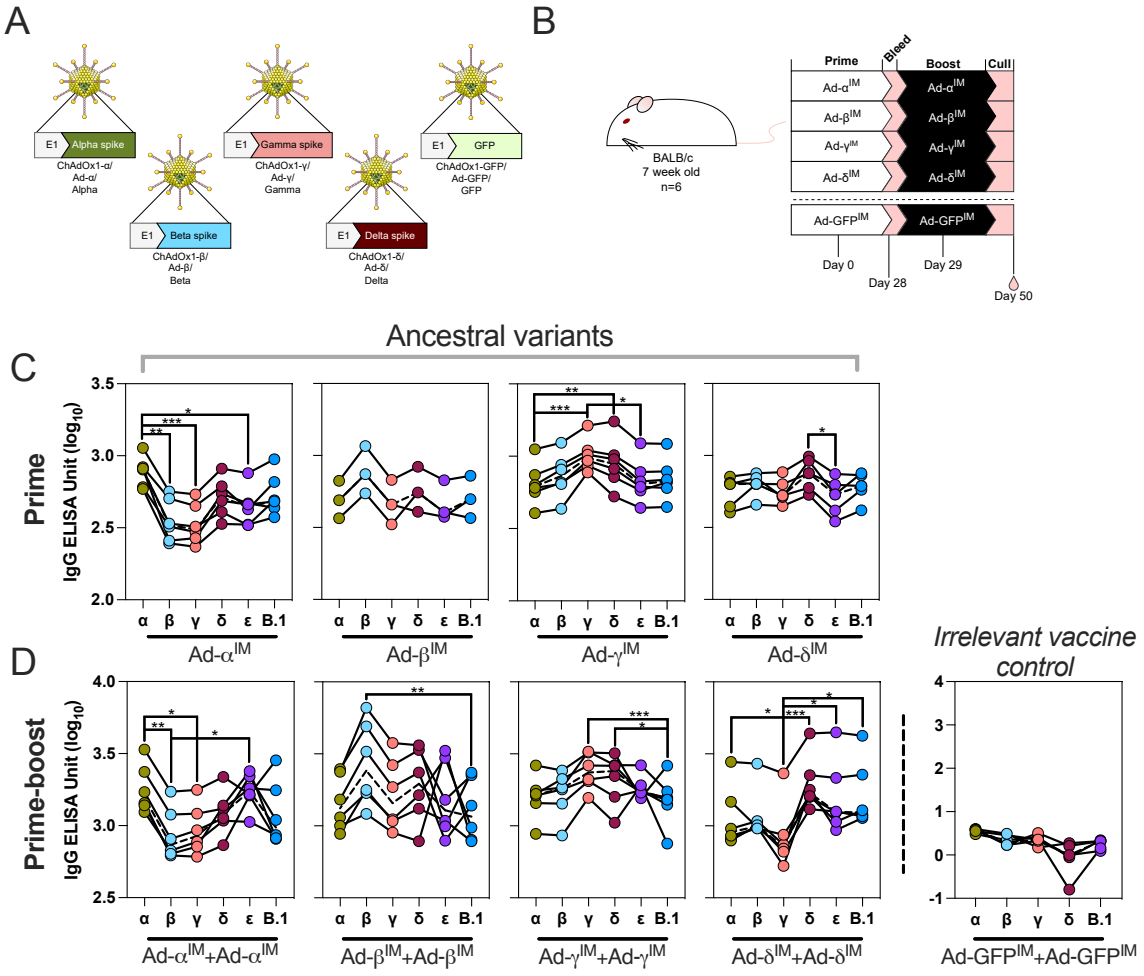

Figure 3.1: Humoral immunogenicity of ancestral variant vaccines

(A) Monovalent ChAdOx1 vaccines encoding the full-length sequences of 'primary cluster' ancestral variants alpha, beta, gamma and delta, as well as negative control vaccine encoding irrelevant antigen GFP. (B) Vaccination schedule for the homologous IM prime-boost of BALB/c mice (n=6). The vaccination experiment was completed once. Alpha (α)-, beta (β)-, gamma (γ)-, delta (δ)-, epsilon (ε)- and B.1-reactive IgG (log_{10} ELISA units) in serum of mice 4 weeks post-prime (C) and 3 weeks post-boost (D), measured via ELISA. B.1 spike antigen was chosen as opposed to WT spike, as the D614G mutation was gained by WT spike early on in the pandemic, and was the available antigen at the time of the experiment. The epsilon variant spike antigen was additionally used as this antigen was temporarily a variant of interest at the time of the experiment, and a variety of variants were tested on to evaluate the breadth of response. In (C) and (D), a dashed line in graphs represents the group median response. To test for significant differences in levels of antibody response to different variant spikes following each regimen, a paired non-parametric Friedman multiple comparisons test was completed (*=P<0.05, **=P<0.01, ***=P<0.001). A list of P values for all graphs is present in Supplemental Table 2. Insufficient sera was collected following Ad-β-prime for three samples, hence only three samples could be measured for antibodies.

The ability of spike-reactive serum antibodies to block ACE-2 binding to spike ("ACE-2-competition") was also measured via Luminex assay, as a surrogate of virus neutralisation (Figure 3.3); when the ACE-2 competition assay was compared with an alternative lentivirus pseudoneutralisation assay, the data were shown to positively correlate (Figure 3.2).

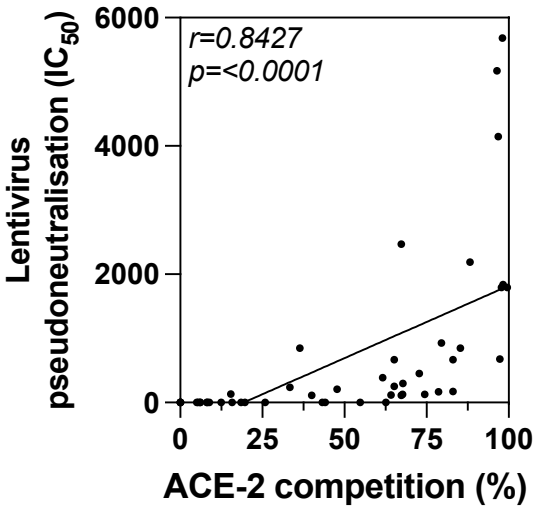

Figure 3.2: Correlation between lentivirus pseudoneutralisation and ACE-2 competition by anti-spike antibodies

A) Correlation between lentivirus (expressing omicron spike) pseudoneutralisation (IC_{50}) and ACE-2 competition (o-$ACE2^{comp}$-Abs; % competition), by anti-omicron spike antibodies generated in the serum of mice prime-boost vaccinated with ChAdOx1 omicron vaccine. A non-parametric Spearman r value of 0.8427 was calculated (P≤0.0001).

The ACE-2 competition capacity of spike-reactive IgG in sera following variant vaccine priming followed a similar trend to levels of IgG; the highest levels of ACE-2-competing antibodies ($ACE2^{comp}$-Abs) detected following each regimen were those that were reactive to cognate antigen (Figure 3.2A). In contrast to antigen-specific IgG however, the levels of cross-reactive $ACE2^{comp}$-Abs varied much more following vaccine prime (Figure 3.3A). Following boosting, the levels of $ACE2^{comp}$-Abs reactive to cognate and non-cognate antigen increased (Figure 3.3B).

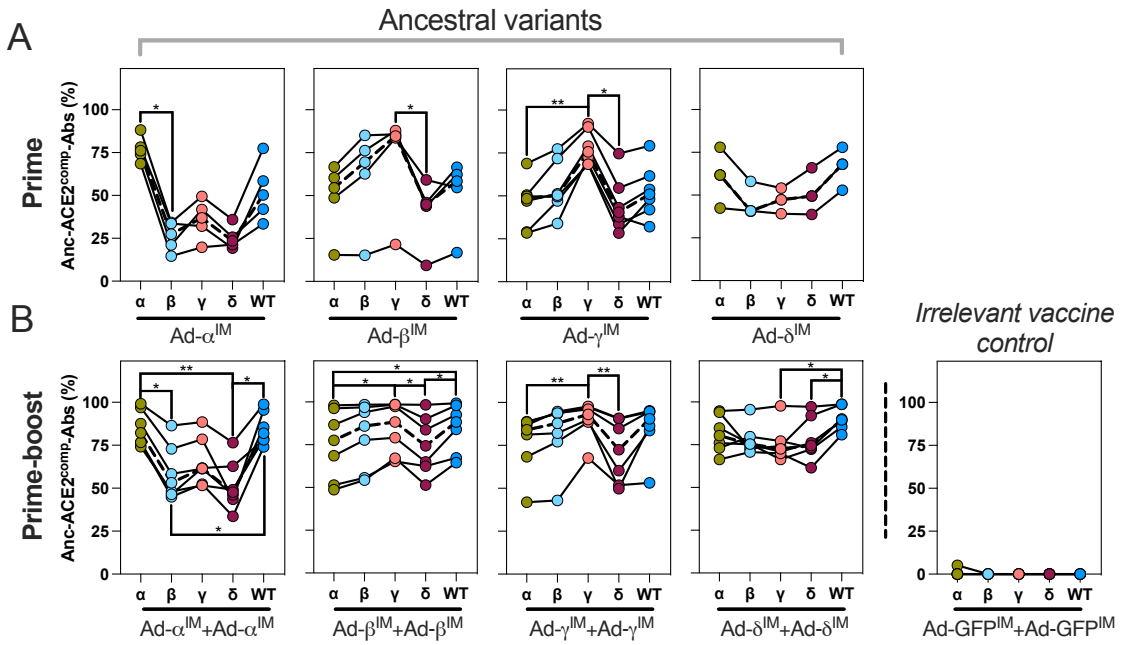

Figure 3.3: ACE-2-competing antibodies following ancestral variant spike vaccine immunisation

Measurement of the capacity of alpha (α)-, beta (β)-, gamma (γ)-, delta (δ)-, and WT-reactive serum antibodies (ACE2^{comp}-Abs) to outcompete ACE-2 binding with spike (% ACE-2 competition), following prime (A; Ad-α^{IM}, Ad-β^{IM}, Ad-γ^{IM} or Ad-δ^{IM}) and boost (B; Ad-α^{IM}+Ad-α^{IM}, Ad-β^{IM}+Ad-β^{IM}, Ad-γ^{IM}+Ad-γ^{IM} or Ad-δ^{IM}+Ad-δ^{IM}) vaccination with ancestral variant vaccines, measured by Luminex assay. Sera was collected 4 weeks post-prime, or 3 weeks post-boost. The vaccination experiment was completed once. A dashed line in graphs represents the group median response. To test for significant differences in levels of antibody response to different variant spikes following each regimen, a paired non-parametric Friedman multiple comparisons test was completed (*=P<0.05, **=P<0.01). A list of P values for all graphs is present in Supplemental Table 3. Insufficient sera was collected following Ad-δ-prime for three samples and for Ad-β-prime for one sample, hence only three samples and five samples could be measured for antibodies for these regimens, respectively.

In summary, vaccination with one or two doses of Ad-α, Ad-β, Ad-γ or Ad-δ vaccine resulted in cross-reactive antibodies in mouse serum, with some variation in the magnitude of response to non-cognate antigen. The levels of cross-reactive ACE2^{comp}-Abs following one dose of vaccine were much more variable, however broadened after homologous vaccine boosting.

2.2.2 Heterologous vaccination with ancestral variant (pre-omicron emergence) spike vaccines

2.2.2.1 Serum IgG responses following heterologous vaccination with ancestral variant (pre-omicron emergence) spike vaccines

To assess whether priming the immune system with a particular ancestral variant spike antigen influenced the latter immune response to a secondary, different variant antigen, mice were vaccinated heterologously; mice were primed with Ad-α and then boosted with either Ad-β or Ad-γ vaccine (Ad-α^{IM}+Ad-β^{IM} and Ad-α^{IM}+Ad-γ^{IM}), or vaccinated in the reverse order (Ad-β^{IM}+Ad-α^{IM} and Ad-γ^{IM}+Ad-α^{IM}) for comparison (Figure 3.4). The assessment of imprinting following Ad-α vaccination was specifically chosen at (as opposed to the Ad-WT vaccine), as the alpha variant was prominent within the U.K. population at the time of the experiment; the Ad-β and Ad-γ vaccines were selected as beta and gamma variants had emerged around a similar time, and have divergent spike sequence identities to the alpha virus spike sequence (Figure 1.1). By comparing the antibody responses following the heterologous regimens and the prime-only regimens presented in Figure 3.1 and Figure 3.3, two indications of immunological imprinting could be investigated: firstly, back boosting, as measured in a bias in antibody response towards the prime vaccine antigen, and secondly, suppression of de novo responses to the boost antigen, measured by comparing with levels generated after one prime dose of vaccine.

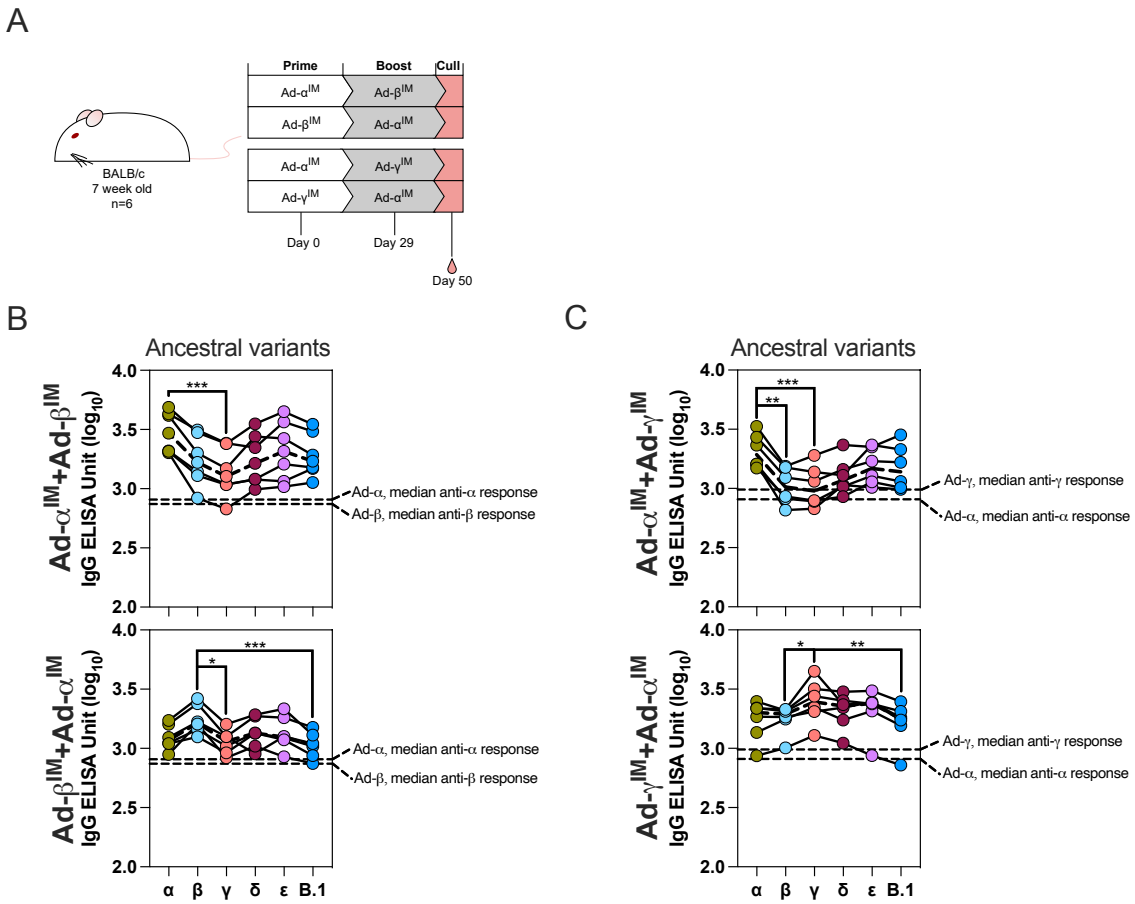

Figure 3.4: Heterologous vaccination with ancestral variant spike vaccines

(A) Vaccination schedule for the heterologous prime-boost of BALB/c mice (n=6) with Ad-α and Ad-β or Ad-γ. Blood was collected 3 weeks post-boost for serologic analyses. The vaccination experiment was completed once. (B) Alpha (α)-, beta (β)-, gamma (γ)-, delta (δ)-, epsilon (ε)- and B.1-reactive IgG (log_{10} ELISA units) in serum of mice vaccinated Ad-α^{IM}+Ad-β^{IM} and Ad-β^{IM}+Ad-α^{IM} (B), or Ad-α^{IM}+Ad-γ^{IM} and Ad-γ^{IM}+Ad-α^{IM} (C), measured via ELISA. In (B) and (C), a dashed line in graphs represents the group median response. To test for significant differences in levels of antibody response to different variant spikes following each regimen, a paired non-parametric Friedman multiple comparisons test was completed (*=P<0.05, **=P<0.01, ***=P<0.001). A list of P values for all graphs is present in Supplemental Table 4.

Following Ad-α^{IM}+Ad-β^{IM} vaccination, the highest levels of spike-reactive serum IgG were observed against alpha spike antigen, which was the antigen encoded in the prime vaccine (Figure 3.4B). The levels of anti-alpha spike IgG were 1.2 log_{10}-fold higher than the levels measured after one dose of Ad-α^{IM} administered in a naïve mouse (median response represented as a dashed line on graph); this suggested a back boosting of antibody

responses derived from prime vaccination occurred. The levels of anti-alpha spike IgG were 1.08 log_{10}-fold higher than anti-beta spike IgG; this suggested a bias in antibody response towards the antigen of prime vaccination.

Levels of anti-beta spike IgG following Ad-α^{IM}+Ad-β^{IM} vaccination were higher (1.12 log_{10}-fold) than the levels measured after one dose of Ad-β^{IM} administered in a naïve mouse (median response represented as a dashed line on graph); this indicated that the priming of mice with non-cognate vaccine (Ad-α^{IM}) enhanced the latter Ad-β^{IM} boost response to cognate beta antigen, and implied that cross-reactive responses were recalled following heterologous boosting. Levels of gamma-, delta-, epsilon- and B.1-reactive IgG were also detected following Ad-α^{IM}+Ad-β^{IM} vaccination.

When mice were vaccinated in the reverse order (Ad-β^{IM}+Ad-α^{IM}), a similar trend was observed, with the highest serum IgG responses measured towards the antigen of the prime vaccine (anti-beta IgG 1.05 log_{10}-fold higher than anti-alpha IgG) (Figure 3.4B). Also, in alignment with the trend observed following Ad-α^{IM}+Ad-β^{IM} vaccination, the responses to alpha and beta antigen were higher than in mice that received Ad-α^{IM} or Ad-β^{IM} vaccine as a single dose. Cross-reactive IgG were detected that bound to the other tested variants.

Vaccinating mice Ad-α^{IM}+Ad-γ^{IM} and Ad-γ^{IM}+Ad-α^{IM} resulted in a similar bias of serum IgG response to prime antigen compared with the antigen of boost vaccination (Figure 3.4C). Following Ad-α^{IM}+Ad-γ^{IM} vaccination, the anti-gamma IgG levels were equivalent to those measured after one dose of Ad-γ^{IM}, signifying that the Ad-γ^{IM}-boosting of Ad-α^{IM}-primed mice did not result in the expansion of dual gamma-alpha cross-reactive IgG. With the reverse regimen however (Ad-γ^{IM}+Ad-α^{IM}), an expansion of these cross-reactive antibodies was observed.

In conclusion, the antigen of prime vaccination was shown to influence the serum IgG responses to secondary antigen; an observed bias in magnitude of IgG responses to the antigen of prime vaccination following heterologous boosting agrees with the antigenic seniority model, that requires the back boosting of prime-derived responses. The trend of higher measured IgG levels specific to the boost vaccine antigen upon heterologous vaccination compared with following prime-only regimen (e.g. Ad-β^{IM}+Ad-α^{IM}> Ad-α^{IM} for anti-alpha IgG), suggested an expansion of cross-reactive antibodies upon heterologous boosting.

2.2.2.2 ACE-2-competition capacity of spike-reactive antibody following heterologous vaccination with ancestral (pre-omicron emergence) variant spike vaccines

The capacity of these antigen-specific antibodies to inhibit ACE-2 binding to spike was then assessed (Figure 3.5). Interestingly, the bias in response to antigen of prime vaccine following heterologous boost noted with IgG data was only partially observed with $ACE2^{comp}$-Ab data. Following both Ad-β^{IM}+Ad-α^{IM} and Ad-α^{IM}+Ad-β^{IM} vaccination, the highest levels of ACE-2 competition were observed by anti-alpha and anti-WT spike antibodies (Figure 3.5A). Following both Ad-α^{IM}+Ad-γ^{IM} and Ad-γ^{IM}+Ad-α^{IM} vaccination, more gamma spike-reactive (γ-$ACE2^{comp}$-Abs) ACE-2-competing antibodies were detected compared with other ancestral variant spike-specific $ACE2^{comp}$-Abs (Figure 3.5B). Antibodies specific to all tested antigens were able to compete with ACE-2 nevertheless. A broader, more cross-reactive response was elicited following Ad-α^{IM}+Ad-β^{IM} vaccination than Ad-β^{IM}+Ad-α^{IM} vaccination. The cross-reactive breadth of responses following Ad-α^{IM}+Ad-γ^{IM} and Ad-γ^{IM}+Ad-α^{IM} however, was similar.

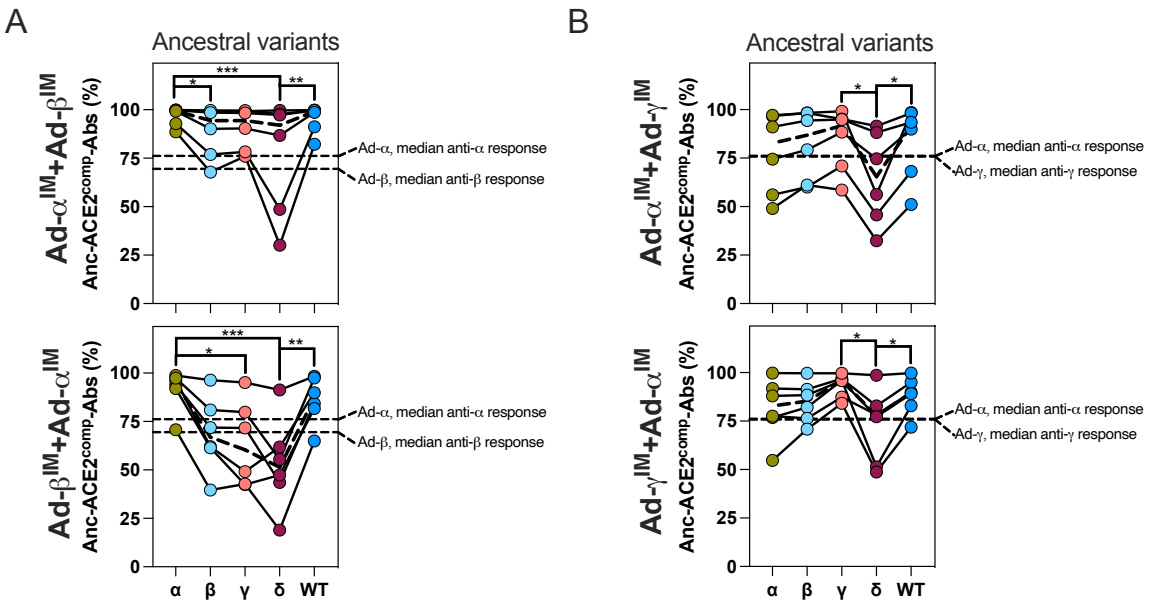

Figure 3.5: ACE-2-competing antibodies following heterologous ancestral variant spike vaccination

Measurement of the capacity of alpha (α)-, beta (β)-, gamma (γ)-, delta (δ)-, and WT-reactive serum antibodies ($ACE2^{comp}$-Abs) to outcompete ACE-2 binding with spike (% ACE-2 competition), following Ad-α^{IM}+Ad-β^{IM} and Ad-β^{IM}+Ad-α^{IM} (A), or Ad-α^{IM}+Ad-γ^{IM} and Ad-γ^{IM}+Ad-α^{IM} (B) vaccination (n=6), measured by Luminex assay. The vaccination experiment was completed once. A dashed line in graphs represents the group median response. To test for significant differences in levels of antibody response to different variant spikes following each regimen, a paired non-parametric Friedman multiple comparisons test was completed (*=P<0.05, **=P<0.01, ***=P<0.001). A list of P values for all graphs is present in Supplemental Table 4.

Therefore, it was less clear what effect priming with a particular ancestral antigen had on latter $ACE2^{comp}$-Ab responses to heterologous antigen, compared with the measured IgG responses.

2.2.3 Heterologous vaccination with omicron and wildtype or alpha vaccines

2.2.3.1 Omicron- and WT-specific responses following heterologous vaccination with omicron and wildtype vaccine

Following the emergence of the antigenically-shifted omicron variant, an omicron vaccine was constructed in-house (ChAdOx1-ο, abbreviated to Ad-ο). The potential influence of immunity derived from WT spike vaccination on latter responses to omicron

vaccine was investigated, given the clinical relevance at the time; omicron vaccines had started being used as boosters in humans (who had been previously vaccinated with WT spike-based vaccines). Importantly, unlike the primary ancestral variants, omicron spike antigen harbours many sequence mutations (Figure 1.3). Hence, there was particular interest in understanding how the immunity from WT spike vaccination influenced the immune responses to omicron spike.

In similar fashion to the experiments completed to investigate imprinting with primary ancestral variants, mice were heterologously vaccinated, using Ad-WT and Ad-o vaccines: Ad-WT^{IM}+Ad-o^{IM} was compared with the reverse regimen Ad-o^{IM}+Ad-WT^{IM}, and homologous (Ad-WT^{IM}+Ad-WT^{IM} and Ad-o^{IM}+Ad-o^{IM}) and prime-only Ad-WT^{IM} and Ad-o^{IM} regimens (Figure 3.6A and Figure 3.6B).

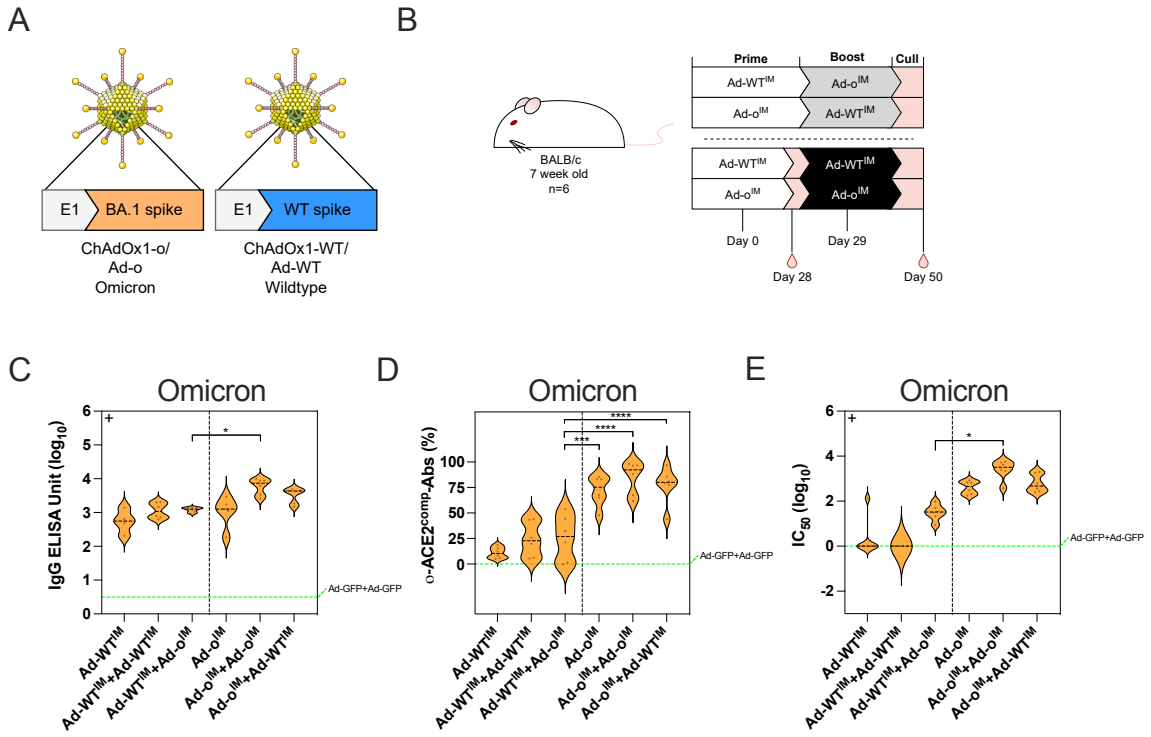

Figure 3.6: Heterologous vaccination with omicron and WT spike-encoding vaccines

(A) Monovalent ChAdOx1 vaccines encoding the full-length sequences of omicron (Ad-ο) and original "WT" (Ad-WT) spike. (B) Vaccination schedule for the heterologous and homologous IM prime-boost of BALB/c mice with Ad-WT and/or Ad-ο vaccines (n=6). Heterologous and homologous experiments were completed separately. Vaccination experiments were completed once. Sera was collected from mice in the homologous prime-boost regimens 4 weeks post-prime to measure for prime-only responses, and 3 weeks post-boost for prime-boost regimens. (C) Levels of total omicron spike-reactive IgG were measured by standardised ELISA and presented as $\log_{10}$ ELISA units (EU). (D) ACE-2-competing omicron S1-specific antibodies (ο-ACE2^{comp}-Abs) were measured by Luminex assay and presented in % ACE-2 competition. (E) Pseudoneutralisation of omicron spike-expressing lentivirus (ο-NAbs) was presented as $\log_{10}$ IC_{50}. Median responses of negative control sera from mice vaccinated with an irrelevant vaccine (ChAdOx1-GFP "Ad-GFP") were included as a green dashed line on graphs. For data in (C), (D), and (E), Ad-WT^{IM}+Ad-ο^{IM} was compared against all other groups statistically. Parametric one-way ANOVA tests were completed when data was normally distributed, otherwise a non-parametric Kruskal-Wallis test was performed (indicated with a "+" at the top left of the graph) (*=P<0.05, ***=P<0.001 and ****=P≤0.0001). On violin plots, the dashed black line represents the group median response.

Omicron spike-binding responses were measured in serum following final vaccination (Figure 3.6C, D and E). Three weeks post-boost, all tested regimens had detectable anti-omicron spike IgG in sera (Figure 3.6C). Ad-WT^{IM}+Ad-ο^{IM}-vaccinated mice had lower anti-omicron spike IgG than Ad-ο^{IM}+Ad-WT^{IM}- and Ad-ο^{IM}+Ad-ο^{IM}-vaccinated (P=0.0105) mice, but had comparable levels to a single IM dose of Ad-ο.

While anti-omicron spike IgG was detected post-Ad-WT^{IM}+Ad-ο^{IM} vaccination, these antibodies were strikingly poor at neutralising omicron (Figure 3.6D). ο-ACE2^{comp}-Ab levels following Ad-WT^{IM}+Ad-ο^{IM} (26.94%) were equivalent to that following Ad-WT^{IM}+Ad-WT^{IM} vaccination (22.82%) (Figure 3.6D). These ο-ACE2^{comp}-Ab levels were significantly lower than those measured following Ad-ο^{IM}+Ad-WT^{IM} (2.97-fold lower; P=0.0001), Ad-ο^{IM}+Ad-ο^{IM} (3.42-fold lower; P≤0.0001) and even Ad-ο^{IM} (2.8-fold lower; P≤0.0001) vaccination. Hence, priming with the WT vaccine resulted in compromised ο-ACE2^{comp}-Ab responses following Ad-ο^{IM} vaccination.

The neutralisation of omicron by serum antibodies was also assessed through a different assay to confirm the results of the ACE-2 competition assay, using in-house omicron pseudotyped virus (Figure 3.6E). A similar trend was noted with levels of omicron pseudotyped virus neutralisation (ο-NAbs), with Ad-WT^{IM}+Ad-ο^{IM} vaccination generating lower levels of ο-NAbs compared with Ad-ο^{IM}+Ad-WT^{IM} (1.91-fold lower), Ad-ο^{IM}+Ad-ο^{IM} (2.35-fold lower) and Ad-ο^{IM} (1.75-fold lower) (Figure 3.6E). In summary, the priming WT vaccine dose strongly limited the ability of heterologous omicron vaccination to induce ο-ACE2^{comp}-Abs and ο-NAbs.

It was then assessed whether a reciprocated effect occurred with anti-WT spike responses (Figure 3.7). The Ad-ο^{IM}+Ad-WT^{IM} regimen was able to generate detectable anti-WT spike IgG titres of comparable level to cognate Ad-WT^{IM} and Ad-WT^{IM}+Ad-WT^{IM} and heterologous Ad-WT^{IM}+Ad-ο^{IM} regimens (Figure 3.7A). However, Ad-ο^{IM}+Ad-WT^{IM} vaccination generated lower levels of WT-ACE2^{comp}-Abs (1.33-fold lower) and WT-NAbs (1.57-fold lower; P=0.0272) than Ad-WT^{IM}+Ad-ο^{IM} (Figure 3.7B and Figure 3.7C). Although slight differences were observed based on the specific antigen, the same trend was seen in both cases: functional antibody responses were biased towards the priming strain regardless of the booster vaccine used. Interestingly, this contrasted the type of imprinting noted between heterologous ancestral variant vaccine regimens demonstrated earlier, where a suppression of latter heterologous booster response because of previous immunity from vaccine-priming was not observed, but solely antigenic seniority; the suppression of responses noted here are indicative of the alternative primary addiction model of imprinting.

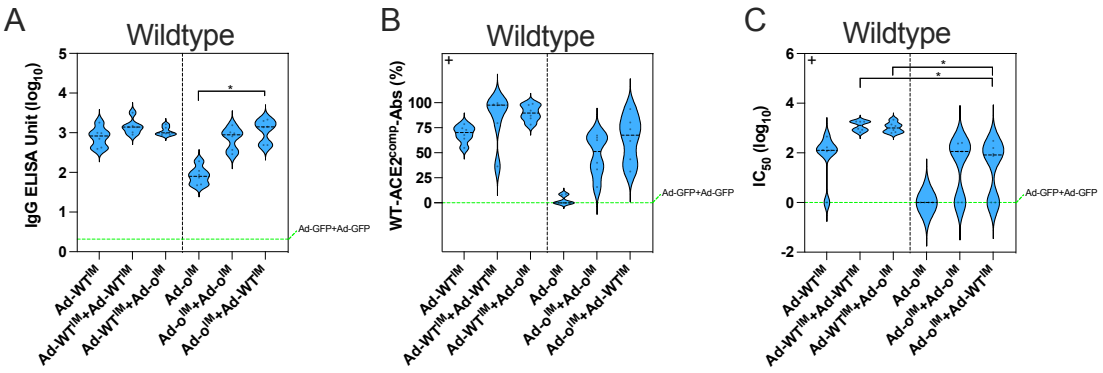

Figure 3.7: WT spike-reactive responses following heterologous and homologous regimens containing Ad-WT and/or Ad-o vaccine

Anti-WT spike immunity in serum following heterologous (Ad-WT^{IM}+Ad-o^{IM} and Ad-o^{IM}+Ad-WT^{IM}) and homologous regimens (Ad-WT^{IM}, Ad-WT^{IM}+Ad-WT^{IM}, Ad-o^{IM} and Ad-o^{IM}+Ad-o^{IM}) containing Ad-WT and/or Ad-o^{IM} (n=6). Vaccination experiments were completed once. Sera was collected from mice in the homologous prime-boost regimens 4 weeks post-prime to measure for prime-only responses, and 3 weeks post-boost for prime-boost regimens. Heterologous and homologous experiments were completed separately. (A) Levels of total B.1 spike-reactive IgG were measured by standardised ELISA and presented as log_{10} ELISA units (EU). (B) ACE-2-competing WT S1-specific antibodies (WT-ACE2^{comp}-Abs) were measured by Luminex assay and presented in % ACE-2 competition. (C) Pseudoneutralisation of WT spike-expressing lentivirus (WT-NAbs) was presented as log_{10} IC_{50}. Median responses of negative control sera from mice vaccinated with an irrelevant vaccine (ChAdOx1-GFP "Ad-GFP") were included as a green dashed line on graphs. For data in (A), (B), and (C), Ad-WT^{IM}+Ad-o^{IM} was compared against all other groups statistically. Parametric one-way ANOVA tests were completed when data was normally distributed, otherwise a non-parametric Kruskal-Wallis test was performed (indicated with a "+" at the top left of the graph) (*=P<0.05). On violin plots, the dashed black line represents the group median response.

2.2.3.2 Cross-reactive responses to ancestral variants following heterologous vaccination with omicron and WT vaccines

The cross-reactive responses to primary ancestral variant spike antigens alpha, beta, gamma and delta were assessed following heterologous regimens (Figure 3.8). Both Ad-WT^{IM}+Ad-o^{IM} and Ad-o^{IM}+Ad-WT^{IM} regimens generated cross-reactive IgG of comparable level (Figure 3.8A). Ad-o^{IM}+Ad-WT^{IM} vaccination however, generated less cross-reactive ancestral spike-binding ACE2^{comp}-Abs (Anc-ACE2^{comp}-Abs) compared with

Ad-WT^{IM}+Ad-o^{IM}-vaccinated mice, although this was not statistically significant (Figure 3.8B).

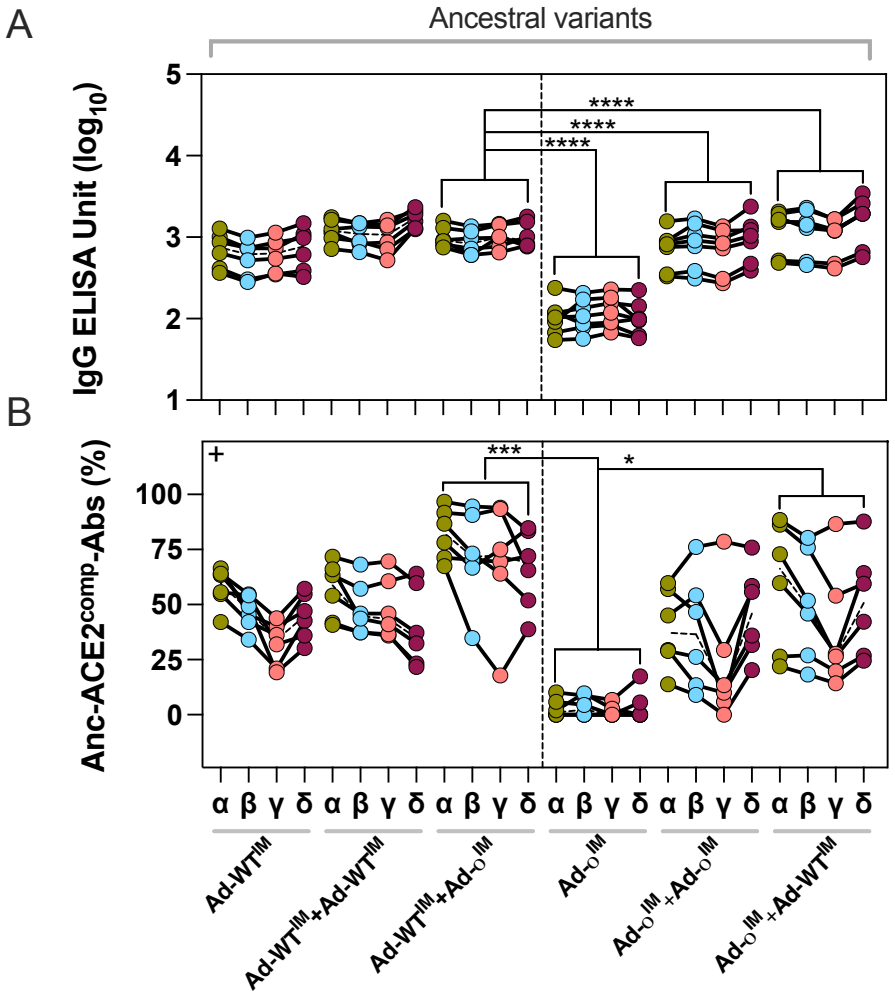

Figure 3.8: Cross-reactive responses to earlier ancestral variants following heterologous and homologous regimens containing Ad-WT and/or Ad-o vaccine

Anti-ancestral spike immunity in serum following heterologous (Ad-WT^{IM}+Ad-o^{IM} and Ad-o^{IM}+Ad-WT^{IM}) and homologous regimens (Ad-WT^{IM}, Ad-WT^{IM}+Ad-WT^{IM}, Ad-o^{IM} and Ad-o^{IM}+Ad-o^{IM}) containing Ad-WT and/or Ad-o^{IM} (n=6). Vaccination experiments were completed once. Sera was collected from mice in the homologous prime-boost regimens 4 weeks post-prime to measure for prime-only responses, and 3 weeks post-boost for prime-boost regimens. Heterologous and homologous experiments were completed separately. (A) IgG and (B) ACE2^{comp}-Ab responses to ancestral variant alpha, beta, gamma and delta spike in serum Ad-WT^{IM}+Ad-o^{IM} was compared with all other regimens statistically using a parametric one-way ANOVA test for (A) or a non-parametric Kruskal-Wallis test for (B) (*=P<0.05, ***=P<0.001 and ****=P≤0.0001). A dashed line represents the group median response.

2.2.3.3 Depletion of WT-spike-reactive omicron RBD-specific antibodies

The measured omicron-reactive antibodies in Ad-WT^{IM}+Ad-o^{IM}-vaccinated mice could be due to either cross-reactive antibodies initially induced by Ad-WT^{IM} and back-boosted by Ad-o^{IM}, or by induction of de novo omicron-specific responses by Ad-o^{IM}. To dissect the origin of the omicron-reactive IgG detected following Ad-WT^{IM}+Ad-o^{IM} vaccination, and distinguish these two aforementioned scenarios, a WT spike pre-absorption assay was completed similarly to that described by Pušnik *et al* (Figure 3.9A)[253]. The Ad-o^{IM}+Ad-WT^{IM} group was also examined for comparison. Samples from either group were pre-incubated with increasing concentrations of WT spike, prior to measuring total IgG against the o-RBD by ELISA. In doing so, levels of IgG that were specific for distinct, mutated epitopes of omicron RBD were measured. The area under the titrated curves (AUC) was used as a measure of level of non-cross-reactive, o-RBD-specific IgG. Following Ad-o^{IM}+Ad-WT^{IM} vaccination, higher titres of non-cross-reactive, o-RBD-specific IgG were detected in sera compared with Ad-WT^{IM}+Ad-o^{IM} vaccination, which induced mostly WT-reactive o-RBD-specific IgG (P=0.0203; Figure 3.9B and Supplemental Figure 1A). Thus, Ad-WT^{IM}+Ad-o^{IM} vaccination induced more of a cross-reactive "back-boosted" as opposed to de novo omicron-specific Ab response.

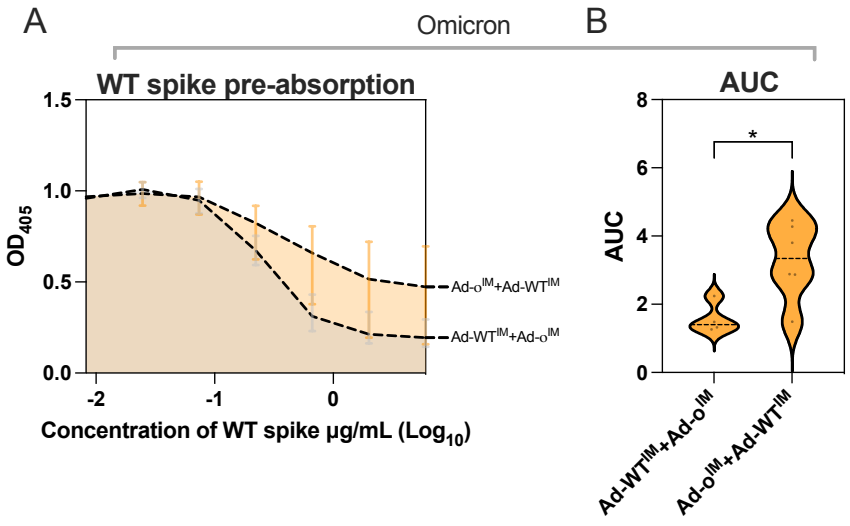

Figure 3.9: Depletion of WT spike-reactive anti-omicron RBD serum IgG

Levels of non-cross-reactive, o-RBD-specific IgG in sera following Ad-WT^{IM}+Ad-o^{IM} and Ad-o^{IM}+Ad-WT^{IM} regimens (n=6, completed once) collected 3 weeks post-boost, as measured through WT spike pre-absorption (depletion) assay. The group median o-RBD IgG levels in samples that were pre-incubated with a range of WT spike concentrations is shown in (A), with error bars representing the ranges at each WT spike concentration. The area under the curve (AUC) values are shown in (B). A parametric t test was completed to compare groups in (B) (*=P<0.05). On violin plots, the dashed black line represents the group median response.

2.2.3.4 Heterologous vaccination with omicron and alpha spike vaccines

To investigate whether the suppression of omicron booster vaccine responses was not a solely WT antigen-specific phenomenon, the previous Ad-WT^{IM}+Ad-o^{IM} experiment was recapitulated however mice were primed with Ad-α^{IM} instead of Ad-WT^{IM} (Ad-α^{IM}+Ad-o^{IM}); the reverse regimen (Ad-o^{IM}+Ad-α^{IM}), as well as homologous (Ad-o^{IM}+Ad-o^{IM} and Ad-α^{IM}+Ad-α^{IM}) and prime only (Ad-α^{IM} and Ad-o^{IM}) regimens were also completed for comparison (Figure 3.10A and Figure 3.10B). The Ad-α^{IM} vaccine was chosen as the alpha variant emerged early towards the beginning of the COVID-19 pandemic, and the alpha variant is more antigenically similar to WT relative to the other variant spike vaccines that we constructed in-house (Figure 1.1 and Table 3.1).

An identical trend in omicron-specific IgG and o-ACE2^{comp}-Abs was observed following Ad-α^{IM}+Ad-o^{IM} to that following Ad-WT^{IM}+Ad-o^{IM} vaccination (Figure 3.7C and Figure 3.7D). Ad-α^{IM}+Ad-o^{IM} vaccination generated detectable omicron spike-reactive IgG of similar level to that generated following Ad-o^{IM} vaccination, but to a lower level than Ad-o^{IM}+Ad-α^{IM} (P=0.0012). o-ACE2^{comp}-Ab levels however, were very low following Ad-α^{IM}+Ad-o^{IM} vaccination: 7.03-fold lower than following Ad-o^{IM} (P≤0.0001) and 7.67-fold lower than Ad-o^{IM}+Ad-α^{IM} (P≤0.0001) (Figure 3.10D).

Likewise, a reciprocated trend was observed with anti-alpha responses (Figure 3.10E and Figure 3.10F). Ad-α^{IM}+Ad-o^{IM} and Ad-o^{IM}+Ad-α^{IM} regimens generated anti-alpha spike IgG of similar level, however, the Ad-α^{IM}+Ad-o^{IM} regimen induced higher levels of α-ACE2^{comp}-Abs than Ad-o^{IM}+Ad-α^{IM} (1.54-fold higher) (Figure 3.10F).

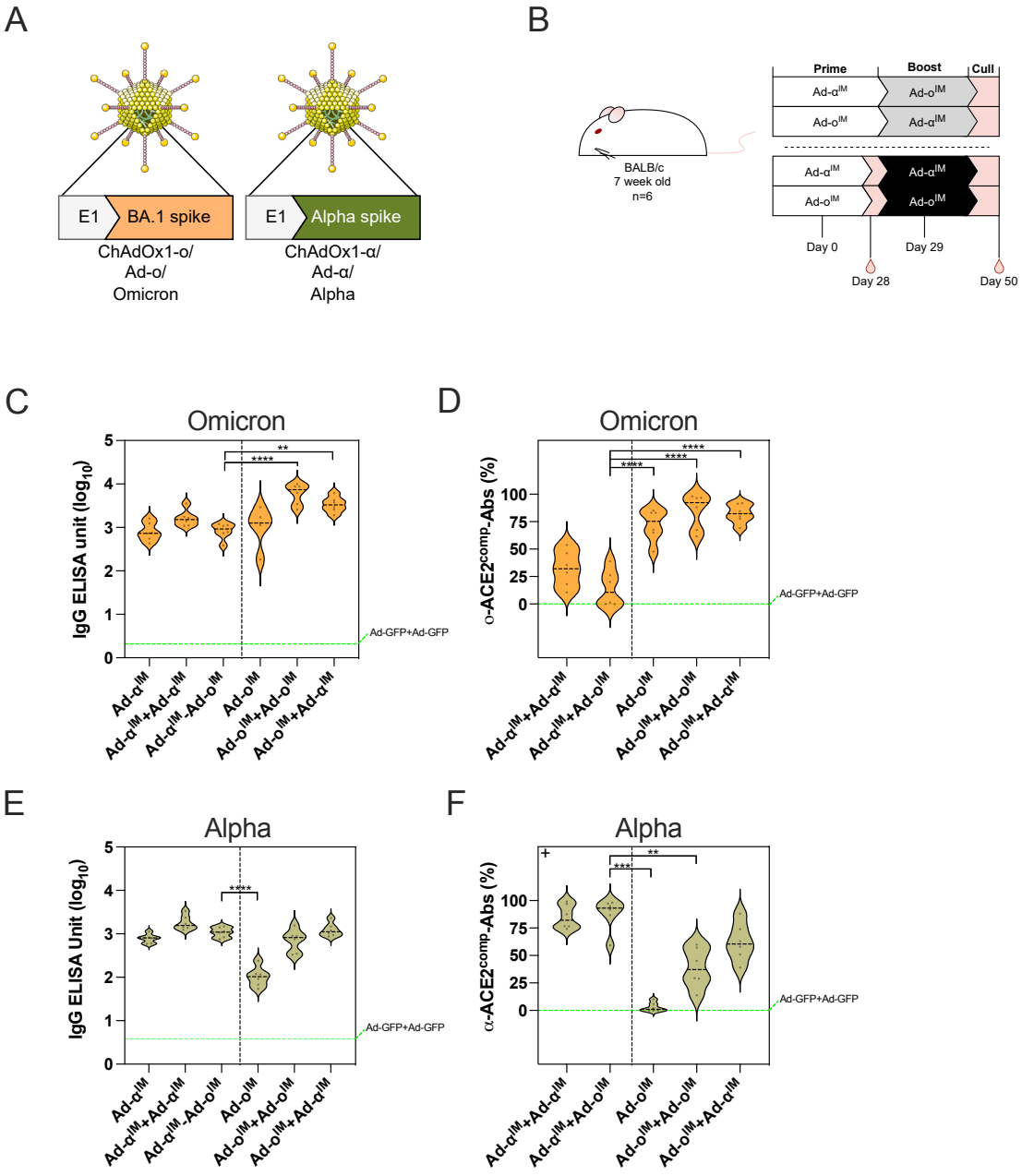

Figure 3.10: Heterologous vaccination with alpha and omicron spike-encoding vaccines

(A) Monovalent ChAdOx1 adenovirus vaccines encoding omicron BA.1 spike (Ad-o) or alpha spike ("Ad-α") sequences. (B) Vaccination schedule for the comparison of heterologous IM prime-boost regimens (Ad-WT^{IM}+Ad-α^{IM} and Ad-o^{IM}+Ad-α^{IM}) and homologous IM prime-boost regimens (Ad-α^{IM}+Ad-α^{IM} and Ad-o^{IM}+Ad-o^{IM}), (n=6); homologous and heterologous experiments were performed separately following identical schedule, and once completed once. Sera were collected from mice in the homologous prime-boost regimens 4 weeks post-prime to measure prime-only responses, and 3 weeks post-boost for prime-boost regimens. (C) Levels of total omicron spike-specific IgG were measured by standardised ELISA and presented as log_{10} ELISA units (EU). (D) ACE-2-competing omicron S1-specific antibodies (o-ACE2^{comp}-Abs) were measured by Luminex assay. Median responses of negative control sera from mice vaccinated with an irrelevant vaccine (ChAdOx1-GFP) were included as a green dashed line on graphs. (E) Levels of total α spike-specific IgG and (F) α-ACE2^{comp}-Abs were measured and presented as in (C) and (D). For IgG and ACE2^{comp}-Abs data in (C), (D), (E) and (F), Ad-α^{IM}+Ad-o^{IM} was compared against all other groups statistically. Parametric one-way ANOVA (Dunnett's multiple comparisons) tests were completed when data was normally distributed, otherwise a non-parametric Kruskal-Wallis test was performed (as indicated with a "+" at the top left corner of the graph). For all data, *=P<0.05, **=P<0.01, ***=P<0.001 and ****=P≤0.0001. On violin plots, the dashed black line represents the group median response.

Cross-reactive IgG to beta, gamma, delta and WT spike were also induced following either Ad-α^{IM}+Ad-o^{IM} or Ad-o^{IM}+Ad-α^{IM} vaccination (Figure 3.11A); levels of IgG were comparable between either regimen. Although not statistically significant, the levels of Anc-ACE2^{comp}-Abs were lower following Ad-o^{IM}+Ad-α^{IM} compared with Ad-α^{IM}+Ad-o^{IM}, aligning with the trend observed in relative levels of Anc-ACE2^{comp}-Abs between Ad-WT^{IM}+Ad-o^{IM} and Ad-o^{IM}+Ad-WT^{IM} observed previously (Figure 3.11B).

Hence, priming with alpha antigen has a similar suppressive effect on latter omicron-specific functional antibody responses to Ad-o^{IM} boost.

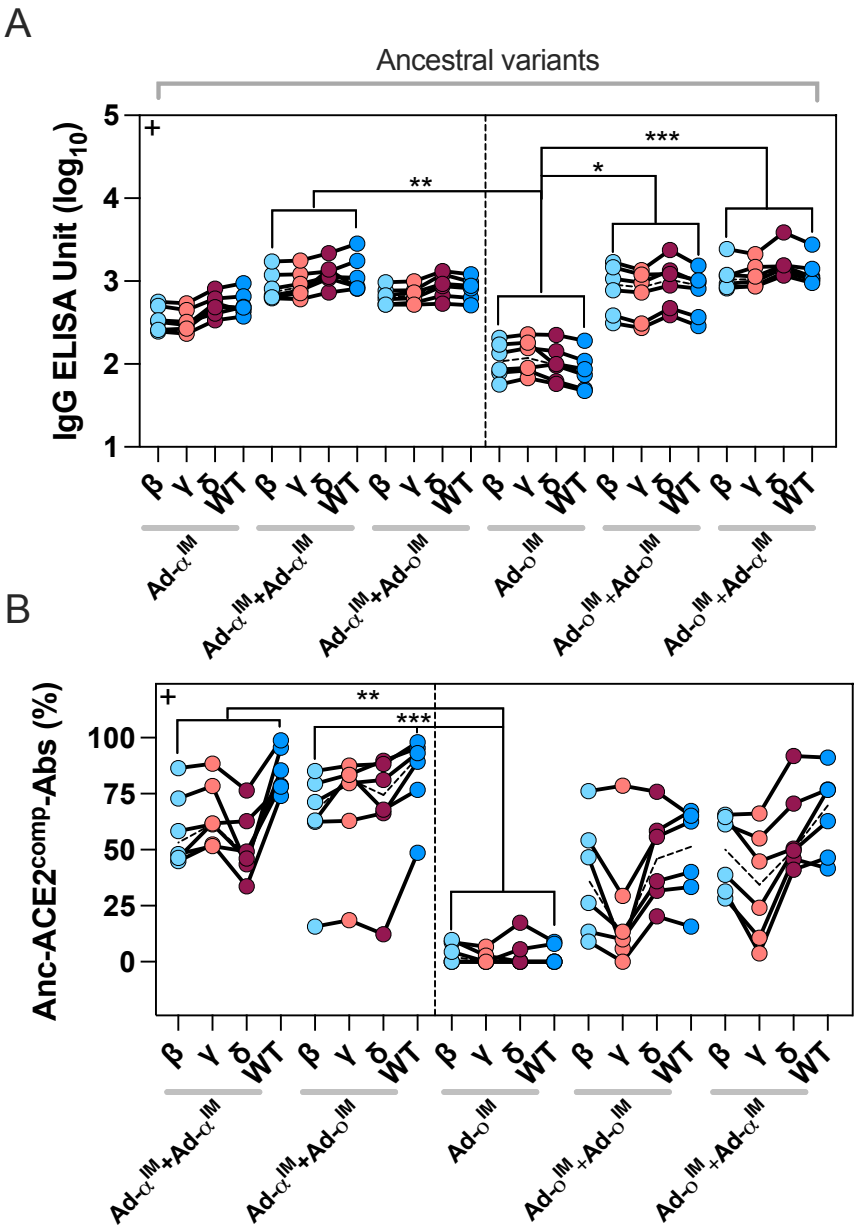

Figure 3.11: Cross-reactive responses to ancestral variants following heterologous vaccination

IgG (A) and ACE2^{comp}-Ab (B) responses to ancestral (variant) beta, gamma, delta and WT spike in serum following heterologous (Ad-WT^{IM}+Ad-α^{IM} and Ad-o^{IM}+Ad-α^{IM}) and homologous (Ad-α^{IM}+Ad-α^{IM} and Ad-o^{IM}+Ad-o^{IM}) regimens, (n=6); Homologous and heterologous experiments were performed separately following identical schedule, and only completed once. Sera were collected from mice in the homologous prime-boost regimens 4 weeks post-prime to measure prime-only responses, and 3 weeks post-boost for prime-boost regimens. Ad-α^{IM}+Ad-o^{IM} was compared with all other regimens statistically using a non-parametric Kruskal-Wallis test for both (A) and (B), as data were non-normally distributed (*=P<0.05, **=P<0.01 and ***=P<0.001). A dashed line represents the group median response.

2.2.3.5 Heterologous vaccination with omicron and other non-ChAdOx1-based WT vaccines

It was then assessed whether priming with other non-ChAdOx1-based WT spike vaccines also influenced the latter omicron-specific responses upon Ad-o^{IM} boost, to confirm that the imprinting observed following Ad-WT^{IM} vaccination was not a ChAdOx1 vaccine-specific phenomenon; this would also ensure that the apparent immunological imprinting observed in the Ad-containing prime-boost regimens was not solely as a result of suppressive anti-ChAdOx1 immunity (anti-vector immunity) established after prime vaccination.

To do this, mice were vaccinated with three other WT spike vaccines: ChAdOx2-WT (abbreviated Ad2-WT), an adenovirus vector vaccine derived from the AdC68 serotype (as opposed to Y25 for ChAdOx1), Pfizer-WT (Pfizer-BioNTech BNT162b2), an mRNA vaccine encoding WT spike, and Novavax-WT (NVX-CoV2373), a recombinant WT spike protein vaccine formulated with adjuvant (Figure 3.12A). Blood was sampled 4 weeks post-prime, and then mice were boosted with Ad-o, and blood collected 3 weeks post-boost for analysis. The reverse order regimens (Ad-o-prime, WT spike vaccine-boost) were completed for comparison.

The omicron spike-specific IgG responses were measured in sera following prime and prime-boost, and compared along with reference IgG responses following Ad-WT^{IM} and Ad-o^{IM} (Figure 3.12B, C and D). Following priming with Ad2-WT, Pfizer-WT or Novavax-WT, levels of cross-reactive omicron spike-binding IgG were detected in serum, to similar levels generated in mice that received one Ad-o^{IM} dose. In regimens where WT vaccine was used for the prime and Ad-o^{IM} for the boost (Ad2-WT^{IM}+Ad-o^{IM}, Pfizer-WT^{IM}+Ad-o^{IM}, Novavax-WT^{IM}+Ad-o^{IM}), increased amounts of anti-omicron spike IgG were measured following

boost compared with the levels measured after prime, and higher levels were measured compared with the levels induced after Ad-oIM prime: Ad2-WTIM+Ad-oIM>Ad2-WTIM; P<0.0001, Ad2-WTIM+Ad-oIM>Ad-oIM; P=0.0007, Novavax-WTIM+Ad-oIM>Novavax-WTIM; P<0.0001, Novavax-WTIM+Ad-oIM>Ad-oIM; P<0.00001. Such observations indicated that Ad-oIM-boosting of (non-ChAdOx1) WT vaccine-primed mice boosted pre-existing antibody responses, resulting in a higher magnitude of omicron-specific IgG than generated after Ad-oIM prime. This contrasted what was observed earlier following Ad-WTIM+Ad-oIM vaccination, where Ad-oIM-boosting resulted in levels of anti-omicron spike IgG of statistically comparable, slightly lower level to that measured after Ad-oIM prime, as opposed to higher levels.

Higher levels omicron spike IgG were observed in the heterologous regimens where Ad-oIM was the prime vaccine (Ad-oIM+Ad2-WTIM, Ad-oIM+Pfizer-WTIM, Ad-oIM+Novavax-WTIM) compared with the reverse regimens where WT spike vaccine was the prime vaccine (Ad2-WTIM+Ad-oIM, Pfizer-WTIM+Ad-oIM, Novavax-WTIM+Ad-oIM): Ad-oIM+Ad2-WTIM>Ad2-WTIM+Ad-oIM; P=0.0003.

To further dissect the serological IgG responses, omicron RBD (o-RBD)-reactive IgG levels in sera were also measured (Figure 3.12E, F and G). The reference levels of anti-o-RBD following the Ad-oIM-prime group were not completed, hence not present on graphs. Interestingly, levels of o-RBD-specific IgG did not statistically increase following Ad-oIM-boost, as was observed with omicron spike-reactive IgG levels. This likely indicated that the boost in omicron spike-reactive IgG observed following WT spike-prime, Ad-oIM-boost regimens in Figure 3.12B, C and D was mainly towards non-RBD epitopes that were conserved between WT and omicron spike antigens. In alignment with the trend in anti-

omicron spike IgG observed in Figure 3.12B, C and D, the heterologous prime-boost regimens where Ad-o^{IM} was the prime antigen, generated greater quantities of anti-o-RBD IgG than the reverse regimens where WT spike vaccine was the prime vaccine: Ad-o^{IM}+Ad2-WT^{IM}>Ad2-WT^{IM}+Ad-o^{IM}; P=0.0028, Ad-o^{IM}+Pfizer-WT^{IM}>Pfizer-WT^{IM}+Ad-o^{IM}; P=0.0002, Ad-o^{IM}+Novavax-WT^{IM}>Novavax-WT^{IM}+Ad-o^{IM}; P=0.0054 (Figure 3.12E, F and G).

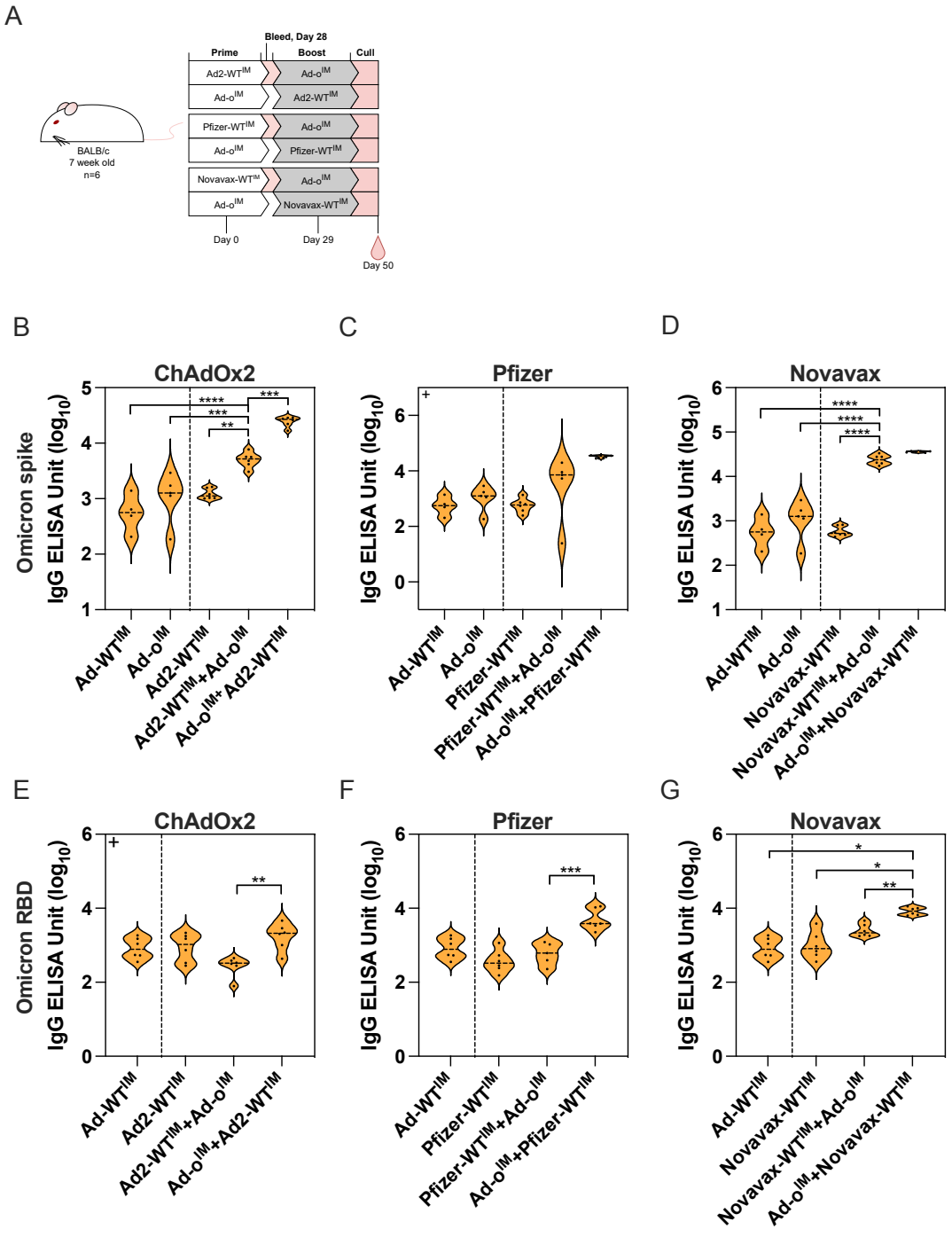

Figure 3.12: Heterologous vaccination of mice with non-ChAdOx1 WT spike vaccines and ChAdOx1 omicron vaccine

(A) Vaccination schedule for the heterologous prime-boost of mice with ChAdOx2-WT (Ad2-WT), Pfizer-WT or Novavax-WT (all non-ChAdOx1 WT spike vaccines) with Ad-o^{IM} (n=6). The vaccination experiment was only completed once. Blood sampling was completed 4 weeks post-WT spike vaccine prime, and 3 weeks post-boost vaccination for all regimens. Levels of omicron spike-reactive IgG in serum following regimens containing ChAdOx2-WT (Ad2-WT) (B), Pfizer-WT (C), or Novavax-WT (D) vaccines, measured by ELISA. Levels of omicron RBD (o-RBD)-reactive IgG in serum following regimens containing ChAdOx2-WT (Ad2-WT) (E), Pfizer-WT (F), or Novavax-WT (G) vaccines, measured by ELISA. Reference levels of IgG following one dose of Ad-o^{IM} and Ad-WT^{IM} were included from separate experiments to the graphs and separated to the left by dashed black lines. The WT spike vaccine-prime, Ad-o^{IM}-boost regimen was statistically compared to all other groups using a one-way ANOVA (Dunnett's multiple comparisons) when data were normally distributed, or using a Kruskal-Wallis test when data were non-normally distributed (as indicated by a "+" at the top left corner of the graph). (*=P<0.05, **=P<0.01, ***=P<0.001 and ****=P<0.0001). On violin plots, the dashed black line represents the group median response. During vaccinations, one mouse died due to reasons unrelated to the vaccinations within the Pfizer-WT+Ad-o group, hence five instead of six datapoints are present on figures for this group. Moreover, there was insufficient sera collected following Ad-WT-prime for two samples, hence only four instead of six datapoints are present on figures for this group.

The neutralisation capacity of sera following the heterologous non-ChAdOx1 WT spike-containing regimens was assessed via ACE-2 competition Luminex assay and pseudoneutralisation assay (Figure 3.13). For reasons of limited sample availability, the prime-only regimens were not included for this analysis. Importantly, very high ACE-2-competing responses were observed following all heterologous regimens tested in this experiment; thus, these samples were diluted 4X more than the previous Ad-WT^{IM}+Ad-o^{IM} experiment presented in Figure 3.6D, so the o-$ACE2^{comp}$-Ab data presented here cannot be directly compared with that presented in Figure 3.6D.

The trend observed with omicron spike- and RBD-reactive IgG was also noted with relative levels of o-$ACE2^{comp}$-Abs and o-NAbs; the regimens with Ad-o^{IM} as the prime vaccine and non-ChAdOx1 WT spike vaccine as the boost elicited higher levels of o-

ACE2^{comp}-Abs and o-NAbs than the reverse regimens: for o-ACE2^{comp}-Abs, Ad-o^{IM}+Ad2-WT^{IM}>Ad2-WT^{IM}+Ad-o^{IM}; P=0.0068, Ad-o^{IM}+Novavax-WT^{IM}>Novavax-WT^{IM}+Ad-o^{IM}; P=0.0152, and for o-NAbs, Ad-o^{IM}+Ad2-WT^{IM}>Ad2-WT^{IM}+Ad-o^{IM}; P=0.0280, Ad-o^{IM}+Novavax-WT^{IM}>Novavax-WT^{IM}+Ad-o^{IM}; P=0.0256 (Figure 3.13A and Figure 3.13B). Although not statistically significant, the Pfizer-WT-containing regimens showed similar trend in relative levels of o-ACE2^{comp}-Abs and o-NAbs.

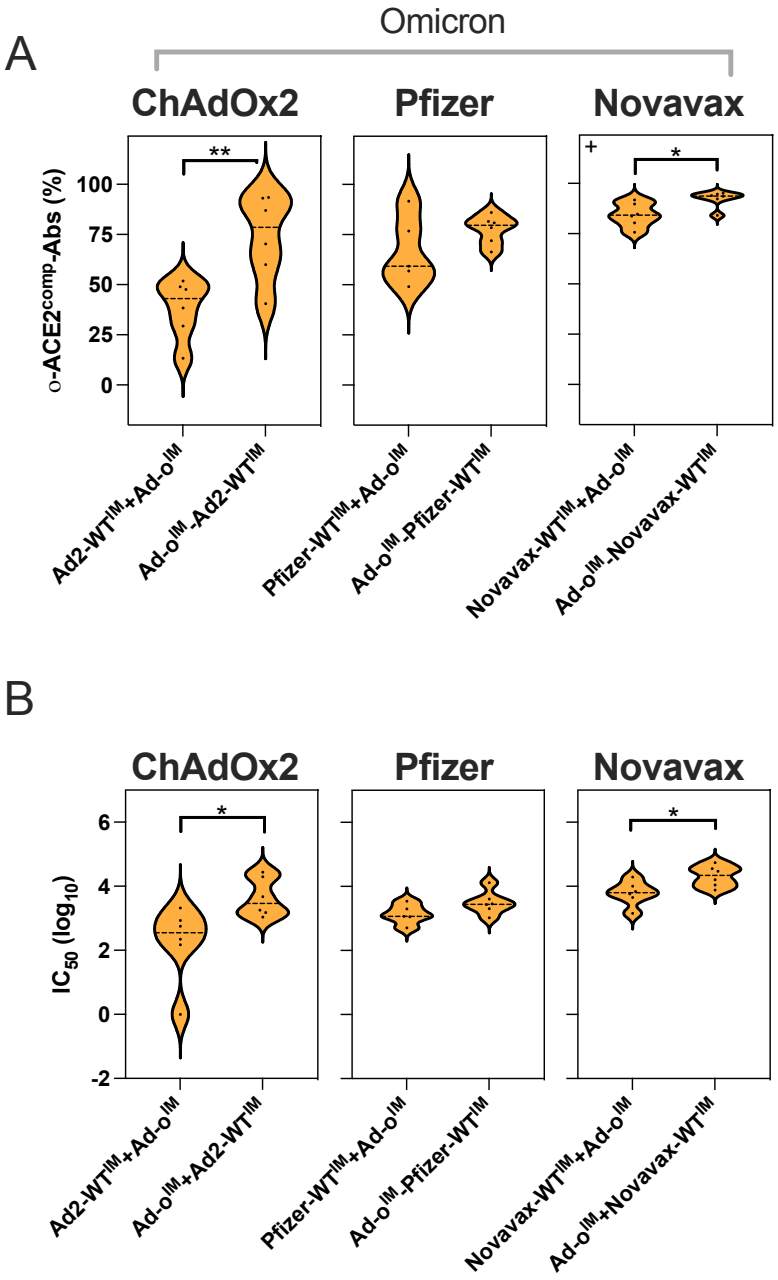

Figure 3.13: Neutralisation capacity of serum following heterologous vaccination of mice with non-ChAdOx1 WT spike vaccines and ChAdOx1 omicron vaccine

(A) ACE-2-competing omicron S1-specific antibodies (ο-ACE2^{comp}-Abs) and (B) omicron pseudovirus-neutralising antibodies (ο-NAbs) in the sera of mice vaccinated in heterologous prime-boost regimens containing ChAdOx2-WT, Pfizer-WT or Novavax-WT and Ad-ο^{IM} (n=6, only completed once, and blood sampling conducted 3 weeks post-boost). To compare regimens statistically, an unpaired t test (for normal data) or Mann-Whitney test (for non-normal data, as indicated by a "+" at the top left corner of the graph) was performed. *=P<0.05, **=P<0.01. On violin plots, the dashed black line represents the group median response. During vaccinations, one mouse died due to reasons unrelated to the vaccinations within the Pfizer-WT+Ad-ο group, hence five instead of six datapoints are present on figures for this group.

Despite these relative reductions in omicron neutralisation in the regimens that were primed with the WT spike vaccine compared with the reverse regimens, the levels of neutralisation measured were still much higher than those following the Ad-WT^{IM}+Ad-ο^{IM} regimen, where measured responses were lower than a single dose of Ad-ο^{IM}, and Ad-WT^{IM} priming appeared to have a suppressive effect on the magnitude of omicron-specific response upon Ad-ο^{IM} boost. Henceforth, although in mice primed with non-ChAdOx1 WT vaccine, Ad-ο^{IM}-boosting generated limited ο-RBD IgG, the overall magnitudes of omicron neutralising antibodies were high; nevertheless, the antigen of prime vaccination was still shown to influence the latter boost response, as a bias in magnitude of omicron-specific antibody response was observed. The overall elevated magnitude in neutralisation noted in these heterologous non-ChAdOx1 WT vaccine-containing regimens compared with the Ad-WT^{IM}+Ad-ο^{IM} and Ad-ο^{IM}+Ad-WT^{IM} regimens presented earlier, could be due to a lack of suppressive anti-vector-mediated immunity, or possibly differences in the intrinsic immunogenicity of the non-ChAdOx1 WT vaccines (compared with ChAdOx1 WT vaccine) and the particular immunogenicity of the non-ChAd^{IM}+ChAd^{IM} and ChAd^{IM}+non-ChAd^{IM}

prime-boost combinations. The role of anti-vector immunity will be explored further later in this chapter.

2.2.3.6 Depletion of WT spike-reactive omicron RBD-specific antibodies derived from heterologous non-ChAdOx1 WT spike vaccine and Ad-ο regimens

To further dissect the origin of the omicron-reactive IgG detected after vaccinating mice by priming them with Ad2-WT, Pfizer-WT or Novavax-WT vaccine and then boosting them with Ad-ο (and the reverse orientation), WT spike pre-absorption assay was conducted as completed previously in Figure 3.9. I hypothesised that the origin of the ο-RBD-reactive IgG detected following the Ad2-WT^{IM}+Ad-ο^{IM}, Pfizer-WT^{IM}+Ad-ο^{IM} and Novavax-WT^{IM}+Ad-ο^{IM} regimens was from the prime, as opposed to boost vaccination. This hypothesis was formed from two previous observations:

- Ad-WT^{IM}+Ad-ο^{IM}-derived ο-RBD IgG was prime-derived (Figure 3.9), and I predicted that a similar observation would be noted with these non-ChAdOx1 WT spike vaccine-containing regimens
- Similar levels of ο-RBD IgG were measured following prime with non-ChAdOx1 WT spike vaccine, and non-ChAdOx1 WT spike vaccine-prime, Ad-ο-boost regimens, which suggested a lack of de novo response to Ad-ο and subsequent ο-RBD IgG formation (Figure 3.12)

In alignment with this hypothesis, the Ad2-WT^{IM}+Ad-ο^{IM} regimen elicited less ο-RBD-specific IgG that was non-WT spike-cross-reactive, i.e., derived from a de novo antibody response to Ad-ο^{IM}, compared with the reverse regimen (Ad-ο^{IM}+Ad2-WT^{IM}) (P=0.0087) (Figure 3.14A). The Novavax-WT-containing regimens also had a similar trend in relative levels of non-cross-reactive ο-RBD-specific IgG; Ad-ο^{IM}+Novavax-

WT^{IM}>Novavax-WT^{IM}+Ad-ο^{IM}, P=0.0094 (Figure 3.14C). The Pfizer-WT vaccine-containing regimens interestingly however, did not share this trend, with ο-RBD-reactive IgG having been depleted by WT spike to a comparable degree (Figure 3.14B).

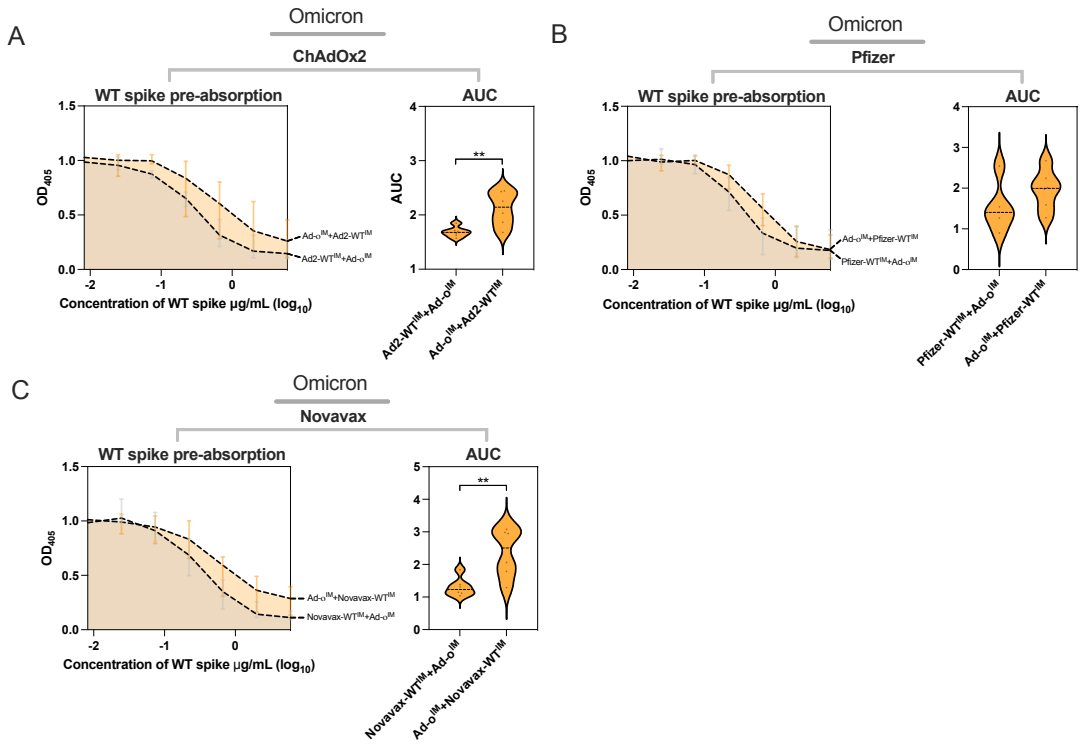

Figure 3.14: Depletion of WT spike-reactive anti-omicron RBD serum IgG

Levels of non-cross-reactive, o-RBD-specific IgG in sera following Ad2-WT^{IM}+Ad-ο^{IM} and Ad-ο^{IM}+Ad2-WT^{IM} (A), Pfizer-WT^{IM}+Ad-ο^{IM} and Ad-ο^{IM}+Pfizer-WT^{IM} (B), and Novavax-WT^{IM}+Ad-ο^{IM} and Ad-ο^{IM}+Novavax-WT^{IM} (C) (all n=6, with vaccination experiments completed only once, and blood sampling conducted 3 weeks post-boost), as measured through WT spike pre-absorption (depletion) assay. The group median o-RBD IgG levels in samples that were pre-incubated with a range of WT spike concentrations, with error bars representing the ranges at each WT spike concentration. The area under the curve (AUC) values are shown on the right. Parametric t tests were completed to compare AUC values in (A), (B) and (C) (*=P<0.05, **=P<0.01). On violin plots, the dashed black line represents the group median response. The raw data for the depletion curves is present in Supplemental Figure 1B. During vaccinations, one mouse died due to reasons unrelated to the vaccinations within the Pfizer-WT+Ad-ο group, hence five instead of six datapoints are present on figures for this group.

In summary, indications of imprinting were observed in regimens where non-ChAdOx1-based WT spike vaccines were used as the prime vaccine and then Ad-ο as the

booster vaccine, however, priming with these non-ChAdOx1-based WT spike vaccines did not seem to result in suppression of Ad-ο responses to the same extent the Ad-WT vaccine did.

2.3 Passive antibody transfer

Following observation that the priming of mice with Ad-WT vaccine resulted in reduced Ad-ο immunogenicity, I hypothesised that suppressive, cross-reactive WT spike antibodies and/or anti-vector antibodies derived from prime vaccination were limiting the de novo responses to omicron vaccine booster. In order to understand this further, a passive serum transfer experiment was performed (Figure 3.15A). In brief, serum generated from WT spike-vaccinated donor mice was intravenously (IV) injected into naïve recipient mice. Recipient mice were then vaccinated IM with Ad-ο, with immune responses assessed a further 3 weeks later. Donor mice were vaccinated following a prime-boost rather than prime-only regimen to increase the antibody concentration of the sera for transfer, as the IV injection volume could not exceed 100 μL; this enabled greater quantities of antibody to be passively transferred to the recipient mice, closer to the levels generated in a mouse following an active immune response. The influence of sera from mice vaccinated with different WT spike vaccines (Novavax NVX-CoV2373, Pfizer-BioNTech BNT162b2) was assessed in addition to Ad-WT-derived sera. Additionally, to assess whether anti-ChAdOx1 ("anti-vector") antibodies were suppressive to the latter Ad-ο response and part of the Ad-WT imprint, serum that was derived from mice primed and boosted with the same vector encoding an irrelevant GFP antigen (ChAdOx1-GFP) was transferred into a separate group.

A range of WT spike-reactive IgG levels were detected between groups prior to IM administration of Ad-ο (Figure 3.15B). Mice that received sera from Novavax-WT^{IM}+Novavax-WT^{IM}-vaccinated mice had the highest levels of transferred anti-WT IgG, followed by those that received Pfizer-WT^{IM}+Pfizer-WT^{IM} sera, and then Ad-WT^{IM}+Ad-WT^{IM} sera. Only mice that received ChAdOx1 vaccine sera had detectable anti-ChAdOx1 IgG (Figure 3.15B). Anti-WT spike IgG levels following serum transfer of Novavax-WT^{IM}+Novavax-WT^{IM}- or Pfizer-WT^{IM}+Pfizer-WT^{IM}-vaccinated mice were equivalent to or higher than serum levels seen in mice directly IM vaccinated with Ad-WT, confirming the level of serum IgG was physiologically relevant to that expected in mice following in vivo responses.

Omicron spike-reactive IgG and ο-$ACE2^{comp}$-Abs were measured in recipient mouse serum post-transfer to assess the differences in baseline level of cross-reactivity prior to the vaccination with Ad-ο (Figure 3.15C). Levels of omicron spike-reactive IgG were detected in mice that received Ad-WT^{IM}+Ad-WT^{IM}, Novavax-WT^{IM}+Novavax-WT^{IM} and Pfizer-WT^{IM}+Pfizer-WT^{IM}, and were strongly associated with overall anti-WT spike antibody levels. Low but detectable levels of ο-$ACE2^{comp}$-Abs were measured in mice that received Novavax-WT^{IM}+Novavax-WT^{IM} and Pfizer-WT^{IM}+Pfizer-WT^{IM} sera as well (Figure 3.15C).

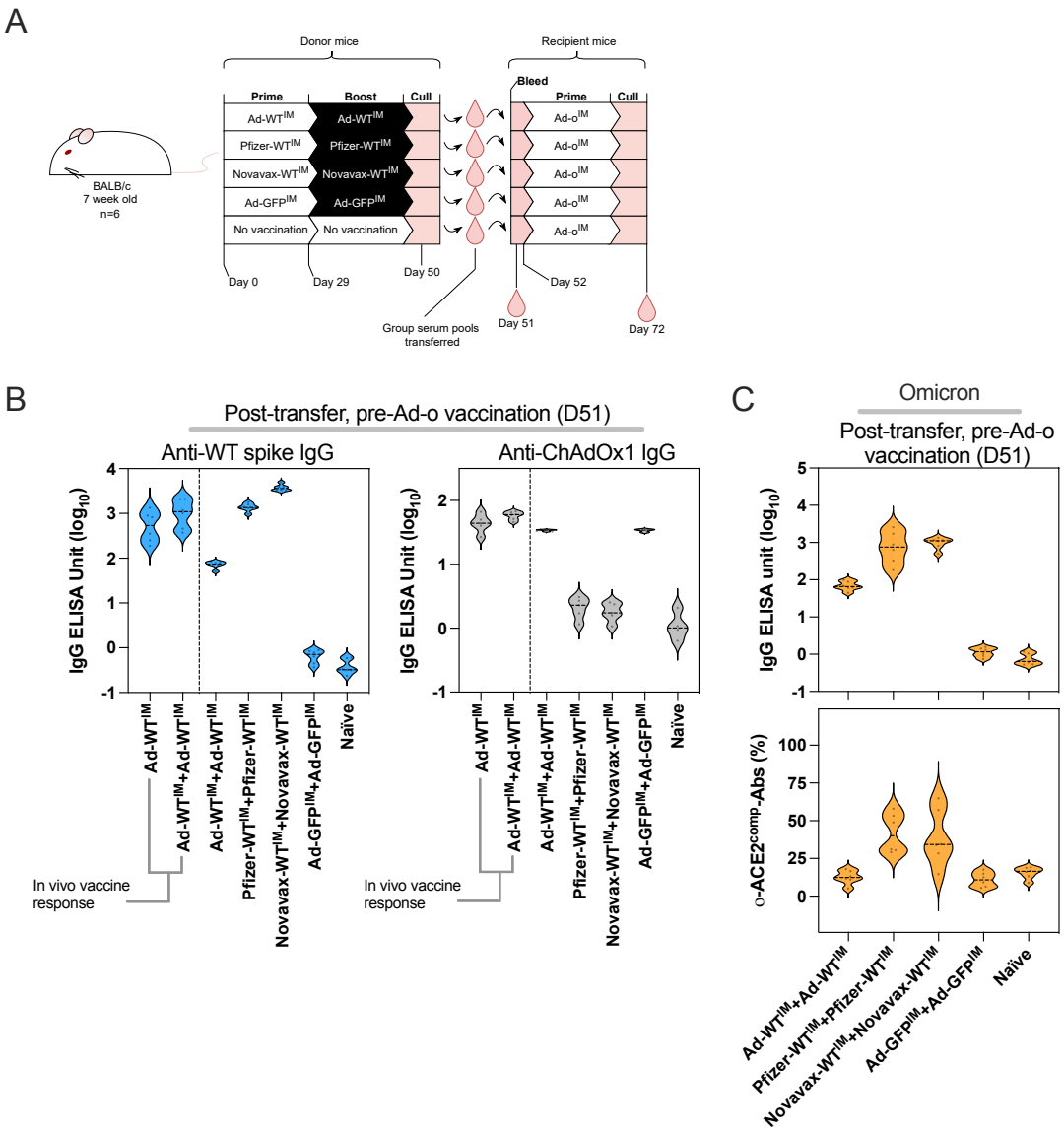

Figure 3.15: Passive transfer of WT spike vaccine sera and ChAdOx1 omicron vaccination

(A) Vaccination and serum transfer schedule. Donor mice (n=6) were vaccinated (or left unvaccinated for negative control), with sera then collected and transferred to naïve recipient mice (n=6). Recipient mice were then vaccinated with Ad-o IM. The experiment was only completed once. Sera from recipient mice were collected after transfer of donor sera before vaccination (day 51) and 3 weeks post Ad-o vaccination (day 72). (B) Levels of anti-WT spike IgG and anti-ChAdOx1 IgG in recipient mice sera, post-transfer of donor sera, and before Ad-o vaccination (day 51). Reference levels of IgG following an in-vivo Ad-WT^{IM} and Ad-WT^{IM}+Ad-WT^{IM} were added to graphs. (C) Levels of anti-omicron spike IgG and o-ACE2^{comp}-Abs in mice sera, post-transfer of donor sera, and before Ad-o vaccination (day 51). On violin plots, the dashed black line represents the group median response.

3 weeks after Ad-ο vaccination, mice that received vaccinated mouse sera had reduced omicron spike-specific IgG and ο-ACE2^{comp}-Ab levels compared with control mice that received naïve sera (Figure 3.16A). The omicron spike IgG levels were significantly lower than those following naïve serum transfer control group in mice that received Ad-WT^{IM}+Ad-WT^{IM} (P≤0.0001), Novavax-WT^{IM}+Novavax-WT^{IM} (P=0.0055) and Ad-GFP^{IM}+Ad-GFP^{IM} (P=0.0014) sera. Likewise, these groups had significantly lower ο-ACE2^{comp}-Abs than the control naïve serum transfer group (Ad-WT^{IM}+Ad-WT^{IM}, P=0.0127; Novavax-WT^{IM}+Novavax-WT^{IM}, P≤0.0001; Ad-GFP^{IM}+Ad-GFP^{IM}, P=0.0421). Mice that received Pfizer-WT^{IM}+Pfizer-WT^{IM} sera had lower levels of omicron-specific response to the naïve control, however, these differences were not statistically significant.

As the transferred sera had some level of omicron-reactive IgG (Figure 3.15C) that could have contributed to the post-vaccination responses measured (Figure 3.16A), the fold change in omicron-specific response was calculated (omicron post-transfer to post-Ad-ο) to assess the degree of de novo response to Ad-ο that was induced by Ad-ο vaccination (Figure 3.16B). Differences in fold change (log_2) indicated that mice that received WT spike vaccine sera had generated much lower de novo omicron spike IgG in response to Ad-ο vaccination than the naïve group, that had a median 10.17-log_2fold change (Ad-WT^{IM}+Ad-WT^{IM}: median 1.90-log_2fold change, Novavax-WT^{IM}+Novavax-WT^{IM}: median -1.31-log_2fold change and Pfizer-WT^{IM}+Pfizer-WT^{IM}: median -0.50-log_2fold change; P≤0.0001 for all vs. naïve). The Ad-GFP^{IM}+Ad-GFP^{IM} group, however, showed far less suppression of de novo response (median 8.25-log_2fold change in omicron spike-specific IgG), but was still lower than the naïve group (P=0.0014). Interestingly, for mice that received Novavax-WT^{IM}+Novavax-WT^{IM} and Pfizer-WT^{IM}+Pfizer-WT^{IM} sera, the median log_2 fold change was negative, meaning that de novo Ad-ο response was not induced and

instead only a waning of transferred cross-reactive IgG (after day 51) was observed. This trend of lower fold change in groups that received sera from WT spike-vaccinated mice was also observed with measured o-ACE2^{comp}-Ab levels. Ad-WT^{IM}+Ad-WT^{IM} mice had lower fold changes in omicron response relative to naïve and Ad-GFP^{IM}+Ad-GFP^{IM} groups, however, differences were not statistically significant. This suggests that pre-existing anti-Ad vector antibodies had only a modest impact on the ability of Ad-o to induce an omicron-specific response, especially in comparison to the groups that received anti-WT spike antibodies.

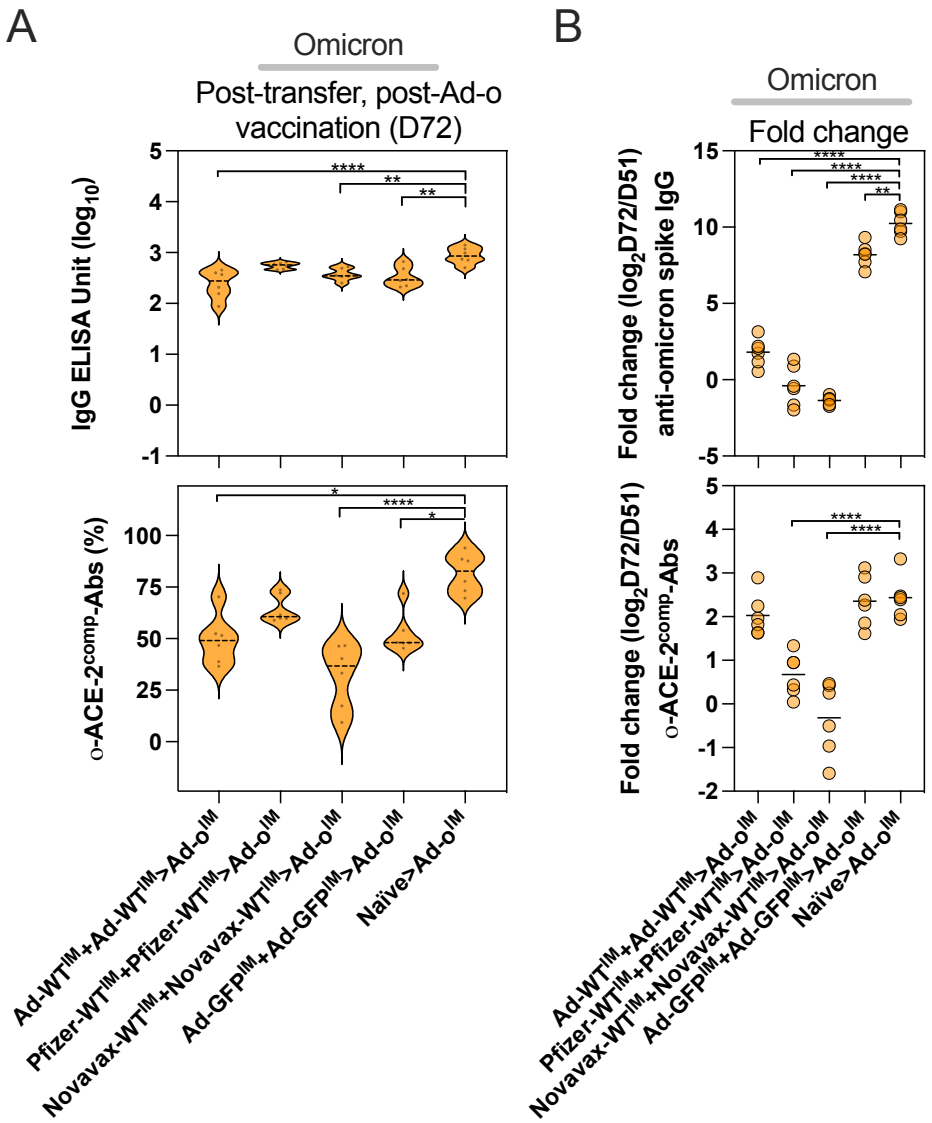

Figure 3.16: Omicron-specific responses following omicron vaccination in mice that received prior passive transfer of WT spike vaccine sera

Omicron-specific responses in recipient mice (n=6) following the transfer of donor sera, and then IM omicron vaccination. The experiment was completed only once. (A) Levels of anti-omicron spike IgG and ο-ACE2^{comp}-Abs in mouse sera, post-transfer of donor sera, and after Ad-ο vaccination (day 72). A one-way ANOVA test was completed on IgG data, and Kruskal-Wallis test on ο-ACE2^{comp}-Abs data, to compare regimens statistically. (B) Fold change in anti-omicron spike IgG and ο-ACE2^{comp}-Ab levels between days 51 and 72. Fold change was calculated as log_2(Day 72/Day 51). One-way ANOVA tests were used to statistically compare groups. For all data, *=P<0.05, **=P<0.01, ***=P<0.001 and ****=P≤0.0001. On violin plots, the dashed black line represents the group median response.

To determine whether the level of anti-WT antibody had an impact on the induction of omicron-specific responses, the fold change in omicron-specific response vs. amount of anti-WT spike IgG were compared (Figure 3.17). Both the magnitude of omicron spike-specific IgG (Figure 3.17A) and ο-ACE2^{comp}-Ab (Figure 3.17B) response post-Ad-ο vaccination were negatively correlated with quantity of WT spike IgG transferred; r=-0.9747 (P≤0.0001) and r=-0.8254 (P≤0.0001), for omicron spike-specific IgG vs. WT spike IgG and ο-ACE2^{comp}-Abs vs. WT spike IgG, respectively.

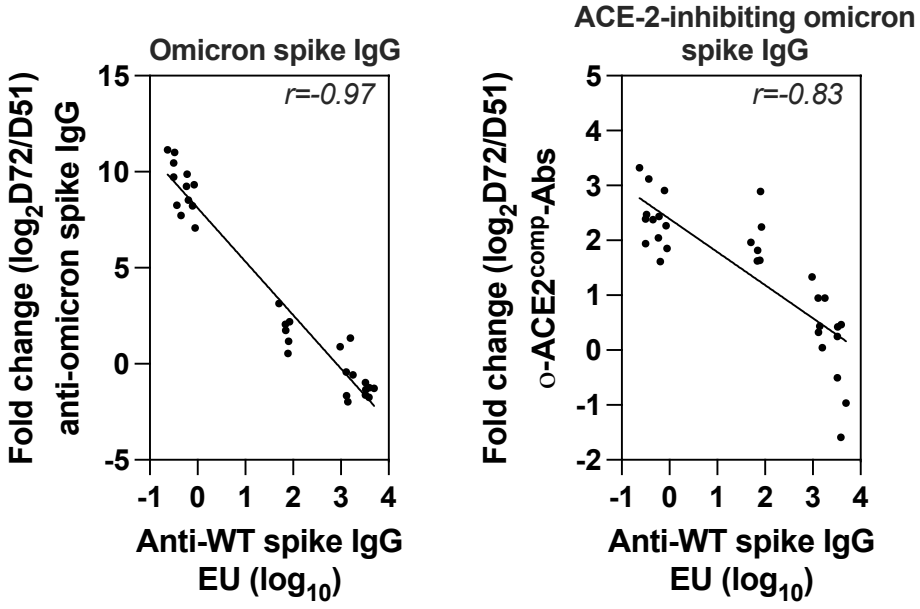

Figure 3.17: Correlation of quantity of WT spike vaccine sera transferred and fold change in omicron-specific response

Correlation of fold change in anti-omicron spike IgG (A) and ο-ACE2^{comp}-Ab (B) levels (log_2(Day 72/Day 51)) against levels of anti-WT spike IgG transferred (measured on Day 51) for the serum transfer experiment detailed in Figure 3.14. To calculate the r values, Pearson correlations were completed. The dots in both plots represent samples from all experimental groups.

In summary, transferring sera derived from WT spike vaccination prior to Ad-ο vaccination resulted in a reduction of the latter omicron-specific responses to Ad-ο. Additionally, anti-ChAdOx1 (anti-vector) IgG was shown to suppress the latter Ad-ο response, however, to a lesser extent than anti-WT spike IgG. The quantity of anti-WT spike IgG transferred was shown to have a tight inverse correlation with omicron-specific response to Ad-ο.

3. Discussion

In this chapter it was demonstrated that pre-existing immunity can have a profound impact on sequential heterologous immunisation humoral responses. Specifically, it was shown that:

- An immune imprint formed after intramuscular ChAdOx1-WT vaccination limited the responses to latter omicron vaccine boost
- Antibodies derived from vaccination with different WT spike vaccines were suppressive to latter de novo responses to omicron booster vaccine
- Anti-ChAdOx1 “anti-vector” antibodies were minimally suppressive to the latter de novo responses to omicron booster vaccine in comparison with anti-WT spike antibodies

Updated variant booster vaccines against SARS-CoV-2 are typically administered via the intramuscular route (IM). This route is effective in inducing immunity for protection against severe disease, but less effective at providing protection against infection, with various studies suggesting this is due to the involvement of immunological imprinting restricting the variant IM booster responses, a phenomenon largely described in the context of influenza virus[80,81,83,84,263]. Imprinting derived from sequential WT spike vaccination may limit the protection conferred by variant booster vaccines by suppressing de novo responses to variant spike and perpetuating the ancestral WT spike response.

At the beginning of this chapter, it was first investigated whether immunological imprinting occurred when mice were exposed to a particular earlier ancestral variant and then exposed to a different ancestral variant afterwards, following these specific vaccination schedules: Ad-α^{IM}+Ad-β^{IM}, Ad-β^{IM}+Ad-α^{IM}, Ad-α^{IM}+Ad-γ^{IM} and Ad-γ^{IM}+Ad-α^{IM}. Although a clear bias in IgG response to the antigen of prime vaccination was detected upon heterologous boosting, which indicated the occurrence of back boosting and fit an antigenic seniority-type imprinting model, this trend was not held with regards to ACE-2-competing antibodies. Irrespective of the vaccines used in each regimen, the heterologous regimens induced higher magnitudes of IgG against the vaccine antigens than when the vaccines were administered in a prime alone; e.g., Ad-α^{IM}+Ad-β^{IM} induced higher levels of anti-alpha spike IgG than Ad-α^{IM}, and higher anti-beta spike IgG than Ad-β^{IM}. These findings reflected the high level of relative homology in spike sequence shared between the alpha, beta and gamma variant antigens compared with more distant variants such as omicron and it's subvariants (Figure 1.1, Figure 1.2 and Figure 1.3)[325]. However, relative ACE-2-competing antibody levels did not display as clear of a trend as relative levels of IgG. Schiepers *et al* describe immunological imprinting as a function of antigenic distance;

imprinting is likely to occur to a greater extent when the antigen of secondary exposure is more homologous in sequence to the antigen of initial exposure, as opposed to more distant in sequence identity[248].

Although back boosted IgG responses following heterologous ancestral variant regimens were detected, a clear suppression in ACE-2-competing antibodies to boosting antigen as a result of heterologous priming was not observed. I hypothesise that this is due to the high level of homology between alpha, beta and gamma spike antigens; pre-existing antibody and back boosted antibody responses have substantial cross-neutralisation capacity, likely as certain epitopes are conserved between these variants that are targeted by neutralising antibody. This hypothesis is illustrated for better understanding in the following diagram: Figure 3.18A. To better understand the origins of the antibodies induced following boost vaccination, antibody depletions could have been completed, however, these were not conducted for this part of the study.

In summary, it appeared that the immunological imprinting observed in these regimens was “beneficial”, rather than deleterious, with no indication of a suppression of quality neutralising responses to the heterologous boost antigen.

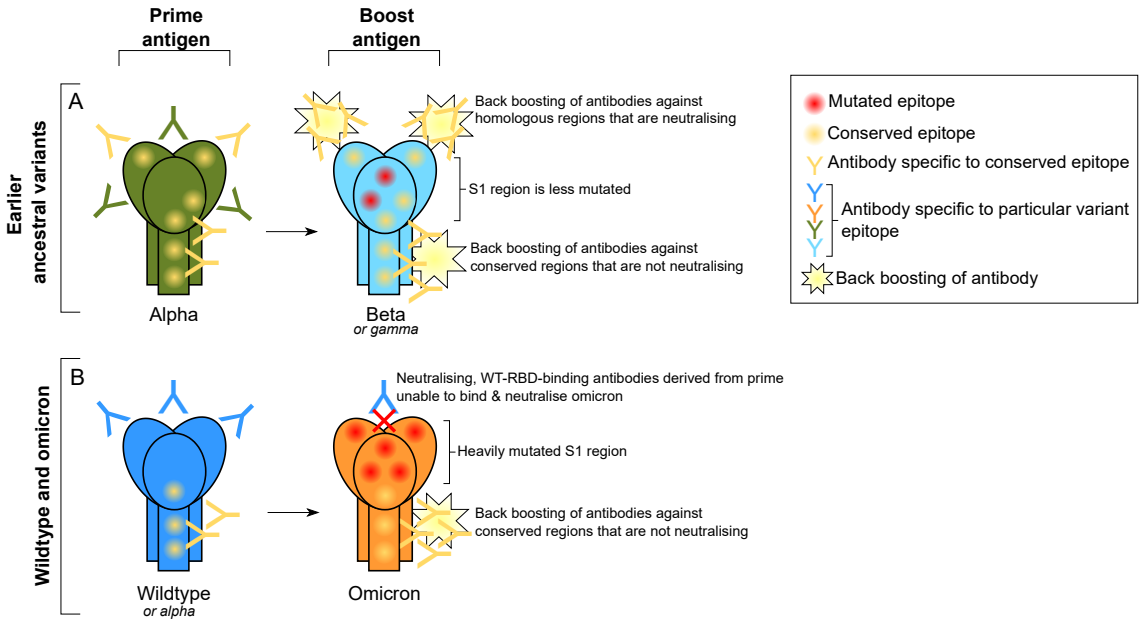

Figure 3.18: Schematic for the comparison of antibody responses following heterologous regimens containing vaccines encoding omicron and WT spike antigen, or earlier primary cluster ancestral spike antigens

Whereas certain epitopes within the S1 region of spike antigen are conserved between earlier ancestral variants of the primary cluster, and back boosted upon heterologous vaccination, less homology is present between WT and omicron spikes within this region, resulting in back boosting to non-neutralising regions of spike contributing to a compromised functional antibody response to omicron virus.

In contrast to the findings above, when a more distant, recently emerged variant vaccine (Ad-ο omicron vaccine) was administered as a booster in original WT spike-encoding Ad-WT-primed mice (Ad-WT^{IM}+Ad-ο^{IM}), it was unable to induce substantial omicron-specific, functional humoral responses. Although anti-omicron spike IgG were detected in serum, the majority of these antibodies were WT-reactive, suggesting they were derived from a back boosting response to WT spike induced initially with the prime vaccine, rather than de novo response to omicron booster vaccine antigen. Back boosting was also indicated by the higher neutralisation of WT pseudotyped virus in sera following Ad-WT^{IM}+Ad-ο^{IM} vaccination compared with Ad-WT^{IM} prime-only samples.

The neutralisation capacity of the omicron spike-binding IgG was low, and levels of neutralisation were lower than that of sera following Ad-o^{IM} prime-only (in contrast to what was observed with the heterologous ancestral spike-encoding vaccine regimens), indicating suppression of a de-novo Ad-o^{IM} response. This trend was identical when mice were vaccinated with another "early" spike antigen species, i.e., alpha spike vaccine: the levels of omicron neutralisation were suppressed by the prior priming with alpha vaccine. As the WT and omicron spike antigens (especially the RBD region) are considerably distant from each other, the back boosting of antibodies observed here was likely focused towards conserved areas of the spike between omicron and WT spike, that when bound by antibody do not lead to the neutralisation of virus (Figure 3.18B). Henceforth, the lack of de novo response to omicron antigen was clearer when the functional antibody responses following the Ad-WT^{IM}+Ad-o^{IM} and Ad-o^{IM}+Ad-WT^{IM} regimens were examined, compared with when the functional responses the following Ad-α^{IM}+Ad-β^{IM}, Ad-β^{IM}+Ad-α^{IM}, Ad-α^{IM}+Ad-γ^{IM} and Ad-γ^{IM}+Ad-α^{IM} regimens were examined.

An important factor to consider regarding both the ancestral variant heterologous regimens, as well as the heterologous regimens involving omicron vaccine, is the potential impact of the varied VP doses administered depending on the particular variant vaccine used. Discrepancies in VP dose administered are a consequence of the varied infectivity between stocks; as dose was determined by infectivity (IU), some groups received more virus than others. Virus that does not infect (hence fail to induce host cell antigen expression) may still contribute to the immune response by activating the innate response and also initiating an adaptive response to the vector itself (anti-vector immunity). Additionally, the different variant spike antigens may have differing stabilities, expression efficiencies and immunogenicity; as such they cannot be interpreted as "equivalents" apart

from their differing sequences. These factors could potentially explain certain unexpected findings in this chapter, such as how the trends in anti-WT spike immunity did not completely mirror the trends in anti-omicron spike immunity following the Ad-WT^{IM}+Ad-o^{IM} and Ad-o^{IM}+Ad-WT^{IM} regimens.

To assess whether the suppressive imprint formed after Ad-WT^{IM} priming was a ChAdOx1 vaccine-specific occurrence, mice were primed with different WT spike-based vaccines in standard doses and then boosted with Ad-o. Here too, indications of imprinting were observed: like in the Ad-WT^{IM}+Ad-o^{IM} regimen, levels of IgG reactive to omicron spike were boosted upon Ad-o^{IM} boost (Ad-WT^{IM}+Ad-o^{IM}>Ad-WT^{IM}, Ad2-WT^{IM}+Ad-o^{IM}>Ad2-WT^{IM}, Pfizer-WT^{IM}+Ad-o^{IM}>Pfizer-WT^{IM}, Novavax-WT^{IM}+Ad-o^{IM}>Novavax-WT^{IM}). However, levels of omicron RBD-reactive IgG generally did not increase, which suggested that the omicron-reactive antibodies induced upon Ad-o^{IM} boost were derived from a back boosting of more conserved, non-RBD regions of spike with higher homology between omicron and WT, as opposed to a de novo response to mutated omicron spike epitopes. This was confirmed via the completion of a WT spike-reactive antibody depletion assay, in which greater quantities of omicron RBD-reactive IgG were depleted by incubation with WT spike compared with the reverse regimens where Ad-o^{IM} was the priming vaccine (with the exception of the Pfizer-WT-containing regimens). Across both IgG and functional surrogate neutralisation assays, a trend of greater omicron-responses following the Ad-o^{IM}-prime, WT-spike vaccine-boost regimens compared with the reverse orientation was observed. This finding aligned well with that observed with the Ad-WT^{IM}+Ad-o^{IM} regimen data.

However, in the non-ChAdOx1 WT spike vaccine heterologous regimens, much higher levels of neutralisation irrespective of orientation of the regimen, were measured in comparison with the Ad-WT^{IM}+Ad-o^{IM} (and Ad-o^{IM}+Ad-WT^{IM}) regimen. I hypothesised

this was as a result of the greater immunogenicity achieved with these heterologous platforms, compared with regimens only containing ChAdOx1 vaccines. These findings also did not rule out the possibility of a role of ChAdOx1-derived anti-vector antibodies in the suppression of Ad-o^{IM} booster responses.

Upon further investigation (using passive transfer of serum), it was confirmed that WT spike vaccine-derived antibody was contributing to the suppressive effect of immunological imprinting noted following the Ad-WT^{IM}+Ad-o^{IM} regimen, and that anti-vector antibodies only had a marginal effect on latter de novo Ad-o^{IM} responses in comparison with the suppressive effect of WT spike antibodies. Nonetheless, these data did not definitively exclude the involvement of anti-vector immunity in the suppression of responses, and anti-vector antibodies still elicited a statistically significant reduction in fold change in anti-omicron spike IgG compared with the naïve positive control group. It is likely that the suppression observed with the Ad-only containing prime-boost regimens was via the concerted action of both anti-vector and anti-spike antibodies.

To more definitively understand the relative contribution of anti-vector antibodies and anti-WT spike antibodies following Ad-WT^{IM} on suppression of the Ad-o^{IM} boost response, an experiment could be conducted whereby the anti-ChAdOx1 antibodies within the Ad-WT^{IM}+Ad-WT^{IM} donor pool are pre-absorbed before transfer into the naïve mouse (and subsequent Ad-o^{IM} boost); this would allow direct quantification of their respective contributions.

Importantly, the suppressive action of anti-vector antibodies and anti-spike antibodies on the ChAdOx1 boost response will occur at different stages; anti-WT spike IgG will be able to bind any expressed antigen that is accessible (i.e., antigen draining to the LNs) over a wider window of time, whereas anti-vector immunity can only act within the

early stages of vaccination to prevent vector entry into host cells. Vector administered IM largely remains in the local vicinity and infects muscle cells in muscular tissue, with marginal dissemination of whole, uninternalised vector into circulation and/or lymph; hence, the opportunity of anti-vector antibodies to access and prevent vector entry is likely to be less than the opportunity by which anti-spike antibody can access and mask more widely disseminated spike antigen that can remain in the tissues for a longer timeframe

The transfer of IgG from sera derived from other non-ChAdOx1 WT spike vaccines was also shown to suppress latter de novo Ad-o^{IM} responses, further confirming that the observed immunological imprinting was not solely a ChAdOx1-specific phenomenon. The transferred WT spike-reactive antibodies, that were shown to be cross-reactive with omicron spike, may be competing omicron vaccine immunogenicity in what has been previously referred to as "antigenic blunting": cross-reactive antibody binding and masking omicron antigen expressed following vaccination, preventing B cell recognition and downstream omicron-specific antibody responses[326,327]. In addition to this, these cross-reactive antibodies may be facilitating the accelerated effector-cell-mediated clearance of omicron antigen-expressing cells upon vaccination in an Fc-dependent manner, also impairing the ability of B cell to recognise antigen[266]. These observed and proposed phenomena are summarised in the following illustration (Figure 3.19).

The quantity of anti-WT spike transferred was positively correlated with the suppression of latter Ad-o^{IM} response, however, other antibody properties may also influence of the extent to which an antibody pool can suppress Ad-o^{IM}. These include for example, avidity (which is highly influenced by factors such as vaccine type, interval between prime and boost, and time after final vaccination); it is likely that antibodies of higher avidity to omicron spike would be more suppressive for instance. As avidity can be

easily measured through the use of a chaotropic agent on samples that have been normalised with respect to quantity of IgG (or IgA), an experiment in which anti-WT spike antibodies of increasing avidity to WT spike be transferred into naïve mice (with those mice subsequently Ad-o^{IM} vaccinated, could aid in understand this antibody properties' specific contribution to suppression. Additionally, the ability of antibody to engage FcR via it's Fc region and subsequently initiate antibody-dependent cell-mediated cytotoxicity (ADCC) could be measured through ADCC assay to understand how this particular proposed mechanism contributes to the suppression of responses observed[266].

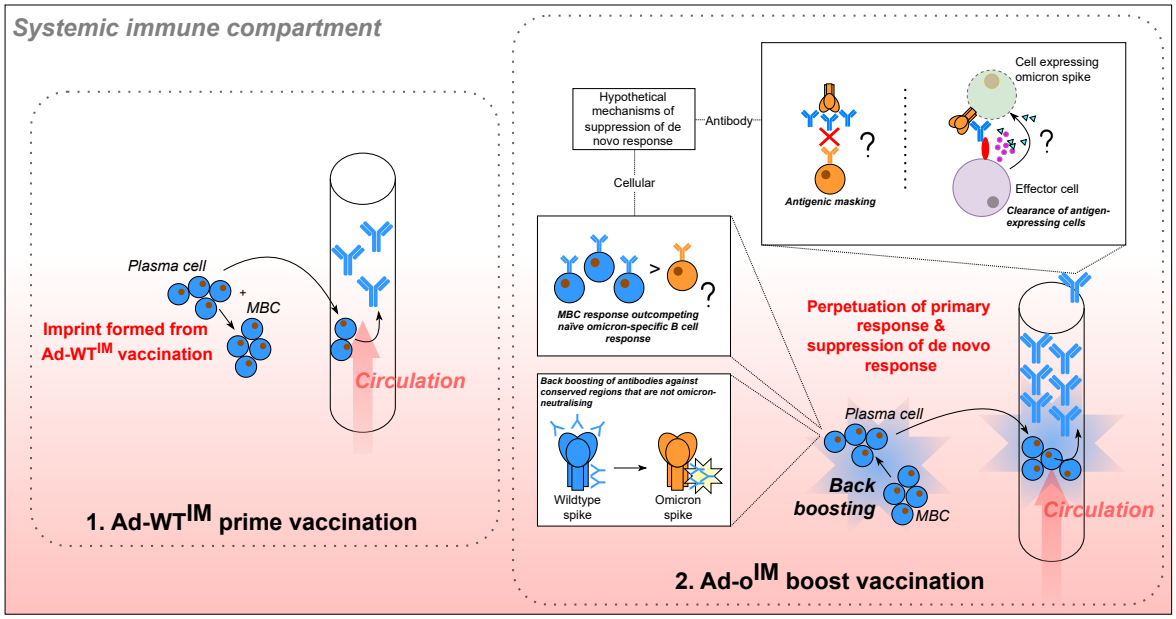

Figure 3.19: The suppressive Ad-WT^{IM}-derived imprint

Schematic summarising two phenomena that occurred in Ad-WT^{IM}-primed mice when they were boosted with Ad-o^{IM}: the back-boosting of non-neutralising, cross-reactive antibodies, and the suppression of de novo responses to omicron vaccine. Two proposed hypothetical mechanisms for the suppression of de novo response are featured: antigenic blunting and antigenic clearance via Fc-FcR interactions.

Importantly, primary addiction is not solely described as an antibody-driven phenomenon; the recall of pre-existing WT spike-vaccine-derived primary B cell cohorts, that outcompete novel B cell responses, and also perpetuate such the suppressive, non-

neutralising antibody responses, are also a key element underpinning the imprinting process[248]. The recall of primary B cell cohorts was indirectly observed through the aforementioned back boosting observed in sera (Ad-WT^{IM}+Ad-ο^{IM}>Ad-WT^{IM}; anti-WT responses), but would need more direct methods of measurement to be concluded.

Other observations support the hypothesis that immunological imprinting, rather than solely an inhibitory antibody scenario, was influencing the Ad-WT^{IM}+Ad-ο^{IM} regimen responses; for instance, there was a clear boost in the cognate neutralisation responses in the homologous setting, i.e., between the Ad-ο^{IM} and Ad-ο^{IM}+Ad-ο^{IM} regimens (regarding anti-omicron neutralisation) and between the Ad-WT^{IM} and Ad-WT^{IM}+Ad-WT^{IM} regimens (regarding anti-WT neutralisation) despite the presence of potentially inhibitory antibody following the prime vaccination that would affect the boost vaccination responses. In other words, in the heterologous setting, there was a unique suppression that was only observed when the antigen of prime (WT) and antigen of boost (ο) differed, which favoured more of an immunological imprinting, rather than simply immune-dampening scenario, that could occur even in the homologous setting.

Completion of an experiment in which Ad-WT^{IM}-derived MBCs are transferred into naïve mice, that are subsequently vaccinated Ad-ο^{IM}, could provide further insight into the specific impact of MBC on perpetuating inhibitory antibody and subsequently affecting the latter de novo responses to Ad-ο^{IM}; and enable ascertainment of whether the source of the suppression of de novo response is not solely the effect of pre-existing antibody but also the competition between B cells. Likewise, an experiment as completed by Schiepers *et al* where antibodies are tagged based on the vaccination timepoint, could more directly demonstrate the reactivation of B cell and downstream antibody in a recall response scenario[248].

Understanding of the role of MBC in this context is warranted given the possible scenario whereby an individual has a low quantity of suppressive antibodies due to waning of response, however, an existing MBC population that may still be stimulated upon boosting and subsequently perpetuate a downstream suppressive antibody response that then impacts the immune response to booster vaccine, and/or may simply be re-activated and outcompete the potential naïve B cell responses.

Other clinical and preclinical studies have observed the impairment of both omicron vaccine responses and omicron breakthrough responses as a result of a pre-existing immunological imprint derived from WT spike vaccination[69,80–82]. One clinical study found that triple-WT-vaccinated, omicron-infected individuals mounted recall responses to shared regions of spike between WT and omicron variant, yet failed to mount a de novo response to omicron antigen[253]. In another clinical study, monovalent WT spike-encoding, and bivalent WT and BA.5 spike-encoding mRNA booster vaccines induced comparable antibody responses in individuals; the wildtype spike antigen within the bivalent vaccine was suggested to have contributed a "deep immunological imprint" limiting the booster vaccine's potential[80]. The data within this chapter indicated that even when monovalent omicron vaccine is administered without WT antigen, a pre-existing WT imprint was capable of suppressing the omicron vaccine response. Other preclinical studies using different vaccine platforms have noted a similar inefficacy of heterologous IM omicron booster to this present study[302,328,329].

In summary, this chapter demonstrates that vaccination with the SARS-CoV-2 spike antigen establishes an immunological imprint in mice that will shape latter immune responses to heterologous SARS-CoV-2 variant antigen. Although immunological imprinting was detected when mice were exposed to different ancestral primary cluster

variant spike antigens, this did not result in a detectable suppression of neutralising antibody, which I hypothesise is as a result of the higher relative homology amongst these spike antigens, especially within the S1/RBD region which is targeted by many NAbs. In contrast, when mice were vaccinated with WT spike antigen vaccine, and then exposed to the more distant omicron antigen, a more striking, suppressive form of imprinting was observed. Specifically, WT spike vaccination was shown to “lock” the immune system into a back boosted antibody response upon omicron vaccine boost, and WT spike vaccine-derived antibodies were shown to be suppressive to the latter de novo omicron vaccine response. The dual effect of the perpetuation (back boosting) of non-functional antibody responses, and suppression of de novo responses (that would result in functional omicron-specific antibody responses) by prime-derived antibodies, led to a form of imprinting that impaired the omicron booster response.

4

Mucosal administration of heterologous omicron vaccine

4. Mucosal administration of heterologous omicron vaccine

3. Discussion

1. Introduction and aims

Certain shortcomings have been associated with the intramuscular route (IM) for the administration of SARS-CoV-2 variant booster vaccines, which are likely contributing in part to the occurrence of breakthrough infection[298]; these include:

- A susceptibility to immunological imprinting derived from previous WT spike vaccination, which was observed in Chapter 3, and which has been reported in various other studies[80–82,302]
- A failure to stimulate the mucosal immune compartment and subsequently induce mucosal immunity
- A failure to induce robust, long-lasting responses[330]

In this chapter, the alternative mucosal route (intranasal) for the administration of omicron booster vaccine (Ad-o) was tested, to assess whether it could overcome imprinting, augment immunogenicity and in addition, generate responses at the site of infection[291]. The mucosal route for the administration of heterologous booster vaccine was chosen for the following reasons:

- The respiratory mucosa targeted by mucosal vaccination is immunologically and anatomically distinct from the wider parenteral, systemic compartment[331], thus, vaccine responses may not be similarly affected by suppressive, circulating prime vaccine-derived antibodies or competitive MBC in the wider system as IM vaccine responses are.
- Mucosal vaccination is more effective than IM vaccination at inducing mucosal immunity, which has been associated with enhanced protection against SARS-CoV-2 infection in non-human primate studies[279,299,332]. *As mentioned in Chapter 3, there is a need for variant booster vaccines that are able to induce*

forms of protection that reduce viral replication, as opposed to those that solely perpetuate pre-existing protective, cross-reactive immunity[298] .

By targeting the respiratory airways through mucosal vaccination, respiratory mucosa-resident memory $CD8^+$ T cells (T_{RM}), which facilitate the rapid clearance of infected cells, as well as $CD4^+$ T_{RM}, resident B cells (B_{RM}) and downstream virus-neutralising mucosal IgA, which contribute to the local humoral response, can be elicited[333,334]. The presence of such immunity at the site of viral entry serves the advantage of faster response to virus exposure and greater subsequent control of infection, compared with the less localised immunity following IM vaccination. In this chapter the intranasal (IN) route is specifically tested; IN vaccination can stimulate the inductive nasal-associated lymphoid tissue (NALT), in doing so generate a response in the URT. Adenovirus vector vaccines against SARS-CoV-2 have been administered via the IN route in previous studies (both preclinical and clinical), with some reporting strong immunogenicity[278,279,292,298,335].

While the inherent benefit of mucosal delivery of vaccine to induce immunity within the lung has been established, such a vaccine strategy has not been extensively explored and compared with standard IM delivery within the context of deleterious antigenic imprinting, as demonstrated in Chapter 3. Exploration of this alternative route of delivery is warranted given the potential impact it may have on enhancing protection against diseases such as COVID-19. In this chapter, the IM and IN routes for administration of heterologous omicron booster vaccine are compared by assessing the immune responses after either regimen.

2. Results

2.1 Effect of passive WT spike antibody transfer on subsequent mucosal omicron vaccination

2.1.1 Effect of passive transfer of Ad-WT vaccine-derived antibodies on subsequent mucosal omicron vaccination

IM omicron vaccine (Ad-ο) responses were shown to be suppressed by antibodies derived from WT spike vaccination, that form part of the immunological imprint (Chapter 3;2.3). Given the mucosal immune compartment is anatomically and immunologically distinct from the wider systemic compartment, it was then assessed whether an IN omicron vaccine response was similarly affected by circulating anti-WT spike antibodies to IM omicron vaccination.

Akin to the previous antibody transfer experiment (Figure 3.15), sera from WT spike-vaccinated mice were transferred into naïve mice, however, mice were then vaccinated with omicron vaccine via the IN route, with IM omicron vaccination included for direct comparison (Figure 4.1A). The effect of Ad-WT^{IM}+Ad-WT^{IM} sera was specifically assessed for this experiment. ELISA and Luminex assays were used to measure the quantities of antigen-reactive antibody and ACE-2 competition capacity, respectively.

Post-transfer, pre-vaccination levels of WT spike IgG and ChAdOx1 were comparable between both groups as expected (Figure 4.1B). Baseline levels of omicron-reactive IgG were detected following Ad-WT^{IM}+Ad-WT^{IM}-transfer above the negative control (naïve serum transfer) (P≤0.0001), however, ο-ACE2^{comp}-Ab levels were very low and comparable to the negative control; this confirmed that the transferred antibodies were cross-reactive to omicron spike, but showed little functional capacity to neutralise omicron (Figure 4.1C).

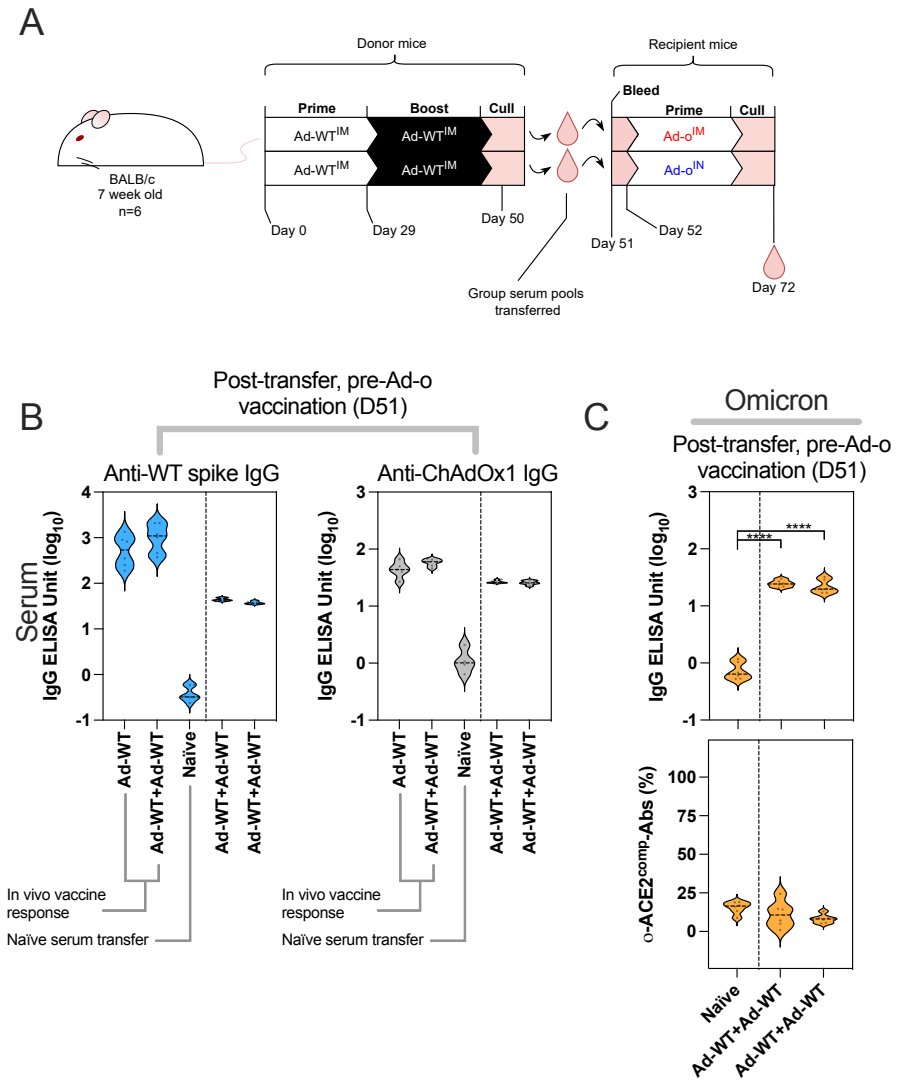

Figure 4.1: Passive transfer of WT spike vaccine sera and ChAdOx1 omicron mucosal vaccination

(A) Vaccination and serum transfer schedule. Donor mice (n=6) were vaccinated, with sera then collected and then transferred to naïve recipient mice (n=6). Recipient mice were then vaccinated with Ad-o IM or IN. The experiment was conducted twice, with data representative of once experiment shown. Sera from recipient mice were collected after transfer of sera before vaccination (day 51) and 3 weeks post Ad-o vaccination (day 72). (B) Levels of anti-WT spike IgG and anti-ChAdOx1 IgG in recipient mice sera, post-transfer of donor sera, and before Ad-o vaccination (day 51). Reference negative control levels of IgG on day 51 in mice that received naïve sera were also included in the figure. (C) Levels of anti-omicron spike IgG and o-ACE2^{comp}-Abs in mice sera, post-transfer of donor sera, and before Ad-o vaccination (day 51). Data in (C) were normally distributed, and a one-way ANOVA test was completed to measure statistically significant differences between regimens (****=P≤0.0001). Dashed black lines on violin plots represent group medians.

3 weeks after IN omicron vaccination, the levels of serum omicron spike-reactive IgG and o-ACE2^{comp}-Abs were of similar level to those following Ad-o^{IN} and Ad-o^{IM} prime-only regimens that did not receive antibodies (Figure 4.2A). In the groups of mice that received antibodies, omicron spike-reactive IgG and o-ACE2^{comp}-Abs were significantly higher following subsequent Ad-o^{IN} vaccination than the levels following subsequent Ad-o^{IM} vaccination (IgG: P=0.0064 and o-ACE2^{comp}-Abs: P≤0.0001) (Figure 4.2A). A higher fold change in serum omicron spike-specific IgG and o-ACE2^{comp}-Abs following vaccination was also observed in the Ad-o^{IN} group, compared with the Ad-o^{IM} group (IgG: P=0.0008 and o-ACE2^{comp}-Abs: P=0.0001) (Figure 4.2B). Thus, IN Ad-o responses were not suppressed by the circulating WT-spike vaccine-induced antibodies.

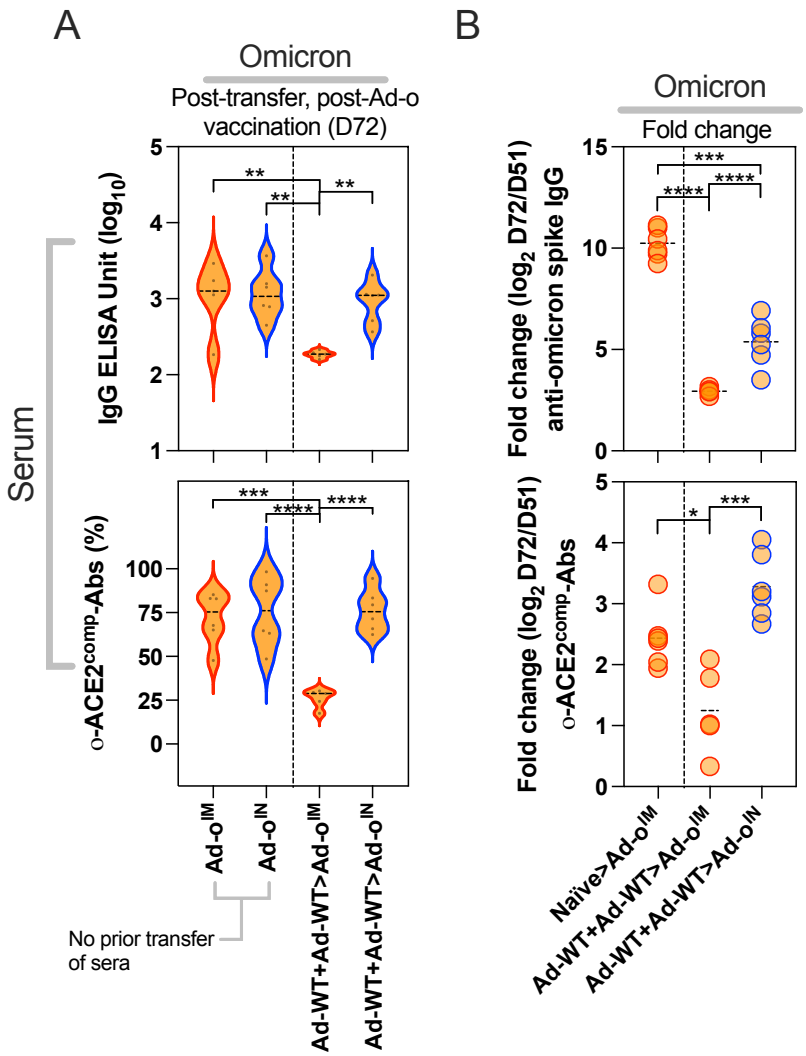

Figure 4.2: Omicron-specific responses following mucosal vaccination with omicron vaccine in mice that received prior transfer of WT spike vaccine sera

Omicron responses post-serum transfer, and omicron vaccination (n=6). The experiment was conducted twice, with data representative of once experiment shown. (A) Levels of anti-omicron spike IgG and ο-ACE2^{comp}-Abs in mouse sera, post-transfer of donor sera, and after Ad-ο vaccination (day 72). On violin plots, the dashed black line represents the group median response. Reference group median levels of IgG and ο-ACE2^{comp}-Abs following Ad-ο^{IM} and Ad-ο^{IN} were included in graphs as dashed red and blue lines, respectively. (B) Fold change in anti-omicron spike IgG and ο-ACE2^{comp}-Ab levels between days 51 and 72. Fold change was calculated as log_2(Day 72/Day 51). Dashed black lines on scatter plots represent the group median values. Data in (A) and (B) were normally distributed, and one-way ANOVA tests were completed to measure statistically significant differences between regimens (**=P<0.01, ***=P<0.001, ****=P≤0.0001).

2.1.2 Effect of passive transfer of Novavax-WT vaccine-derived antibodies on subsequent mucosal omicron vaccination

Following the observation that Ad-$\omicron^{IN}$-boost responses were not affected by the previous transfer of Ad-WT^{IM}+Ad-WT^{IM} sera, it was assessed whether this observation was held when higher quantities of WT spike antibody were present in circulation. To do this, the experiment completed in 2.1.1 was recapitulated (Figure 4.1A), however, serum was transferred from mice that were vaccinated with Novavax-WT vaccine (Novavax-WT^{IM}+Novavax-WT^{IM}) instead of Ad-WT vaccine (Figure 4.3A); previously, this prime-boost regimen elicited much higher levels of anti-WT spike antibody and omicron spike-reactive IgG in sera, and the transfer of this sera significantly suppressed Ad-$\omicron^{IM}$ boost responses, as shown in Chapter 3 (Figure 3.16).

Following the transfer of Novavax-WT^{IM}+Novavax-WT^{IM} sera into naïve mice, detectable levels of anti-WT spike IgG were measured, with the group median titre (3.39 EU ($\log_{10}$)) 2-$\log_{10}$fold higher than the median titres measured in the previous transfer experiment where Ad-WT^{IM}+Ad-WT^{IM} sera was transferred (1.61 EU ($\log_{10}$)) (Figure 4.3B and Figure 4.1B). As expected, mice that received Novavax-WT^{IM}+Novavax-WT^{IM} sera did not have detectably high anti-ChAdOx1 IgG titres; consistent with the previous experiment where Novavax-WT^{IM}+Novavax-WT^{IM} sera was transferred, a marginal level of ChAdOx1 reactivity was measured above naïve negative control, which could be attributed to cross-reactivity. The Novavax-WT^{IM}+Novavax-WT^{IM} sera transferred also exhibited measurable cross-reactivity to omicron (Novavax-WT^{IM}+Novavax-WT^{IM} group 2 vs. Naïve; P=0.0007), and cross-reactive antibody showed poor but detectable ACE-2-competing capacity (Novavax-WT^{IM}+Novavax-WT^{IM} group 1 vs. Naïve; P=0.0020, Novavax-WT^{IM}+Novavax-WT^{IM} group 2 vs. Naïve; P=0.0001) (Figure 4.3C).

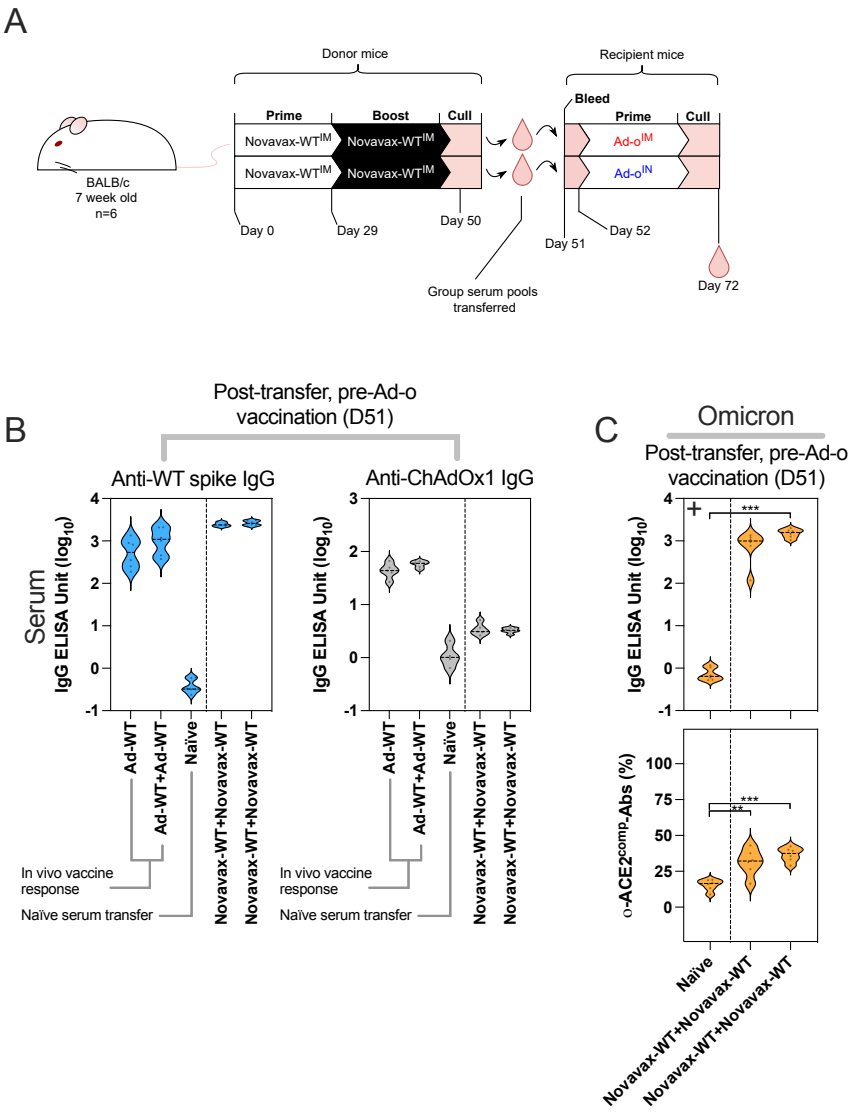

Figure 4.3: Passive transfer of Novavax-WT vaccine sera and ChAdOx1 omicron mucosal vaccination

(A) Vaccination and serum transfer schedule. Donor mice (n=6) were vaccinated, with sera then collected and then transferred to naïve recipient mice (n=6). Recipient mice were then vaccinated with Ad-o IM or IN. The experiment was only completed once. Sera from recipient mice were collected after transfer of sera before vaccination (day 51) and 3 weeks post Ad-o vaccination (day 72). (B) Levels of anti-WT spike IgG and anti-ChAdOx1 IgG in recipient mice sera, post-transfer of donor sera, and before Ad-o vaccination (day 51). Reference negative control levels of IgG on day 51 in mice that received naïve sera were also included in the figure. (C) Levels of anti-omicron spike IgG and o-ACE2^{comp}-Abs in mice sera, post-transfer of donor sera, and before Ad-o vaccination (day 51). Groups plotted in (C) were measured for statistically significant differences through either a Kruskal-Wallis test (upper graph) or one-way ANOVA test (lower graph) (**=P<0.01, ***=P<0.001). Dashed black lines on violin plots represent group medians.

Three weeks post-Ad-ο vaccination, lower levels of omicron-reactive IgG and ο-ACE2^{comp}-Abs were measured in groups that received antibodies compared with the levels measured in the reference control groups of mice that did not receive antibodies prior to vaccination: Ad-ο^{IM} vs. Novavax-WT^{IM}+Novavax-WT^{IM}>Ad-ο^{IM}; P≤0.0001, Ad-ο^{IM} vs. Novavax-WT^{IM}+Novavax-WT^{IM}>Ad-ο^{IN}; P=0.0014, Ad-ο^{IN} vs. Novavax-WT^{IM}+Novavax-WT^{IM}>Ad-ο^{IM}; P≤0.0001, Ad-ο^{IN} vs. Novavax-WT^{IM}+Novavax-WT^{IM}>Ad-ο^{IN}; P=0.0005, all for ο-ACE2^{comp}-Abs (Figure 4.4A). The route of Ad-ο did not significantly impact the anti-omicron immunity elicited, although the Ad-ο^{IN} group did have slightly higher titres of ο-ACE2^{comp}-Abs (1.66-fold higher).

The fold change in omicron-specific immunity upon vaccination was measured to correct for baseline levels of omicron cross-reactivity in transferred sera (Figure 4.4B). Both groups of mice that received prior transfer of Novavax-WT^{IM}+Novavax-WT^{IM} sera, irrespective of route of Ad-ο vaccination, had lower fold changes in omicron immunity compared with control group: for anti-omicron spike IgG, Novavax-WT^{IM}+Novavax-WT^{IM}>Ad-ο^{IM}; P≤0.0001 and Novavax-WT^{IM}+Novavax-WT^{IM}>Ad-ο^{IN}; P≤0.0001 and for ο-ACE2^{comp}-Ab levels, Novavax-WT^{IM}+Novavax-WT^{IM}>Ad-ο^{IM}; P≤0.0001 and Novavax-WT^{IM}+Novavax-WT^{IM}>Ad-ο^{IN}; P≤0.0001. Henceforth, it appeared that the transfer of Novavax-WT^{IM}+Novavax-WT^{IM} sera, with much higher quantities of anti-WT spike IgG than what is generated following Ad-WT^{IM}+Ad-WT^{IM} vaccination, suppressed both the responses to Ad-ο^{IM} and Ad-ο^{IN}; mucosal administration was not able to bypass the suppressive antibody imprint in this case.

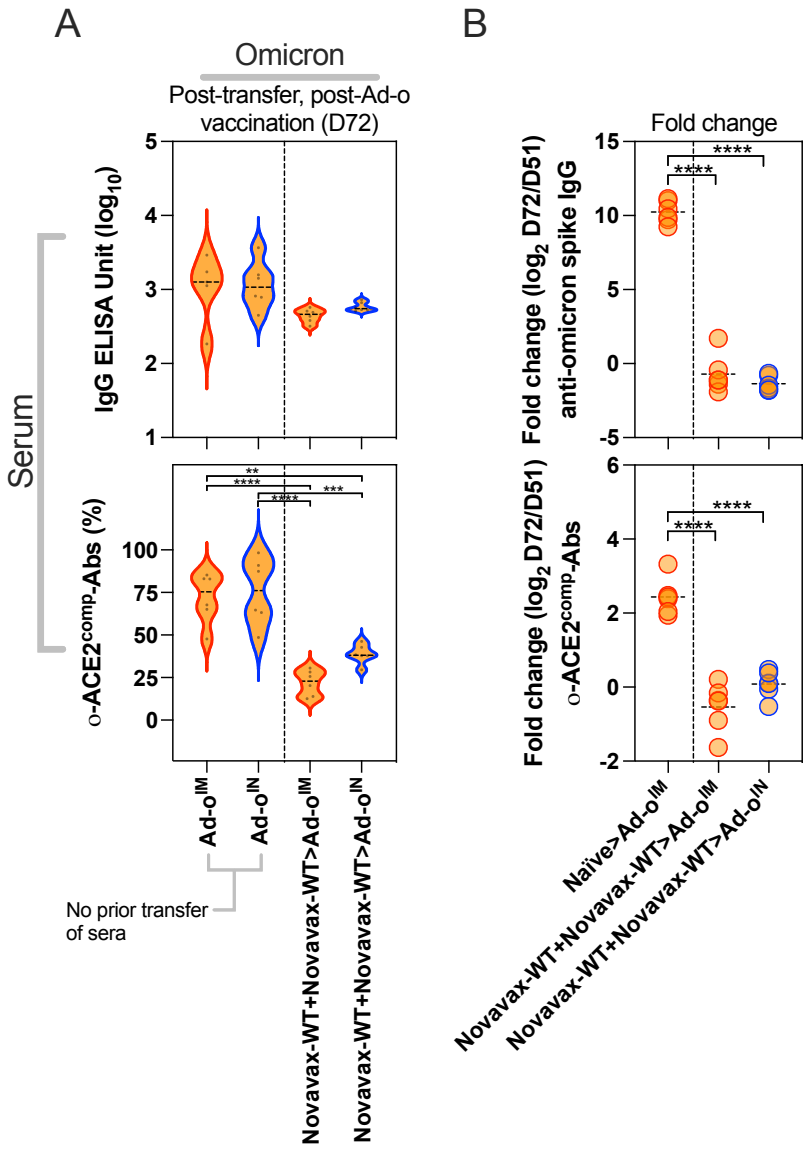

Figure 4.4: Omicron-specific responses following mucosal vaccination with omicron vaccine in mice that received prior transfer of Novavax-WT spike vaccine sera

Omicron responses post-serum transfer, and omicron vaccination (n=6). The experiment was only conducted once. (A) Levels of anti-omicron spike IgG and o-ACE2^{comp}-Abs in mice sera, post-transfer of donor sera, and after Ad-o vaccination (day 72). On violin plots, the dashed black line represents the group median response. Reference group median levels of IgG and o-ACE2^{comp}-Abs following Ad-o^{IM} and Ad-o^{IN} were included in graphs as dashed red and blue lines, respectively. (B) Fold change in anti-omicron spike IgG and o-ACE2^{comp}-Ab levels between days 51 and 72. Fold change was calculated as log_2(Day 72/Day 51). Dashed black lines on scatter plots represent the group median values. Data in (A) and (B) were normally distributed, and one-way ANOVA tests were completed to measure statistically significant differences between regimens (**=P<0.01, ***=P<0.001, ****=P≤0.0001).

2.2 Mucosal boosting of omicron vaccine in WT spike vaccine-primed mice

Given that the transfer of Ad-WT spike vaccine-derived antibodies did not affect the responses to Ad-ο mucosal vaccination, it was then assessed whether the mucosal administration of heterologous omicron vaccine in mice that were primed with Ad-WT^{IM} was more immunogenic than the standard intramuscular route (IM), which was shown to be suppressed. In this experiment, the potential involvement of prime-derived MBC on IN-boosting could also be indirectly assessed, as opposed to solely the effect of suppressive WT-vaccine antibodies. To do this, mice were first vaccinated with Ad-WT IM and then either boosted with Ad-ο IM (Ad-WT^{IM}+Ad-ο^{IM}) or IN (Ad-WT^{IM}+Ad-ο^{IN}) 4 weeks later, with systemic (spleens and sera) and mucosal (lungs, respiratory fluids) immunogenicity measured a further 5 weeks later (Figure 4.5A). The aim was to assess if omicron-specific and mucosal immunity were augmented.

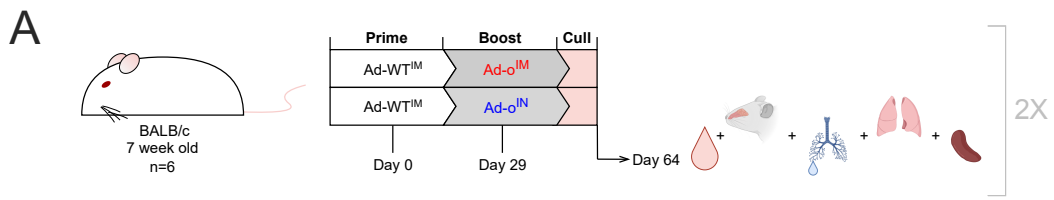

Figure 4.5: Mucosal boosting of omicron vaccine in WT vaccine-primed mice

(A) 7-week-old inbred BALB/c mice (n=6) were vaccinated with Ad-WT intramuscularly on day 0. 4 weeks later, mice were heterologously boosted with Ad-ο vaccine either via the intramuscular or intranasal route. 5 weeks post-boost, mice were sacrificed, with blood, NALT palate, BAL fluid, lungs and spleens harvested for analyses. The experiment was repeated once to generate sufficient sample volume for analyses.

2.2.1 Antibody responses following mucosal boosting of omicron vaccine

2.2.1.1 Antibody responses in the serum following mucosal boosting of omicron vaccine

IN-boosting with Ad-ο resulted in higher levels of omicron spike-specific IgG (P=0.0001) and IgA (P≤0.0001) in sera compared with IM-boosting (Figure 4.6A and B). Higher levels of ο-ACE2^{comp}-Abs were observed in sera following IN-boosting of Ad-ο compared with IM-boosting, with values all above 90% ACE-2 competition (P≤0.0001) (Figure 4.6C). IN-boosting also induced higher levels of omicron pseudotyped virus-neutralising antibodies (ο-NAbs) compared with IM-boosting in sera and NALT (P=0.0022) (Figure 4.6D). Hence, IN-boosting of Ad-ο resulted in greater anti-omicron immunity in the sera of mice compared with IM-boosting.

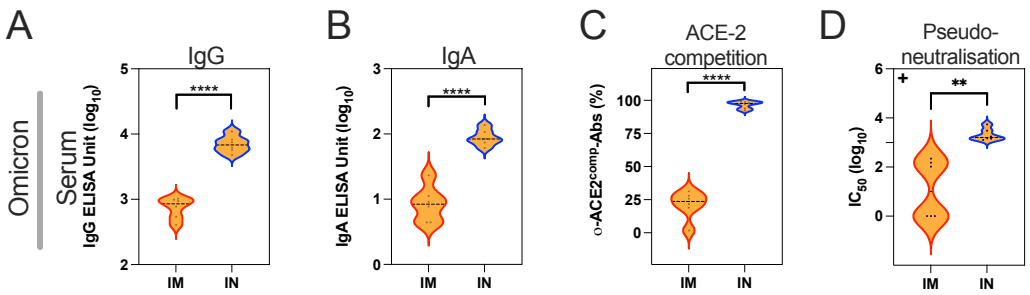

Figure 4.6: Anti-omicron antibody responses in the serum of omicron vaccine-boosted mice

Omicron-specific antibody responses in the serum following Ad-WT^{IM}+Ad-ο^{IM} (abbreviated "IM") and Ad-WT^{IM}+Ad-ο^{IN} (abbreviated "IN") regimens (n=6). The experiment was completed twice, and representative data from one repeat is shown. Serum was collected 5 weeks post-boost. Levels of total omicron spike-specific IgG (A) and IgA (B) were measured by standardised ELISA and presented as log_{10} ELISA units. (C) ACE-2-competing omicron S1-specific antibodies (ο-ACE2^{comp}-Abs) were measured by Luminex assay and presented as % ACE-2 competition, which was calculated by using the reduction in measured binding compared to a negative internal control. (D) Pseudoneutralisation of omicron spike-expressing lentivirus (ο-NAbs) was presented as log_{10} IC_{50}, which was calculated from sample titration curves. Statistically significant differences between groups in all figures were determined through parametric t tests or non-parametric Mann-Whitney tests (**=P<0.01, ****=P≤0.0001); when data did not follow a normal distribution, a "+" was added to the left corner of the graph. On violin plots, the dashed black line represents the group median response.

2.2.1.2 Depletion of WT spike-reactive anti-omicron RBD serum IgG following mucosal boosting of omicron vaccine

A WT spike depletion assay was then conducted as described earlier in Chapter 3, to assess whether the elevated levels of anti-omicron antibody in the serum following IN-boosting were derived from a de novo response to Ad-ο or a back boosting of immunity derived from the Ad-WT^{IM}-prime (Figure 4.7). I hypothesised that the Ad-WT^{IM}+Ad-ο^{IN} regimen would generate more non-cross-reactive, ο-RBD-specific IgG than the Ad-WT^{IM}+Ad-ο^{IM} regimen.

Unexpectedly, both regimens were depleted by WT spike to an equal extent, suggesting that the additional levels of anti-omicron IgG generated in the serum in the IN-boost group were derived from back-boosting (Figure 4.7A and B). Hence, although the suppressed omicron-reactive antibody responses in the serum in the Ad-WT^{IM}+Ad-ο^{IM} regimen appeared to be augmented to significantly higher levels, the anti-omicron antibody immunity generated at least in the systemic compartment, was towards shared epitopes between WT and omicron spike and not as a result of a more "de novo", less-suppressed-type response to Ad-ο.

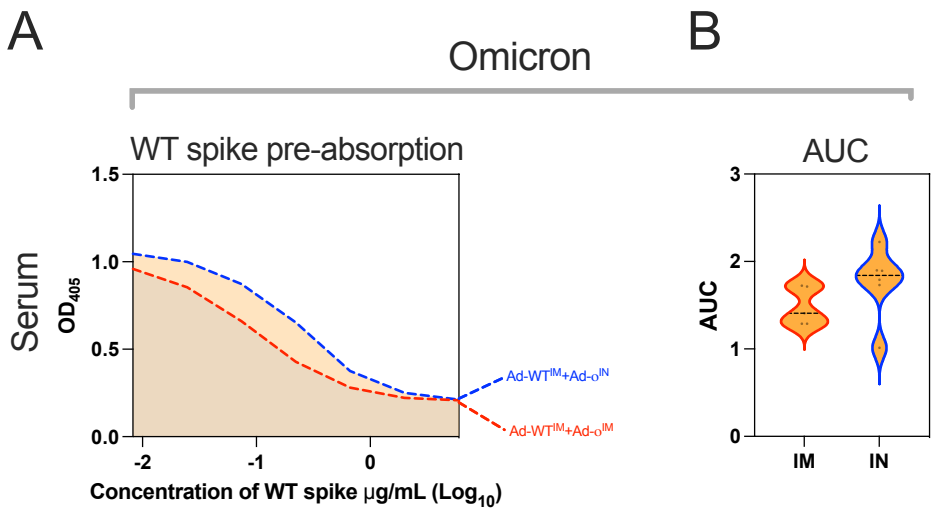

Figure 4.7: Depletion of WT spike-reactive anti-omicron RBD serum IgG

Levels of non-cross-reactive, o-RBD-specific IgG in sera following Ad-WT^{IM}+Ad-o^{IM} and Ad-WT^{IM}+Ad-o^{IN} regimens (n=6, experiment repeated twice with one dataset shown), as measured through WT spike pre-absorption (depletion) assay. (A) The group median o-RBD IgG levels in samples that were pre-incubated with a range of WT spike concentrations. (B) The area under the curve (AUC) values are shown on the right. On violin plots, the dashed black line represents the group median response. One sample within the IM boost group failed to pass QC and such datapoint was subsequently not included in the figures.

2.2.1.3 Antibody responses in mucosal fluids following mucosal boosting of omicron vaccine

The levels of omicron-reactive antibodies in nasal-associated lymphoid tissue (NALT) fluid (URT) and broncho-alveolar lavage fluid (BALF) (LRT) were then assessed (Figure 4.8). IN-boosting resulted in higher levels of omicron spike-reactive IgG and IgA in NALT fluid (Figure 4.8A; IgG: P=0.0002, Figure 4.8B; IgA: P=0.0022) and BALF (Figure 4.8E; not statistically significant, Figure 4.8F; IgA: P=0.0411) compared with the IM-boosted group.

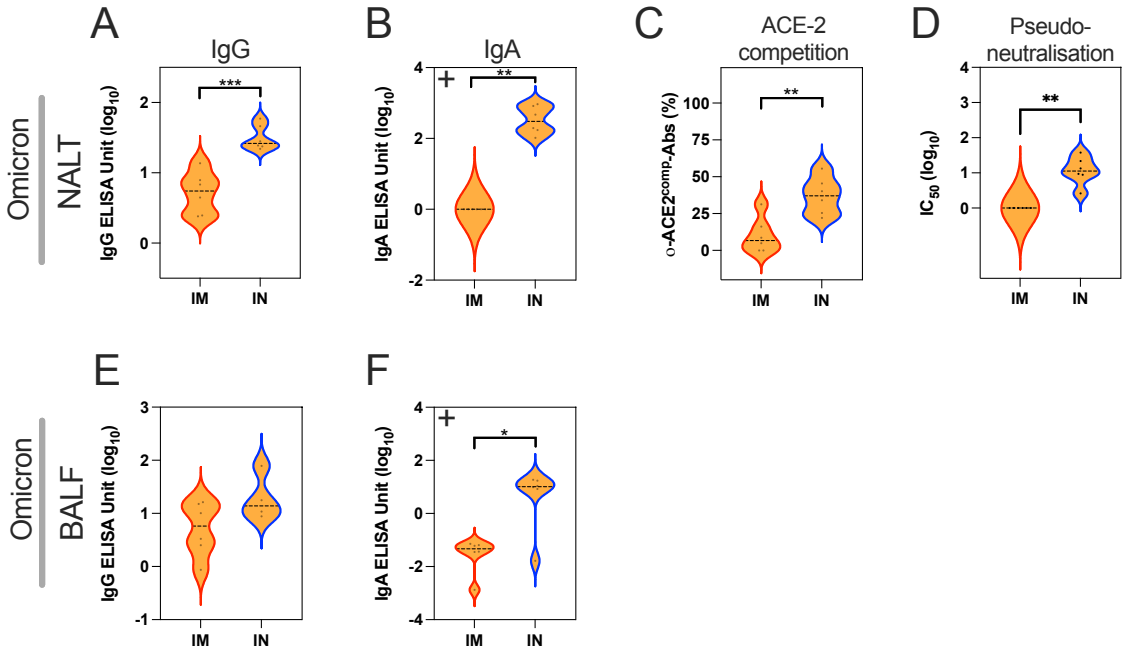

Figure 4.8: Anti-omicron antibody responses in mucosal fluids following mucosal boosting of omicron vaccine

Omicron-specific antibody responses in NALT fluid (A), (B), (C), (D) and BALF (E) and (F), following Ad-WT^{IM}+Ad-ο^{IM} and Ad-WT^{IM}+Ad-ο^{IN} regimens (n=6, experiment completed twice with one representative data set shown). Levels of total omicron spike-specific IgG (A), (E) and IgA (B), (F) were measured by standardised ELISA and presented as log_{10} ELISA units. (C) ACE-2-competing omicron S1-specific antibodies (ο-ACE2^{comp}-Abs) were measured by Luminex assay and presented as % ACE-2 competition, which was calculated by using the reduction in measured binding compared to a negative internal control. (D) Pseudoneutralisation of omicron spike-expressing lentivirus (ο-NAbs) was presented as log_{10} IC_{50}, which was calculated from sample titration curves. Statistically significant differences between groups in all figures were determined through parametric t tests or non-parametric Mann-Whitney tests (*=P<0.05, **=P<0.01, ***=P<0.001); when data did not follow a normal distribution, a "+" was added to the left corner of the graph. On violin plots, the dashed black line represents the group median response.

The neutralising capacity of NALT fluid was also assessed via Luminex ACE-2 competition assay (Figure 4.8C) and lentivirus pseudoneutralisation assay (Figure 4.8D). Higher levels of ο-ACE2^{comp}-Abs (P=0.0035) and ο-NAbs (P=0.0022) were generated following IN-boosting compared with IM-boosting. Hence, IN-boosting resulted in elevated antibody responses to omicron locally in the respiratory compartment.

2.2.1.4 Antibody responses to earlier ancestral variants in serum and NALT fluid

It was then assessed whether elevated cross-reactive humoral responses to earlier ancestral variants (and WT) were elicited systemically in the blood and locally in the NALT following IN-boosting with Ad-ο, compared with IM-boosting (Figure 4.9). Following IN-boosting, elevated levels of both IgG and IgA against all tested ancestral variants were observed in both sera and NALT fluid compared with levels following IM-boosting (Ad-WT^{IM}+Ad-ο^{IN}>Ad-WT^{IM}+Ad-ο^{IM}, P≤0.0001 and P=0.0006, for sera (Figure 4.9A) and NALT (Figure 4.9D) IgG, respectively, and P=0.0022 for sera (Figure 4.9B) and NALT (Figure 4.9E)

IgA. Ancestral variant-binding antibodies in serum and NALT fluid also strongly inhibited ACE-2 binding (Anc-ACE2^{comp}-Abs) in the Luminex assay following IN-boosting: Ad-WT^{IM}+Ad-o^{IN}>Ad-WT^{IM}+Ad-o^{IM}, P=0.0022 and P=0.0006, for sera (Figure 4.9C) and NALT (Figure 4.9F). Collectively, administering Ad-o as an IN-boost resulted in higher levels of cross-reactive response to ancestral variants both in sera and in NALT, compared with IM administration.

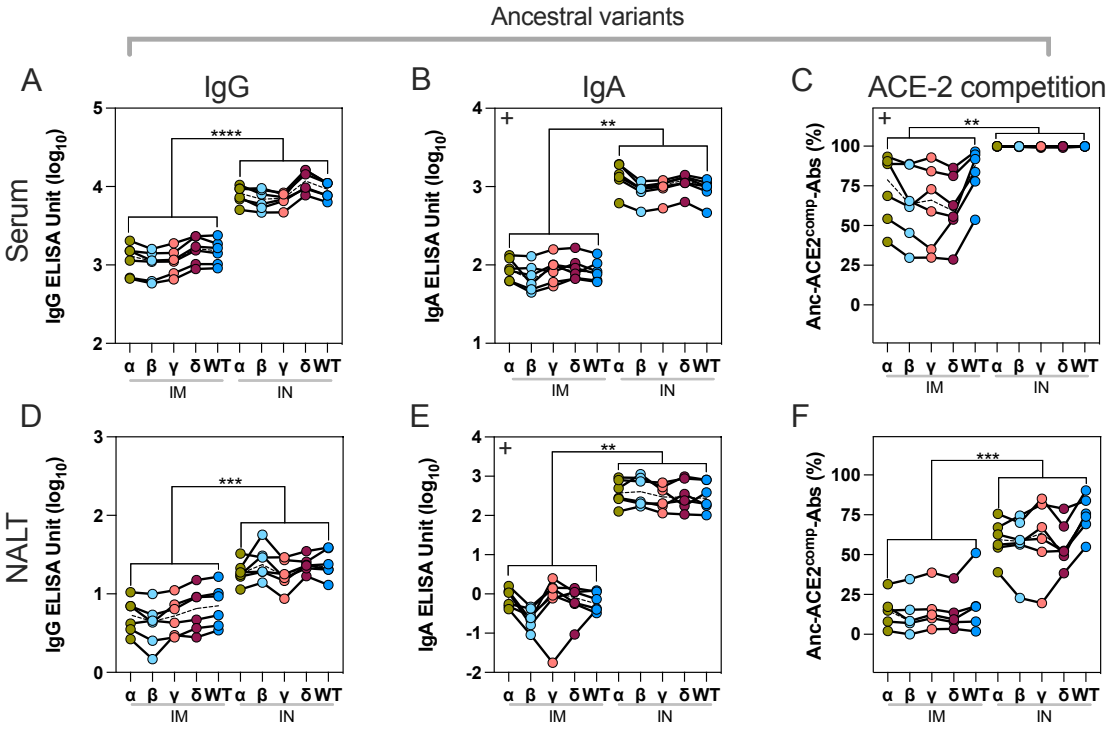

Figure 4.9: Antibody responses to earlier ancestral variants in serum and NALT fluid

Serum IgG (A), IgA (B) and ACE2^{comp}-Ab (C) and NALT fluid IgG (D), IgA (E) and ACE2^{comp}-Ab (F) responses to ancestral (variant) alpha, beta, gamma, delta and WT spike in serum following Ad-WT^{IM}+Ad-o^{IM} and Ad-WT^{IM}+Ad-o^{IN} regimens (n=6, experiment completed twice with one representative dataset shown). Regimens were compared statistically using either parametric T tests or non-parametric Kruskal-Wallis tests, depending on whether data were normally or non-normally distributed, respectively (**=P<0.01, ***=P<0.001 and ****=P≤0.0001). When data did not follow a normal distribution, a "+" was added to the left corner of the graph. On plots, the dashed black line represents the group median response.

2.2.1.5 Antibody responses to omicron subvariants

Given the observation that Ad-WT^{IM}+Ad-o^{IN} vaccination elicited a very strong cross-reactive response to earlier ancestral variants, it was then assessed whether antibody responses extended to newer omicron subvariant spike antigens. To do this, an omicron subvariant bead panel was created and Luminex ACE-2 competition assay performed with serum samples (Figure 4.10A). The measurement of ACE-2-competing NALT fluid antibodies could not be completed due to limited sample volume. The quantity of ACE-2-competing BA.1, BA.2, BA.4/5/5.1, BQ.1.1, XBB.1.5 and XBB.1.16 spike-reactive antibodies was measured.

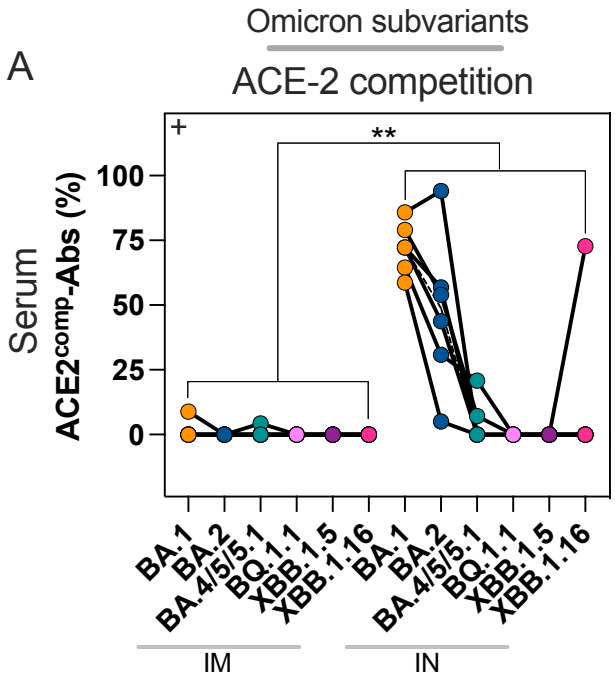

Figure 4.10: Antibody responses to omicron subvariants

(A) ACE2^{comp}-Abs reactive to omicron subvariant full spike: BA.1, BA.2, BA.4/5/5.1, BQ.1.1, XBB.1.5 and XBB.1.16 measured in the serum of mice following Ad-WT^{IM}+Ad-o^{IM} and Ad-WT^{IM}+Ad-o^{IN} regimens (n=6, experiment completed twice with one representative dataset shown). Regimens were compared statistically using a non-parametric Kruskal-Wallis test, as data was non-normally distributed (as indicated with the "+" symbol) (**=P<0.01). On plots, the dashed black line represents the group median response.

Following Ad-WT^{IM}+Ad-ο^{IM} vaccination, no detectable anti-omicron subvariant spike ACE-2-competing antibodies were measured in serum. Contrastingly, the Ad-WT^{IM}+Ad-ο^{IN} regimen did elicit detectable BA.2-ACE2^{comp}-Abs and certain mice generated trace amounts of BA.4/5/5.1-ACE2^{comp}-Abs, although, the overall levels of omicron subvariant spike-binding ACE2^{comp}-Abs were low in following this regimen as well (P=0.0022). These findings reflect the considerable antigenic distance between the omicron subvariants tested relative to the higher homology amongst 'primary' cluster earlier ancestral variants alpha, beta, gamma, delta and wildtype[325]. Therefore, although the cross-reactivity of serum following Ad-WT^{IM}+Ad-ο^{IN} extended to BA.2 spike, the overall cross-reactivity to the selected omicron subvariants tested here was poor.

2.2.2 Cellular responses following mucosal boosting of omicron vaccine

The cellular responses following IN- or IM-boosting were measured by flow cytometry using a pan-B and T cell panel (Table 2.4) and the gating strategy featured in Supplemental Figure 2. Anti-CD45 antibody was intravenously (IV) injected just prior to culling the mice to enable the exclusion of circulatory B and T cells from the measured lung-resident B and T cell populations.

2.2.2.1 B cell responses in the lungs following mucosal boosting of omicron vaccine

IN-boosted mice had greater numbers of class-switched lung B cells (CD45^{IV-} CD19^{+}IgD^{-}IgM^{-}) compared with IM-boosted mice (P=0.0174, Figure 4.11A). IN-boosted mice also had higher frequencies of class-switched ο-RBD-specific lung-resident B cells (defined as CD45^{IV-}CD19^{+}IgD^{-}IgM^{-}ο-RBD^{+}, non-significant) and o-RBD-specific plasma cells (defined as CD19^{-}CD138^{+}IgD^{-}IgM^{-}ο-RBD^{+}, P=0.0014) compared with IM-boosted mice

(Figure 4.11B). Greater numbers of lung B cells ($CD45^{IV-}CD19^{+}$) expressing common memory markers PD-L2, CD73 and CD80 (all non-statistically significant difference) were observed following IN-boosting compared with that following IM-boosting (Figure 4.11C)[336].

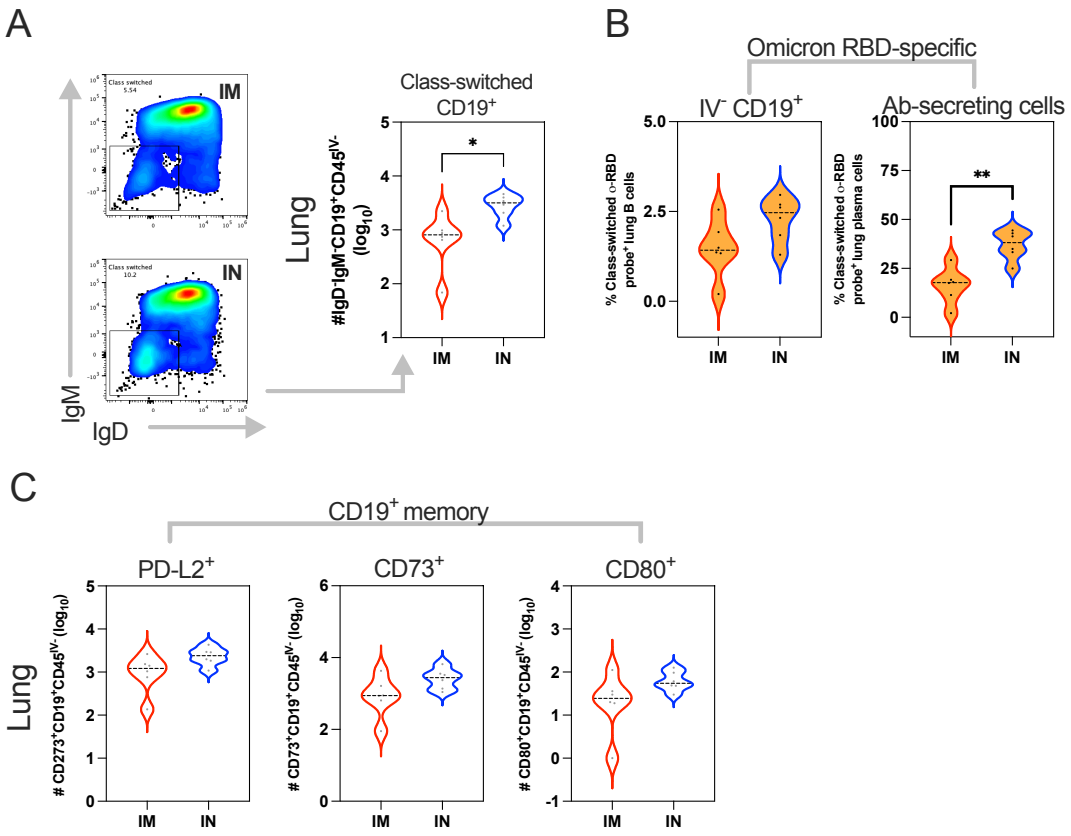

Figure 4.11: B cell responses in the lungs following mucosal boosting of omicron vaccine

B cell responses in the lungs of mice 5 weeks following Ad-WT^{IM}+Ad-o^{IM} and Ad-WT^{IM}+Ad-o^{IN} regimens (n=6, experiment completed twice with one representative dataset shown). (A) Total numbers (log_{10}) of class-switched lung B cells ($IgD^{-}IgM^{-}CD19^{+}CD45^{IV-}$) as measured through cell staining and flow cytometry. (B) Frequencies of o-RBD probe-specific lung plasma cells ($CD19^{-}CD138^{+}IgD^{-}IgM^{-}o\text{-}RBD^{+}$) and o-RBD probe-specific lung-resident B cells ($CD45^{IV-}CD19^{+}IgD^{-}IgM^{-}o\text{-}RBD^{+}$). (C) Total numbers ($log_{10}$) of PD-L2-, CD73- and CD80-expressing lung B cells ($CD19^{+}CD45^{IV-}$). Regimens were compared statistically using parametric T tests, as all data were normally distributed (*=P<0.05 and **=P<0.01). Group medians were represented as black dashed lines on violin plots.

2.2.2.2 T cell responses following mucosal boosting of omicron vaccine

The impact of IN-boosting on the T cell responses was next examined. Omicron-specific IFN$_\gamma$ T cell responses in the spleen and lungs were measured using ELISpot assay (Figure 4.12A). Cells were stimulated with peptides spanning the S1 domain of spike that contained omicron-specific mutations (Supplemental Table 1). A higher number of S1 spike-specific lung cells were observed in IN-boosted mice compared with IM-boosted (P=0.0022, Figure 4.12A), however in the spleen comparable numbers of IFN$_\gamma$-producing cells were measured following peptide stimulation (Figure 4.12A). Lung tissue-resident memory T cells (T_{RM}) were defined as $CD45^{IV-}CD69^+CD103^+CD62L^-CD44^+$ (for $CD8^+$) or $CD45^{IV-}CD69^+CD62L^-CD44^+$ (for $CD4^+$) and effector memory T cells (T_{EM}) as $CD62L^-CD44^+CD127^+$ (for both $CD4^+$ and $CD8^+$). Higher numbers of $CD8^+$ and $CD4^+$ lung T_{RM} ($CD8^+$ P=0.0030, $CD4^+$ P=0.0046, Figure 4.12B), and T_{EM} ($CD8^+$ P=0.0089, $CD4^+$ P=0.0004, Figure 4.12C) were observed by IN-boosting when compared with IM-boosting.

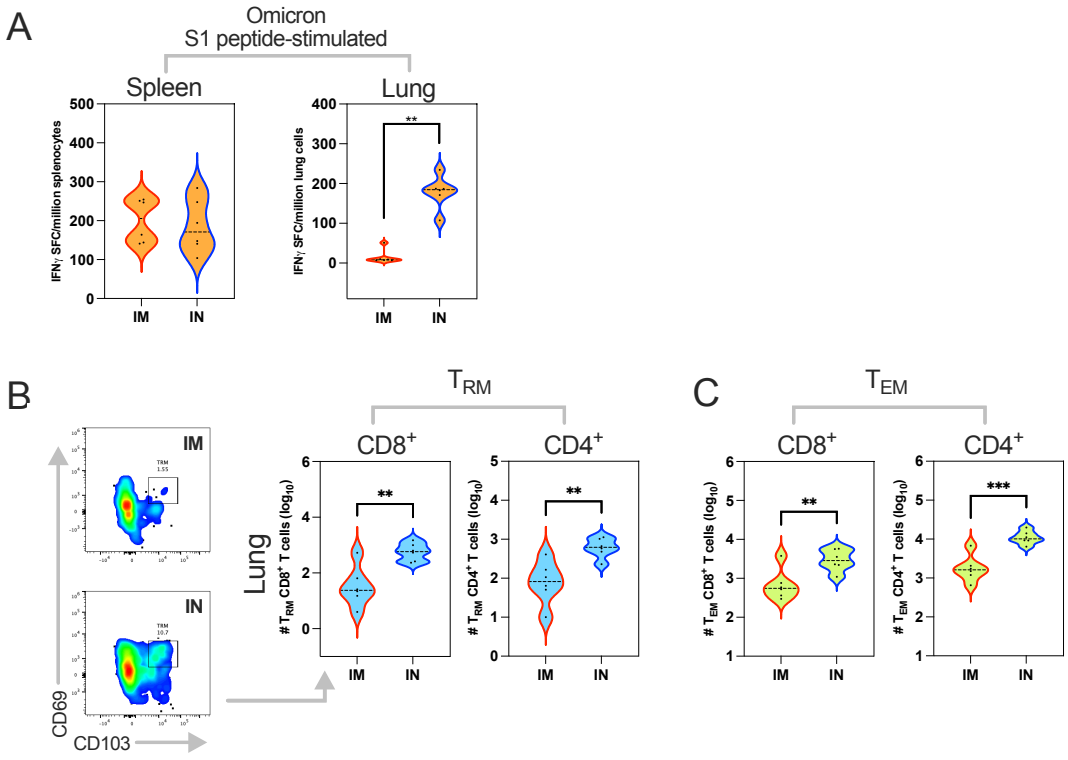

Figure 4.12: T cell responses following mucosal boosting of omicron vaccine

T cell responses in the lungs and spleens of mice 5 weeks following Ad-WT^{IM}+Ad-o^{IM} and Ad-WT^{IM}+Ad-o^{IN} regimens (n=6, experiment completed twice with one representative dataset shown). (A) Frequency of lung cells and splenocytes that released detectable IFNγ following stimulation with omicron S1 peptides (antigen-specific), measured by IFNγ ELISpot assay. (B) Total numbers (log_{10}) of lung-resident memory CD8$^+$ (CD45^{IV-}CD69$^+$CD103$^+$CD62L$^-$CD44$^+$) and CD4$^+$ (CD45^{IV-}CD69$^+$CD62L$^-$CD44$^+$) T cells. (C) Total numbers (log_{10}) of lung CD8$^+$ and CD4$^+$ effector memory T cells (CD62L$^-$CD44$^+$CD127$^+$). Regimens were compared statistically using parametric T tests, as all data were normally distributed (**=P<0.01 and ***=P<0.001). Group medians were represented as black dashed lines on violin plots.

Collectively, IN administration of Ad-o resulted in enhanced lung T and B cell responses compared with when administered IM, with non-inferiority of systemic T cell responses.

2.3 Mode of vaccinaₜion and the formation of immunological imprints

To further understand the relationship between mode of vaccination and the formation of immunological imprint, a series of experiments were conducted where mice were vaccinated with different combinations of routes for the prime and the boost, using the Ad-WT and Ad-o vaccines.

2.3.1 Mucosal boosting of omicron vaccine in mice primed with mucosal WT vaccine

The IM-priming of Ad-WT vaccine resulted in a suppressive imprint that was partially bypassed by the mucosal administration of Ad-o; I hypothesised this bypassing was a reflection of the anatomical separation of the respiratory compartment and the wider systemic compartment. Therefore, I wanted to investigate whether changing the route of the Ad-WT prime to the mucosal route (IN) also resulted in a suppressive imprint,

and whether mucosal administration of Ad-ο booster in IN-primed mice was able to overcome this potential suppression of omicron-specific response. To do this, an experiment was devised where mice were primed IN with Ad-WT, and then boosted IN with Ad-ο: Ad-WT^{IN}+Ad-ο^{IN} (Figure 4.13A). The reverse regimen was completed for comparison Ad-ο^{IN}+Ad-WT^{IN}. Omicron-reactive antibody responses were then assessed in the serum of mice.

A trend of elevated omicron-reactive response in the group of mice that received Ad-ο^{IN} as the prime vaccine, compared to the group of mice that received Ad-WT^{IN} as the prime vaccine, was noted when observing omicron spike-specific IgG, ο-ACE2^{comp}-Abs and ο-NAbs in serum, but not omicron spike-specific serum IgA: Ad-ο^{IN}+Ad-WT^{IN}>Ad-WT^{IN}+Ad-ο^{IN}, IgG: P=0.0223, ο-ACE2^{comp}-Abs: ****=P≤0.0001 and ο-NAbs: P=0.0022 (Figure 4.13B, D and E). The levels of serum IgG following Ad-WT^{IN}+Ad-ο^{IN} were similar to those generated when mice were primed with Ad-ο^{IN} only (shown as a dashed blue line on figures), however median levels of serum ο-ACE2^{comp}-Abs were much lower (median 7.38 % ACE-2-competition) than the reference Ad-ο^{IN} prime-only levels (median 76.09 % ACE-2-competition) (Figure 4.13D). Certain mice also had undetectable ο-NAbs, with a group median response of 1.32 IC_{50} (log_{10}), which was also lower than the levels following Ad-ο^{IN} prime-only (3.00 IC_{50} (log_{10})) (Figure 4.13E).

Anti-omicron spike IgA levels in the serum were comparable between Ad-ο^{IN}+Ad-WT^{IN} and Ad-WT^{IN}+Ad-ο^{IN} regimens, as well as with the Ad-ο^{IN} prime-only group (Figure 4.13C). Hence, following Ad-WT^{IN}+Ad-ο^{IN}, omicron spike-reactive IgG and IgA were generated in sera, yet the functional capacity of these antibodies was low.

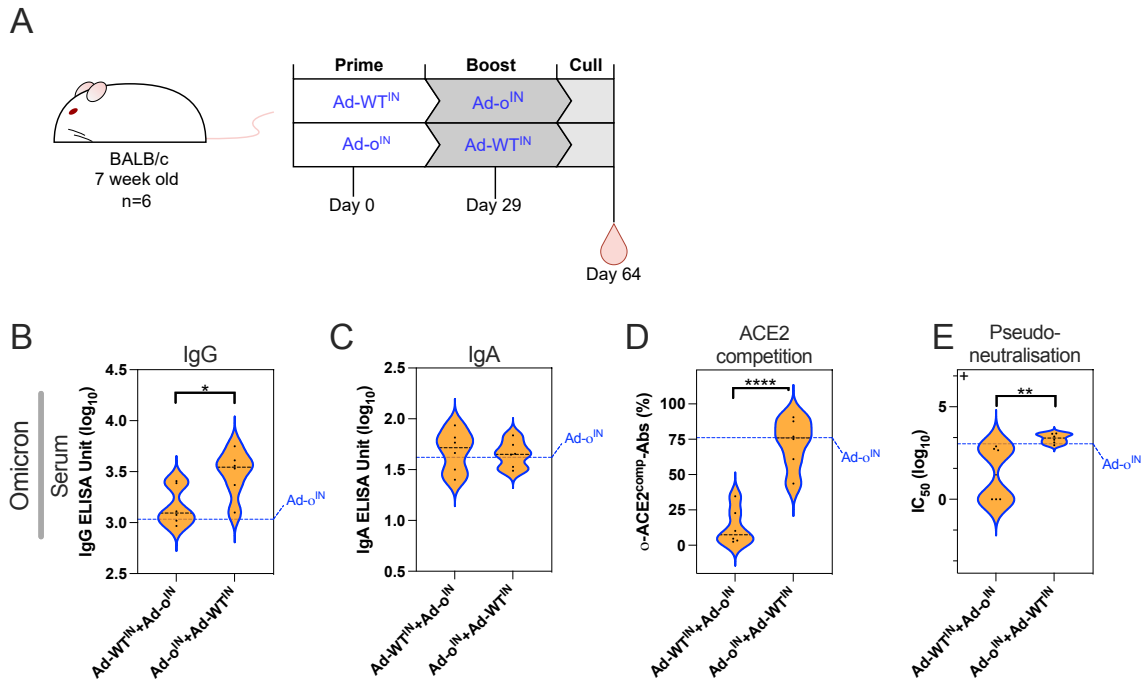

Figure 4.13: Mucosal boosting of omicron vaccine in mice primed with mucosal WT vaccine

(A) Vaccination schedule for the heterologous vaccination of mice with intranasally administered Ad-WT and Ad-o vaccine. 7-week-old BALB/c mice (n=6) were vaccinated on day 0 and day 29, with blood collected 5 weeks post-boost. The vaccination experiment was only completed once. Levels of total omicron spike-specific IgG (B) and IgA (C) were measured by standardised ELISA and presented as log_{10} ELISA units. (D) ACE-2-competing omicron S1-specific antibodies (o-$ACE2^{comp}$-Abs) were measured by Luminex assay and presented as % ACE-2 competition, which was calculated by using the reduction in measured binding compared to a negative internal control. (E) Pseudoneutralisation of omicron spike-expressing lentivirus (o-NAbs) was presented as log_{10} IC_{50}, which was calculated from sample titration curves. For graphs (B), (C), (D) and (E), the median group response following Ad-o^{IN} prime-only was added as a reference (shown as a dashed blue line) to assess whether the Ad-WT^{IN}-prime had a negative influence on latter Ad-o^{IN} response. The complete data for Ad-o^{IN} is featured in Chapter 5. Statistically significant differences between groups in all figures were determined through parametric t tests or non-parametric Mann-Whitney tests (*=P<0.05, **=P<0.01, ****=P≤0.0001); when data did not follow a normal distribution, a "+" was added to the left corner of the graph. On violin plots, the dashed black line represents the group median response.

In summary, Ad-WT^{IN} vaccination was shown to have a suppressive effect on latter omicron-neutralising responses to mucosal Ad-o^{IN} vaccination; mucosal administration of Ad-o^{IN} did not overcome imprint formed after Ad-WT^{IN} vaccination.

2.3.2 Intramuscular boosting of omicron vaccine in mice mucosally primed with WT vaccine

Given that the IN-boosting of omicron vaccine in Ad-WT IM-primed mice not only enhanced mucosal, but systemic responses, and the fact that IN-priming of Ad-WT vaccine resulted in a suppressive imprint that could not be bypassed by IN-boosting of the omicron vaccine, it is likely that the mucosal and systemic compartments may have a unidirectional relationship: I hypothesise that IN-priming results in an immune response that 'spills' from the lungs into the wider circulation, resulting in an imprint that extends beyond the mucosal compartment. In contrast, IM-priming results in an antibody response that is restricted to the blood, hence the immune imprint does not reach the lungs and affect heterologous IN-boosting responses in IM-primed mice (explaining the strong immunogenicity of the Ad-WT^{IM}+Ad-o^{IN} regimen).

To test this hypothesis, mice were prime-boost vaccinated with Ad-WT and Ad-o, but with the routes of vaccination reversed in order, so that the mode of prime vaccination was IN and the mode of boost IM (i.e., IN-IM, instead of IM-IN): Ad-WT^{IN}+Ad-o^{IM} (Figure 4.14A). The reverse order of vaccines for priming and boosting was also tested for comparison: Ad-o^{IN}+Ad-WT^{IM} (Figure 4.14A). The Ad-WT^{IM}+Ad-o^{IN} regimen that was tested previously was included in the figures to compare with the Ad-WT^{IN}+Ad-o^{IM} regimen; in such a way, it could be assessed whether Ad-o^{IM}-boosting failed to bypass the systemic imprint established from Ad-WT^{IN}-priming, unlike the Ad-WT^{IM}+Ad-o^{IN} regimen, where Ad-o^{IN}-boosting was able to bypass the suppressive Ad-WT^{IM}-prime-derived imprint (Figure 4.6). In addition, the reference median values of omicron-reactive immunity expected after Ad-o^{IM}-prime were added, so that any suppression could be identified (as indicated by

responses that are lower than the median Ad-o^{IM}-prime responses), as well as the reference median values expected after Ad-o^{IN}-prime, to assess for any boosting effect of the Ad-WT^{IM}-boost in the Ad-o^{IN}+Ad-WT^{IM}.

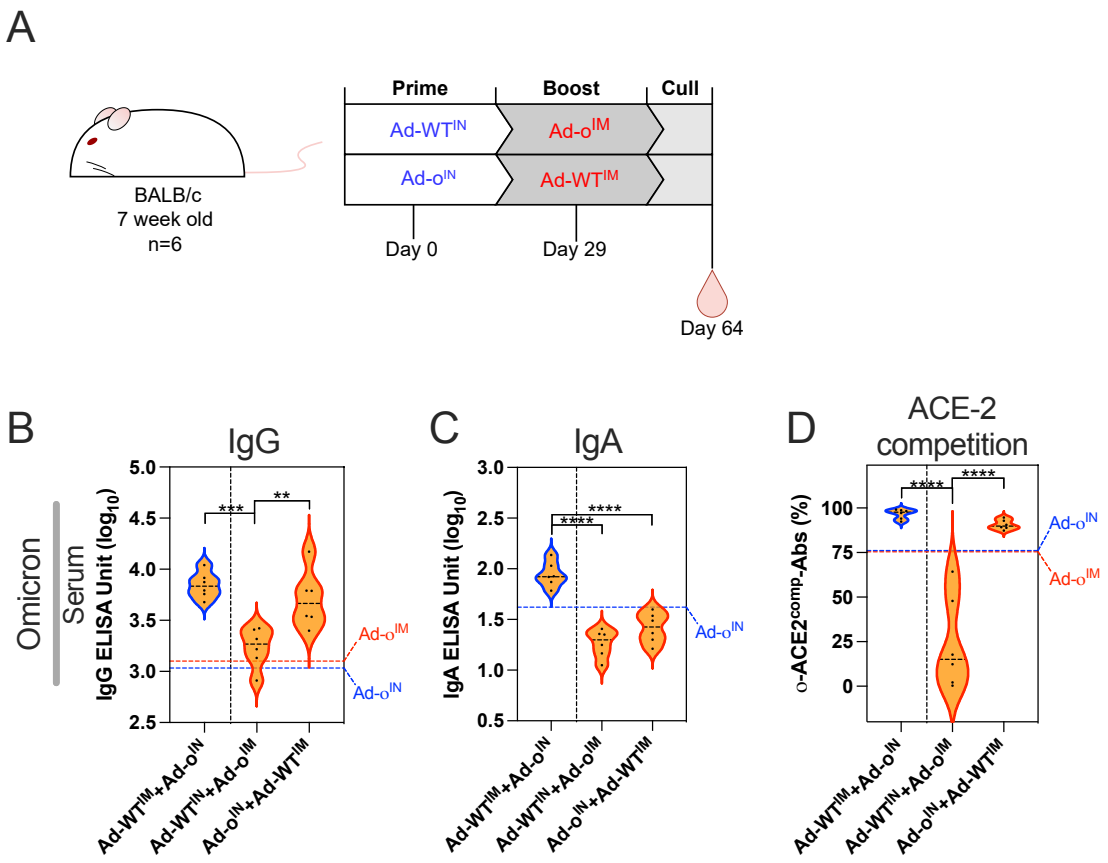

Figure 4.14: Intramuscular boosting of omicron vaccine in mice mucosally primed with Ad-WT vaccine

(A) Vaccination schedule for the heterologous vaccination of mice 7-week-old BALB/c mice (n=6) via Ad-WT^{IN}+Ad-o^{IM} and Ad-o^{IN}+Ad-WT^{IM} regimens. Mice were primed on day 0 and boosted on day 29. The vaccination experiment was only completed once. Sera was collected 5 weeks post-boost for the measurement of responses. Levels of total omicron spike-specific IgG (B) and IgA (C) were measured by standardised ELISA and presented as log_{10} ELISA units. (D) ACE-2-competing omicron S1-specific antibodies (o-ACE2^{comp}-Abs) were measured by Luminex assay and presented as % ACE-2 competition, which was calculated by using the reduction in measured binding compared to a negative internal control. For comparison, the responses after Ad-WT^{IM}+Ad-o^{IN} (measured previously in a separate experiment) were added on the left of graphs, separated by a black dashed line. For graphs (B) and (D), the median group response following Ad-o^{IM} prime-only was added as a reference (shown as a dashed red line) to assess whether the Ad-WT^{IN}-prime had a negative influence on latter Ad-o^{IM} response. Statistically significant differences between groups in all figures were determined through parametric t tests (**=P<0.01, ***=P<0.001, ****=P≤0.0001). On violin plots, the dashed black line represents the group median response.

5 weeks post-boost, the serum omicron spike-reactive IgG, IgA and ο-ACE2^{comp}-Ab responses were lower in the Ad-WT^{IN}+Ad-ο^{IM} group compared with the reference Ad-WT^{IM}+Ad-ο^{IN} group (Figure 4.14B, C and D); IgG: P=0.0004, IgA: P≤0.0001 and ο-ACE2^{comp}-Ab: P≤0.0001. Although the levels of serum IgG generated following Ad-WT^{IN}+Ad-ο^{IM} were comparable to the reference median level expected after Ad-ο^{IM} prime-only (Figure 4.14B), the levels of serum ο-ACE2^{comp}-Abs were far lower (median 15.04% ACE-2-competition) than the levels expected after Ad-ο^{IM} prime-only (median 75.39% ACE-2-competition). Together, the poor responses following Ad-WT^{IN}+Ad-ο^{IM} suggested the imprint formed after Ad-WT^{IN} vaccination could not be overcome by Ad-ο^{IM} vaccination.

In addition, the IgG and ο-ACE2^{comp}-Ab responses following Ad-WT^{IN}+Ad-ο^{IM} were lower than the reverse vaccine orientation regimen (Ad-ο^{IN}+Ad-WT^{IM}) (Figure 4.14B and D): IgG: P=0.0038 and ο-ACE2^{comp}-Ab: P=0.0004. The Ad-ο^{IN}+Ad-WT^{IM} regimen IgG and ο-ACE2^{comp}-Ab responses were higher than the Ad-ο^{IN} prime-only reference values, suggesting that the heterologous boosting of Ad-WT^{IM} vaccine back boosts responses developed after Ad-ο^{IN}-priming.

These observations support the hypothesis of a unidirectional relationship between the compartment targeted (i.e., mode of vaccination) in which anatomical regions (blood or respiratory mucosa/lungs) are subsequently stimulated, henceforth, form an immunological imprint. The direct comparison of the levels of omicron ACE-2-competing antibodies in the serum following Ad-WT^{IM}+Ad-ο^{IN} and Ad-WT^{IN}+Ad-ο^{IM} regimens highlighted this non-reciprocal relationship, whereby Ad-WT^{IM} did not result in an imprint that affected Ad-ο^{IN} responses, but Ad-WT^{IN} vaccination resulted in an imprint that impacted the Ad-ο^{IM} (and Ad-ο^{IN}, as shown in Figure 4.13) responses. The boosting of

omicron-reactive responses in the Ad-$\omicron^{IN}$+Ad-WT^{IM} regimen also supported the idea that IN vaccination stimulated not only the mucosa compartment but the wider systemic compartment; if the IN mode of vaccination resulted in a respiratory mucosa-restricted response, the IM vaccination of Ad-WT would presumably not result serum omicron-reactive responses that were higher than Ad-$\omicron^{IN}$ prime-only.

3. Discussion

In this chapter, it was demonstrated that by altering the route of vaccine administration, the effect of pre-existing immunity induced by intramuscular immunisation could be circumvented, and immune responses in the mucosa at the site of infection can be advantageously generated. Importantly however, this observed bypassing of the suppressive antibody imprint was shown to be dependent on the amount of circulating antibody present, and also influenced by the mode of previous WT prime vaccination. Specifically, it was observed that:

- De novo responses to Ad-$\omicron^{IN}$ were not suppressed by the prior transfer of Ad-WT^{IM}+Ad-WT^{IM}-derived anti-WT spike antibody serum, but that Novavax-WT^{IM}+Novavax-WT^{IM}-derived antibody serum did suppress responses.
- Suppressed omicron-reactive antibody responses in the blood were augmented when Ad-$\omicron$ was administered IN in Ad-WT^{IM}-primed mice, but not in Ad-WT^{IN}-primed mice
- IN-boosting elicited strong cellular and antibody responses in the respiratory mucosa in Ad-WT^{IM}-primed mice

- IN-boosting elicited broad, cross-reactive antibody responses in the serum and the respiratory mucosa in Ad-WT^{IM}-primed mice

Through passive antibody transfer experiments, it was observed that IN but not IM administration of omicron vaccine could bypass the suppression mediated by Ad-WT^{IM} spike vaccine-derived antibodies that form part of the immune imprint. I hypothesise this is due to the anatomically and immunologically distinct nature of the mucosal immune compartment; circulating, systemically-derived antibodies may not have as great a suppressive effect within the mucosal compartment, where circulatory IgG especially, has limited access, thus enabling a stronger de novo response to vaccine[331]. Mechanistically, the lack of suppressive antibody within defined mucosal niches is likely to result in reduced blunting of antigen expressed following Ad-ο vaccination, hence greater antigenic recognition by B cells. Through previous experiments, and following the IM-IM regimens tested in Chapter 3 and this Chapter, IM vaccination was shown to poorly stimulate the mucosal immune response; this suggests the prime-derived imprint is restricted to the systemic compartment which includes the circulatory system, but not the defined mucosal niches. As shown in Chapter 3, the transfer of anti-vector antibodies did reduce the immunogenicity of Ad-ο^{IM}, albeit to a much less extent than the transfer of anti-WT spike antibodies; as anti-vector antibodies may bind to vector and prevent subsequent antigen expression, their absence in the mucosal compartment is also likely to contribute to an extent to the enhanced responses following the mucosal boost route compared with the IM boost route.

When greater quantities of anti-WT spike antibody were transferred that were produced by Novavax-WT^{IM}+Novavax-WT^{IM}-vaccinated mice, the de novo responses to Ad-ο were suppressed even when it was administered via the mucosal route, indicating that

the ability of mucosal vaccine administration to bypass a suppressive imprint is contingent on the concentration of pre-existing suppressive antibodies, and potentially, the composition and features of the polyclonal antibodies that were transferred (that are reflective of the vaccine modality in the inbred mouse model). These findings warrant further investigation of the relationship between blood antibody concentration and the ability to bypass the suppressive imprint, possibly via a dose response-type passive antibody transfer experiment, as well as investigation of the how mechanistically the transferred Novavax-WT^{IM}+Novavax-WT^{IM} serum antibodies suppress these de novo responses to omicron vaccine. I hypothesise that circulatory IgG from Novavax-WT^{IM}+Novavax-WT^{IM} vaccination enters the mucosal compartment via either passive transudation or FcRn-mediated transcytosis; it is possible that at higher or "saturating" circulatory antibody concentrations transudation occurs to a greater extent (i.e., transudation is a function of concentration of circulatory antibody), with IgG "spilling" into the mucosa compartment and subsequently negatively interfering with the local de novo responses to booster vaccine[337].

The relationship between transudation of antibody and mucosal vaccination is unclear; it would be interesting to investigate how mucosal vaccination influences the likelihood of transudation and transcytosis of circulatory antibody, i.e., whether mucosal vaccination, e.g., through augmenting lung inflammation poises the lungs for greater influx of circulatory antibody. To investigate this further, an experiment could be devised where antibody sera is transferred into naïve mice via IV injection, and then the mice either vaccinated IN with irrelevant vaccine control (e.g., Ad-GFP) or left unvaccinated. Three weeks post-vaccination, WT spike-specific antibodies could be measured in the respiratory

mucosa fluids to determine whether Ad-GFP^{IN} vaccination has had an influence on the influx of transferred, circulatory antibody into the mucosa or not.

Of important note, murine IgA that is generated systemically is known to efficiently cross into the mucosa via transcytosis (via the polymeric Ig receptor (pIgR)), unlike in humans[245]; should the concentration of IgA in the Novavax-WT^{IM}+Novavax-WT^{IM}-vaccinated sera that was transferred be higher than in the Ad-WT^{IM}+Ad-WT^{IM}-vaccinated sera, more suppressive IgA may have then entered the mucosal compartment and interfered with the de novo responses to Ad-o. Henceforth, the two following approaches could provide further mechanistic insight to the findings: firstly, measurement of the relative levels of WT spike-reactive IgA in the Ad-WT^{IM}+Ad-WT^{IM} and Novavax-WT^{IM}+Novavax-WT^{IM} sera pools that were transferred into mice, and secondly, comparison of the effect of prior transfer of WT spike-reactive IgG or IgA isotypes on Ad-o immunogenicity. These potential mechanisms have important implications when considering the outcome of heterologous mucosal boosting in humans: as human monomeric IgA produced in the blood following systemic vaccination is less effective at reaching the mucosa, this could influence how circulatory antibodies at higher concentrations impact the de novo response to mucosally-administered Ad-o in humans. Lastly, investigation of other differences to the antibody composition of the serum pools and specific features of the antibodies produced from the Novavax-WT^{IM}+Novavax-WT^{IM}- and Ad-WT^{IM}+Ad-WT^{IM}-vaccinated donor mice could be of interest for understanding the differences observed in the data. For example, serum antibody from the respective Novavax-WT^{IM}+Novavax-WT^{IM} and Ad-WT^{IM}+Ad-WT^{IM} groups could be normalised and FcR-engagement subsequently measured, such as to determine whether a certain antibody profile is more effective in localising to the mucosa. As mentioned earlier in Chapter 3, the

avidity of antibody is also likely to influence the suppressive capacity of the antibody; the general differences between avidity between IgA (dimeric, but generally lower affinity) and IgG (generally higher affinity via the GC reaction, but monomeric) should be considered when moving forward with these proposed experiments, and can be measured via normalised avidity assay.

When the Ad-o omicron vaccine was administered IN in mice that were primed with Ad-WT IM, strong omicron-specific antibody responses were elicited both locally in the respiratory mucosa and systemically, contrasting the much poorer responses that were measured when Ad-o was administered IM. Additionally, the responses elicited following IN-boosting were much more cross-reactive to earlier ancestral variants locally in the mucosa, and systemically in the serum. As expected, elevated levels of mucosal immunity were measured in the IN-boost group: antigen-specific IgA, T_{RM}, B_{RM} and NAbs. Hence, IN-boosting was shown to not only result in superior systemic omicron-specific responses compared with the IM boost group, but additionally augment the mucosal immunity in mice. The assessment of Ad-o as a mucosal booster vaccine in mice vaccinated with other WT spike vaccines, especially those that elicit higher titres of antibody, such as Novavax-WT, would be a relevant area of further exploration.

The benefit of an IM-prime, IN-boost (IM-IN) regimen or 'prime-pull' strategy has previously been demonstrated with WT spike-encoding vaccines, where the same target antigen (homologous) is used for the prime and the boost[92,303–305,338]. Studies have noted enhanced systemic responses, as well as increased respiratory mucosal IgA, IgG, NAbs and lung T_{RM} levels, following the dual-mode IM-IN regimen when compared with regimens solely involving IN or IM vaccination[303–305,338]. More recently, preclinical studies have tested heterologous IN-boosting with a range of different omicron vaccines in WT spike-primed

mice, including a recombinant omicron RBD-nucleoprotein fusion protein booster, an MVA booster encoding omicron spike, and an Ad5-based omicron spike booster[300–302]. In alignment with the findings presented in this chapter, such studies described enhanced omicron-specific respiratory mucosal immunity; they also reported reduced omicron replication upon challenge, when booster vaccine was administered IN.

A particularly relevant study that strongly supported the findings in this chapter compared the protection provided by a bivalent WT and BA.5 spike adenovirus booster vaccine that was administered via the IN or aerosol route, with the protection provided by a dual WT and BA.5-encoding mRNA vaccine that was administered IM, following XBB.1.16 challenge in NHPs[298]. The mucosal routes tested were able to provide upper airway protection, which was uniquely correlated with mucosal IgA, whereas the IM boost route only offered lower airway protection, which was correlated with lung IgA, IgG and T cell responses[298].

Interestingly, when the fraction of omicron RBD-reactive serum IgG derived from the IN-boost group was further dissected through a WT spike depletion assay, most of the omicron RBD-reactive IgG was shown to be cross-reactive with WT spike, and IgG from either regimen (Ad-WT^{IM}+Ad-o^{IN} and Ad-WT^{IM}+Ad-o^{IM}) were out-depleted to the same extent. This suggested that at least on a serological level, the elevated levels of omicron-specific IgG immunity following IN-boosting were still likely derived from back-boosting of the pre-existing Ad-WT^{IM}-derived imprint, and not from a de novo-type response to omicron vaccine. I had initially hypothesised that part of the reasoning for the observed bypassing of the suppression of the omicron responses was a more de novo-like immune response to omicron vaccine. I hypothesise that the phenotype of the immune response to IN-boost is dependent on the identity of the immune compartment, i.e., more de novo-like

in the respiratory mucosa, and more back-boosting-like in the systemic compartment/blood, and that the mucosal IgA induced upon IN-boost would have a de novo-type origin (Figure 4.15). Due to a limited sample volume, WT spike depletion assays with mucosal fluid samples could not be completed, which would help in understanding whether mucosal antibodies were derived from a back boosting response or more de novo-like response. In addition to this, the reactivity of MBC within the NALT could be examined through stimulation of the extracted NALT palates with omicron or WT RBD and subsequent measurement of the secreted antibody within the culture supernatant; it would be expected that the Ad-WT^{IM}+Ad-ο^{IN} regimen would generate greater quantities of omicron-specific mucosal MBC compared with WT-specific MBC, and that more omicron-reactive antibody would be secreted into culture fluid when omicron spike used as stimulant compared with when using WT spike as stimulant.

The draining of antigen from the respiratory tract into lymph nodes may subsequently stimulate and perpetuate a pre-existing primary B cell cohort established from systemic IM-priming, whereas the more "naïve" respiratory mucosa less influenced by suppressive antibody, may support a more de novo-like response to Ad-ο. Nevertheless, the presence of cross-reactive and cross-neutralising (reactive to ancestral variants) antibody in the NALT still indicated the possibility of a back boosted response in the mucosa; in such scenario perhaps the overall greater immunogenicity of the vaccine within the mucosa as a result of less interference from pre-existing antibody promoted a stronger, more functional/quality cross-reactive response to omicron than what was measured following omicron IM-boosting.

Finally, when the mode of Ad-WT prime was changed from IM to IN, it was observed that 1. IN-priming with Ad-WT also established a suppressive imprint and that 2. Neither

the IN-boosting nor the IM-boosting of Ad-ο were able to bypass the suppressive imprint and augment the omicron-reactive responses in the blood. The formation of a suppressive imprint following IN reflected the unidirectional relationship between IM and IN modes of vaccination and their capacity to stimulate mucosal and/or systemic compartments: IM vaccination stimulated systemic immunity, but did not readily stimulate the mucosal compartment, however IN vaccination was capable of stimulating both local mucosal and wider systemic compartments. Importantly, the IN vaccination route in mice involved administering 25 µL of vaccine through the nostrils, and previous experiments completed by Marta Ulaszewska and Alexandra Spencer (unpublished data, The Jenner Institute) showed that at such a volume, vaccine likely reaches the lung airways in addition to the nasal passages. Hence, the presence of vaccine in the URT and LRT together, and subsequent draining of antigen ("spill"), induced a more systemic-type response in addition to the more localised URT response, thus explaining the suppressive imprint formed following Ad-WT^{IN} vaccination. It would be of interest to measure the omicron-neutralising responses within the mucosal fluids following the Ad-WT^{IN}+Ad-ο^{IN} regimen to confirm that these responses are equally suppressed in the mucosal compartment, however, this was not completed for this experiment.

In addition to the generation of anti-WT spike antibodies in the mucosa following Ad-WT^{IN}-prime that would contribute to the suppression of Ad-ο^{IN} boost responses, is the potential contribution of Ad-WT^{IN}-prime-derived ChAdOx1 NAbs (anti-vector). As mentioned in Chapter 3, the window of opportunity by which anti-vector antibodies bind and prevent ChAdOx1 infection of host cell is likely to be minimal and anti-vector antibodies cannot physically access the muscular tissue; in contrast to this, anti-vector antibodies could be secreted into the mucosa following Ad-ο^{IN}-prime and more readily

access and neutralise ChAdOx1 virus if the booster is also administered mucosally. Henceforth, anti-vector immunity located in the mucosa may have a greater suppressive effect than when located in the systemic compartment. Further exploration of the relative levels of contribution of anti-vector immunity to suppression of the de novo response between mucosal and systemic compartments is warranted; this could be assess through IN-priming with non-ChAdOx1 WT spike vaccine, and then Ad-υ^{IN} boost (i.e. Novavax-WT^{IN}+Ad-WT^{IN} or Pfizer-WT^{IN}+Ad-υ^{IN}).

The observation of elevated immunogenicity following the heterologous Ad-WT^{IM}+Ad-υ^{IN} regimen presented in this chapter prompted further investigation the potential mechanisms underpinning these responses (Chapter 5).

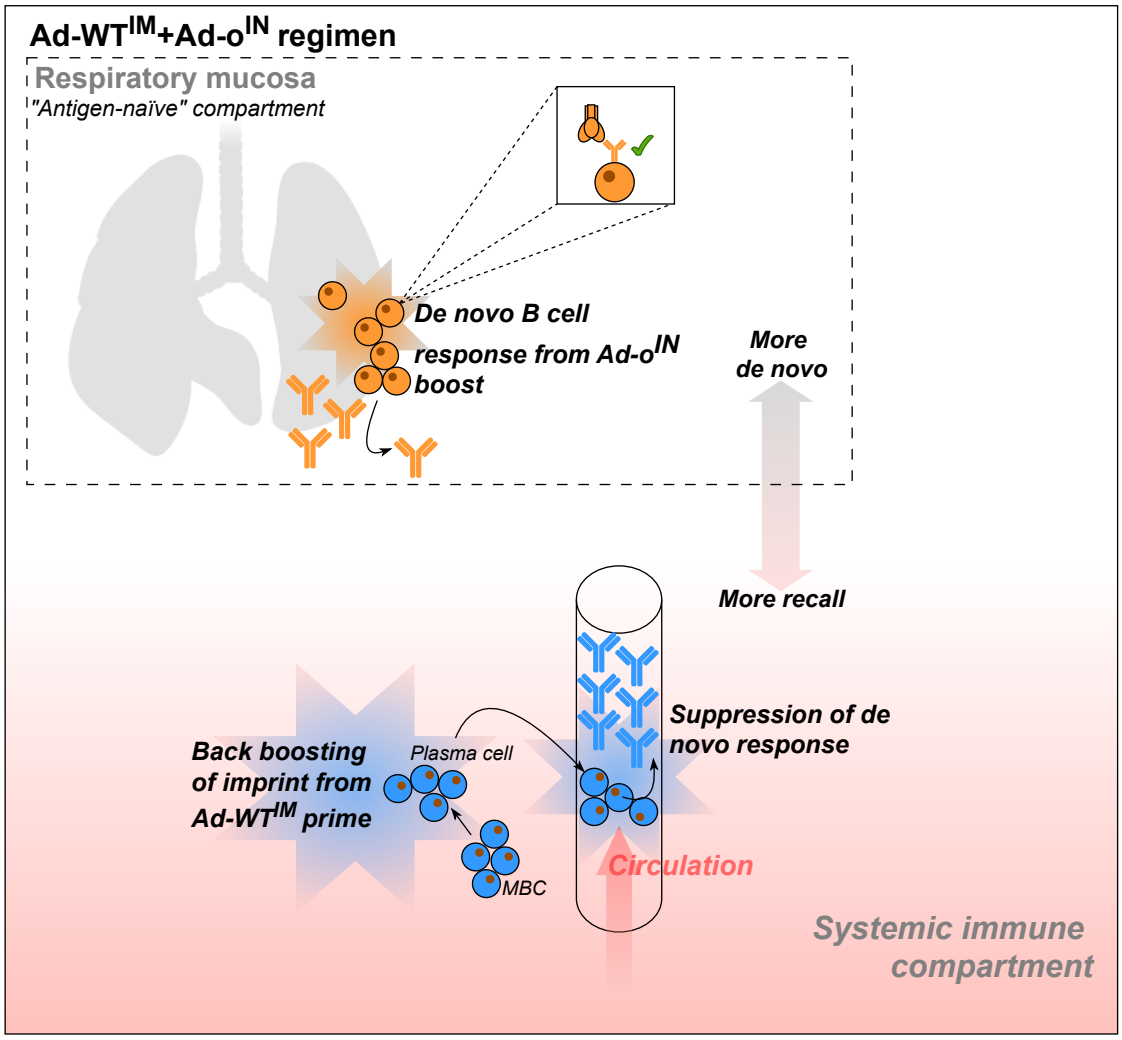

Figure 4.15: Schematic depicting features of the immune responses in the respiratory and systemic compartments following the Ad-o^{IN}-boost of Ad-WT^{IM}-primed mice

Orange antibodies and B cells represent de novo responses to omicron antigen following Ad-o-boosting. Blue antibodies and B cells are those generated following prime vaccination with Ad-WT, and subsequently re-stimulated upon Ad-o-boosting. The arrow depicts a de-novo-to-recall immune response axis model in which the mucosal and systemic compartments undergo different types of immune response. The tubular drawing depicts a blood vessel in which suppressive antibodies from priming and back-boosting reside.

5

Further delineation of the mechanisms driving the heterologous omicron vaccine mucosal boost response

5. Further delineation of the mechanisms driving the heterologous omicron vaccine mucosal boost response

1. Introduction and aims
2. Results

2.1 Origins of MBC generated in the lungs following Ad-WT^{IM}+Ad-o^{IN}

2.1.1 Cell lineage tracing of GC B cells derived from the Ad-WT^{IM}-prime vaccination following omicron vaccine boost

2.2 Assessing the potential involvement of memory T cells derived from Ad-WT^{IM} vaccination on the Ad-o^{IN} boost responses

2.2.1 The benefit of Ad-WT^{IM}-prime vaccination on latter antibody responses to Ad-o^{IN} vaccination

2.2.2 Adoptive cell transfer of splenocytes generated from Ad-WT^{IM} vaccination prior to mucosal-boosting

3. Discussion

1. Introduction and aims

Administering the Ad-ο omicron booster vaccine via the mucosal route (Ad-$\omicron^{IN}$) bypassed the suppressive effects of a pre-existing imprint established by Ad-WT^{IM} vaccination (Chapter 4). In addition to Ad-$\omicron^{IN}$ vaccination rescuing the suppressed omicron-reactive responses in the blood, the regimen was able to induce strong cross-reactive responses both locally in the respiratory mucosa and systemically in the blood. I thus hypothesised that the Ad-WT^{IM}-prime might provide a certain 'benefit', contributing to the elevated latter omicron-specific, and cross-reactive antibody responses. I hypothesised that this could be due to the contribution of pre-existing, cross-reactive T cells from the Ad-WT^{IM} vaccination, as T cells are more broadly reactive and less affected by the drifting and shifting of SARS-CoV-2 spike antigen[339], and thus may positively contribute to the latter Ad-$\omicron^{IN}$ response.

As passively transferred antibodies derived from Ad-WT vaccination did not suppress the subsequent de novo responses to Ad-$\omicron^{IN}$ vaccine, I proposed that the part of the mechanism leading to the enhanced omicron-specific immunogenicity of the Ad-WT^{IM}+Ad-$\omicron^{IN}$ regimen was a more de novo-type B cell response, as opposed to back boosted response, in the respiratory mucosa. To investigate this more directly, the antigen-experienced B cells derived from prime vaccination were directly traced and measured in the lungs following vaccine boost, with the aim of determining whether the lung B cell pool was seeded by pre-existing, systemically-derived MBC that homed to the lungs following Ad-$\omicron^{IN}$ boost recall response, or whether naïve mucosa-derived B cells that encountered omicron antigen upon the boost vaccination seeded and predominated the lung B cell response.

In this chapter, the aim was to further dissect the mechanisms driving the bypassing of suppressed omicron-reactive responses and the generation of broad antibody immunity with the Ad-WT^{IM}+Ad-ο^{IN} regimen. To do this, cell transfer and cell lineage-tracing experiments were devised to track lymphocytes derived from Ad-WT^{IM}-prime vaccination following the Ad-ο^{IN} boost. Specifically, the potential role of the following were examined:

1. Ad-WT^{IM}-derived MBC on the latter Ad-ο^{IN} response in the lungs
2. Ad-WT^{IM}-derived splenic (systemic) T cells on the latter Ad-ο^{IN} response in the lungs

2. Results

2.1 Origins of MBC generated in the lungs following Ad-WT^{IM}+Ad-o^{IN} vaccination

2.1.1 Cell lineage tracing of GC B cells derived from the Ad-WT^{IM} prime vaccination following omicron vaccine boost

I hypothesised that one of the mechanisms behind the bypassing of the omicron-specific responses was a more de novo-like B cell response in the respiratory mucosa following IN-boosting; this hypothesis is supported by the observation of a lack of suppressive effect of passive transfer of Ad-WT antibodies in mice prior to Ad-ο^{IN} vaccination. To further investigate this hypothesis, the origins of omicron-specific B cells present in the lungs were deciphered, to discern whether they were derived from the primary cohort of memory B cells generated following the Ad-WT^{IM} prime vaccination response (recall), or whether they are (local) naïve B cells that have been activated solely upon IN-boost (de novo).

To track B cells from the Ad-WT prime vaccination, transgenic B cell reporter mice were utilised; these mice were bred, maintained and vaccinated by Lyn Yong, who also performed the sample processing, flow cytometry experiments and data collection. The data were then analysed by Cameron Bissett. The transgenic mice were of a C57BL6/J

background (as opposed to BALB/c, as the latter were not available for use), and constitutively expressed a tamoxifen-inducible Cre recombinase-estrogen receptor 2 fusion protein (ERT2cre) under the S1pr2 promoter, which is expressed in all germinal centre (GC) B cells (Figure 5.1A)[268]. The gene for a red fluorescent protein "tdTomato" was also inserted under a constitutively expressed promoter, but downstream of a stop cassette that must be excised by ERT2cre (bound by tamoxifen) to be expressed[268]. Henceforth, during the tamoxifen treatment of these mice, all GC B cells (i.e. antigen-experienced), as well as their descendants, permanently express tdTomato and can be identified[268].

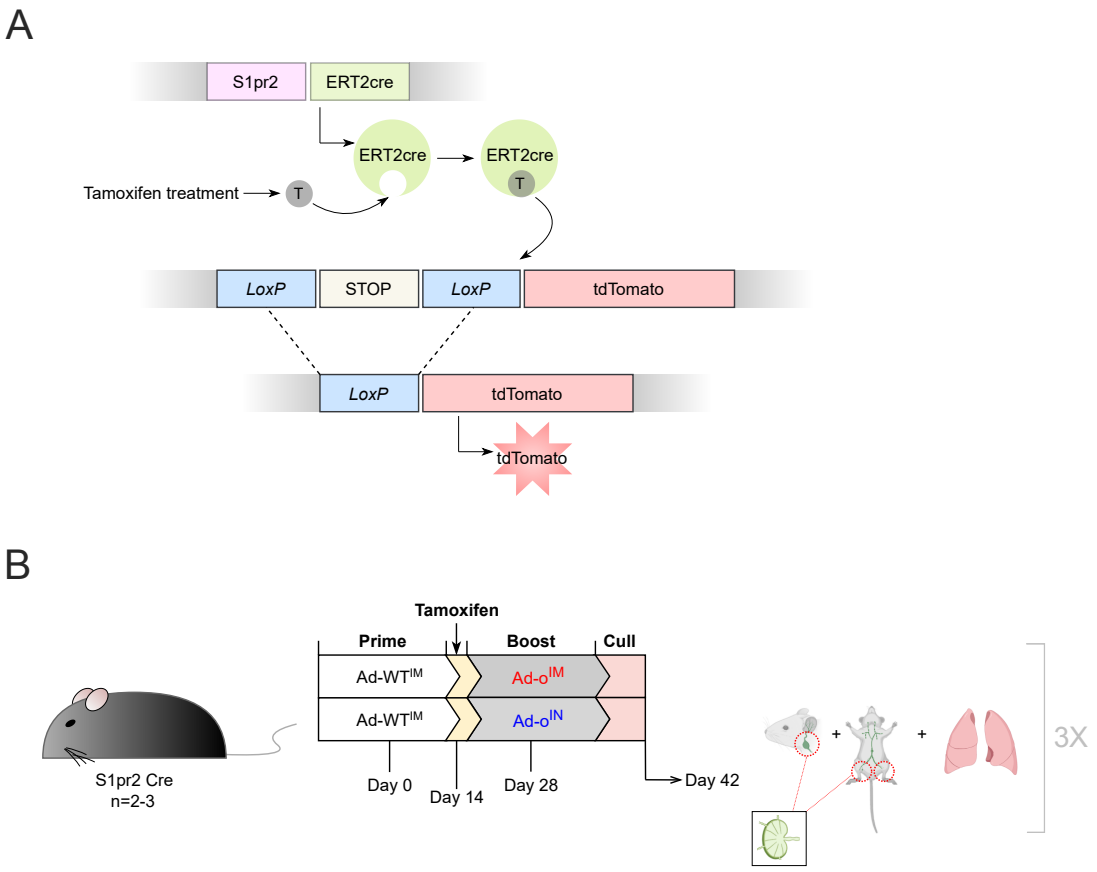

Figure 5.1: S1pr2 transgenic mouse model for the labelling of Ad-WT^{IM}-prime B cells

(A) The transgenic S1pr2 (Sphingosine-1-phosphate Receptor 2)-Cre tdTomato mouse system: The tamoxifen-induced ERT2cre recombinase gene was added downstream of the germinal centre B cell-expressed promoter S1pr2. Upon tamoxifen treatment, ERT2cre is able to catalyse the excision of a stop codon upstream of red fluorescent protein tdTomato, leading to its expression and subsequently permanently labelling the cell. (B) Vaccination schedule using transgenic "S1pr2-Cre tdTomato" fate tracking mice. Tamoxifen was administered in mice 14 days post-prime at time of optimal germinal centre (GC) B cell production. Mice were culled two weeks post-boost, with left and right inguinal lymph nodes (LILN and RILN, respectively), cervical lymph nodes (CLN) and lungs removed for analysis. The experiment was completed three times, with data compiled from the three separate repeats (n=2-3). The vaccination experiment, tissue processing, cell staining and flow cytometry was conducted by Lyn Yong.

The transgenic mice were primed with Ad-WT IM, and then either boosted with Ad-ο IM or IN 28 days later (Figure 5.1B), with tamoxifen treatment occurring 14 days post-Ad-WT IM prime, a period of optimal GC B cell output, to label prime vaccination GC B cells with tdTomato[268]. The immune responses in the lungs, as well as cervical lymph nodes (CLN), and right and left inguinal lymph nodes (RILN and LILN) were assessed 2 weeks after booster vaccination by cell staining and flow cytometry. The lymph nodes (LN) were assessed due to their abundance of GC B cells; specific LN were harvested due to their proximity to site of vaccination, i.e., CLN and IN vaccination, and RILN, IM vaccination, with the LILN serving as a control for comparison to the RILN. The lungs were also assessed to identify the potential presence of prime-derived, tdTomato$^+$ cells.

GC B cells were defined as cells expressing Fas$^+$GL7$^+$IgD$^-$B220$^+$ (Figure 5.2A). The total frequencies of GC B cells (labelled and unlabelled) measured reflected the route of vaccination, with higher frequencies observed in the LNs nearest to the site of vaccination; mice that received two IM doses of vaccine (Ad-WT^{IM}+Ad-ο^{IM}) in the right inner thigh muscle had higher measurable frequencies of GC B cells in the RILN node compared with mice that were vaccinated Ad-WT^{IM}+Ad-ο^{IN} (receiving one IM dose) (Figure 5.2B,

P=0.0022). In contrast, a higher frequency of GC B cells were observed in the respiratory draining LNs (CLN) following IN-boosting compared with IM-boosting (Figure 5.2D, non-significant difference). Frequencies of GC B cells in the LILN and lungs were low and comparable between IM- and IN-boosted mice (Figure 5.2C and E). Within the relevant draining LN (RILN following IM and CLN following IN), a greater proportion of GC B cells that were tdTomato$^+$ following IM boost (40% tdTomato$^+$) were detected, compared with IN boost (25% tdTomato$^+$) (Figure 5.2B and D). Interestingly, the large tdTomato$^+$ fraction (despite low overall frequency of GC B cells) seen in the RILN following IN boost (58% tdTomato$^+$) appeared to reflect the residual GC response after IM prime, as similar results were seen if no IN boost was given (Supplemental Figure 4). Similarly, the low overall GC B cell frequency, but high fraction tdTomato$^+$, seen in in the CLN after IM immunisation (51%

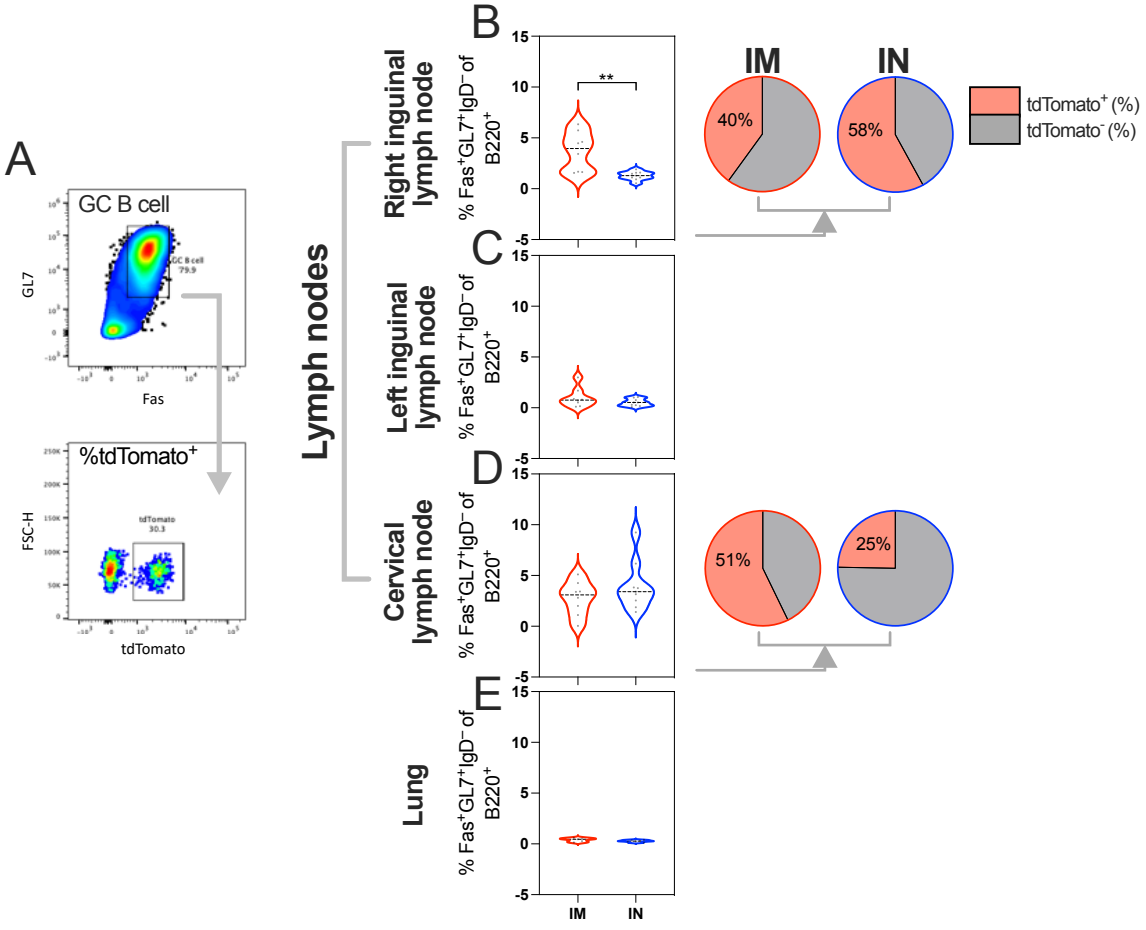

Figure 5.2: Frequencies of Ad-WT^{IM}-derived germinal centre B cells in the lymph nodes and lungs post-Ad-o mucosal boost

Tracking of Ad-WT^{IM} B cells following Ad-o^{IM} or Ad-o^{IN} vaccination in the lungs. Experiment was completed three times, with data compiled from the three separate repeats. The vaccinations, tissue processing and staining and flow cytometry were conducted by Lyn Yong. The data were visualised and analysed by Cameron Bissett. (A) Example flow plot of a gated GC B cell population (Fas$^+$GL7$^+$IgD$^-$B220$^+$), with the frequency of tdTomato$^+$ gated downstream. Frequencies of GC B cells in RILN (B), LLIN (C), CLN (D) and lungs (E), as measured by cell staining and flow cytometry. For RILN and CLN cells that had measurable frequencies of GC B cells, the proportion of Ad-WT^{IM} prime-derived (tdTomato$^+$) cells (median group response) were indicated in pie charts. Data were normally distributed, and unpaired T tests were completed to test for statistically significant differences between groups (**=P<0.01). Black dashed lines on violin plots represent the group medians.

tdTomato$^+$) appeared to be linked to a minor response induced by the IM prime (Supplemental Figure 4). These data reflect a scenario where more naïve B cells contributed to the GC response in the LNs draining the respiratory mucosa following IN-boosting, compared with IM-boosting.

The frequencies of o-RBD$^+$ B cells were measured in the lungs, CLN, LLIN and RILN (Figure 5.3). Of important note, this measured o-RBD$^+$ B cell population was gated on IgD$^-$ B220$^+$ B cells, hence was not limited to GC-specific B cells, thus includes the descendants of GC B cells (which would also be labelled should the precursor cells be labelled following tamoxifen treatment) (Figure 5.3A). Frequencies of o-RBD$^+$ B cells were higher in the lungs and CLN (Figure 5.3E and D, respectively) following IN-boosting compared with IM-boosting, however this was not statistically significant. A small frequency of the o-RBD$^+$ population was tdTomato$^+$ in the lungs following both IM (2%) and IN (6%) vaccination. Higher frequencies of tdTomato$^+$ o-RBD$^+$ B cells were detected in RILN (28% IM and 21% IN), that were comparable between IM- and IN-boosted mice (Figure 5.3B). Frequencies of tdTomato$^+$ o-RBD$^+$ B cells in the LILN were low and comparable between groups (5% IM

and 7% IN) (Figure 5.3C). A higher frequency of tdTomato$^+$ o-RBD$^+$ B cells in the CLN were observed following IM-boosting compared with IN-boosting (15% IM and 4% IN), suggesting limited participation of the GC-derived B cells from prime in the IN boost response (Figure 5.3D).

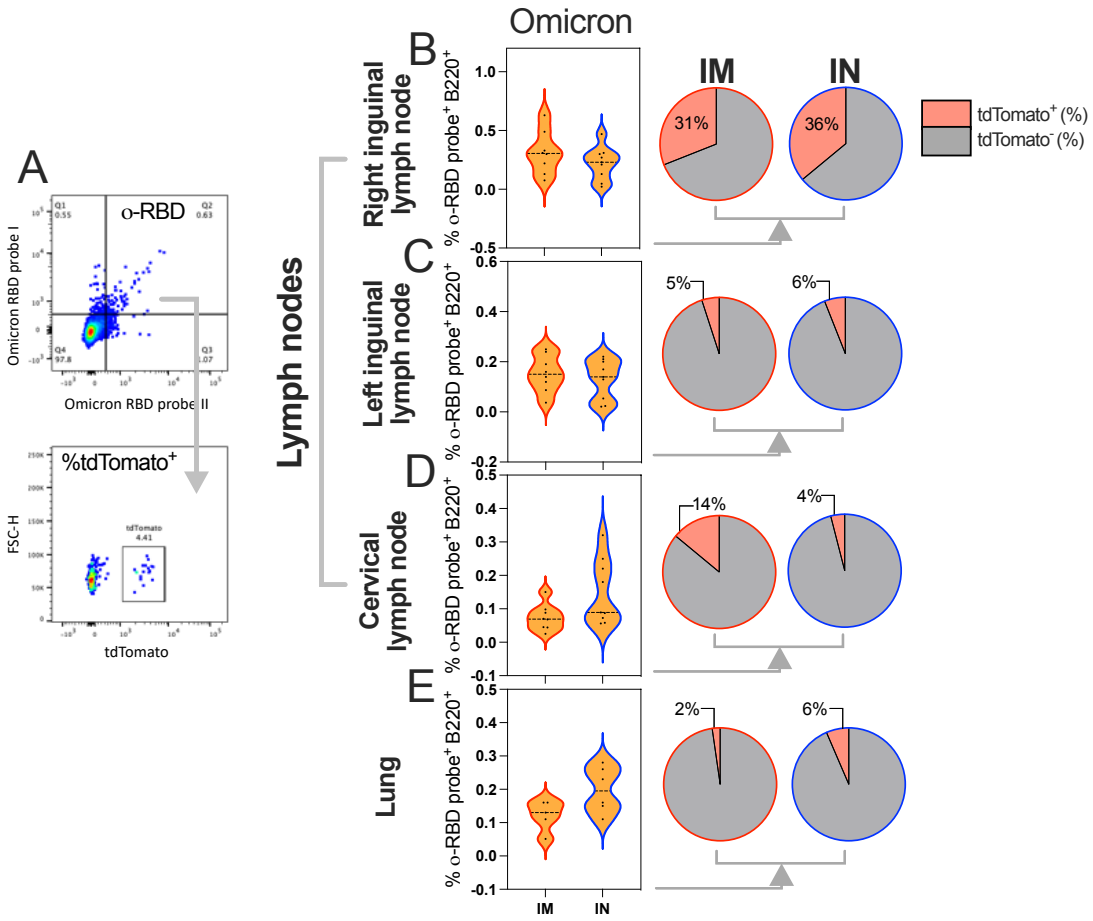

Figure 5.3: Frequencies of omicron-RBD$^+$ Ad-WT^{IM}-derived B cells in the lymph nodes and lungs post-Ad-o mucosal boost

Tracking of Ad-WT^{IM} B cells following Ad-o^{IM} or Ad-o^{IN} vaccination in the lungs. Experiment was completed three times, with data compiled from the three separate repeats. The vaccinations, tissue processing and staining and flow cytometry were conducted by Lyn Yong. The data were then visualised and analysed by Cameron Bissett. (A) Example flow plot for the gating of omicron RBD probe$^+$ B cells (B220$^+$), with the frequency of tdTomato$^+$ gated downstream. Frequencies of o-RBD$^+$ B cells in RILN (B), LLIN (C), CLN (D) and lungs (E). The proportion of o-RBD$^+$ B cells that were Ad-WT^{IM} prime-derived (tdTomato$^+$) (median group response) were indicated in pie charts. Black dashed lines on violin plots represent the group medians.

In summary, tdTomato^{+} Ad-WT IM-prime-derived B cells comprised a small fraction of the omicron-specific B cell pool in the lungs and CLN after IN boost, especially in comparison to the fraction in the RILN pool. The data suggest that the de-novo naïve B cell population are contributing to the IN Ad-o response in the lungs, in comparison with systemic responses where higher frequencies of Ad-WT IM-prime GC B cells have persisted.

In alignment with this finding, a smaller frequency of WT-cross-reactive PCs were measured following Ad-WT^{IM}-Ad-o^{IN} vaccination compared with following Ad-WT^{IM}+Ad-o^{IM} vaccination within the o-RBD^{+} lung PC population isolated in the initial IN boost experiment featured in Chapter 4, (P=0.0152, Figure 5.4A). Importantly, this experiment used the BALB/c strain, as opposed to the C57BL/6J transgenic strain used in this chapter, hence direct comparisons between these data sets cannot be completed and the influence of particular strain, rather than regimen, on observed immune response should be considered.

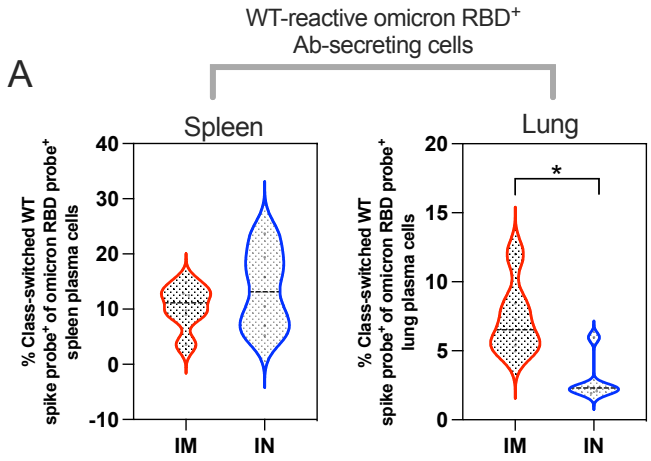

Figure 5.4: Frequency of WT spike cross-reactive omicron RBD^{+} plasma cells in the lungs and spleen

(A) Frequencies of o-RBD probe-specific spleen and lung plasma cells that were WT spike probe reactive (CD19^{-}CD138^{+}IgD^{-}IgM^{-}o-RBD^{+}WT-S^{+}). Data was produced from the experiment featured in Chapter 4. Mann-Whitney tests were completed to test for statistically significant differences between groups (*=P<0.05).

2.2 Assessing the potential involvement of memory T cells derived from Ad-WT^{IM} vaccination on the Ad-o^{IN} boost response

2.2.1 The benefit of Ad-WT^{IM} prime vaccination on latter antibody responses to Ad-o^{IN} vaccination

To confirm that Ad-WT^{IM}-prime had a positive impact on the latter antibody responses to Ad-o^{IN}, an experiment was completed where the immune responses of mice that were solely primed with Ad-o intranasally (Ad-o^{IN}) and mice that were first primed with Ad-WT^{IM} and then boosted with Ad-o intranasally (Ad-WT^{IM}+Ad-o^{IN}) were directly compared (Figure 5.5). Sera, NALT palates, BAL fluid and spleens were harvested from mice 5 weeks following final vaccination for analyses.

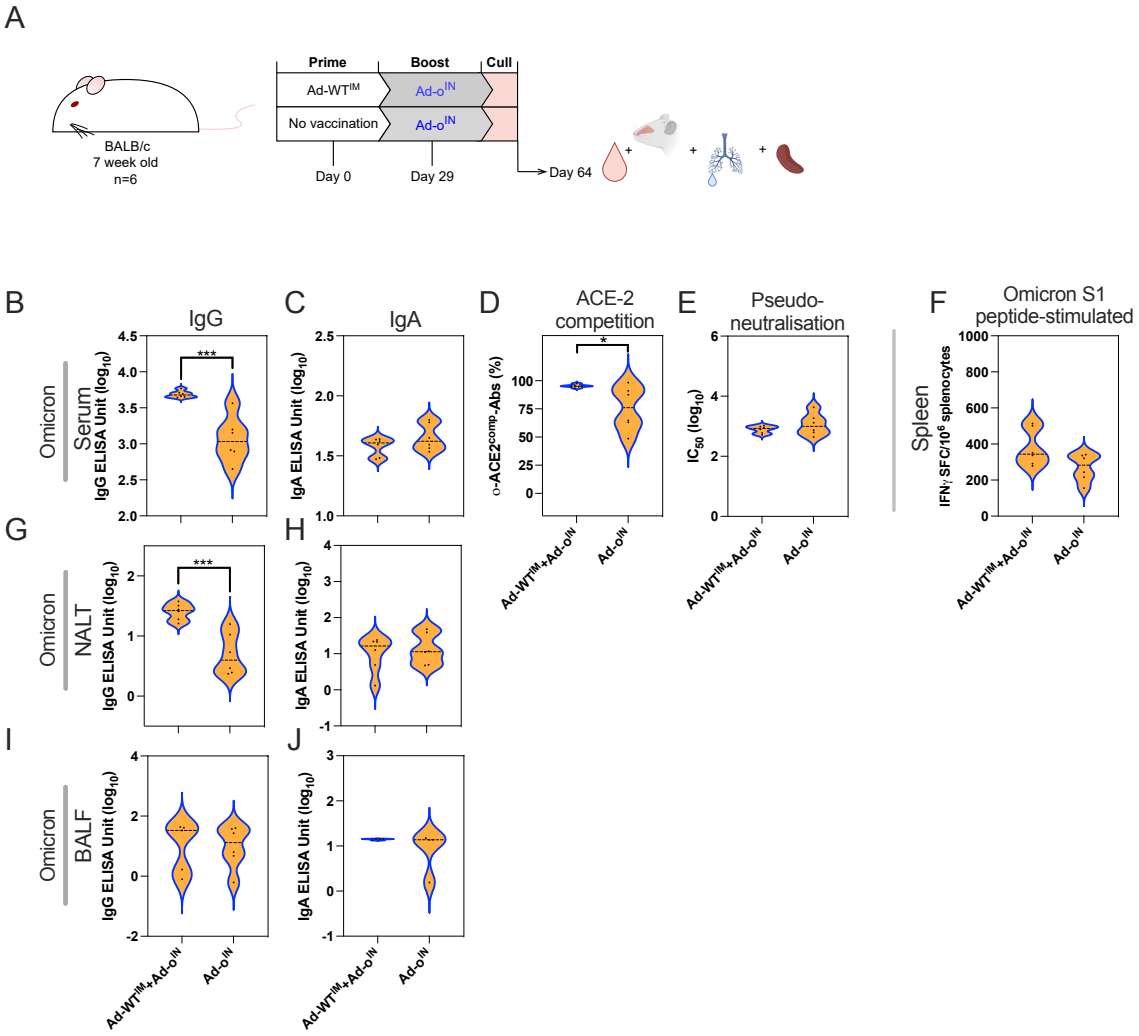

Figure 5.5: Assessing the effect of IM Ad-WT-prime on latter responses to heterologous omicron vaccine boost

(A) Vaccination schedule for the comparison of prime-boost Ad-WT^{IM}+Ad-o^{IN} regimen and prime-only Ad-o^{IN} regimen (n-6). The vaccination experiment was only completed once. 5 weeks post-boost, sera, NALT and BALF were collected for analyses. Omicron spike-reactive IgG in serum (B), NALT (G) and BAL fluid (I). Omicron spike-reactive IgA in serum (C), NALT (H) and BAL fluid (J). Levels of total omicron spike-specific IgG and IgA were measured by standardised ELISA and presented as log_{10} ELISA units. ACE-2-competing omicron S1-specific antibodies (o-ACE2^{comp}-Abs) in serum (D) were measured by Luminex assay on and presented as % competition, which was calculated by using the reduction in measured binding compared to a negative internal control. Pseudoneutralisation of omicron spike-expressing lentivirus (o-NAbs) in serum (E) was presented as log_{10} IC_{50}, which was calculated from titrated sample curves. (F) IFNγ release by splenocytes stimulated with omicron S1 peptides, measured by IFNγ ELISpot assay. To compare between groups, parametric t tests were performed. (*=P<0.05, ***=P<0.001)

The Ad-WT^{IM}+Ad-o^{IN} regimen generated higher levels of omicron spike-reactive IgG in the serum (Figure 5.5B) and NALT fluid (Figure 5.5G), compared with the Ad-o^{IN} prime-only regimen (serum: P=0.0007, NALT: P=0.0010). The Ad-WT^{IM}+Ad-o^{IN} regimen also generated higher levels of o-ACE2^{comp}-Abs in the serum compared with the Ad-o^{IN} regimen (P=0.0323) (Figure 5.5D). Levels of omicron spike-reactive IgA in the serum and mucosal fluids (NALT and BALF) were comparable between regimens (Figure 5.5C, H and J), as well as levels of serum o-NAbs (Figure 5.5E).

In addition to the measurement of antibodies, the frequency of IFNγ-releasing splenocytes was measured following stimulation with omicron S1 peptides that contained mutations (Figure 5.5F). The group median frequency of IFNγ-releasing cells was higher following the Ad-WT^{IM}+Ad-o^{IN} regimen (344 spot-forming cells/10^6 splenocytes) compared with the Ad-o^{IN} regimen (283 spot-forming cells/10^6 splenocytes), however, this difference was not statistically significant.

The levels of ancestral spike-binding, ACE-2-competing antibodies (Anc-ACE2^{comp}-Abs) were also measured in serum (Figure 5.6). As previously observed in Chapter 4, mice following the Ad-WT^{IM}+Ad-o^{IN} regimen generated strong cross-reactive responses to ancestral variants, whereas the Ad-o^{IN} was unable to induce cross-reactive responses (P=0.0022) (Figure 5.6A).

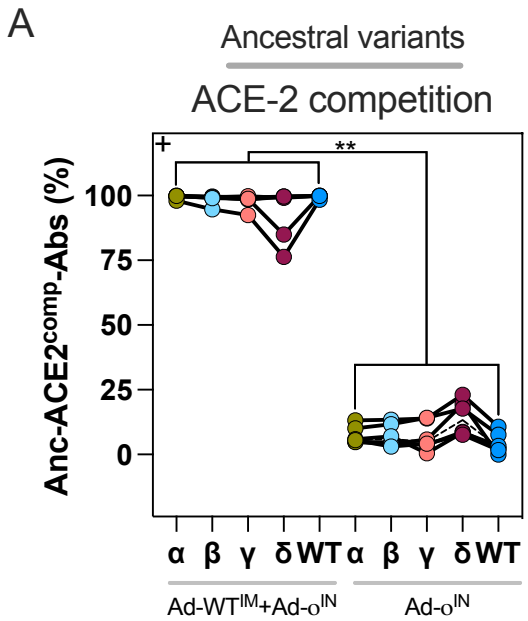

Figure 5.6: Serum antibody responses to ancestral variants following mucosal omicron prime and intramuscular WT prime, mucosal omicron boost regimens

Cross-reactive ACE-2-competing antibody response following Ad-WT^{IM}+Ad-o^{IN} and prime-only Ad-o^{IN} regimen (n-6). The vaccination experiment was only completed once. (A) ACE2^{comp}-Abs reactive to earlier ancestral variant spikes alpha, beta, gamma, delta, and WT: measured in the serum of mice following Ad-WT^{IM}+Ad-o^{IN} and Ad-o^{IN} regimens. Regimens were compared statistically using a non-parametric Kruskal-Wallis test, as data was non-normally distributed (as indicated with the "+" symbol) (**=P<0.01). On plots, the dashed black line represents the group median response.

In summary, Ad-WT^{IM}-priming was shown to have a positive effect on the latter responses to Ad-o^{IN} booster vaccination. Specifically, elevated levels of serum and NALT omicron spike-reactive IgG, as well as serum o-ACE2^{comp}-Abs, were measured. Additionally,

Ad-WT^{IM}-priming resulted in broader, cross-reactive responses to ancestral variants in the blood following Ad-ο^{IN}-boosting, compared with Ad-ο^{IN}-priming alone.

2.2.2 Adoptive cell transfer of splenocytes generated from Ad-WT^{IM} vaccination prior to mucosal boosting

Since the magnitude of the responses following the Ad-WT^{IM}+Ad-ο^{IN} regimen surpassed those elicited from an IN prime of Ad-ο alone (Figure 5.5 and Figure 5.6), the potential involvement of pre-existing memory T cells derived from Ad-WT^{IM}-priming in the latter Ad-ο^{IN} response was investigated. Unlike B cells, which did not contribute largely to the latter Ad-ο response in the lungs, memory T cells derived from WT vaccination may be contributing to a greater extent given their high level of cross-reactivity to omicron antigen.

To better understand the potential role of memory T cells derived from the Ad-WT^{IM} prime vaccination on the Ad-ο mucosal boost responses, an adoptive cell transfer experiment was devised using CD45.1^{+} donor mice and CD45.2^{+} (hence CD45.1^{-}) recipient mice. To generate WT spike vaccine-derived memory cells, congenic donor mice were either vaccinated Ad-WT^{IM}+Ad-WT^{IM} or were left unvaccinated, and then splenocytes harvested from vaccinated mice were then IV transferred into recipient mice (Figure 5.7A). Recipient mice were subsequently vaccinated with either Ad-ο IM or IN, or not vaccinated, with immune responses assessed 3 weeks after Ad-ο vaccination by flow cytometry using anti-CD45.1 antibodies to discriminate between donor- and host-derived cells.

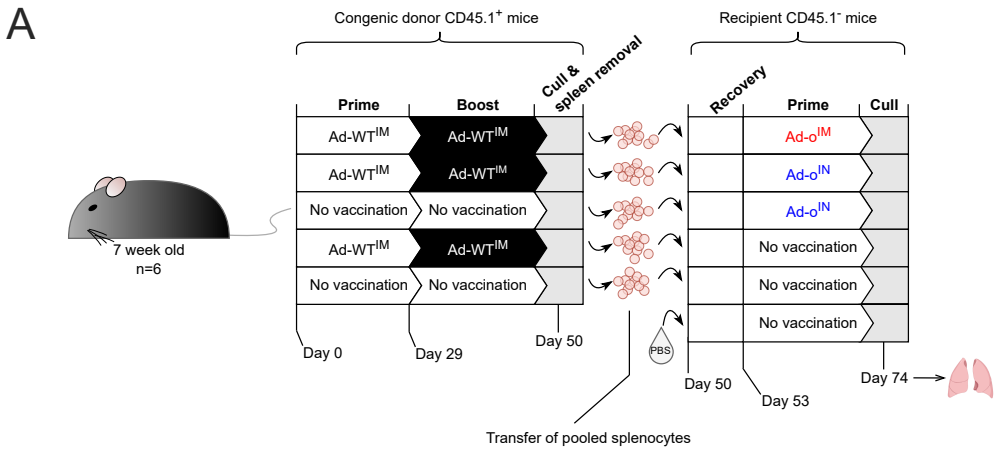

Figure 5.7: Schedule for the adoptive cell transfer of Ad-WT^{IM}-derived splenocytes and subsequent Ad-o mucosal boosting

(A) Donor CD45.1^{+} mice (n=6) were prime-boost vaccinated (or left unvaccinated) with Ad-WT IM. 3 weeks after final vaccination, donor mice were culled and spleens removed, processed and transferred to recipient naïve CD45.2^{+} (CD45.1^{-}) mice (n=6). Three days after receiving the splenocytes, mice were vaccinated with Ad-o either IM or IN. The lungs of mice were harvested 3 weeks post-Ad-o vaccination (day 74). The experiment was only completed once. For the control groups, the group numbers were n=<6: Ad-WT+Ad-WT>No vaccination (n=4), Naïve>No vaccination (n=3) and PBS>No vaccination (n=2).

The highest number of donor cells in the lungs was observed in mice that received splenocytes from Ad-WT^{IM}+Ad-WT^{IM}-vaccinated mice, that were then Ad-o^{IN}-vaccinated (Ad-WT^{IM}+Ad-WT^{IM}>Ad-o^{IN}) (Figure 5.8A). The number of donor-derived cells (CD45.1^{+}) in Ad-WT^{IM}+Ad-WT^{IM}>Ad-o^{IN} lungs were higher than in mice that received naïve donor cells prior to Ad-o^{IN} vaccination (Ad-WT^{IM}+Ad-WT^{IM}>Ad-o^{IN} vs. Naïve>Ad-o^{IN}; P≤0.0001); suggesting that the WT-spike-specific donor cell population had expanded and homed to the lungs upon Ad-o^{IN} vaccination. Ad-WT^{IM}+Ad-WT^{IM}>Ad-o^{IN} CD45.1^{+} lung cells were also significantly higher in number than in mice that received vaccinated-donor cells but remained unvaccinated (vs. Ad-WT^{IM}+Ad-WT^{IM} >No vaccination P≤0.0001 and vs. Naïve>No vaccination P≤0.0001).

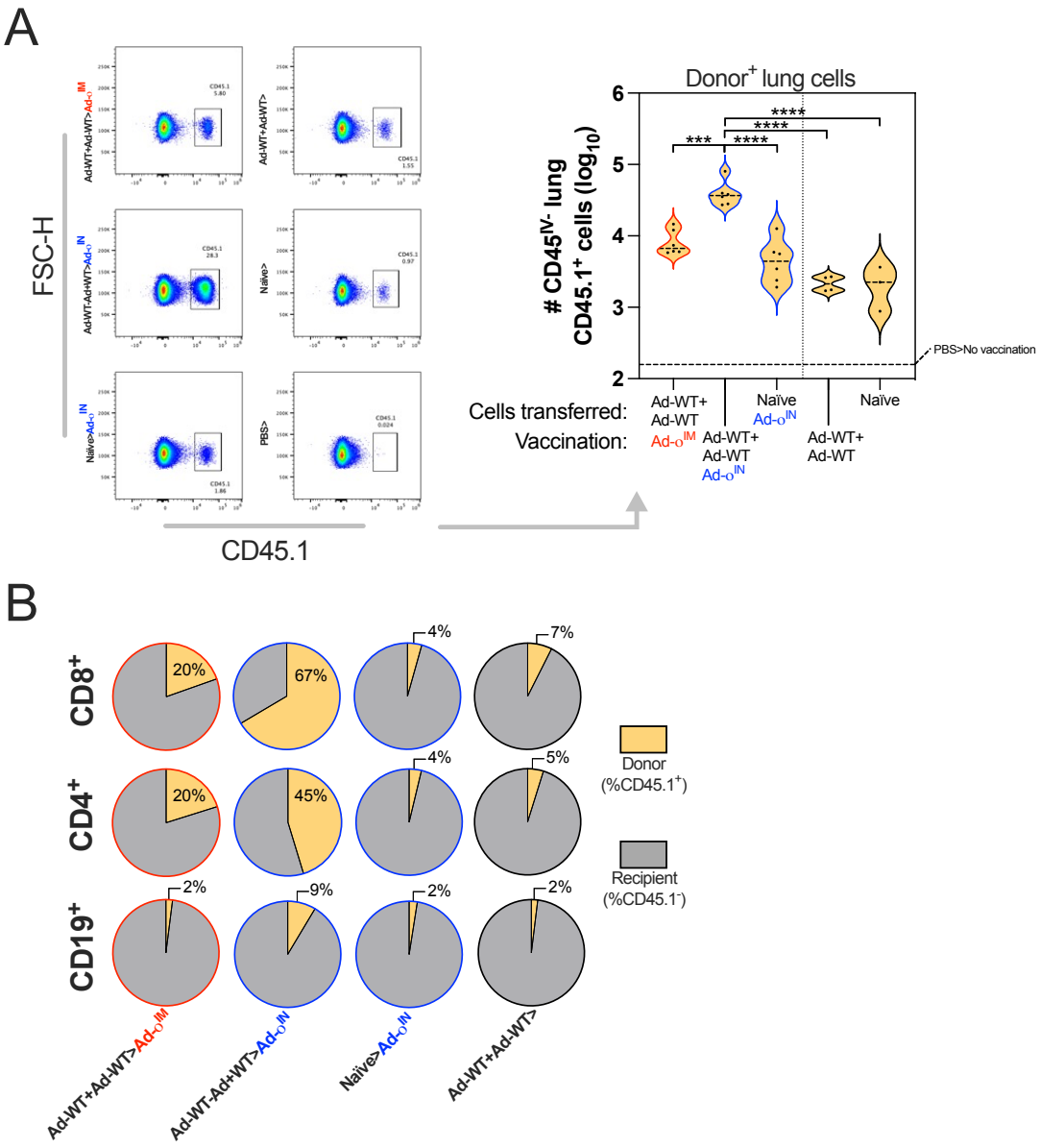

Figure 5.8: Frequency of Ad-WT^{IM}-derived donor cells in lungs following Ad-o^{IN} vaccination

Donor cell populations in recipient mice (n=6) following vaccination with Ad-o IM or IN; the experiment was only completed once. (A) Total numbers (log_{10}) of donor^{+} cells (CD45.1^{+}CD45^{IV-}) in the lungs of mice, as measured via cell staining and flow cytometry. The median response of the negative control mouse group that received PBS instead of cells, and were not vaccinated, is indicated as a dashed horizontal black line on graphs. Example flow plots for each group are located on the left. As data were normally distributed, one-way ANOVA Šidák's multiple comparisons was completed to compare Ad-WT^{IM}+Ad-WT^{IM}>Ad-o^{IN} regimen against all other regimens. (***=P<0.001, ****=P≤0.0001). The dashed black line in (A) represents the median response to the group that received PBS and were not vaccinated. (B) Frequencies of donor^{+} (CD45.1^{+}CD45^{IV-}) CD8^{+}, CD4^{+} and CD19^{+} cells in the lungs. Pie chart values represent group medians. For the control groups, the group numbers were n=<6: Ad-WT+Ad-WT>No vaccination (n=4), Naïve>No vaccination (n=3) and PBS>No vaccination (n=2).

The frequency of donor-derived (CD45.1$^+$) lung CD8$^+$ and CD4$^+$ T cells, as well as CD19$^+$ B cell cells, was also assessed (Figure 5.8B). A large proportion of lung CD8$^+$ T cells in Ad-WT^{IM}+Ad-WT^{IM}>Ad-o^{IN} mice were donor-derived (median 67% CD45.1$^+$) compared with other vaccinated regimens (Ad-WT^{IM}+Ad-WT^{IM}>Ad-o^{IM}, 20% CD45.1$^+$; Naïve>Ad-o^{IN}, 4% CD45.1$^+$). Similarly, the largest proportion of donor CD45.1$^+$ CD4$^+$ T cells were observed following Ad-WT^{IM}+Ad-WT^{IM}>Ad-o^{IN} regimen (median 45% CD45.1$^+$). In contrast, the proportion of donor CD45.1$^+$ B cells across all regimens was low, ranging from 2-9% CD45.1$^+$. The largest contribution of donor CD45.1$^+$ B cells was in the Ad-WT^{IM}+Ad-WT^{IM}>Ad-o^{IN} group, consistent with the T cell responses. Therefore, CD8$^+$ and CD4$^+$ T cells derived from Ad-WT^{IM}+Ad-WT^{IM} vaccination, but not B cells (consistent with the findings in Figure 5.3), contributed considerably to the latter Ad-o^{IN} response in the lungs.

I hypothesised that the major contribution of memory T cells to the Ad-o^{IN} vaccine response was due to cross-reactive responses primed by Ad-WT. The immunodominant H-2K^b (C57BL/6 haplotype) -restricted $S_{539-546}$ epitope is conserved between WT and omicron, and a H-2K^b tetramer of this was used to stain for cross-reactive T cells in the lungs. Ad-WT^{IM}+Ad-WT^{IM}>Ad-o^{IN} and Naïve>Ad-o^{IN} regimens resulted in the generation of more cross-reactive spike-specific CD8$^+$ T cells in the lungs than in Ad-WT^{IM}+Ad-WT^{IM}>Ad-o^{IM} and unvaccinated control groups (Ad-WT^{IM}+Ad-WT^{IM}>Ad-o^{IN} vs. Ad-WT^{IM}+Ad-WT^{IM}>No vaccination P=0.0029 and vs. Naïve>No vaccination P=0.0076) (Figure 5.9A). The proportion of cross-reactive CD8$^+$ T cells that were donor-derived was high in groups that received Ad-WT^{IM}+Ad-WT^{IM} cells and were then vaccinated (93% and 97% for Ad-WT^{IM}+Ad-WT^{IM}>Ad-o^{IM} and Ad-WT^{IM}+Ad-WT^{IM}>Ad-o^{IN} mice, respectively; Figure 5.9B). In mice that received naïve donor cells that were then Ad-o^{IN}-vaccinated, the majority of cross-reactive CD8$^+$ T cells were recipient-derived (96% CD45.1), as expected.

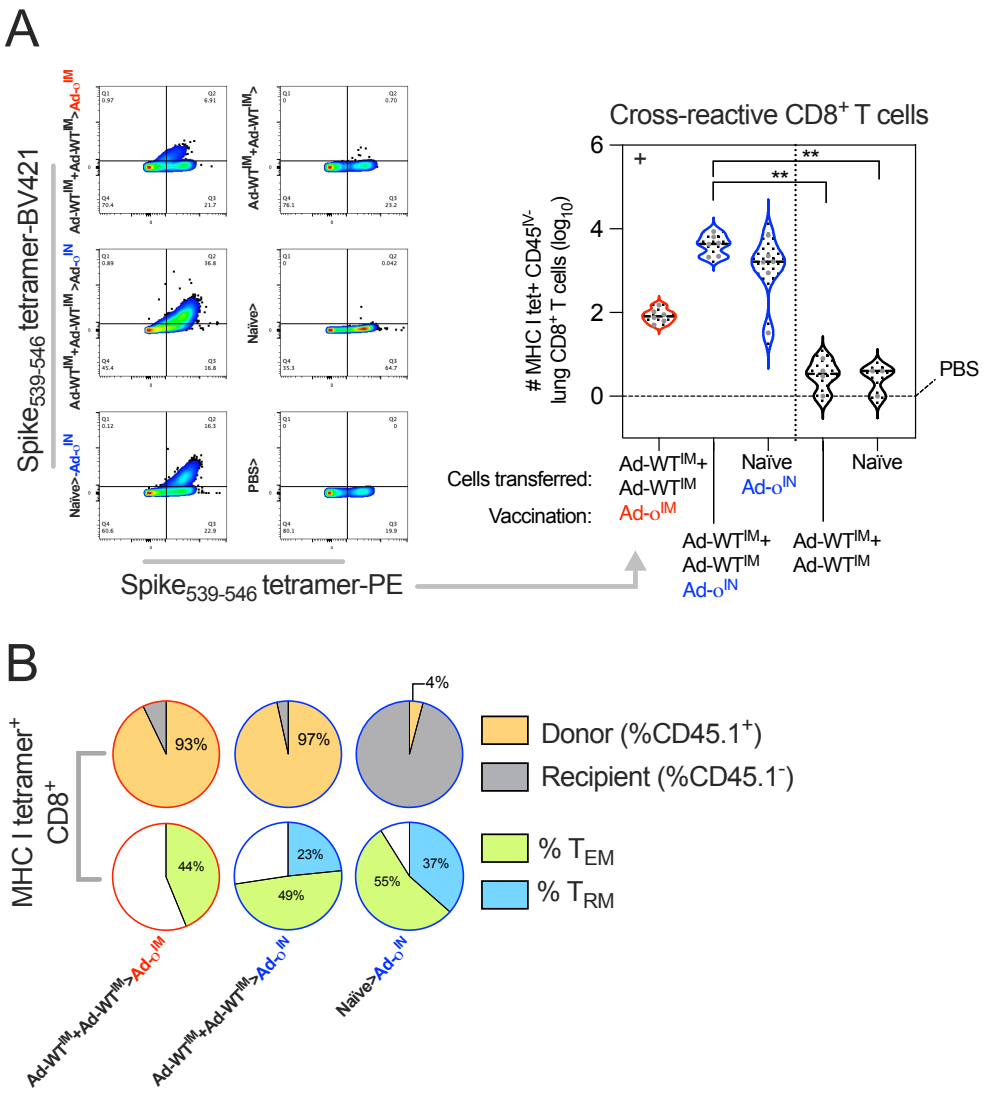

Figure 5.9: Frequency of Ad-WT^{IM}-derived cross-reactive donor T cells in the lungs post Ad-o^{IN} vaccination

Ag^{+} Donor CD8^{+} T cell populations in recipient mice (n=6) following vaccination with Ad-o IM or IN; the experiment was only completed once. (A) Total numbers (log_{10}) of cross-reactive CD8^{+} T cells (MHC I tet^{+}CD45^{IV-}) in the lungs of mice, as measured via cell staining and flow cytometry. A tetramer using the immunodominant H-2K^{b}-restricted $S_{539-546}$ epitope (that is conserved between WT and omicron) was used to stain cross-reactive cells (representative staining plots on the left). As certain data did not follow a normal distribution, Dunn's multiple comparisons was completed to compare Ad-WT^{IM}+Ad-WT^{IM}>Ad-o^{IN} regimen with all other regimens. (**=P<0.01). The dashed black line in (A) represents the median response to the group that received PBS and were not vaccinated. (B) Frequency of donor^{+} cells, and T$_{RM}^{+}$ (CD69^{+}CD103^{+}CD62L^{-}CD44^{+}) and T$_{EM}^{+}$ (CD62L^{-}CD44^{+}CD127^{+}) cells, within the measured cross-reactive lung CD8^{+} T cell (MHC I tet^{+}CD45^{IV-}) population. For the control groups, the group numbers were n=<6: Ad-WT+Ad-WT>No vaccination (n=4), Naïve>No vaccination (n=3) and PBS>No vaccination (n=2).

Out of the MHC I tetramer positive population following Ad-o vaccination, the T cell phenotype in the lungs was different depending on whether the mice were boosted IN or IM with Ad-o (Figure 5.9B). 44% of the cross-reactive $CD8^+$ T cells from Ad-WT^{IM}+Ad-WT^{IM}>Ad-o^{IM} mice were an effector memory phenotype (T_{EM}: $CD45^{IV-}CD44^+CD62L^-CD127^+$) with no T_{RM} detected (Figure 5.9B). Cross-reactive $CD8^+$ T cells from Ad-WT^{IM}+Ad-WT^{IM}>Ad-o^{IN} mice were 49% T_{EM} phenotype and 23% T_{RM} phenotype. Cross-reactive $CD8^+$ T cells from the Naïve>Ad-o^{IN} group, where the response was recipient-derived, were 55% T_{EM} phenotype and 37% T_{RM} phenotype. Thus, while both Ad-o^{IM} and Ad-o^{IN} drove secondary expansion of cross-reactive memory T cells, Ad-o^{IN} was uniquely superior at recruiting these cells to the lungs and converting them to a T_{RM} phenotype.

Therefore, memory T cells derived from Ad-WT^{IM} priming contribute substantially to the lung T cell response following a boosting Ad-o^{IN} vaccination.

3. Discussion

In this chapter, two main observations were made that build upon the findings presented in Chapter 4. The multiple mechanisms driving the Ad-WT^{IM}+Ad-o^{IN} regimen responses are summarised in the following illustration: Figure 5.10. In brief:

1. MBC from Ad-WT^{IM}-prime have a minor contribution to the lung B cell responses following Ad-o^{IN} vaccination
2. Cross-reactive memory T cells from Ad-WT^{IM}-prime vaccination contribute largely to the lung immune response following Ad-o^{IN} vaccination

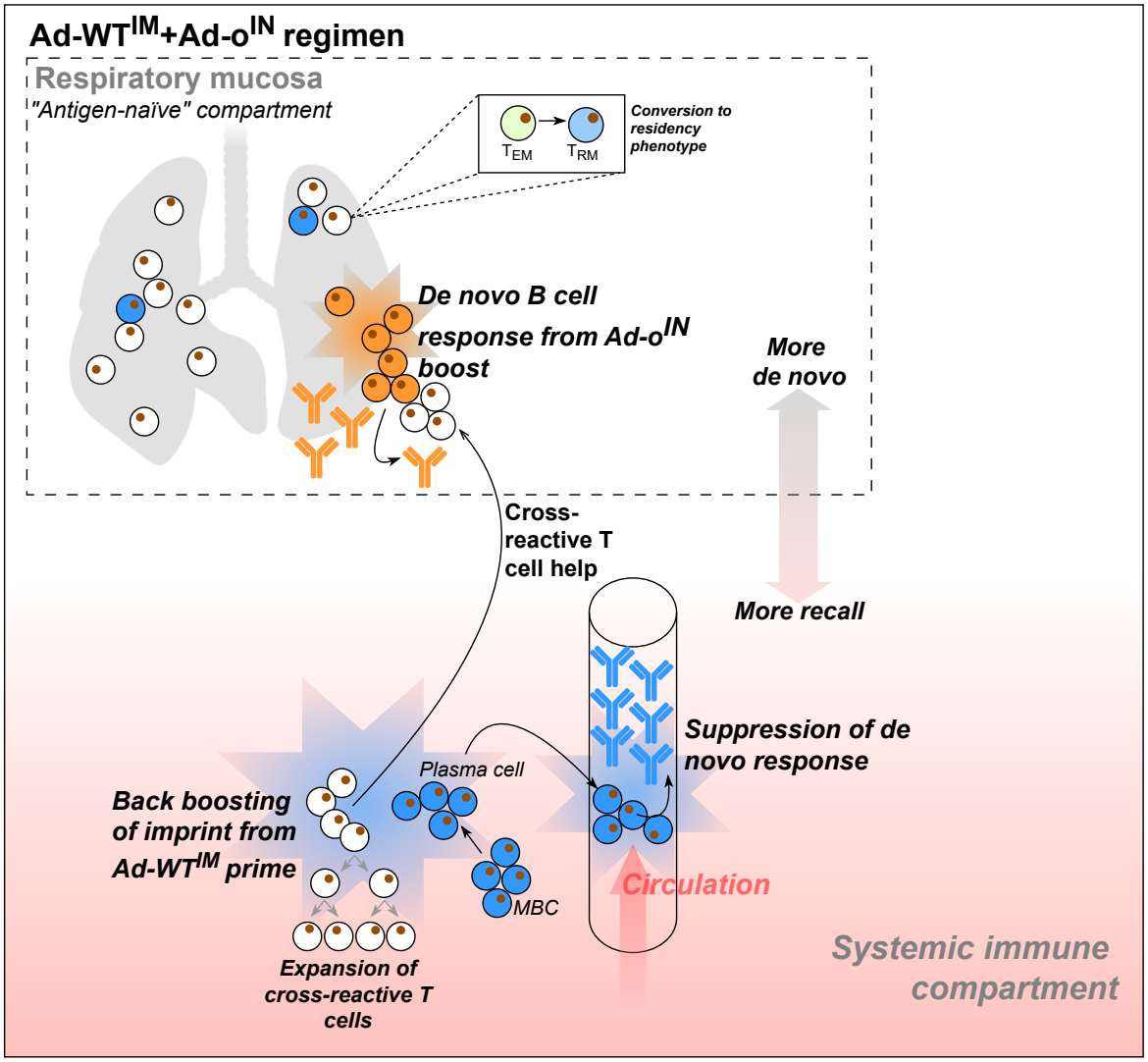

Figure 5.10: Graphical summary of the proposed multi-mechanism model driving the immune responses of the Ad-WT^{IM}+Ad-o^{IN} regimen

Orange antibodies and B cells represent de novo responses to omicron antigen following IN Ad-o-boosting. Blue antibodies and B cells are those generated following prime vaccination with Ad-WT, and subsequently re-stimulated upon Ad-o-boosting. The arrow depicts a de-novo-to-recall immune response axis model in which the mucosal and systemic compartments undergo different types of immune response. The tubular drawing depicts the circulatory system in which suppressive antibodies from priming and back-boosting reside. The cross-reactive memory T cells derived from prime vaccination are labelled in white.

The findings of 1. align with the hypothesis presented in Chapter 4, in which omicron-reactive responses were proposed to be bypassed as a result of multiple factors: the anatomical and immunological separation of the mucosal compartment from the wider systemic and circulatory compartment restricts the access of suppressive antibody formed

from Ad-WT IM prime vaccination, and the mucosal compartment remains largely unstimulated by IM vaccination ("antigen naïve tissue"), accordingly supporting a more de novo-like response in which naïve B cells, recognising omicron-specific epitopes, are provided with a greater opportunity to be activated. These B cells, with access to antigen that is less masked and not rapidly cleared from presentation by circulatory, suppressive prime-derived antibodies, drive a quality, omicron-neutralising antibody response. In addition, the naïve B cells are likely not as burdened by the presence of competitive MBC from prime. Contrastingly (and simultaneously), the systemic immune compartment undergoes more of a back-boosting, recall-type response in which at least on a serological level, the pre-existing prime response is perpetuated (upon Ad-$\omicron^{IN}$ or Ad-$\omicron^{IM}$ boost), that while may be cross-reactive with omicron spike, is however poorly neutralising.

In alignment with these findings, one study described a scenario in which pre-existing MBC re-activated and rapidly differentiated to PB and PC upon boosting, thus generating a dominant serological antibody response that was recall-derived, but that the pre-existing circulatory antibody also served an inhibitory role, preventing the re-entrance of MBC into secondary GCs[267]. The inhibitory antibody promoted the seeding of naïve B cells into secondary GCs that had impaired antigen-binding capacity, and cross-reactive memory T cells were necessary for this seeding process[267]. These observations may explain why the frequencies of GC B cells measured in the S1pr2 experiment in this chapter were never ±100% tomato$^+$ for the Ad-WT^{IM}+Ad-$\omicron^{IM}$ regimen. It is likely naïve B cells contributed to the secondary GCs formed following Ad-$\omicron^{IM}$-boost, thus lowering the relative frequency of tomato$^+$ GC B cells in the RILN. Looking forward, to improve the design of this completed experiment, Ad-WT^{IM}+Ad-WT^{IM} and Ad-WT^{IN}+Ad-WT^{IN} groups could be included as additional, positive controls of a recall response (as the greatest levels of recall would be

expected when the boost antigen is homologous to the prime, as well as the route of vaccination) and used as a reference to compare with the test groups.

Of important note, as evidenced through the supplementary experiment in which the RILNs were analysed 40+ days after Ad-WT^{IM}, the primary GCs were shown to persist following prime (Supplemental Figure 4); this explains the higher frequency of tomato^{+} RILN GC B cells in the Ad-WT^{IM}+Ad-o^{IN} regimen (high frequency of tomato^{+} as only one IM dose, no naïve, secondary GC, but solely persisting prime-derived GCs), compared with the Ad-WT^{IM}+Ad-o^{IM} regimen (lower frequency of tomato^{+} as naïve B cells recruited into secondary GCs following second IM dose).

More generally, a drawback to the S1pr2 experiment was the use the C57BL/6 mouse strain, as opposed to BALB/c strain, as was used for Chapter 3 and Chapter 4 experiments, as well as the adoptive cell transfer experiments within this chapter. When the S1pr2 B cell tracking experiments were conducted, it was necessary to make the assumption that the general trends in difference in immune response between the Ad-WT^{IM}+Ad-o^{IM} and Ad-WT^{IM}+Ad-o^{IN} regimens in the C57BL/6 mice would be similar to those measured previously in the BALB/c strain, despite the differences between the characteristics of these two strains' immune systems; for example, more Th2-leaning antibody responses are typically observed in BALB/cs, whereas more Th1-skewed, antiviral responses are typically observed in C57BL/6 mice[340]. The C57BL/6 background S1pr2 transgenic mice were used due to availability. To better harmonise between the different experiments, recapitulation of the Ad-WT^{IM}+Ad-o^{IM} and Ad-WT^{IM}+Ad-o^{IN} experiment (Figure 4.5) using C57BL/6, and then subsequent measurement of antibody and cellular responses, could be completed; the BALB/c and C57BL/6 data could then be compared, such that strain-specific factors influencing the immune response be identified if present,

or, confirmation of identical trends in immune response following the Ad-WT^{IM}+Ad-o^{IM} and Ad-WT^{IM}+Ad-o^{IN} regimens between the two strains, be made.

In support of the aforementioned hypothesis of the mechanism driving the Ad-WT^{IM}+Ad-o^{IN} response, both the transgenic and adoptive cell transfer cell tracking experiments indicated that there was minimal presence of Ad-WT^{IM}-derived MBC in the lung following the Ad-o^{IN} boost, and that the majority of omicron RBD-reactive B cells were derived from the boost vaccination (i.e., naïve and activated upon boosting). In another study that aligns with these findings, Pušnik *et al* showed that unlike cross-reactive T cell responses originating from WT spike vaccination that were stimulated after omicron breakthrough infection, B cell responses to the mutated regions of omicron spike were impaired due to the pre-existing vaccine imprint[253]. Nevertheless, in the adoptive cell transfer experiment in this chapter, a very small fraction (relative to T cell fractions; 7%) of donor-derived B cells were detected that had expanded and homed to the lungs following IN boost; it is possible that these prime-derived B cells contributed to the broadly-reactive antibody pool measured in the mucosa.

As highlighted in this chapter by directly comparing the Ad-WT^{IM}+Ad-o^{IN} regimen responses with those generated after a prime-only vaccination with Ad-o^{IN}, priming Ad-WT^{IM} resulted in enhanced omicron- and cross-reactive antibody responses in the mucosa and blood following Ad-o^{IN} boost. It was therefore investigated whether memory T cells derived from Ad-WT^{IM}-prime significantly contributed to the lung Ad-o^{IN} response, unlike the Ad-WT^{IM}-derived MBC. It was noted that cross-reactive memory CD8^{+} T cells derived from Ad-WT^{IM} vaccination recalled into the lungs upon Ad-o^{IN} vaccination. Although a stain for cross-reactive CD4^{+} T cells was not included, the expansion and homing of Ad-WT^{IM}-prime-derived CD4^{+} T cells to the lungs was measured. These pre-existing T cells likely assist

in and contribute to the latter Ad-o^{IN} B cell response, and drive the broad, cross-reactive responses locally and systemically measured. Some of the Ad-WT^{IM}-derived memory $CD8^+$ T cells converted to a T_{RM} phenotype upon IN boost, as evidenced by the expanded cross-reactive T_{RM} population measured after IN-boosting in mice that received Ad-WT^{IM}-Ad-WT^{IM} splenocytes. $CD8^+$ T cells have been shown to migrate from circulation to nonlymphoid tissues upon secondary antigen exposure and adopt a T_{RM}-type phenotype[341]. The cross-reactivity of T cells derived from ancestral antigen exposure to omicron antigen has been extensively reported, and it is hypothesised this immunity contributes to the blunted disease elicited via omicron in most individuals[342]. I propose that cross-reactive T cells positively contribute to the local lung and systemic responses upon Ad-o^{IN} boost.

6

Immunogenicity of a bivalent RSV-Influenza ChAdOx1 vaccine

6. Immunogenicity of a bivalent RSV-Influenza ChAdOx1 vaccine

1. Introduction and aims
2. Results

2.1 Immunogenicity of ChAdOx1-NP+M1-mRSV(F)-DS2 when administered via different regimens

2.1.1 Antibody responses to ChAdOx1-NP+M1-mRSV(F)-DS2 in the blood and the mucosa

2.1.2 T cell responses to ChAdOx1-NP+M1-mRSV(F)-DS2 systemically and in the respiratory mucosa

2.2 Protective capacity of ChAdOx1-NP+M1-mRSV(F)-DS2 determined via virus challenge

2.2.1 RSV challenge following ChAdOx1-NP+M1-mRSV(F)-DS2 vaccination

2.2.1.1 Weight change and lung viral load following RSV challenge

2.2.1.2 Antibody and cellular immune responses following RSV challenge

2.2.2 H3N2 challenge following ChAdOx1-NP+M1-mRSV(F)-DS2 vaccination

2.2.2.1 Weight change and lung viral load following H3N2 challenge

2.2.2.2 Antibody and cellular immune responses following H3N2 challenge

2.2.3 H1N1 challenge following ChAdOx1-NP+M1-mRSV(F)-DS2 vaccination

2.2.3.1 Weight change and viral load following H1N1 challenge

2.2.3.2 Antibody and cellular immune responses following H1N1 challenge

3. Discussion

1. Introduction and aims

As emphasised through the findings presented in Chapters 4, 5 and 6, the route of vaccination is an important consideration when designing vaccines against respiratory viruses, having a profound influence on the magnitude and type of response generated. The majority of vaccines used against two other major respiratory viruses that also inflict a major global health burden, RSV and influenza, are also administered via the intramuscular (IM) route. The IM administration of these vaccines leads to protection against severe disease and infections of the LRT (Table 1.5). However, much like the SARS-CoV-2 vaccines administered via the IM route, IM RSV and influenza vaccination is largely ineffective at stimulating the mucosal immune compartment[278,343,344], which is needed to induce forms of protection that would prevent infection of the airways, as well as reduce virus transmission. Optimisation of the vaccination strategies such that they induce protective immunity against infection is warranted. Lessening the transmission of RSV and influenza virus to the elderly and infant populations that are most vulnerable to both RSV- and influenza-elicited disease by vaccinating a wider age range with a vaccine that blocks infection could be a strategy to reduce the immense burden on health imposed by these viruses.

Both clinical and preclinical studies have shown that delivering influenza and RSV vaccines via mucosal routes better induces mucosal immunity, which correlates well with protection[202,345–350]. URT immunity to respiratory syncytial virus (RSV) and influenza virus has been shown to protect against viral infection and disease[351–355]. Tissue-resident memory T and B cells (T_{RM} and B_{RM}), as well as neutralising IgA within the URT, contribute to rapid response and control of viral infection at the site of viral entry[356].

Previously, Susan Morris *et al* constructed a bivalent ChAdOx1 vaccine encoding the pre-fusion stabilised RSVF protein, and nucleoprotein (NP) and matrix 1 (M1) internal influenza proteins at the Jenner Institute. The stabilised RSV F pre-fusion antigen is an ideal candidate for RSV vaccines as it is capable of inducing potently neutralising, protective antibodies, and the antigen is conserved across viral subtypes; it is now used in three licensed vaccines that are effective at reducing RSV-LRTD in older adults and/or infants born from pregnant, vaccinated individuals[145,146,148,357,358]. The NP and M1 internal influenza proteins are favourable T cell antigens for an influenza vaccine as they are highly conserved across viral subtypes, thus may accommodate the regular antigenic drift of influenza virus. The presence of NP- and M1-reactive memory T cells, especially within the airways, could facilitate more rapid clearance of influenza virus. A suitable vector for the delivery and expression of influenza NP and M1 T cell antigens, and RSV F B cell antigen, is adenovirus ChAdOx1. The clinical safety profile of this platform has been well-studied for vaccines against various pathogens, including SARS-CoV-2[273–277]; IM immunisation with ChAdOx1 has been used in global vaccination schemes, and this vaccine technology can be administered safety via the mucosal IN route[278,279].

The aim of this chapter was to assess the immunogenicity and protective capacity of a newly constructed bivalent viral vector vaccine, ChAdOx1-NP+M1-RSVF, when administered homologously in naïve mice. ChAdOx1-NP+M1-RSVF is aimed to simultaneously protect against both RSV and influenza virus infection and disease. The vulnerable infant and elderly populations are affected by both RSV and influenza virus, hence a vaccine regimen capable of inducing dual protection would be an attractive, cost-effective, and convenient strategy. The vaccine was designed to induce broad, cross-protective tissue-resident T cells against heterosubtypic influenza viruses and neutralising

antibodies against RSV in the respiratory mucosa and systemically. The IM-IN regimen was tested alongside other homologous regimens using the IM or IN vaccination route, to assess which were best able to induce such form of immunity. With the collaborative help of John Tregoning *et al*, the regimens' protective capacity against challenge with the following viruses was examined: RSV A, influenza A H3N2 and influenza A H1N1.

2. Results

2.1 Immunogenicity of ChAdOx1-NP+M1-mRSV(F)-DS2 when administered via different regimens

2.1.1 Antibody responses to ChAdOx1-NP+M1-mRSV(F)-DS2 in the blood and respiratory mucosa

The ChAdOx1-NP+M1-RSVF vaccine was constructed prior to this project, by inserting the influenza and RSV antigenic sequences within the ChAdOx1 backbone. In brief, a pre-fusion-stabilised RSV A2-F (DS2) sequence was inserted at the E4-deleted gene site, and a sequence encoding the H3N2 NP and M1 proteins, attached to each other by a flexible linker, was inserted at the E1-deleted gene site (Figure 6.2A). Importantly, the H3N2 NP sequence is highly conserved with other influenza subtype sequences, relative to poor conservation between surface glycoprotein antigens, as exemplified in a table presented later in this chapter (Table 6.1).

A variety of prime-only and prime-boost regimens involving IM and/or IN routes of vaccination were tested to determine which regimens induced both systemic, and respiratory mucosal immune responses to RSV and influenza A antigens and optimal immunogenicity (Figure 6.2B). An outbred (CD-1) mouse strain was chosen, such that immune responses to vaccination better represented an outbred population as is similar to humans.

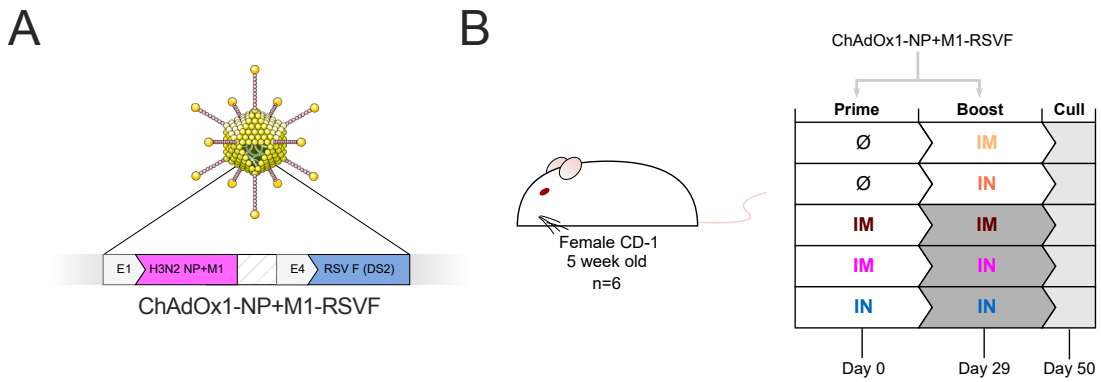

Figure 6.1: ChAdOx1-NP+M1-RSV(F) vaccination

(A) ChAdOx1-NP+M1-RSVF adenovirus vaccine (B) Vaccination schematic for the assessment of the immunogenicity of ChAdOx1-NP+M1-RSVF administered through different regimens in outbred, 5-week-old, CD-1 mice (n=6). Mice were culled on day 50, with sera, lungs, spleens, nasal-associated lymphoid tissue (NALT) and bronchioalveolar lavage fluid (BALF) harvested. The experiment was completed twice, with the repeat experiment only including the prime-boost regimen. Data from the first experiment is presented for antibody measurements and intracellular staining.

Three weeks after final vaccination the levels of IgG, IgA and IgM specific to RSV A2-F, H1N1-NP and H1N1-M1 (Figure 6.2) antigens were measured via ELISA in the serum of vaccinated mice. Influenza A NP and M1 from the H1N1 subtype were selected due to availability at the time of experiment (as opposed to H3N2 which was the subtype used for the vaccine), however, as stated earlier, high sequence conservation exists between the H1N1 and H3N2 internal proteins (Table 6.1). Serum IgG titres against all antigens were detected. As expected, all prime-boost regimens induced higher IgG levels compared with the prime-only regimens. Specifically, the IM-IN and IN-IN regimens elicited significantly higher IgG titres than the prime-only regimens; this finding was consistent across all three antigens (RSV A2-F (Figure 6.2A), H1N1-NP (Figure 6.2B) and H1N1-M1 (Figure 6.2G)) (P values located in Supplemental Table 5). The IM-IN and IN-IN regimens also elicited between 2- and 5-fold higher $\log_{10}$ IgG ELISA units (EUs) than in IM-IM-vaccinated mice, however, these differences were not statistically significant. IM-IM vaccination did not

elicit significantly higher IgG titres in sera compared with prime-only groups. Increased antigen-specific IgA levels in the serum were observed in the IM-IN and IN-IN groups compared with the IM and IM-IM groups, specific against RSV A2-F (Figure 6.2B), H1N1-NP (Figure 6.2E) and H1N1-M1 (Figure 6.2H) (P values located in Supplemental Table 5). The levels of antigen-specific IgM were comparable across all regimens (Figure 6.2C, F and I). Because the levels of serum anti-influenza A NP and M1 IgG and IgA were positively correlated (r=0.8841), only the NP antigen was used in subsequent assays as the representative influenza A antigen (Figure 6.2J).

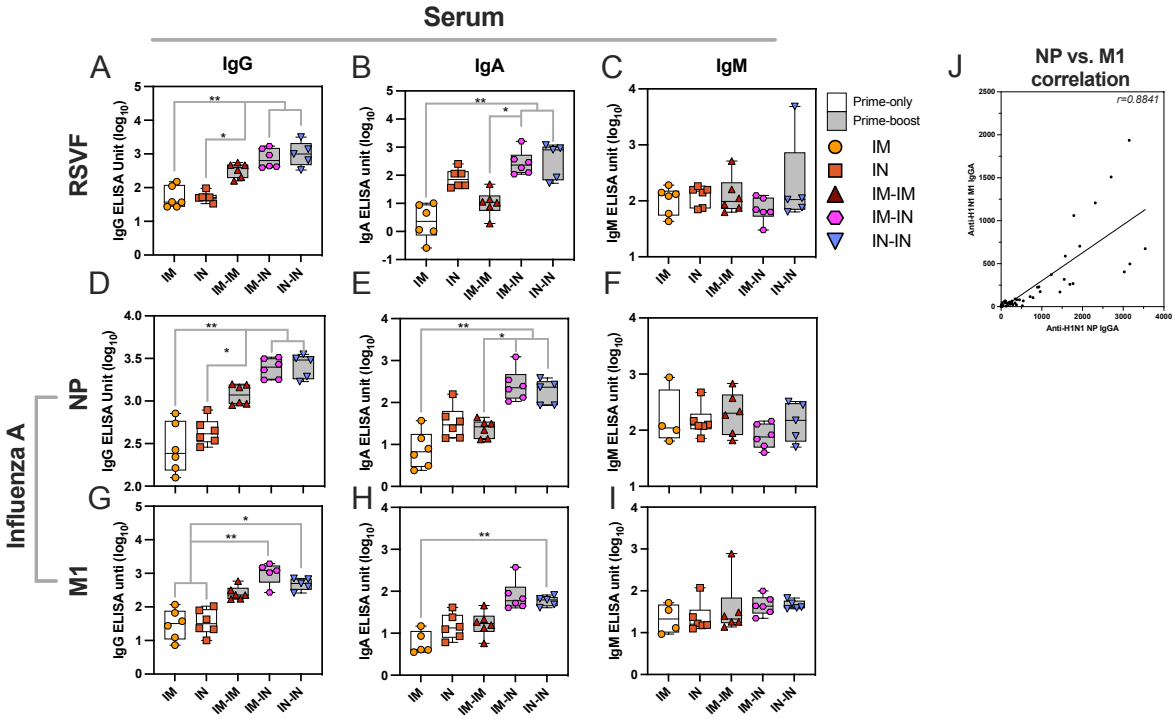

Figure 6.2: Antibody responses in the blood following ChAdOx1-NP+M1-mRSV(F) vaccination

IgG, IgA and IgM responses against RSVF (A, B, and C, respectively), influenza A NP (D, E and F, respectively) and M1 (G, H and I, respectively) (H1N1) in sera three weeks post-final vaccination, measured by ELISA. Values are displayed as ELISA units (EUs) (log_{10}). Individual mouse values are represented as symbols. Values were analysed using non-parametric Kruskal-Wallis tests to assess for statistically significant differences between groups, which are then expressed as P values (*=P<0.05, **=P<0.01). (J) Correlation of influenza A NP and M1 IgGA with Spearman r value (r=0.8841). For boxplots, whisker endings represent upper and lower extremes, the box bounds represent upper and lower quartiles, respectively, and the central line represents the group median. The P values for these graphs are present in Supplemental Table 5. For the IN-IN vaccination group, one datapoint is missing due to the sample having insufficient volume for the antibody measurements.

To assess the mucosal antibody responses, respiratory fluid IgA specific to H1N1-NP and RSV A2-F was tested (Figure 6.3). Higher levels of H1N1 NP- and RSV A2 F-specific IgA were detected following IM-IN and IN-IN vaccination within the nasal-associated lymphoid tissue (NALT), broncho-alveolar lavage fluid (BALF) and lung homogenate supernatant (LHS), compared with the levels following IM and IM-IM vaccination (Figure 6.3 and Supplemental Table 6). The IN-IN regimen elicited the highest titres of IgA in NALT, BALF and LHS. The IM-IN-vaccinated group had IgA titres comparable to the IN-IN-vaccinated group in the NALT, BALF and LHS.

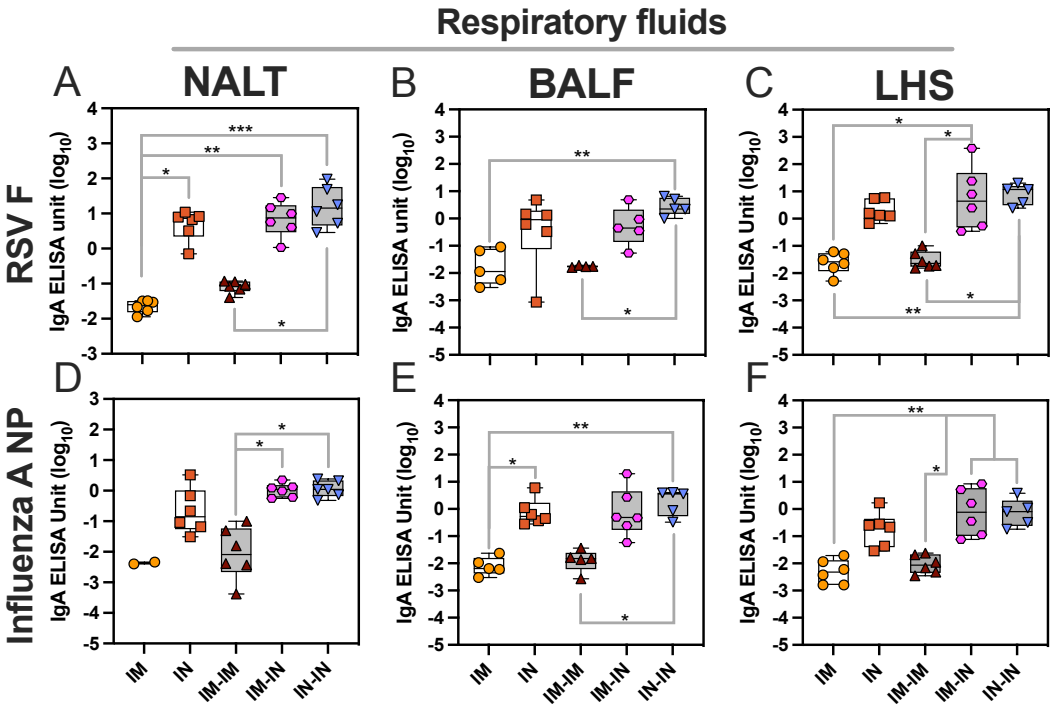

Figure 6.3: Antibody responses in respiratory fluids following ChAdOx1-NP+M1-mRSV(F) vaccination

Antibody responses (isotypes) following ChAdOx1-NP+M1-mRSV(F) vaccination (n=6). Data shown is from the first of two repeat experiments. Levels of IgA specific to RSV F in NALT (A), BALF (B) and lung homogenate supernatant (LHS) (C) and influenza A NP (H1N1) in NALT (D), BALF (E) and (LHS) (F) collected from mice three weeks post-final vaccination as measured by ELISAs (*=P<0.05, **=P<0.01, ***=P<0.001). For boxplots, whisker endings represent upper and lower extremes, the box bounds represent upper and lower quartiles, respectively, and the central line represents the group median. The P values for data are available in Supplemental Table 6. When datapoints in groups were less than a sum of 6, this was due to insufficient sample volume required to complete the assay.

The relative levels of antigen-specific IgG subclasses can reflect the type of T cell responses that have occurred[359]. To assess if regimens elicited Th1 (increased relative IgG2a) or Th2 (increased relative IgG1) responses, the relative abundances of IgG subclasses specific to NP and RSVF antigens in serum were then assessed. IM, IM-IM and IM-IN regimens elicited high relative levels of IgG2a among subclasses, suggesting a Th1-type response (Figure 6.4A)[360]. IN and IN-IN groups however, did not elicit clear Th1-type IgG subclass responses, with reduced relative levels of IgG2a, and either balanced levels across all five subclasses (H1N1 NP-specific) or elevated IgG2b (RSVF-specific) (Figure 6.4B). The IN and IN-IN regimens had low IgG2a to IgG1 ratios compared with the IM, IM-IM and IM-IN regimens (Figure 6.4B).

In summary, the IM-IN and IN-IN regimens induced higher systemic and respiratory mucosal antibody responses against RSV and influenza viral antigens compared with other regimens tested. However, IM-IN-vaccinated mice had a clear Th1-type systemic IgG subclass profile, whereas IN-IN vaccinated mice possessed a mixed IgG subclass profile and IgG2b-dominant profile, for influenza NP-specific and RSVF-specific IgG, respectively.

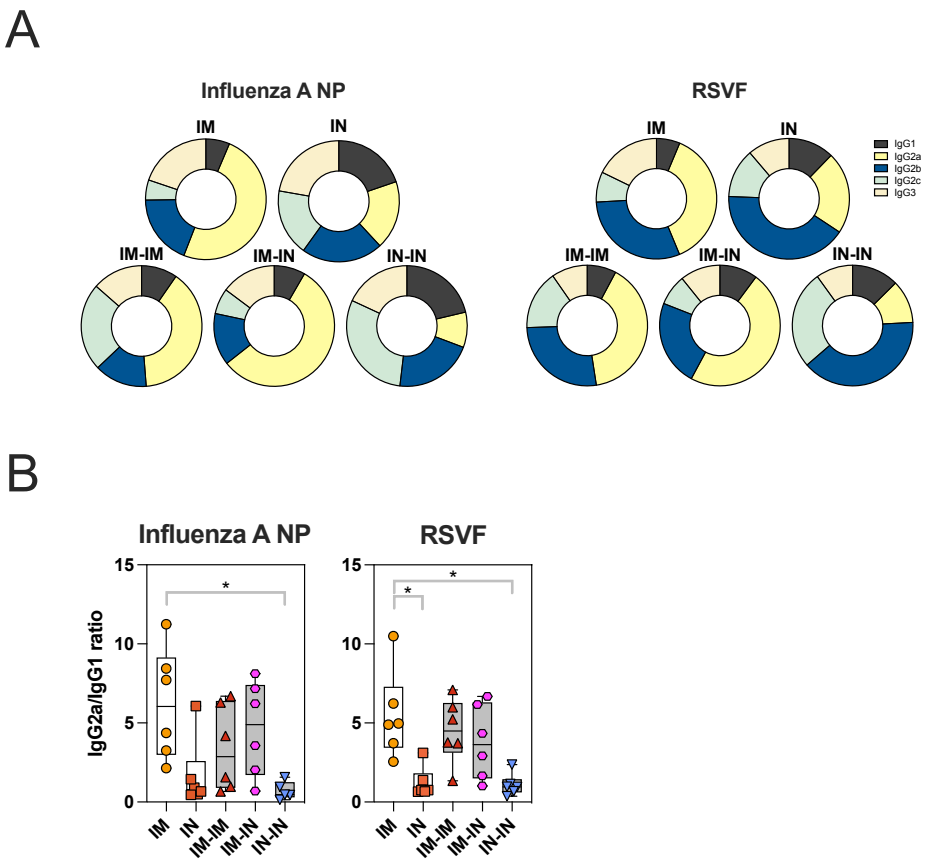

Figure 6.4: Trends in systemic IgG subclasses following ChAdOx1-NP+M1-mRSV(F) vaccination

Antibody responses (IgG subclasses) following ChAdOx1-NP+M1-mRSV(F) vaccination (n=6). Data shown is from the first of two repeat experiments. (A) Relative levels of anti-influenza A NP (H1N1) and anti-RSVF IgG subclasses in serum (IgG1, IgG2a, IgG2b, IgG2c and IgG3), as measured by tIgG-normalised indirect ELISA. Relative IgG subclass levels following each regimen are presented as individual doughnut charts, with each section of the doughnut representing the median IgG subclass OD_{405nm} response. Bar charts with individual sample responses per subclass per regimen are present in Supplemental Figure 5. (B) Serum antigen-specific IgG2a to IgG1 subclass ratios (IgG2a OD_{405nm} /IgG1 OD_{405nm}). Group differences of data in (B) were analysed using non-parametric Kruskal-Wallis tests *=P<0.05. For boxplots, whisker endings represent upper and lower extremes, the box bounds represent

2.1.2 T cell responses to ChAdOx1-NP+M1-mRSV(F)-DS2 systemically and in the respiratory mucosa

The T cell responses were then measured in the spleen and lungs to determine the systemic and respiratory cellular responses, respectively, following vaccination. Antigen

peptide stimulation and subsequent intracellular staining (ICS) of cytokines IFNγ, TNF, IL-4 and IL-2 was performed to determine the frequency of $CD8^+$ and $CD4^+$ T cells expressing each cytokine, and subsequent T cell phenotype (Figure 6.5A (spleen) and Figure 6.5B (lung)).

Splenocytes were stimulated with NP and M1 peptides, and following IM-IN vaccination, $CD4^+$ T cells demonstrated a trend of highest levels of IFNγ and TNF production and minimal IL-4 and IL-2, compared with other regimens (Figure 6.5A). RSVF-stimulated splenocytes of IN and IN-IN vaccinated mice had strikingly higher levels of IL-2 staining in $CD4^+$ T cells compared with IM and IM-IM regimen $CD4^+$ T cells (IN>IM and IN-IN>IM, P=0.0082 and P=0.0297, respectively). The relative levels of staining of the other cytokines IFNγ, TNF and IL-4, however, remained statistically comparable between regimens following RSVF peptide stimulation.

Following NP and M1 peptide stimulation, the $CD8^+$ T cell splenocytes had a trend across all regimens of minimal IL-4 and IL-2 expression, and higher levels of IFNγ and TNF expression, which were highest following the IM-IN regimen (Figure 6.5A). Following RSVF peptide stimulation, the $CD8^+$ T cell splenocytes following IM-IN mirrored this trend. Other regimens did not have clear trends in the expression of the four cytokines measured, showing more balanced levels of expression across the cytokines. The IM and IN-IN regimen $CD8^+$ T cell splenocytes had minimal levels expression of all four cytokines in comparison with other tested regimens.

Cytokine positive responses were detected in $CD4^+$ and $CD8^+$ lung T cells to varying degrees (Figure 6.5B). Lung $CD4^+$ and $CD8^+$ T cells of IM-IN vaccinated mice expressed the highest levels of IFNγ, TNF and IL-4 following NP- and M1-peptide stimulation (Figure 6.5B). Notably, lung cell cytokine responses following IN-IN vaccination were generally low

compared with other regimens. Overall, the measured lung CD4⁺ and CD8⁺ T cell cytokine responses had a mixed profile post-peptide-stimulation.

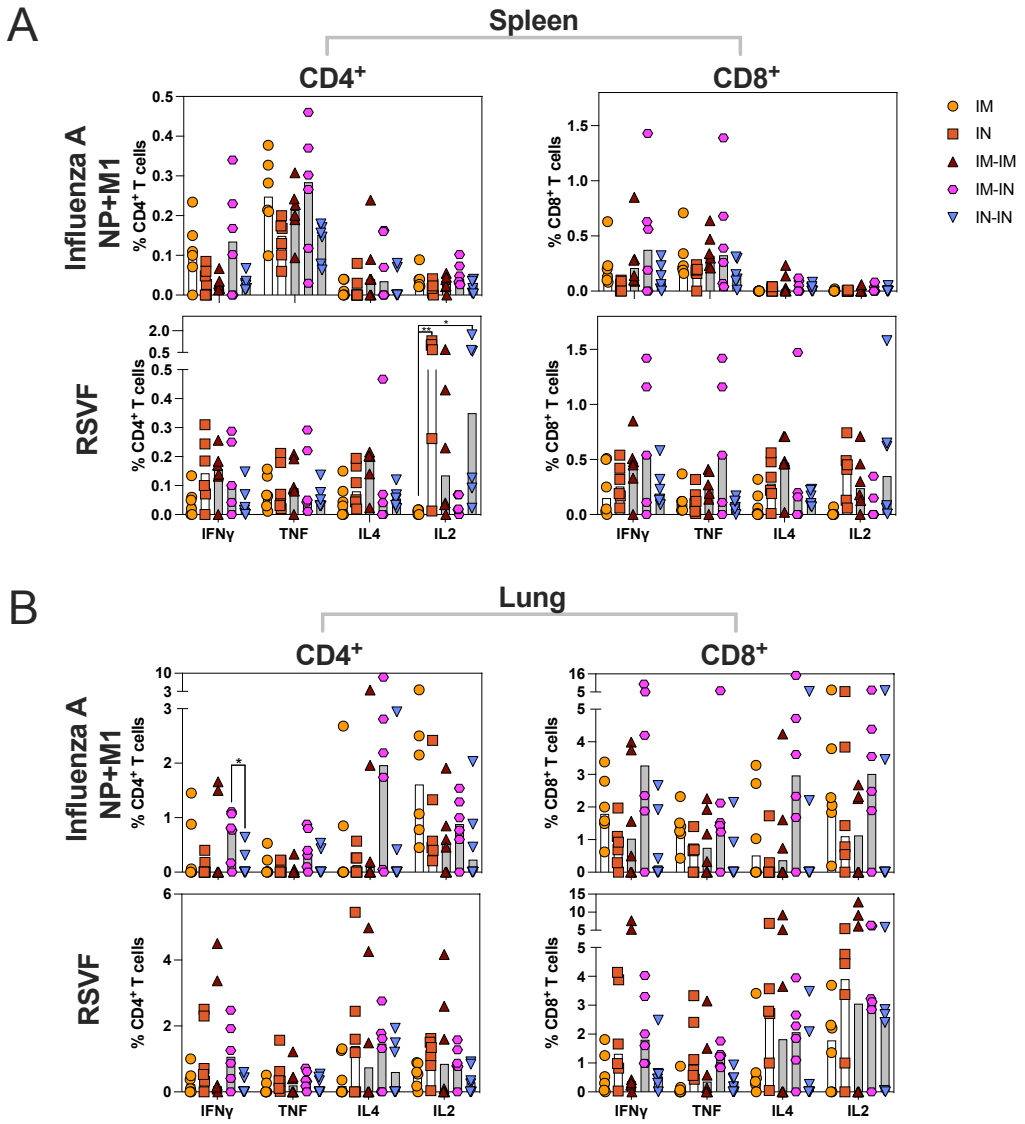

Figure 6.5: T cell cytokine responses in spleen and lungs following ChAdOx1-NP+M1-mRSV(F)

Cytokine responses following ChAdOx1-NP+M1-mRSV(F) vaccination (n=6). Data shown is from the first of two repeat experiments. (A) Cytokine responses in CD4⁺ and CD8⁺ splenocytes that were separately stimulated with influenza A (H1N1) NP+M1- and RSVF-spanning peptides; % cytokine⁺ T cells were determined through intracellular staining. Basal frequencies of cytokine⁺ T cells (unstimulated sample) were subtracted from stimulated sample frequencies. Median responses in each group are displayed as the top lines of bars on graphs on the left-hand side of the figure, with symbols representing individual mice, grey-shaded bars prime-boost regimens and white bars prime-only regimens. (B) Cytokine responses in CD4⁺ and CD8⁺ lung cells harvested from mice, separately stimulated with influenza A (H1N1) NP+M1- and RSVF-spanning peptides. Group differences of data in (A) and (B) were analysed using non-parametric Kruskal-Wallis tests (*=P<0.05, **=P<0.01).

An additional experiment was conducted, repeating the prime-boost regimens IM-IM, IM-IN and IN-IN, so that further cellular immunogenicity analyses could be completed (Figure 6.6A). The frequencies of IFNγ-releasing cells following peptide stimulation were assessed through IFNγ ELISpot assay (Figure 6.6B). Following RSVF peptide stimulation, IM-IM and IM-IN vaccinated mice had comparable frequencies of IFNγ-releasing splenocytes that were statistically higher than the frequencies in the control, unvaccinated mouse group (P=0.0057 and P=0.0065, IM-IM>unvaccinated control and IM-IN>unvaccinated control, respectively) (Figure 6.6B). Following NP+M1 peptide stimulation, the IM-IM, IM-IN and IN-IN mouse groups all had higher frequencies of IFNγ-releasing splenocytes compared with unvaccinated control group (P=0.0256, P=0.0100, P=0.0291, IM-IM>unvaccinated control, IM-IN>unvaccinated control, and IN-IN>unvaccinated control, respectively) (Figure 6.6B).

The total numbers of lung tissue-resident memory T cells (T_{RM}) were measured via antibody staining and flow cytometry. T_{RM} were defined as expressing a $CD3^{IV-}CD69^{+}CD103^{+}CD62L^{-}CD44^{+}$ phenotype, where anti-CD3 antibody was intravenously (IV) injected into mice to exclude all circulatory T cells (Figure 6.6C). Lung $CD8^{+}$ T_{RM} counts were highest following IM-IN vaccination (IM-IN>IM-IM, P=0.0197 and IM-IN>unvaccinated control, P=0.0005). IN-IN vaccinated mice had T_{RM} counts lower than IM-IN, but that were still higher than unvaccinated control mice (IN-IN>unvaccinated control, P=0.0197). Additionally, T_{EM} ($CD3^{IV-}CD44^{+}CD62L^{-}CD127^{+}$) counts were highest following IM-IN vaccination (Figure 6.6C).

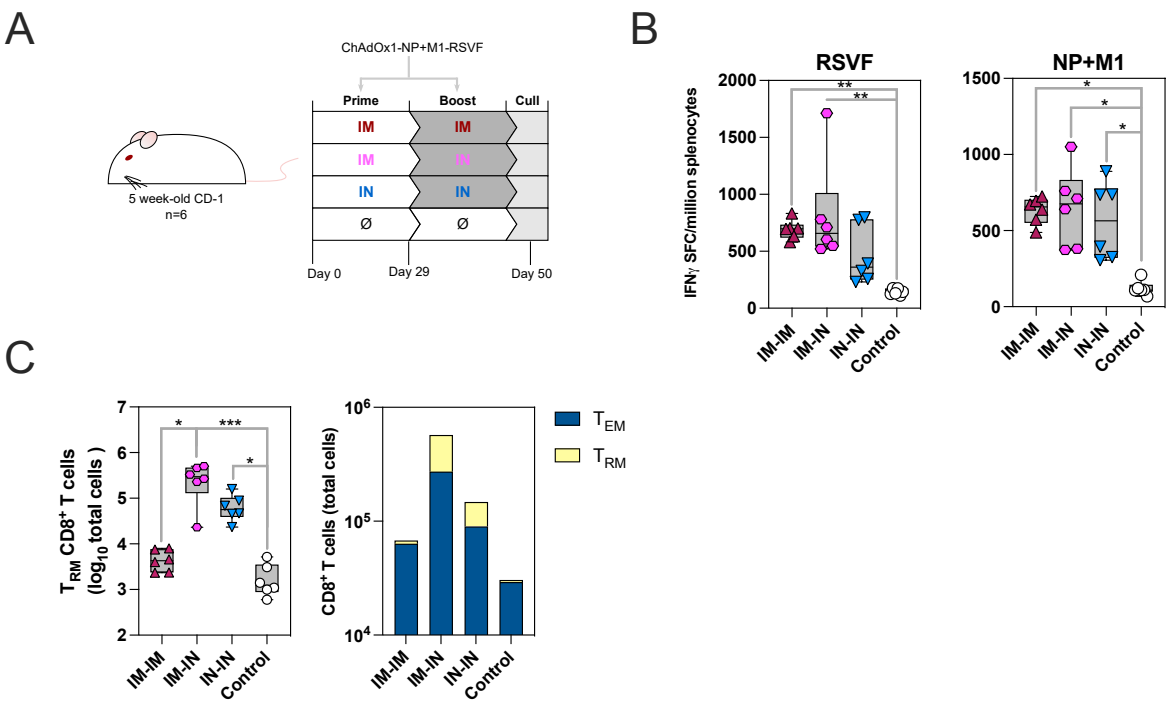

Figure 6.6: Further assessment of the cellular immunogenicity of ChAdOx1-NP+M1-mRSV(F) when administered via a prime-boost regimen

(A) Vaccination schematic for the continued assessment of the cellular immunogenicity of ChAdOx1-NP+M1-RSVF (n=6). (B) IFNγ responses in splenocytes stimulated with NP+M1- and RSVF-spanning peptides (IFNγ spot-forming cells (SFCs)/million splenocytes), as measured by IFNγ enzyme-linked immunosorbent spot (ELISpot) assay. (C) Total counts of CD8+ T_{RM} cells (left), as well as relative counts of $CD8^+$ T_{EM} and T_{RM} cells (right) in lungs post-vaccination (all non-antigen-specific). T_{RM} cells were defined as $CD8^+CD44^+CD62L^-CD103^+CD69^+$, and negative for intravenous (IV) circulatory $CD3^+$ T cell stain. T_{EM} cells were defined as $CD8^+CD44^+CD62L^-CD127^+$, and negative for IV circulatory $CD3^+$ T cell stain. Group differences of data in (A), (B), (D) and (E) were analysed using non-parametric Kruskal-Wallis tests (*=P< 0.05, **=P<0.01, ***=P<0.001). For all boxplots, whisker endings represent upper and lower extremes, the box bounds represent upper and lower quartiles, respectively, and the central line represents the group median.

The overall magnitudes of T cell cytokine responses tended to be higher in IM-IN-vaccinated groups both systemically in the spleen and locally in the lung. In the spleen, these responses were generally IFNγ- and TNF-biased, whereas in the lungs a mixed cytokine profile was detected. IM-IM and IM-IN-vaccinated mouse splenocytes also released high levels of IFNγ as measured by ELISpot assay. The IM-IN regimen was also able to potentiate higher counts of T_{RM} and T_{EM} in the lungs compared with other regimens. A

summary of the magnitude of immune response following reach regimen is represented through a normalised heatmap in Figure 6.7A.

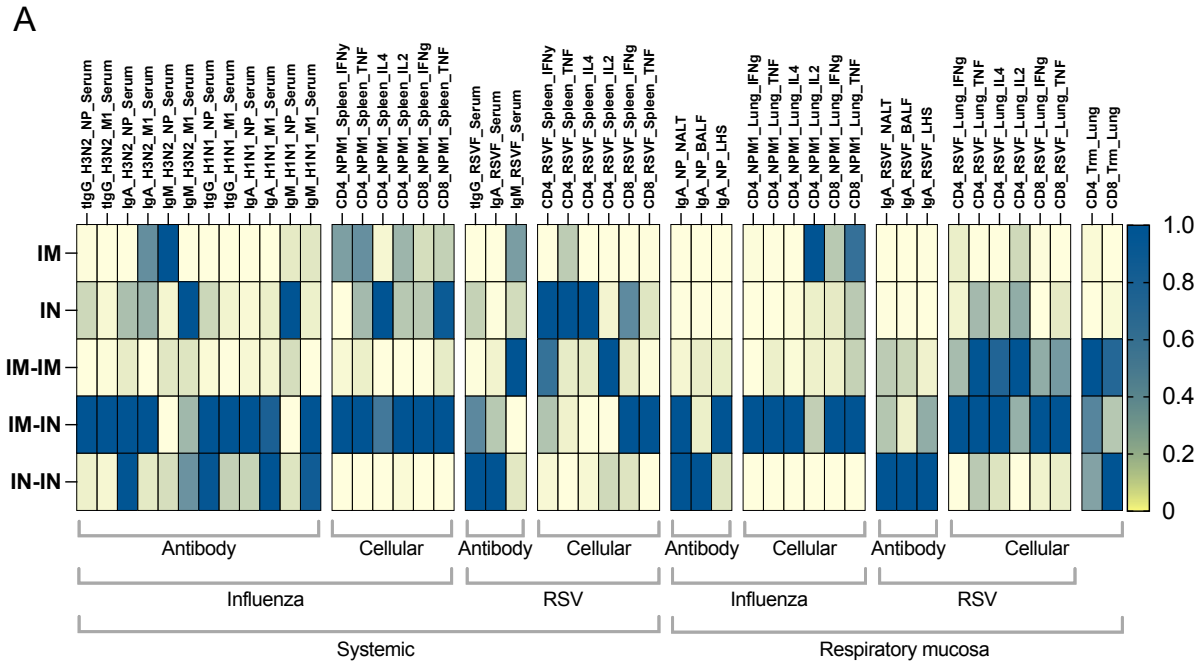

Figure 6.7: Summary of the magnitude of immune responses following different vaccination regimens

(A) A heatmap of the compiled immunogenicity responses following different vaccination regimens. Data is derived from both immunogenicity experiments (n=6). Data were min-max (1.0=max, 0.0=min) normalised across regimens per assay readout. Each assay readout is represented as a column, with the specific readout labelled at the top of columns. Each regimen is represented by a row. Readouts are organised into either an antibody or cellular response measurement, influenza antigen- or RSV antigen-specific, and also systemic or respiratory mucosa response. The T_{RM} data is not antigen-specific.

2.2 Protective capacity of ChAdOx1-NP+M1-mRSV(F)-DS2 determined via virus challenge

The protective capacity of ChAdOx1-NP+M1-RSVF administered via different prime-boost routes in mice was assessed via virus challenge experiment. John Tregoning, Ziyin Wang, Robert F. Cunliffe and Hadijatou Sallah, abbreviated John Tregoning *et al* (all Imperial College London) conducted the mouse virus challenge experiments and subsequent ex-vivo cell staining, flow cytometry and viral load measurements as part of a

collaboration study. Serum and mucosal fluid ELISAs from these experiments, as well as data analysis and visualisation, were conducted by Cameron Bissett.

Certain animal models such as the ferret influenza challenge model and the cotton rat RSV challenge model are well-established and favoured over the mouse model, as they better reflect certain aspects of the human immune response to virus; despite this, the mouse model is still incredibly useful and established for RSV and influenza challenge studies[361,362]. The mouse challenge model is useful for determining the immunogenic and protective potential of certain regimens/vaccines. Additionally, it has significant overlaps with aspects of human infection, especially severe disease following infection[125,361–368]. The inbred BALB/c strain, rather than the CD-1 outbred strain (used in the immunogenicity studies), was chosen for these challenge experiments as the challenge models were previously established in the BALB/c strain.

One RSV strain was selected (RSV A2) for assessment of the protective immunity induced by ChAdOx1-NP+M1-RSVF vaccination against RSV infection and disease, however, two strains were selected for influenza: H3N2 (X-31) and H1N1 (A/California/7/2009), so that the protection against different subtypes (heterosubtypic protection) of influenza could be assessed. The internal influenza antigens of the vaccine and the two challenge strains are highly conserved as determined through pBLAST (Table 6.1), however, these challenge strains differ in terms of their pathogenicity in mice, as well as the identities of their glycoproteins[369].

Table 6.1: Homology of the influenza antigens of strains that are relevant to Chapter 6

ChAdOx1-NP+M1-RSVF antigen strain	Challenge strain	Antigen	Amino acid sequence identity (%)
Influenza A H3N2 A/Panama/2007/1999	Influenza A H1N1 A/California/7/2009	NP	89
		M1	92
		HA	44
		NA	44
	Influenza A H3N2 A/X-31	NP	91
		M1	95
		HA	88
		NA	87

2.2.1 RSV challenge following ChAdOx1-NP+M1-mRSV(F)-DS2 vaccination

2.2.1.1 Weight change and lung viral load following RSV challenge

The level of protection against RSV following IM-IM, IM-IN or IN-IN ChAdOx1-NP+M1-RSVF vaccination regimens was assessed via virus challenge. 5-week-old BALB/c mice were vaccinated, and then challenged IN with $7.7x10^5$ PFU RSV-A2 21 days-post boost (Figure 6.8A).

Weight loss was measured daily in mice post-challenge as a readout of deteriorating health and disease. All vaccinated mice, irrespective of regimen, followed a trend of less weight loss compared with unvaccinated, challenged, control mice (Figure 6.8B). Weight loss between days 4 and 7 post-infection within the IM-IN-vaccinated group was significantly less when compared with the control group (Figure 6.8, P values located in Supplemental Table 7). The area under the curve (AUC) values for the IM-IN-vaccinated mouse weight loss curves also indicated that overall less weight had been lost compared with the unvaccinated, challenged control group mice: IM-IN>control; P=0.0097 (Figure 6.8C). No significant differences in weight loss were measured between immunisation regimens.

To assess the degree of viral replication in the respiratory tract, lung RSV viral loads were measured after mice were culled on day 7. IM-IN and IN-IN-vaccinated mice had statistically lower viral loads within lungs compared with unvaccinated, challenged controls (P=0.0166 and P=0.0055, IM-IN>unvaccinated control and IN-IN>unvaccinated control, respectively) (Figure 6.8D).

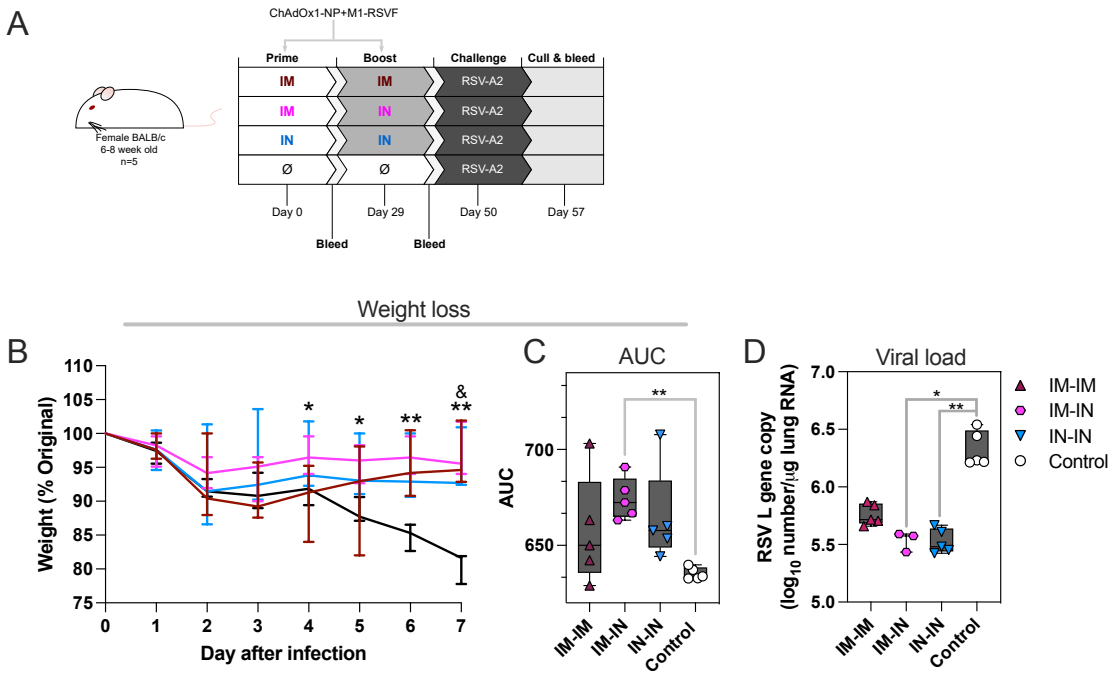

Figure 6.8: Challenging ChAdOx1-NP+M1-mRSV(F)-vaccinated mice with RSV

(A) Vaccination and challenge schematic for the assessment of the protective capacity of ChAdOx1-NP + M1-RSVF against RSV-A2 infection. Mice (n=5) were prime-boost-vaccinated, then challenged with RSV-A2, and culled 7 days later with tissues and fluids harvested. Blood sampling was performed 4 weeks post-prime and 3 weeks post-boost. The experiment was completed only once. (B) Weight change in mice over time post-challenge, measured as % of pre-challenge weight. At each timepoint, lines represent group medians, and bars represent group bodyweight ranges. Significant differences between IM-IN and control groups are represented with *, between IM-IM and control as & (* or & =P<0.05, **=P<0.01). Exact P values are present in Supplemental Table 7. (C) AUC values for the weight change curves presented in (B). (D) Viral load in lungs 7 days post-challenge, measured as number of RSV L gene copies/µg lung RNA (log_{10}). The viral load of two samples was not included as these samples did not generate a CT during the PCR process. Vaccinations, virus challenge, mouse culls and bleeds, were conducted by John Tregoning et al, as well as the generation weight change data, and viral load. The data were then visualised and analysed by Cameron Bissett.

2.2.1.2 Antibody and cellular immune responses following RSV challenge

The antibody and cellular immune responses systemically and in the respiratory tract were assessed on day 7 of challenge (Figure 6.9). Serum RSV A2-F-specific IgG and IgA levels were additionally measured 4 weeks post-prime and 3 weeks post-boost (Figure 6.9A). Although serum IgG levels were statistically comparable between all vaccinated regimens post-boost, pre-challenge, serum IgA levels were higher in the IM-IN and IN-IN regimens compared with the IM-IM regimen (IN-IN>IM-IM; P=0.0044) (Figure 6.9A). IgG and IgA antibodies against RSV A2-F were detected above control baseline in all regimens in serum 7 days post-challenge (Figure 6.9B). Within serum, nasal washes (NWs), BALF and LHS, IN-IN vaccinated mice had significantly higher titres of IgG and IgA compared with IM-IM vaccinated mice post-challenge, whilst IM-IN vaccinated mice had intermediate values between such regimens: serum IgG: P=0.0486, NW IgG: P=0.0327, LHS IgG: P=0.0486, serum IgA: P=0.0027, NW IgA: P=0.0089, BALF IgA: P=0.0016, LHS IgA: P=0.0016 (Figure 6.9B).

Total counts of T_{RM} (defined as $CD3^+CD8^+CD69^+CD103^+CD62L^-CD44^+$, and H-$2K^d$ $KYKNAVTEL^+$) in BAL and lungs were measured via cell staining and flow cytometry. The pentamer included in the T_{RM} staining definition was H-$2K^d$-restricted, and contained an RSV F glycoprotein epitope (KYKNAVTEL, $RSVF_{85-93}$), such that antigen-experienced T_{RM} were specifically measured. The overall counts of BAL and lung $CD8^+$ T_{RM} within all vaccinated, challenged groups were higher than unvaccinated, challenged control sample levels (Figure 6.9C and D). Levels of $CD8^+$ T_{RM} in BAL and lungs were of statistically insignificant difference between regimens, and only IN-IN vaccinated mice demonstrated statistically higher levels compared with unvaccinated control (P=0.0134 for BAL and P=0.0028 for lung cells) (Figure 6.9C and D). Nevertheless, IM-IN and IN-IN regimens had

BAL and lung T_{RM} levels of much smaller range compared with IM-IM vaccinated mice; the IM-IM vaccinated group had a larger range of T_{RM} levels, with two mice with having undetectable levels of T_{RM}. All vaccinated, RSV-challenged mice had numbers of T_{EM} $CD8^+$ T cells similar value to naïve, challenged mice in BAL and lungs.

In summary, all vaccinated animals were protected from overt disease, with IM-IN and IN-IN immunised mice having a significant reduction of lung viral load following RSV challenge.

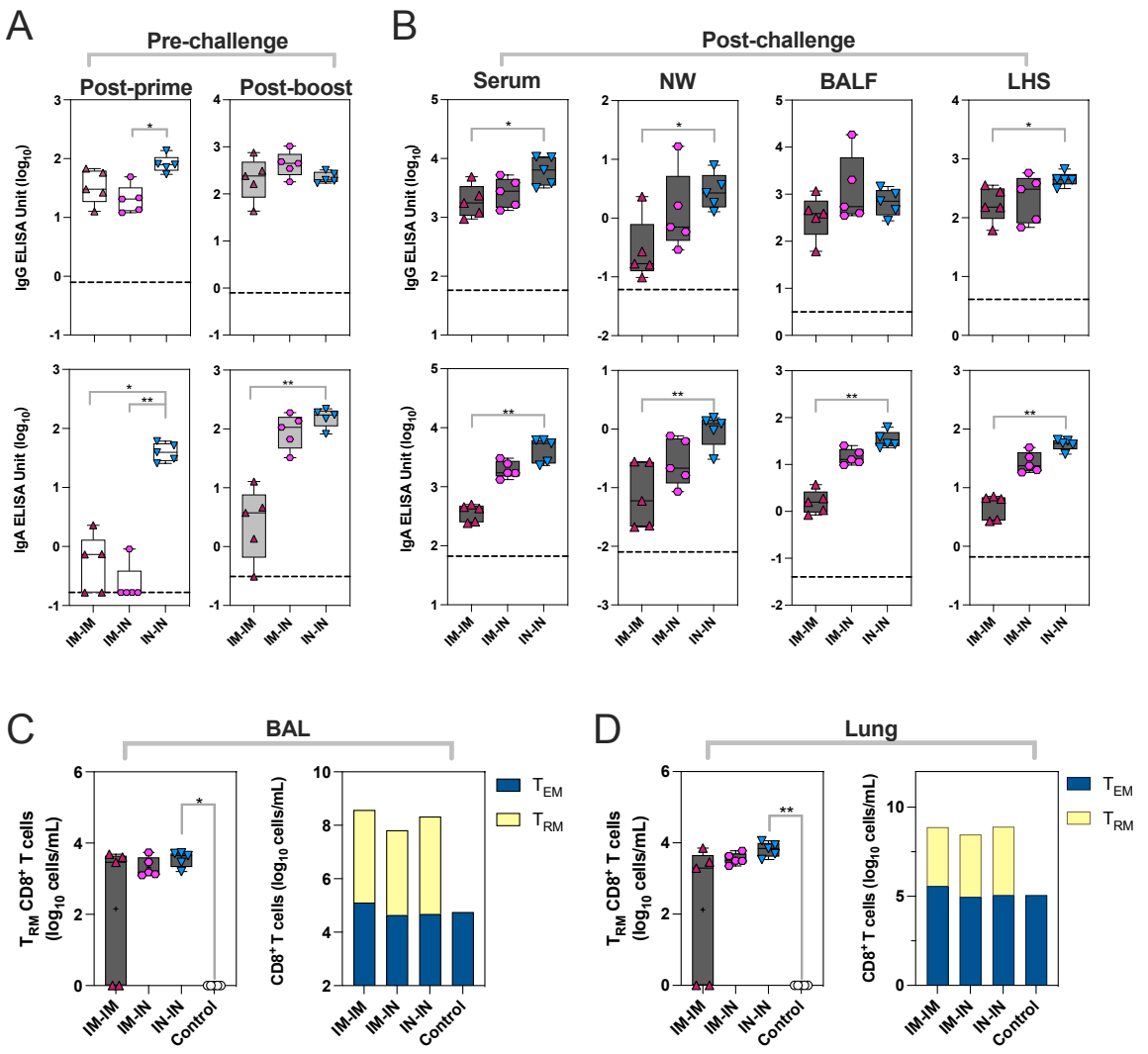

Figure 6.9: Immune responses following RSV challenge of ChAdOx1-NP+M1-mRSV(F)-vaccinated mice

Immunogenicity data for the RSV challenge experiment (n=6; completed once). (A) RSVF-specific IgG and IgA levels in serum 4 weeks post-prime and 3 weeks post-boost, measured by ELISA (B) RSVF-specific IgG and IgA levels in serum, NWs, BALF and LHS 7 days post-challenge, measured by ELISA. Median negative control values are displayed as dashed lines. (C) Levels of antigen-specific $CD8^+$ T_{RM}, and relative levels of antigen-specific $CD8^+$ T_{RM} and T_{EM}, in BAL post-challenge. T_{RM} and T_{EM} cells were defined as $CD3^+CD8^+CD44^+CD62L^-CD103^+CD69^+$, and $CD3^+CD8^+CD44^+CD62L^-$, respectively, and positive for RSV pentamer H-$2K^d$ KYKNAVTEL. In the boxplots of (C) and (D), a black "+" symbol represents the group mean. One mouse in group IM-IN did not have detectable lung T_{RM}. Two mice from the IM-IM-vaccinated group did not have detectable BAL T_{RM}. (D) Levels of antigen-specific $CD8^+$ T_{RM}, and relative levels of antigen-specific $CD8^+$ T_{RM} and T_{EM}, in the lung post-challenge. Two mice from the IM-IM-vaccinated group did not have detectable lung T_{RM}. Group differences for all data were analysed using non-parametric Kruskal-Wallis tests (*=P<0.05, **=P<0.01). For all figure boxplots, whisker endings represent upper and lower extremes, the box bounds represent upper and lower quartiles, respectively, and the central line represents the group median. Serum samples were provided by John Tregoning *et al*. Antibody data was generated by Cameron Bissett by ELISA. BAL and lung cell staining and flow cytometry was completed by John Tregoning *et al.* The data were visualised and analysed by Cameron Bissett.

2.2.2 H3N2 challenge following ChAdOx1-NP+M1-mRSV(F)-DS2 vaccination

2.2.2.1 Weight change and lung viral load following H3N2 challenge

The level of protection induced by ChAdOx1-NP+M1-RSVF vaccination against influenza A H3N2 infection and disease was also assessed via challenge. BALB/c mice were vaccinated IM-IM, IM-IN, IN-IN or left unvaccinated, and then challenged IN with $2x10^5$ PFU influenza A X-31 21 days post-boost (Figure 6.10A).

After virus challenge, all vaccinated groups of mice lost less weight than the unvaccinated controls (Figure 6.10B, P values located in Supplemental Table 7). Mice vaccinated IM-IN or IN-IN lost the least weight upon challenge, as indicated through weight loss AUC values (P=0.0066 and P=0.02332, IM-IN>unvaccinated control and IN-IN>unvaccinated control, respectively) (Figure 6.10C). The IM-IM group of mice lost the most weight out of the vaccinated groups, with a group median weight loss curve that mirrored the unvaccinated control group curve; weight recovery was only indicated after day 4 (Figure 6.10B and C), when IM-IM vaccinated mouse weights began to recover until cull on day 6 post-challenge.

All vaccinated, H3N2-challenged mice had less viral load in lungs (measured as M gene copy number/μg lung RNA) compared with unvaccinated, challenged control mice (Figure 6.10D). Mice vaccinated with following the IM-IN and IN-IN regimens had statistically lower viral loads compared with unvaccinated control mice (P=0.0037 and P=0.0097, IM-IN>unvaccinated control and IN-IN>unvaccinated control, respectively), and viral loads were of a similar level across IM-IN and IN-IN regimens.

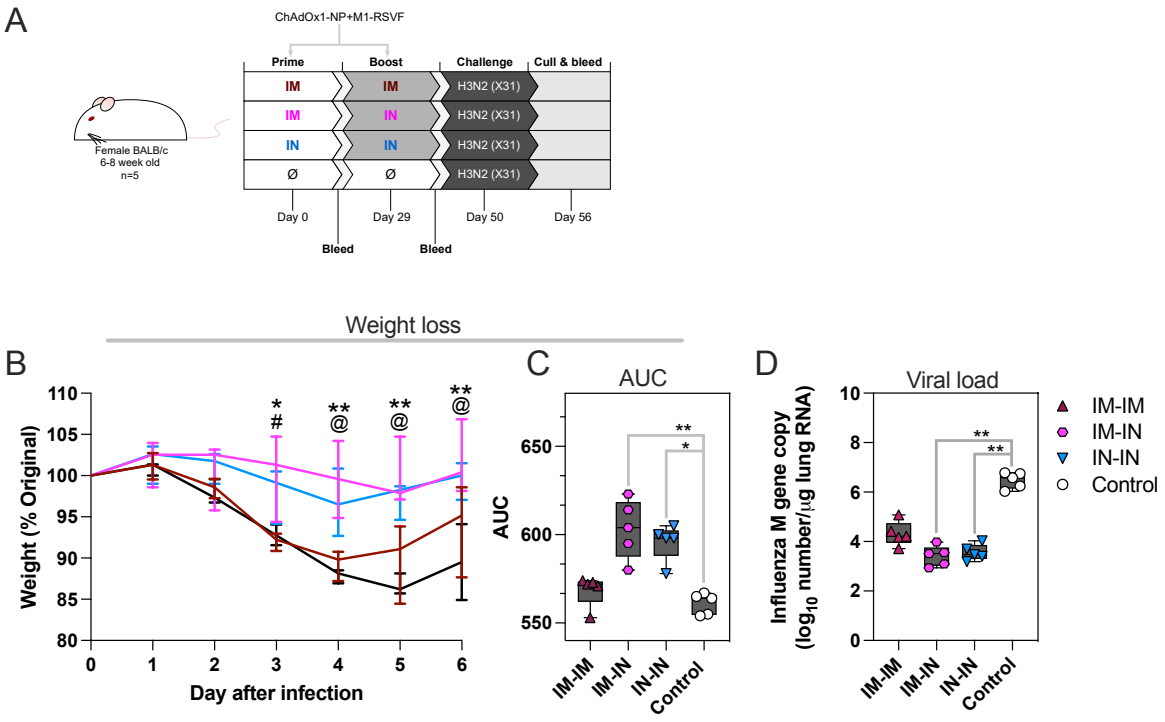

Figure 6.10: Challenging ChAdOx1-NP+M1-mRSV(F)-vaccinated mice with H3N2

(A) Vaccination and challenge schematic for the assessment of the protective capacity of ChAdOx1-NP+M1-RSVF against X31 (H3N2) infection and subsequent disease in mice (n=5). Mice were prime-boost-vaccinated, then challenged with X31, and culled 6 days later with tissues and fluids harvested. Blood sampling was performed 4 weeks post-prime and 3 weeks post-boost. The experiment was only completed once. (B) Weight change in mice over time post-challenge, measured as % of pre-challenge weight. Significant differences at timepoints between IM-IN and control mouse groups are represented with *, between IM-IN and IM-IM as # and between IN-IN and unvaccinated as @ (*, @ or # =P<0.05, **=P<0.01). (C) AUC values for the weight change curves presented in (B). (D) Viral load in lungs 6 days post-challenge (M gene copies/µg lung RNA (log_{10})). Vaccinations, virus challenge, mouse culls and bleeds, were conducted by John Tregoning et al, as well as the generation weight change data, and viral load. The data were visualised and analysed by Cameron Bissett.

2.2.2.2 Antibody and cellular immune responses following H3N2 challenge

The antibody and cellular immune responses systemically and in the respiratory tract were assessed on day 6 of challenge (Figure 6.11). Pre-challenge IgG and IgA levels in the serum were additionally measured (Figure 6.11A); the IM-IN regimen elicited higher levels of serum H3N2 NP-specific IgG and IgA compared with the IM-IM and IN-IN regimens: IM-IN>IM-IM, IgG P=0.0012 and IgA P=0.0028. Serum IgG and IgA antibodies against H3N2-

NP were detected above baseline in all regimens post-challenge (Figure 6.11B). Serum and airway IgG and IgA were significantly higher following IN-IN vaccination and challenge, than IM-IM vaccination and challenge, whilst IM-IN vaccinated mice again had intermediate titres: serum IgG: P=0.0016, serum IgA: P=0.0021, BALF IgA: P=0.0071, NW IgA: P=0.0056 (Figure 6.11B).

$CD8^+$ T_{RM} were defined as $CD3^+CD8^+CD69^+CD103^+CD62L^-CD44^+$, and positive for a H-$2K^d$(BALB/c haplotype)-restricted $TYQRTRALV^+$-epitope-containing pentamer; the TYQRTRALV epitope is present within the nucleoprotein of influenza A, and conserved between the NP sequences of challenge and encoded in the ChAdOx1-NP+M1-RSVF vaccine. $CD8^+$ T_{RM} were detected in BAL and lungs above the level in control, challenged animals in all vaccination regimens (Figure 6.11C and Figure 6.11D). In both BAL and lungs, IM-IN vaccinated, challenged mice had the highest median $CD8^+$ T_{RM} frequencies across immunisation regimens, and were significantly higher than in the unvaccinated control group (P=0.0020 and P=0.0101 for BAL and lung cells, respectively). One IM-IN vaccinated mouse failed to generate detectable lung $CD8^+$ T_{RM} following challenge. Following all regimens, T_{EM} could be detected in BAL and lungs (Figure 6.11C and Figure 6.11D).

In summary, all vaccinated animals were protected from overt disease, with viral titres lower following the IM-IN and IN-IN regimens than the IM-IM regimen, and higher frequencies of a T_{RM} population measured in the IM-IN vaccinated group post-H3N2 challenge compared with other groups.

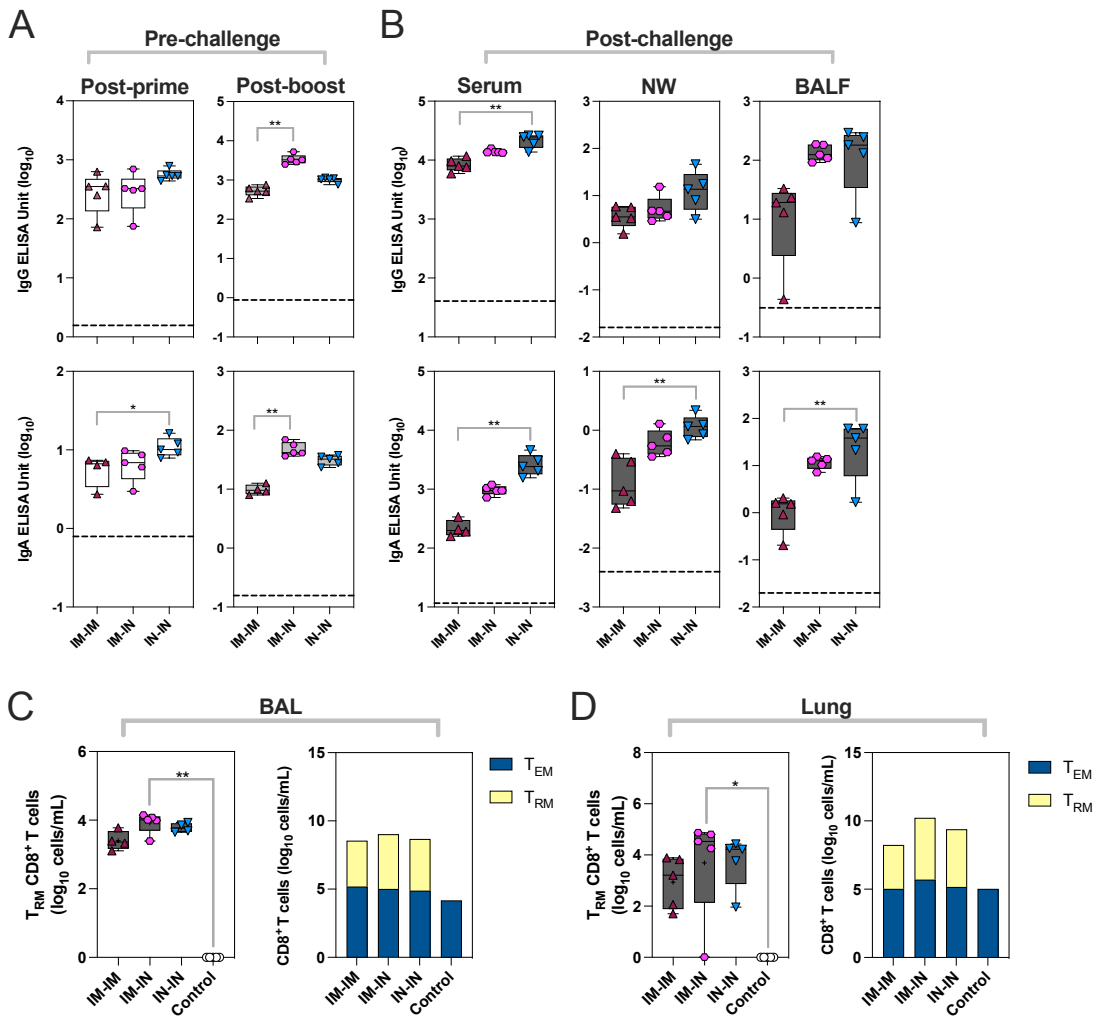

Figure 6.11: Immune responses following H3N2 challenge of ChAdOx1-NP+M1-mRSV(F)-vaccinated mice

Immunogenicity data for the H3N2 challenge experiment (n=6; completed once). (A) H3N2 NP-specific IgG and IgA levels in serum, NWs and BALF post-challenge, as measured by ELISA (log_{10} EU). LHS was not collected for this experiment. Median negative control values are displayed as dashed lines. (C) Levels of antigen-specific $CD8^+$ T_{RM} cells, and relative levels of antigen-specific $CD8^+$ T_{EM} and T_{RM}, in BAL post-challenge. T_{RM} and T_{EM} cells were defined as $CD3^+CD8^+CD44^+CD62LCD103^+CD69^+$, and $CD3^+CD8^+CD44^+CD62L^-$, respectively, and positive for influenza pentamer H-$2K^d$ TYQRTALV. (D) Levels of antigen-specific $CD8^+$ T_{RM} cells, and relative levels of antigen-specific $CD8^+$ T_{EM} and T_{RM}, in the lung post-challenge. In the boxplots of (C) and (D), a black "+" symbol represents the group mean. One mouse in group IM-IN did not have detectable lung T_{RM}. Group differences for all data were analysed using non-parametric Kruskal-Wallis tests (*=P<0.05, **=P<0.01). For all boxplots, whisker endings represent upper and lower extremes, the box bounds represent upper and lower quartiles, respectively, and the central line represents the group median. Serum samples were provided by John Tregoning *et al*. Antibody data was generated by Cameron Bissett. BAL and lung cell staining and flow cytometry was completed by John Tregoning *et al.* The data were visualised and analysed by Cameron Bissett.

2.2.3 H1N1 challenge following ChAdOx1-NP+M1-mRSV(F)-DS2 vaccination

2.2.3.1 Weight change and viral load following H1N1 challenge

The level of protection induced by ChAdOx1-NP+M1-RSVF against infection and disease with a different influenza A strain, H1N1, was tested. The H1N1 strain NP and M1 proteins are similar in sequence to the ones encoded in the ChAdOx1-NP+M1-RSVF vaccine, however, the strain differs in pathology and features different distant glycoprotein identities. 5-week-old BALB/c mice were vaccinated, and then challenged IN with $2.1x10^5$ PFU influenza A H1N1 21 days-post boost (Figure 6.12A).

The weight changes in mice following H1N1 challenge were similar among vaccinated and unvaccinated control groups until day 4 post-challenge, when weight loss in the IM-IN group halted and mouse weight began to increase, unlike the other groups (Figure 6.12B and Figure 6.12C). The weight of IM-IN-vaccinated mice on day 5 was statistically higher than of IM-IM vaccinated mice (IM-IN>IM-IM P=0.0066) (Figure 6.12B).

The viral loads measured in lungs (measured by M gene copy number/μg lung RNA) were all lower in the vaccinated groups, however, only mice vaccinated IM-IN had statistically significant lower viral loads compared with the unvaccinated, challenged control group (P=0.0011, IM-IN vs. unvaccinated control); IM-IN vaccinated mice had the lowest detectable viral loads among all vaccinated regimen mouse groups (Figure 6.12D).

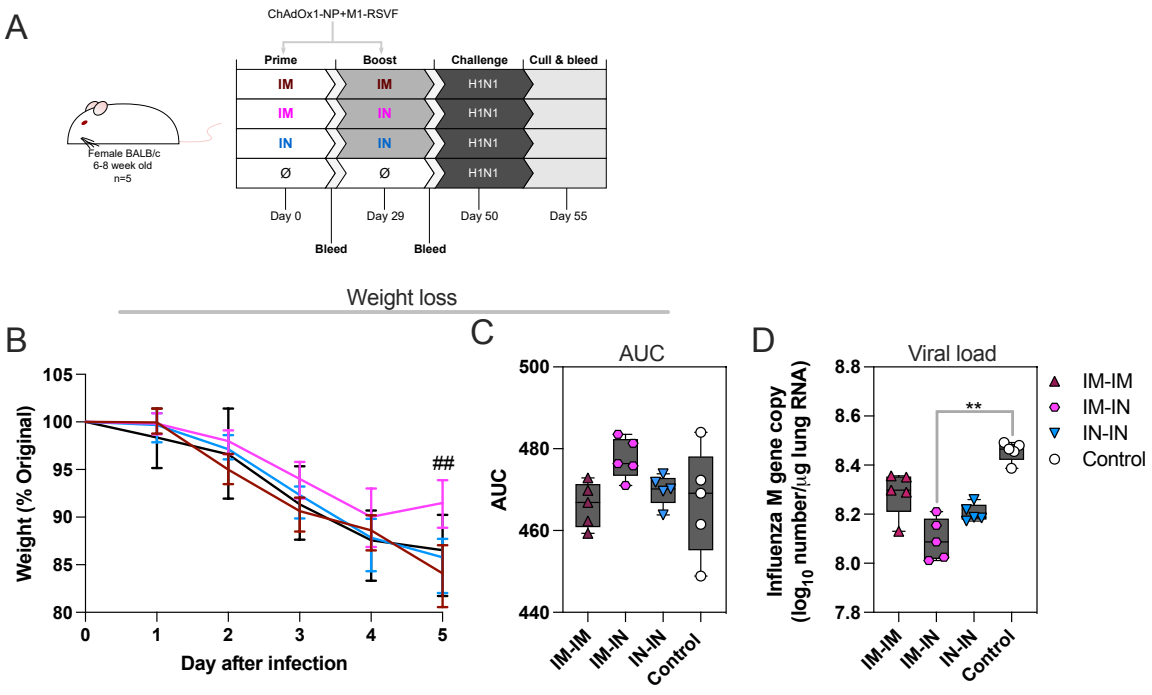

Figure 6.12: Challenging ChAdOx1-NP+M1-mRSV(F)-vaccinated mice with H1N1

(A) Vaccination and challenge schematic for the assessment of the protective capacity of ChAdOx1-NP+M1-RSVF against H1N1 infection and subsequent disease in mice (n=5). Mice were prime-boost-vaccinated, then challenged with H1N1, and culled 5 days later with tissues and fluids harvested. Blood sampling was performed 4 weeks post-priming and 3 weeks post-boosting. The experiment was only completed once. (B) Weight change in mice over time post-challenge, as measured by % of pre-challenge weight. The significant difference between IM-IN and IM-IM mouse groups is represented with ## (##=P<0.01). (C) AUC values for the weight change curves presented in (B). (D) Viral load in lungs 5 days post-challenge (number of M gene copies/µg lung RNA (log_{10})). Vaccinations, virus challenge, mouse culls and bleeds, were conducted by John Tregoning et al, as well as the generation weight change data, and viral load. The data were visualised and analysed by Cameron Bissett.

2.2.3.2 Antibody and cellular immune responses following H1N1 challenge

The antibody and cellular immune responses systemically and in the respiratory tract were assessed on day 5 of challenge (Figure 6.13). Pre-challenge IgG and IgA levels in serum were additionally measured (Figure 6.13A); vaccination regimens elicited comparable levels of serum H3N2 NP-specific IgG and IgA. IgG and IgA antibodies against H1N1-NP were detected above control baseline in all regimens in serum 5 days post-

challenge (Figure 6.13B). Within the airways of IM-IN and IN-IN vaccinated mice, higher IgG and IgA titres were detected compared with IM-IM vaccinated mice post-challenge (Figure 6.13B): IN-IN>IM-IM; BALF IgG: P=0.0486, LHS IgG: P=0.014, NW IgA: P=0.0352, BALF IgA: P=0.0036, LHS IgA: 0.0012 and IM-IN>IM-IM; BALF IgG: P=0.0112 and NW IgA: P=0.0119.

Within BAL and lungs, IM-IN vaccinated, challenged mice had more $CD8^+$ T_{RM} (defined identically to that of H3N2 challenge), and the total number were statistically higher than that measured in IM-IM vaccinated mice (P=0.0379 and P=0.0267 for BAL and lung cells, respectively) (Figure 6.13C and Figure 6.13D). All regimens induced measurable numbers of T_{EM} compared with unvaccinated, challenged control mice. IM-IN vaccination however, induced the greatest numbers of T_{EM} compared with other regimens.

In summary, IM-IN immunised mice demonstrated higher protection compared with other regimens, though not sterilising; increased weight after day 4 of infection and lower viral loads were paired with distinctively higher levels of $CD8^+$ T_{RM} and T_{EM} locally in BAL and lungs.

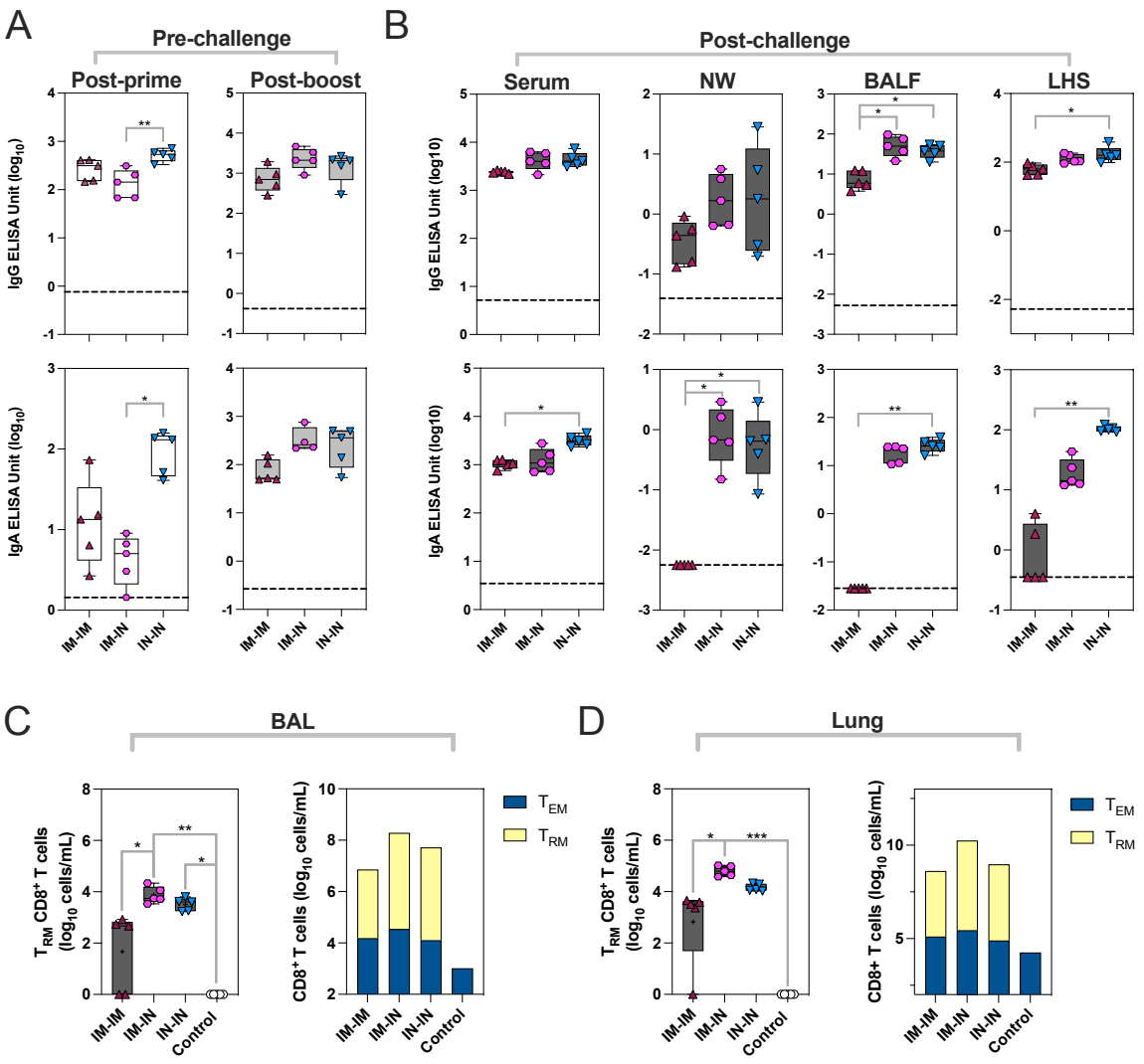

Figure 6.13: Immune responses following H3N2 challenge of ChAdOx1-NP+M1-mRSV(F)-vaccinated mice

Immunogenicity data for the H1N1 challenge experiment (n=6; completed once). (A) H1N1 NP-specific IgG and IgA levels in serum, NWs, BALF and LHS post-challenge, as measured ELISA (log_{10} EU). Median control values are displayed as dashed lines on graphs. (B) Levels of antigen-specific $CD8^+$ T_{RM} cells, and relative levels of antigen-specific $CD8^+$ T_{EM} and T_{RM}, in BAL post-challenge. T_{RM} and T_{EM} cells were defined as $CD3^+CD8^+CD44^+CD62L^-CD103^+CD69^+$, and $CD3^+CD8^+CD44^+CD62L^-$, respectively, and positive for influenza pentamer H-$2K^d$ TYQRTALV. In the boxplots of (C) and (D), a black "+" symbol represents the group mean. One mouse in group IM-IN did not have detectable lung T_{RM}. Two mice in group IM-IM did not have detectable BAL T_{RM}. (C) Levels of antigen-specific $CD8^+$ T_{RM} cells, and relative levels of antigen-specific $CD8^+$ T_{EM} and T_{RM}, in the lung post-challenge. One mouse in group IM-IM did not have detectable Lung T_{RM}. Group differences for all data were analysed using non-parametric Kruskal-Wallis tests (*=P<0.05, **=P<0.01, ***=P<0.001). For all boxplots, whisker endings represent upper and lower extremes, the box bounds represent upper and lower quartiles, respectively, and the central line represents the group median. Serum samples were provided by John Tregoning *et al*. Antibody data was generated by Cameron Bissett. BAL and lung cell staining and flow cytometry was completed by John Tregoning *et al.* The data were visualised and analysed by Cameron Bissett.

3. Discussion

RSV and influenza A continue to inflict a major global health burden, disproportionately affecting children and the elderly. Recently, RSV vaccine candidates and long-lasting antibody therapeutics (Nirsevimab) have been licensed, and vaccines against influenza are used in annual vaccination regimens[141]. Licensed RSV and influenza vaccines are mostly administered intramuscularly; a safe route associated with systemic immunity, and effective at eliminating severe disease. However, the IM route of vaccination has limited capacity to induce respiratory mucosal immunity, which has been associated with the control of respiratory infection[370,371]. A respiratory mucosal route of vaccination capable of inducing durable RSVF-specific memory B cells and neutralising antibodies at viral entry will provide protection and reduce levels of infection[352,372]. Additionally, T_{RM} induced upon mucosal vaccination, resting within the lung parenchyma and airway mucosa, capable of rapid activation upon influenza A infection, are expected to largely enhance the control of virus infection[226,230,373].

As RSV and influenza persist globally, cost-effective, two-in-one bivalent vaccines, capable of inducing simultaneous respiratory and systemic immunity against RSV and influenza present an attractive strategy. In this chapter, a bivalent vaccine that was constructed in-house, ChAdOx1-NP+M1-RSVF, was tested in mice. The findings demonstrated that route of vaccination and regimen have a strong influence on the extent of protection provided by a given vaccine. IM-IN vaccinated mice generally demonstrated higher magnitudes of cellular and humoral responses, and a favourable Th1-skewed IgG subclass response was observed.

Certain hypotheses and observations of Chapters 3, 4 and 5 may explain the trends in immunogenicity observed in this chapter with the different homologous regimens tested. The IM-IN regimen generated superior systemic antibody responses to the IM-IM regimen for example, which could be as a result of the mucosal boost targeting the more antigen-naïve-like mucosa, which would contain less suppressive, in this case, cognate antibodies. The lessened suppression of the mucosal dose of vaccine in result, may have explained the overall enhanced immunogenicity of systemic antibody responses noted following IM-IN. Nonetheless, the action of suppressive cognate antibody, which has been described previously as "antigenic blunting"[262], is limited in the context of homologous boosting as the boost antigen will still be able to stimulate pre-existing MBC and elicit the generation of "relevant/neutralising" antibodies, unlike in the heterologous boost context where back boosted responses may be generated that are poorly-neutralising to the booster antigen.

Henceforth, although the presence of suppressive, cognate antibody in such scenario may have negative influence on the magnitude of immune response to homologous booster, it is unlikely to result in complete suppression of the boost response, and perpetuation of the pre-existing, prime-derived response within this context will be "beneficial". Moving forward, to better understand the mechanisms driving the responses of the IM-IN homologous regimen, it would be relevant to investigate both the impact of the transfer of cognate antibody serum on subsequent IM and IN vaccination, as well as assess the involvement of MBC derived from IM-prime vaccination on mucosal boost responses in the lungs (via adoptive transfer of MBC or cell lineage tracing through a S1pr2 transgenic mouse system as completed in Chapter 6). The latter proposed experiment would help to determine whether the systemic prime-derived MBC population expands

and contributes to the latter homologous mucosal boost response, unlike that noted in the heterologous context observed in Chapter 5. Lastly, as previously demonstrated in Chapter 5, it is likely that systemically-derived memory T cells home and contribute to the latter mucosal response in the lungs, with some converting to a T_{RM} phenotype.

Anti-vector immunity was shown to have less of an impact on the suppression of de novo responses to omicron vaccine in Chapter 3 than anti-spike antibodies, however, still resulted in a detectable reduction in the responses mounted compared with the naïve control group. In the homologous prime-boost regimen examined in this chapter, the presence of anti-vector antibodies following prime vaccination may also explain the enhanced immunogenicity of the bi-compartmental IM-IN regimen over IM-IM and IN-IN regimens; minimal vector-neutralising antibody established in the respiratory mucosa following IM-prime may result in the lessened suppression of ChAdOx1-NP+M1-RSVF booster immunogenicity when administered intranasally. As IN vaccination was shown to establish an antibody imprint, IN-priming may similarly result in a suppressive anti-vector imprint in the mucosa that reduces the immunogenicity of the IN-boost (in the IN-IN regimen). The extent to which anti-vector immunity suppresses the ChAdOx1 response may be reflective of the specific immune compartment it resides; whereas anti-vector antibodies cannot access the local muscle tissue, hence neutralise booster vector and subsequently lower antigenic expression, anti-vector antibodies can be directly secreted into the mucosa, hence more readily neutralise ChAdOx1 vector administered intranasally before it is able to infect epithelial cells and induce a response. It was shown in Chapter 3 that anti-vector antibodies transferred into a circulatory system do cause marginal, yet statistically significant reductions in the immunogenicity of an IM-booster vaccination,

however it is unclear how, or rather where, these antibodies are neutralising the IM-booster; the anti-vector antibodies be accessing vector that is in the lymph or blood.

In light of such hypotheses, an anti-vector neutralisation assay was conducted on the BALF samples from the RSV challenge experiment, in order to determine if the number of IN immunisations positively correlated with the levels of ChAdOx1-neutralising antibodies (ChAdOx1-NAbs) (Figure 6.14); as BALF was only collected after the final timepoint for the challenge experiments, the relative levels of BALF ChAdOx1-NAbs following IM- or IN-prime could not be completed, which would allow for more direct comparison of the pre-boost ChAdOx1-NAbs and post-boost ChAdOx1-NP+M1-RSVF immunogenicity. The IN-IN regimen generated the greatest levels of ChAdOx1-NAbs in the BALF, which were significantly higher than in the IM-IM group (P=0.0032). The IM-IN regimen had intermediate levels of BALF ChAdOx1-NAbs, and the IM-IM regimen had the lowest levels of BALF ChAdOx1-NAbs. Henceforth, it is likely the mucosal ChAdOx1-NAbs established after a single IM-prime would be minimal and support a more optimal ChAdOx1-NP+M1-RSVF IN-boost response, compared with that in IN-primed mice.

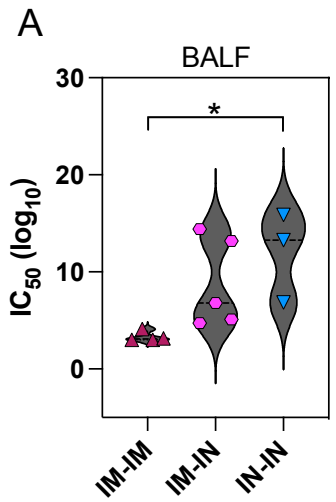

Figure 6.14: Anti-vector neutralisation assay

(A) Levels of anti-ChAdOx1 (anti-vector) neutralisation ($IC_{50}(log_{10})$) in the broncho-alveolar lavage fluid (BALF) of mice vaccinated with ChAdOx1-NP+M1-RSVF in an IM-IM, IM-IN or IN-IN regimen, then challenged with virus. BALF was collected 3 weeks post-boost. To compare groups statistically, a Kruskal-Wallis test was performed. Insufficient BALF volume in two samples of the IN-IN group prevented measurement of anti-vector neutralisation of these samples.

The IM-IN regimen also demonstrated higher overall protection against infection over other homologous route regimens; the extent to which IM-IN vaccination offered greater protection however, varied depending on the virus used in challenge. Furthermore, the protection provided by IM-IN vaccination was likely via different mechanisms depending on whether RSV or influenza virus.

Greater numbers of $CD8^+$ T_{RM} were measured in the lungs and BAL of IM-IN-vaccinated mice challenged with H3N2 and H1N1 influenza A strains, compared with those challenged with RSV. Preclinical studies have used conserved NP and M1 antigens as targets in their influenza vaccines for the generation of cross-protective T cells[201,374–376]. Some of these studies used NP and M1 antigens encoded in ChAdOx-based vectors and detected distinct differences in responses depending on route of vaccination; aerosol vaccination of pre-exposed pigs with ChAdOx2-NP+M1-NA boosted mucosal immunity, and IM vaccination solely peripheral blood immunity[375]. A human trial using a MVA-vectored, NP+M1-encoding vaccine concluded no advantageous protection over control group when administered IM in individuals vaccinated 28 days prior with standard quadrivalent influenza vaccine (QIV)[377]. Here, it was suggested that alternative routes of vaccination, such as aerosol or IN, be considered, for enhanced efficacy of vaccine[377]. It is likely that lung-resident cross-reactive T_{RM} cells are important for greater control over influenza infection than what is provided through systemic vaccination[226,230,373].

In addition to T_{RM} cells, ChAdOx1-NP+M1-RSVF elicited antibody responses against internal influenza A proteins NP and M1. Unlike NP- and M1-reactive $CD8^+$ T cells, it is unclear what role anti-NP and M1 antibodies may contribute, if any, to protection against influenza infection and disease in humans. It has been suggested that anti-NP IgG antibodies that are capable of engaging effector cells via Fc receptor-Fc binding, may contribute to protection; such antibodies have been shown to be common in healthy and influenza-infected adults[378]. However, various small animal model studies have presented conflicting data in support of and against a protective role of anti-NP and M1 influenza protein antibodies[379–382]. MVA viral vector vaccines co-expressing or individually expressing influenza A NP, M2 and M1 internal antigens protected mice against lethal challenge with homologous and heterologous influenza A viruses; here too, not only cellular but also strong anti-NP antibody responses were described following vaccination[363]. It was also shown in previous literature through passive antibody transfer experiments, that anti-NP IgG contributed to protective antiviral activity, but that NP-specific $CD8^+$ T cells were also involved and necessary for this form of protection[380]. When transgenic mice expressing anti-NP human mAbs derived from an infected patient were heterotypically challenged with highly pathogenic influenza virus, resistance to infection was noted[381]. Conversely, in another study, passively transferred anti-NP human mAbs were not protective in a mouse challenge model, despite being able to engage FcRs[383]. These proposed non-neutralising, antibody-mediated mechanism of protection, nevertheless, require that NP and/or M1 antigen be accessible to antibody at some stage within infection[380].

IM-IN-vaccinated mice were less protected against H1N1 (A/California/7/2009) infection and disease, compared with when they were challenged with H3N2 (X31), despite both strains' NP and M1 sequences being conserved to a similarly high degree to that

encoded in the vaccine. Here, T cell immunity and potentially anti-NP and M1 antibodies, were likely not adequate for sterilising protection against A/California/7/2009, which has shown to be more virulent in mouse infection models, compared with X31[369].

All ChAdOx1-NP+M1-RSVF vaccine regimens protected mice against RSV challenge, however, IM-IN and IN-IN vaccinated mice had the lowest viral loads upon challenge. The IM-IN regimen specifically, was more Th1-leaning according to systemic immunogenicity data; IM-IN-vaccinated mice possessed the greatest relative IgG2a levels compared with other subclasses, and the smallest relative IgG1 levels. B cell class-switching to IgG2a is promoted by Th1-associated IFNγ release in the cellular milieu, whereas promotion of class-switching to IgG1 is mediated by Th2-associated cytokine IL-4[384]. In alignment with this, the systemic (spleen) cytokine staining responses observed were generally TNF- and IFNγ-biased, and IM-IN vaccination was shown to induce high levels of IFNγ as measured via ELISpot assay. Th1 responses have been linked to lessened disease during RSV infection, whereas Th2-type responses have been associated with enhanced disease[135,362,385].

NAbs targeting the F protein likely contributed a considerable degree to the protection observed against RSV disease[386–388]. Earlier serum and antibody passive transfer studies and more recent correlate of protection studies have supported the role of humoral immunity in protection from RSV infection and disease[386–388]. A large number of RSV candidates, as well as licensed RSV vaccines Abrysvo and Arexvy, utilise stabilised F protein antigens, which have been widely tested and proven to generate protective neutralising antibodies[138,348,389–391]. The lower measured viral load in IM-IN- and IN-IN-vaccinated mouse lungs may have been as a result of enhanced mucosal antibody responses, or may reflect a more multifactorial mechanism of RSV protection. $CD8^+$ and $CD4^+$ T cells, and specifically T_{RM}, have also been described as important for protection against RSV, and in

other studies, control over RSV infection has been demonstrated by T cells in the absence of RSV-specific antibodies[392–395].

Limited work has explored the employment of RSV and influenza vaccines via a heterologous systemic prime, mucosal boost regimen. However, a range of studies involving RSV and influenza vaccines have tested mucosal vaccinations[348,349,356,396–404]. In such examples, mucosal vaccination (via IN, intrapulmonary and/or aerosol) priming generally generated higher respiratory mucosal responses than parental/systemic routes (IM and intraperitoneal). Nevertheless, within this study, the responses of greatest magnitude and protection against disease and infection were established when systemic priming preceded a mucosal boost; such responses were generally higher in IM-IN vaccinated mice than IN-prime or IN-IN vaccinated mice, highlighting the benefit of hetero-compartmental vaccination. With such combination, the benefits of systemic and respiratory mucosal immunity are both harnessed. IM-priming "secured" an IgG2a>IgG1 response that was maintained following IN boost.

Other systemic-prime, mucosal-boost vaccination regimens have been described in other studies involving SARS-CoV-2 vaccines. One such study used a ChAd-based platform, and showed that combination IM-IN regimen was able to induce potent responses superior to homologous route regimens, with antibody responses of highest magnitude and Th1-skewing, consistent with the results within this thesis[303–305,338]. The "prime-pull" regimen strategy has been used for other mucosal vaccines against non-respiratory pathogens, such as chlamydia; and proven to induce strong immunity within minipigs[405].

Further investigation of the suitability of the ChAdOx1-NP+M1-RSVF and the IM-IN vaccination strategy for use in infants and the elderly, will be important, as infant and older adults cohorts are particularly burdened by RSV and influenza virus[141,406]. Consideration of

current clinical practice regarding vaccination against RSV and influenza and how this vaccine could be used as an auxiliary product will be considered through future clinical development and assessment. These findings further support the exploration of the systemic prime, mucosal boost route regimen combination for vaccines against respiratory viruses. The content of this chapter was used in the following publication where the original draft was written by Cameron Bissett:

- Bissett, C., Belij-Rammerstorfer, S., Ulaszewska, M., Smith, H., Kailath, R., Morris, S., Powers, C., Sebastian, S., Sharpe, H.R., Allen, E.R., et al. (2024). Systemic prime mucosal boost significantly increases protective efficacy of bivalent RSV influenza viral vectored vaccine. npj Vaccines *9*, 1–14. https://doi.org/10.1038/s41541-024-00912-1.

7
Conclusions and future directions

7. Conclusions and future directions

1. Overview
2. Conclusions, limitations and future directions

2.1 Pre-existing vaccine-derived immunity has a strong influence on heterologous variant booster vaccination

2.2 The mucosal vaccination route can overcome deleterious immunological imprinting

2.3 Multiple mechanisms drive the heterologous IM-IN regimen immune response

2.4 The homologous IM-IN regimen generates superior protection against disease and infection

3. Final remarks

1. Overview

Significant progress has been made regarding the development and licensure of respiratory virus vaccines; they are the principal preventative tool against infectious respiratory diseases, which remain as one of the primary causes of death and severe illness globally[407]. However, the outstanding prevalence of these viruses highlights the need for the amelioration of our current strategies. Namely, despite the recognisable benefits of the mucosal vaccination route in protecting against infection, it is often overlooked in favour of the standard intramuscular route. This DPhil project highlights the benefits of mucosal vaccination within two distinct contexts, and supports its implementation in both current and future strategies. The benefits were first exemplified in a heterologous setting, when a mucosal omicron variant booster was tested, and in the homologous setting, when a newly constructed vaccine was administered via a dual mode, intramuscular-prime, intranasal-pull regimen.

2. Conclusions, limitations and future directions

2.1 Pre-existing vaccine-derived immunity has a strong influence on heterologous variant booster vaccination

When vaccines that encoded different SARS-CoV-2 variant spikes were administered heterologously via the intramuscular route in mice, immunological imprinting was apparent, with the outcome dependent on the antigenic distance between the encoded antigens. Heterologous prime-boost regimens using ancestral variant vaccines, where the encoded antigens demonstrated high relative cross-reactivity, displayed an antigenic seniority-type form of imprinting with regards to IgG, in which back boosting responses were cross-neutralising and beneficial to both the boosting antigen and the prime antigen. Contrarily, when mice were primed with wildtype or early alpha variant

vaccine and boosted with the highly divergent omicron vaccine, a “primary addiction”-type imprinting was observed. The inhibition of the de novo omicron response to booster was shown to be mediated, at least in part, by suppressive antibodies.

Whilst immunological imprinting had been proposed in various studies to influence the immune responses to variant infection and variant booster vaccination, its involvement has still been somewhat ambiguous and unclear because clinical studies are hindered by the heterogeneity of the human populations’ infection history, and the tools and scope for ascertaining the role of imprinting are limited. In Chapter 3, by using naïve mice, it was possible to clearly ascribe wildtype vaccination to the formation of an imprint; in such way, wildtype vaccine-prime was representative of a primary series vaccination in humans, and the omicron boost representative of the adapted omicron booster vaccines currently on the market.

A particular limitation to the experiments conducted in Chapter 3 (as well as chapters 4 and 5) was the treatment of the different ChAdOx1 constructs as “equivalents” or identical, apart from the sequence that they encode. The dose of vaccine administered for all variant vaccines was 10^8 IU; discrepancies in the infectivity of virus between stocks meant that the quantity of viral particle (VP) administered between mouse groups varied. Although sequence expression in the host cell is contingent on the vector’s ability to infect the host cell, vector that does not infect the host cell may still contribute to the immune response as the external VP is immunogenic in itself; therefore, viral stocks of poorer infectivity, that necessitate higher VP to be administered to achieve equivalent IU dose, may be more immunogenic than those with higher infectivity. These differences also have important implications for the potential level of anti-vector immunity subsequently established; higher VP doses will likely induce greater anti-vector immunity compared with

lower VP doses, and this may conflate the differences in immunogenicity that may have been ascribed to antigenic species rather than the vector itself. To better understand the influence of differences in VP between stocks, an experiment could be completed where different batches of the same ChAdOx1 vaccine could be administered, with the IU dose identical across groups, but VP different. The impact of change in VP quantity on both antigen immunogenicity, and extent of anti-vector immunity formed could then be assessed. Finally, the different variant antigens may not only differ in regards amino acid sequence and epitope changes, but other properties, such as stability and inherent immunogenicity; this must be considered when treating them as “units”.

A potential improvement to the experiments completed in Chapter 3 could have been the measurement of antibody responses in the mucosal fluids of mice, in addition to the responses measured in the serum. In doing so, it would be possible to confirm that the IM route (irrespective of regimen or vaccine type) is inefficient in stimulating the mucosal compartment; this would support the rationale and hypotheses presented in the following Chapter (Chapter 4) where the alternative IN route for heterologous boosting was explored. This additional data would enable the comparison of mucosal antibody responses following regimens presented in Chapters 3 and 4.

2.2 The mucosal vaccination route can overcome deleterious immunological imprinting

Although mucosal boosting has been explored as a means of enhancing local, respiratory immunity, it has not been readily explored as a means of overcoming or bypassing the effects of deleterious imprinting derived from vaccination. In Chapter 4, by targeting the mucosal compartment, which features distinct immunological and anatomical properties, the negative effects of the wildtype vaccine-derived systemic

imprint were circumvented. In addition, enhanced mucosal T_{RM}, IgA and ACE-2-competing antibodies were measured; these responses were broadly reactive to both omicron and ancestral variants. These findings would support the consideration of a switch from the conventional intramuscular vaccination route for seasonal boosters to the intranasal route, for the promotion of more de novo-like responses to the relevant or matched strains, and to establish more localised immunity.

Nonetheless, the circumvention of immunological imprinting in this chapter was only observed under particular conditions. When greater amounts of WT spike antibody were transferred to mice that were then intranasally vaccinated with omicron, the omicron-specific responses were still suppressed to an extent. Additionally, when mice were primed intranasally with the wildtype vaccine, as opposed to intramuscularly, the intranasal administration of omicron booster vaccine was unable to bypass the suppressive imprint, and the omicron-neutralising responses in the serum were impaired. These observations suggest the need for further investigation of the feasibility and application of IN-boosting in humans as a means of overcoming imprinting; in particular, how the infection history of the individual will influence the efficacy of the IN booster, and how sequentially administered, annual mucosal boosters encoding different variants or strains, will function if an imprint is established in the respiratory mucosa following vaccination.

As reflected via the “IN-IM” reverse route orientation regimen experiment, the IN and IM routes have a unidirectional relationship with regards to the compartments they are able to stimulate. However, the mucosal and systemic immune compartments should not be interpreted as “equivalents” or discrete units, and rather, have different immunological characteristics that are reflective of their functions. On such note, a limitation to this work was the lack of durability experiments that would measure the

immunity generated post-IN omicron vaccine boost over time. Notably, the immunity within the lungs following infection or mucosal vaccination in some studies has been described as transient (in comparison to that induced systemically), with a rapid decline[408]. It would be particularly relevant to assess whether mucosal vaccination in IM-vaccinated individuals would augment the durability of mucosal memory responses compared with stand-alone mucosal vaccinations or immune responses to infection in naïve immune systems, as has been assessed in such durability studies. Contrarily, if lung immunity (and thus the mucosal imprint) wane substantially with time, this could favour annual mucosal boosting campaigns over conventional intramuscular ones, as the mucosal route may hypothetically be less susceptible to immunological imprinting.

2.3 Multiple mechanisms drive the heterologous IM-IN regimen immune response

Through cell lineage tracing and adoptive cell transfer experiments, two main observations were made that provided mechanistic insight into the measured immune responses following the Ad-WT^{IM}+Ad-o^{IN} regimen. Firstly, the B cell response in the mucosa was predominantly de novo following the Ad-o^{IN}-boost, rather than derived from the Ad-WT^{IM}-prime. Secondly, Ad-WT^{IM}-derived, systemic cross-reactive memory T cells migrated to the lungs and likely assisted in the latter lung Ad-o^{IN} B cell responses, with some having converted to a T_{RM} phenotype. The more de novo-type B cell response in the lungs reflected the hypothesis that the mucosal compartment possessed a less-imprinted phenotype following Ad-WT^{IM}-prime, i.e., fewer competitive MBCs and inhibitory antibodies present in the vicinity. The observation of cross-reactive memory T cells derived from WT vaccination contributing to the heterologous responses to omicron antigen is consistent with literature[253]; they have even been demonstrated to support naïve B cell seeding of

secondary GC upon secondary antigen exposure under the presence of inhibitory pre-existing antibody[267].

However, there are certain limitations to these experiments. Notably, the adoptive transfer experiment is reductionist in that it involves the transfer of splenocytes into a naïve mouse, and does not fully recapitulate or "establish" the immunity formed in a mouse that actively mounts an immune response following Ad-WT^{IM} vaccination. More generally, the transfer of splenocytes into the mouse circulatory system is "unnatural"; a considerable proportion of the transferred splenocytes will die upon transfer (with engraftment rates typically as low as 10%) and the homing capacity of these splenocytes following transfer, but before vaccination is unclear. Therefore, although it is insightful to measure and focus on the transferred set of splenocytes, the monitoring and tracing of these populations generated from an active prime response would be an important confirmation of findings, advancing this research.

Regarding the fate-mapping cell lineage tracing experiment completed in this chapter, a particular drawback was that the background strain of the transgenic S1pr2 mice used was C57BL/6, as opposed to the BALB/c strain, which was used in all other experiments. Henceforth, an assumption was made that the trends in immune response between the IM- and IN-boost groups would be similar between the two different strains. To eliminate the possibility of strain-specific differences significantly impacting the comparisons made, head-to-head comparisons of the cellular and antibody responses following the Ad-WT^{IM}+Ad-o^{IM} and Ad-WT^{IM}+Ad-o^{IN} regimens in the BALB/c and C57BL/6 strains could be completed. Should the trends in immune response be identical and reproduced across the different strains, this would strengthen the validity of the findings within this chapter. On a separate note, there are several areas of potential further

exploration regarding the S1pr2 experiment that would enrich the understanding of the relationship between different immune compartments and the IM-IN heterologous regimen; namely more in-depth characterisation and comparison of the antigen-specific MBCs within the different lymph nodes, e.g., whether they are largely IgA or IgG class-switched.

2.4 The homologous IM-IN regimen generates superior protection against disease and infection

In a homologous setting, when a bivalent RSV-influenza vaccine was administered via different prime-boost routes, the dual mode IM-IN regimen provided the strongest protection against infection and disease following influenza A or RSV challenge, outperforming the single-mode regimens. The IM-IN regimen was able to generate both antibody and cellular responses systemically and locally in the respiratory mucosa. The observations in this chapter underscored the significant impact that the route of administration has on protective outcomes.

The homologous dual-mode regimen tested in this chapter exemplifies a potential vaccination strategy for naïve immune systems, such as those in infants. The IM-IN regimen has potential to address the challenges and concerns of mucosal vaccination, that include the potential of inducing an overly reactogenic, inflammatory response in the lungs, or on the contrary, the potential failure to induce robust responses due to the high tolerogenicity of the lungs; the IM-prime in this study was shown to drive a desired Th1-type response that was maintained upon IN-boost, and the IN-boost amplified this pre-existing response, in contrast to the single-mode prime-boost and prime-only regimens. The bivalent candidate used in this chapter serves as an example multivalent vaccine, of which there are certain candidates in clinical trials currently, including a dual SARS-CoV-2 and influenza

vaccine by Pfizer[409]; the simultaneous induction of protection against multiple viruses in infants through one vaccine is a desirable and convenient strategy that should prioritised moving forward.

As was the case in Chapter 5, two mouse strains were used in this Chapter, which was a particular limitation to the study design. Although the use of the CD-1 strain is beneficial in that it better emulates the variability typically observed within the human population with regards to immune response, recapitulation of the different regimens in the BALB/c strain, and measurement of the subsequent immunogenicity (as was completed in CD-1s in this chapter), would better harmonise the different data sets and more accurately link the trends in immunogenicity (pre-challenge) to the trends in protection following virus challenge, which were deduced from BALB/c mouse experiments. Indeed, pre-challenge serology was conducted on the BALB/c mice which allowed for correlation of the pre-challenge serum antibody levels and degree of protection post-challenge, however, conducting a more in-depth immunogenicity study (pre-challenge) with BALB/c mice would allow the measurement of mucosal antibodies, and lung and spleen cellular responses, which could then be more accurately correlated with the separate BALB/c challenge studies.

Another, perhaps superior approach, could involve the recapitulation of the BALB/c virus challenges with greater group numbers, to allow a subset of mice within each group to be culled before challenge (as opposed to challenged, then culled) for the subsequent in-depth evaluation of cellular and antibody immunity responses pre-challenge. Finally, for an even clearer evaluation of the specific correlates of protection against the different viruses tested, it would be relevant to conduct cell and antibody transfer, then challenge,

experiments such that the protective effect of specific types of immunity measured in the immunogenicity studies be linked to a protective effect.

3. Final remarks

The work in this thesis supports the possibility of more optimised vaccine strategies that better control and reduce viral infection in the host, and potentially reduce the transmission and spread of virus at the population level. Particular focus should be placed on the adaptation and optimisation of preclinically-tested mucosal vaccination strategies for their application in humans, as certain promising candidates have failed to translate successfully into human trials. Although the induction of completely sterilising forms of immunity may be an unrealistic goal for vaccines against respiratory viruses, especially those that regularly mutate, the consideration of mucosal vaccination moving forward, along with the implementation of current emerging technologies, including mRNA and viral vector vectors, will surely contribute to the lessened prevalence of these viruses and the reduction of the disease burden they inflict.

References

1. Boncristiani, H. F., Criado, M. F. & Arruda, E. Respiratory Viruses. in *Encyclopedia of Microbiology* 500–518 (Elsevier Inc., 2009). doi:10.1016/B978-012373944-5.00314-X.
2. White, D. O. & Brown, L. E. RESPIRATORY VIRUSES. *Encyclopedia of Virology* 1488–1496 (1999) doi:10.1006/rwvi.1999.0247.
3. COVID-19 deaths | WHO COVID-19 dashboard. *datadot* https://data.who.int/dashboards/covid19/cases.
4. Al-Aly, Z. *et al.* Long COVID science, research and policy. *Nat Med* **30**, 2148–2164 (2024).
5. Justo Arevalo, S. *et al.* What do we know about the function of SARS-CoV-2 proteins? *Front Immunol* **14**, 1249607 (2023).
6. Rashid, F. *et al.* Roles and functions of SARS-CoV-2 proteins in host immune evasion. *Front. Immunol.* **13**, (2022).
7. Bai, C., Zhong, Q. & Gao, G. F. Overview of SARS-CoV-2 genome-encoded proteins. *Sci China Life Sci* **65**, 280–294 (2022).
8. Hikmet, F. *et al.* The protein expression profile of ACE2 in human tissues. *Mol Syst Biol* **16**, e9610 (2020).
9. Malone, B., Urakova, N., Snijder, E. J. & Campbell, E. A. Structures and functions of coronavirus replication–transcription complexes and their relevance for SARS-CoV-2 drug design. *Nat Rev Mol Cell Biol* **23**, 21–39 (2022).
10. Peacock, T. P. *et al.* The furin cleavage site in the SARS-CoV-2 spike protein is required for transmission in ferrets. *Nat Microbiol* **6**, 899–909 (2021).
11. Zhang, J. *et al.* Membrane fusion and immune evasion by the spike protein of SARS-CoV-2 Delta variant. *Science* **374**, 1353–1360 (2021).
12. Jackson, C. B., Farzan, M., Chen, B. & Choe, H. Mechanisms of SARS-CoV-2 entry into cells. *Nat Rev Mol Cell Biol* **23**, 3–20 (2022).
13. Yadav, R. *et al.* Role of Structural and Non-Structural Proteins and Therapeutic Targets of SARS-CoV-2 for COVID-19. *Cells* **10**, 821 (2021).
14. Zhang, Z. *et al.* Structure of SARS-CoV-2 membrane protein essential for virus assembly. *Nat Commun* **13**, 4399 (2022).
15. Medeiros-Silva, J., J. Dregni, A., H. Somberg, N., Duan, P. & Hong, M. Atomic structure of the open SARS-CoV-2 E viroporin. *Science Advances* https://doi.org/10.1126/sciadv.adi9007 (2023) doi:10.1126/sciadv.adi9007.
16. Cubuk, J. *et al.* The SARS-CoV-2 nucleocapsid protein is dynamic, disordered, and phase separates with RNA. *Nat Commun* **12**, 1936 (2021).
17. Kakavandi, S. *et al.* Structural and non-structural proteins in SARS-CoV-2: potential aspects to COVID-19 treatment or prevention of progression of related diseases. *Cell Communication and Signaling* **21**, 110 (2023).
18. Harvey, W. T. *et al.* SARS-CoV-2 variants, spike mutations and immune escape. *Nat Rev Microbiol* **19**, 409–424 (2021).
19. Saldivar-Espinoza, B. *et al.* The Mutational Landscape of SARS-CoV-2. *International Journal of Molecular Sciences* **24**, (2023).
20. Plante, J. A. *et al.* Spike mutation D614G alters SARS-CoV-2 fitness. *Nature* **592**, 116–121 (2021).
21. Pondé, R. A. A. Physicochemical effect of the N501Y, E484K/Q, K417N/T, L452R and T478K mutations on the SARS-CoV-2 spike protein RBD and its influence on agent

fitness and on attributes developed by emerging variants of concern. *Virology* **572**, 44–54 (2022).
22. Mohammadi, M., Shayestehpour, M. & Mirzaei, H. The impact of spike mutated variants of SARS-CoV2 [Alpha, Beta, Gamma, Delta, and Lambda] on the efficacy of subunit recombinant vaccines. *Braz J Infect Dis* **25**, 101606 (2021).
23. SARS-CoV-2 variants of concern as of 27 September 2024. https://www.ecdc.europa.eu/en/covid-19/variants-concern.
24. Liu, Y. *et al.* The N501Y spike substitution enhances SARS-CoV-2 infection and transmission. *Nature* **602**, 294–299 (2022).
25. Harvey, W. T. *et al.* SARS-CoV-2 variants, spike mutations and immune escape. *Nat Rev Microbiol* **19**, 409–424 (2021).
26. Yadav, P. D. *et al.* Isolation and characterization of SARS-CoV-2 Beta variant from UAE travelers. *J Infect Public Health* **15**, 182–186 (2022).
27. Yurkovetskiy, L. *et al.* S:D614G and S:H655Y are gateway mutations that act epistatically to promote SARS-CoV-2 variant fitness. *bioRxiv* 2023.03.30.535005 (2023) doi:10.1101/2023.03.30.535005.
28. Lista, M. J. *et al.* The P681H Mutation in the Spike Glycoprotein of the Alpha Variant of SARS-CoV-2 Escapes IFITM Restriction and Is Necessary for Type I Interferon Resistance. *J Virol* **96**, e0125022 (2022).
29. Harvey, W. T. *et al.* SARS-CoV-2 variants, spike mutations and immune escape. *Nat Rev Microbiol* **19**, 409–424 (2021).
30. Hirotsu, Y. & Omata, M. Discovery of a SARS-CoV-2 variant from the P.1 lineage harboring K417T/E484K/N501Y mutations in Kofu, Japan. *J Infect* **82**, 276–316 (2021).
31. Liu, Y. *et al.* Delta spike P681R mutation enhances SARS-CoV-2 fitness over Alpha variant. *Cell Rep* **39**, 110829 (2022).
32. Krammer, F. & Ellebedy, A. H. Variant-adapted COVID-19 booster vaccines. *Science* **382**, 157–159 (2023).
33. Earnest, R. *et al.* Comparative transmissibility of SARS-CoV-2 variants Delta and Alpha in New England, USA. *Cell Rep Med* **3**, 100583 (2022).
34. Chen, K.-W. K., Tsung-Ning Huang, D. & Huang, L.-M. SARS-CoV-2 variants – Evolution, spike protein, and vaccines. *Biomed J* **45**, 573–579 (2022).
35. Willett, B. J. *et al.* SARS-CoV-2 Omicron is an immune escape variant with an altered cell entry pathway. *Nat Microbiol* **7**, 1161–1179 (2022).
36. Bálint, G., Vörös-Horváth, B. & Széchenyi, A. Omicron: increased transmissibility and decreased pathogenicity. *Sig Transduct Target Ther* **7**, 1–3 (2022).
37. Meng, B. *et al.* Altered TMPRSS2 usage by SARS-CoV-2 Omicron impacts infectivity and fusogenicity. *Nature* **603**, 706–714 (2022).
38. Kemp, S. A. *et al.* SARS-CoV-2 evolution during treatment of chronic infection. *Nature* **592**, 277–282 (2021).
39. Cele, S. *et al.* SARS-CoV-2 prolonged infection during advanced HIV disease evolves extensive immune escape. *Cell Host & Microbe* **30**, 154-162.e5 (2022).
40. Obermeyer, F. *et al.* Analysis of 6.4 million SARS-CoV-2 genomes identifies mutations associated with fitness. *Science* **376**, 1327–1332 (2022).
41. Hadfield, J. *et al.* Nextstrain: real-time tracking of pathogen evolution. *Bioinformatics* **34**, 4121–4123 (2018).
42. GISAID Initiative. https://www.epicov.org/epi3/frontend#ad4a0.

43. Chatterjee, S., Bhattacharya, M., Nag, S., Dhama, K. & Chakraborty, C. A Detailed Overview of SARS-CoV-2 Omicron: Its Sub-Variants, Mutations and Pathophysiology, Clinical Characteristics, Immunological Landscape, Immune Escape, and Therapies. *Viruses* **15**, 167 (2023).
44. Topol, E. A new variant alert. *Ground Truths* https://erictopol.substack.com/p/a-new-variant-alert (2022).
45. Tamura, T. *et al.* Virological characteristics of the SARS-CoV-2 XBB variant derived from recombination of two Omicron subvariants. *Nat Commun* **14**, 2800 (2023).
46. Ma, K. & Chen, J. Omicron XE emerges as SARS-CoV-2 keeps evolving. *Innovation (Camb)* **3**, 100248 (2022).
47. Chakraborty, C., Bhattacharya, M., Sharma, A. R. & Dhama, K. Recombinant SARS-CoV-2 variants XD, XE, and XF: The emergence of recombinant variants requires an urgent call for research – Correspondence. *Int J Surg* **102**, 106670 (2022).
48. GISAID Initiative. https://www.epicov.org/epi3/frontend#159d47.
49. Lamers, M. M. & Haagmans, B. L. SARS-CoV-2 pathogenesis. *Nat Rev Microbiol* **20**, 270–284 (2022).
50. Menter, T. *et al.* Postmortem examination of COVID-19 patients reveals diffuse alveolar damage with severe capillary congestion and variegated findings in lungs and other organs suggesting vascular dysfunction. *Histopathology* **77**, 198–209 (2020).
51. Carsana, L. *et al.* Pulmonary post-mortem findings in a series of COVID-19 cases from northern Italy: a two-centre descriptive study. *Lancet Infect Dis* **20**, 1135–1140 (2020).
52. Stein, S. R. *et al.* SARS-CoV-2 infection and persistence in the human body and brain at autopsy. *Nature* **612**, 758–763 (2022).
53. Zhao, F., Ma, Q., Yue, Q. & Chen, H. SARS-CoV-2 Infection and Lung Regeneration. *Clin Microbiol Rev* **35**, e00188-21.
54. Filippatos, F., Tatsi, E. & Michos, A. Immune response to SARS-CoV-2 in children: A review of the current knowledge. *Pediatr Investig* **5**, 217–228 (2021).
55. Silva, M. G. *et al.* Effect of age on human ACE2 and ACE2-expressing alveolar type II cells levels. *Pediatr Res* **93**, 948–952 (2023).
56. Hoffmann, M. *et al.* SARS-CoV-2 Cell Entry Depends on ACE2 and TMPRSS2 and Is Blocked by a Clinically Proven Protease Inhibitor. *Cell* **181**, 271-280.e8 (2020).
57. Blitshteyn, S. & Verduzco-Gutierrez, M. Long COVID: A Major Public Health Issue. *Am J Phys Med Rehabil* **103**, e131–e132 (2024).
58. England, N. H. S. NHS England » Landmark moment as first NHS patient receives COVID-19 vaccination. https://www.england.nhs.uk/2020/12/landmark-moment-as-first-nhs-patient-receives-covid-19-vaccination/ (2020).
59. COVID-19 vaccines | WHO COVID-19 dashboard. *datadot* https://data.who.int/dashboards/covid19/vaccines.
60. Polack, F. P. *et al.* Safety and Efficacy of the BNT162b2 mRNA Covid-19 Vaccine. *New England Journal of Medicine* **383**, 2603–2615 (2020).
61. Spikevax (previously COVID-19 Vaccine Moderna) | European Medicines Agency (EMA). https://www.ema.europa.eu/en/medicines/human/EPAR/spikevax (2021).
62. Baden, L. R. *et al.* Efficacy and Safety of the mRNA-1273 SARS-CoV-2 Vaccine. *N Engl J Med* **384**, 403–416 (2021).
63. Falsey, A. R. *et al.* Phase 3 Safety and Efficacy of AZD1222 (ChAdOx1 nCoV-19) Covid-19 Vaccine. *New England Journal of Medicine* **385**, 2348–2360 (2021).

64. Sadoff, J. *et al.* Safety and Efficacy of Single-Dose Ad26.COV2.S Vaccine against Covid-19. *New England Journal of Medicine* **384**, 2187–2201 (2021).
65. Dunkle, L. M. *et al.* Efficacy and Safety of NVX-CoV2373 in Adults in the United States and Mexico. *New England Journal of Medicine* **386**, 531–543 (2022).
66. Tanriover, M. D. *et al.* Efficacy and safety of an inactivated whole-virion SARS-CoV-2 vaccine (CoronaVac): interim results of a double-blind, randomised, placebo-controlled, phase 3 trial in Turkey. *The Lancet* **398**, 213–222 (2021).
67. Hogan, A. B. *et al.* Estimating long-term vaccine effectiveness against SARS-CoV-2 variants: a model-based approach. *Nat Commun* **14**, 4325 (2023).
68. Rijkers, G. T. & van Overveld, F. J. The “original antigenic sin” and its relevance for SARS-CoV-2 (COVID-19) vaccination. *Clinical Immunology Communications* **1**, 13–16 (2021).
69. Huang, C. Q., Vishwanath, S., Carnell, G. W., Chan, A. C. Y. & Heeney, J. L. Immune imprinting and next-generation coronavirus vaccines. *Nat Microbiol* **8**, 1971–1985 (2023).
70. Maltseva, M., Keeshan, A., Cooper, C. & Langlois, M.-A. Immune imprinting: The persisting influence of the first antigenic encounter with rapidly evolving viruses. *Hum Vaccin Immunother* **20**, 2384192.
71. Faraone, J. N. & Liu, S.-L. Immune imprinting as a barrier to effective COVID-19 vaccines. *Cell Reports Medicine* **4**, 101291 (2023).
72. Evans, J. P. & Liu, S.-L. Challenges and Prospects in Developing Future SARS-CoV-2 Vaccines: Overcoming Original Antigenic Sin and Inducing Broadly Neutralizing Antibodies. *The Journal of Immunology* **211**, 1459–1467 (2023).
73. Spikevax (previously COVID-19 Vaccine Moderna) | European Medicines Agency (EMA). https://www.ema.europa.eu/en/medicines/human/EPAR/spikevax (2021).
74. Research, C. for B. E. and. Novavax COVID-19 Vaccine, Adjuvanted. *FDA* https://www.fda.gov/vaccines-blood-biologics/coronavirus-covid-19-cber-regulated-biologics/novavax-covid-19-vaccine-adjuvanted (2024).
75. Research, C. for B. E. and. Pfizer-BioNTech COVID-19 Vaccine. *FDA* https://www.fda.gov/vaccines-blood-biologics/coronavirus-covid-19-cber-regulated-biologics/pfizer-biontech-covid-19-vaccine (2024).
76. Research, C. for B. E. and. Moderna COVID-19 Vaccine. *FDA* https://www.fda.gov/vaccines-blood-biologics/coronavirus-covid-19-cber-regulated-biologics/moderna-covid-19-vaccine (2024).
77. A guide to the spring 2024 COVID-19 vaccination campaign. *GOV.UK* https://www.gov.uk/government/publications/covid-19-vaccination-spring-booster-resources/a-guide-to-the-covid-19-spring-booster-2023.
78. Gardner, B. J. & Kilpatrick, A. M. Predicting Vaccine Effectiveness for Hospitalization and Symptomatic Disease for Novel SARS-CoV-2 Variants Using Neutralizing Antibody Titers. *Viruses* **16**, 479 (2024).
79. Antunes, L. *et al.* Effectiveness of the adapted bivalent mRNA COVID-19 vaccines against hospitalisation in individuals aged ≥ 60 years during the Omicron XBB lineage-predominant period: VEBIS SARI VE network, Europe, February to August, 2023. *Euro Surveill* **29**, 2300708 (2024).
80. Wang, Q. *et al.* Deep immunological imprinting due to the ancestral spike in the current bivalent COVID-19 vaccine. *Cell Reports Medicine* 101258 (2023) doi:10.1016/j.xcrm.2023.101258.

81. Tortorici, M. A. *et al.* Persistent immune imprinting occurs after vaccination with the COVID-19 XBB.1.5 mRNA booster in humans. *Immunity* **57**, 904-911.e4 (2024).
82. Yisimayi, A. *et al.* Repeated Omicron exposures override ancestral SARS-CoV-2 immune imprinting. *Nature* **625**, 148–156 (2024).
83. Zaeck, L. M. *et al.* Original COVID-19 priming regimen impacts the immunogenicity of bivalent BA.1 and BA.5 boosters. *Nat Commun* **15**, 4224 (2024).
84. Collier, A. Y. *et al.* Immunogenicity of BA.5 Bivalent mRNA Vaccine Boosters. *N Engl J Med* NEJMc2213948 (2023) doi:10.1056/NEJMc2213948.
85. Andersson, N. W. *et al.* Comparative effectiveness of bivalent BA.4-5 and BA.1 mRNA booster vaccines among adults aged ≥50 years in Nordic countries: nationwide cohort study. *BMJ* **382**, e075286 (2023).
86. Carreño, J. M., Singh, G., Simon, V., Krammer, F., & PVI study group. Bivalent COVID-19 booster vaccines and the absence of BA.5-specific antibodies. *Lancet Microbe* **4**, e569 (2023).
87. Aydillo, T. *et al.* Immunological imprinting of the antibody response in COVID-19 patients. *Nature Communications 2021 12:1* **12**, 1–13 (2021).
88. Topol, E. J. & Iwasaki, A. Operation Nasal Vaccine—Lightning speed to counter COVID-19. *Science Immunology* **7**, eadd9947 (2022).
89. Waltz, E. China and India approve nasal COVID vaccines — are they a game changer? *Nature* **609**, 450–450 (2022).
90. 康希诺生物 CanSinoBIO. https://www.cansinotech.com/html/1/179/180/1100.html.
91. Singh, C. *et al.* Phase III Pivotal comparative clinical trial of intranasal (iNCOVACC) and intramuscular COVID 19 vaccine (Covaxin®). *npj Vaccines* **8**, 1–9 (2023).
92. Madhavan, M. *et al.* Tolerability and immunogenicity of an intranasally-administered adenovirus-vectored COVID-19 vaccine: An open-label partially-randomised ascending dose phase I trial. *eBioMedicine* **85**, (2022).
93. Doty, B., Ghaswalla, P., Bohn, R. L., Stoszek, S. K. & Panozzo, C. A. Incidence of RSV in Adults: A Comprehensive Review of Observational Studies and Critical Gaps in Information. *The Journal of Infectious Diseases* jiae314 (2024) doi:10.1093/infdis/jiae314.
94. Jain, H., Schweitzer, J. W. & Justice, N. A. Respiratory Syncytial Virus Infection in Children. in *StatPearls* (StatPearls Publishing, Treasure Island (FL), 2024).
95. Tin Tin Htar, M., Yerramalla, M. S., Moïsi, J. C. & Swerdlow, D. L. The burden of respiratory syncytial virus in adults: a systematic review and meta-analysis. *Epidemiol Infect* **148**, e48.
96. Glezen, W. P., Taber, L. H., Frank, A. L. & Kasel, J. A. Risk of Primary Infection and Reinfection With Respiratory Syncytial Virus. *American Journal of Diseases of Children* **140**, 543–546 (1986).
97. Li, Y. *et al.* Global, regional, and national disease burden estimates of acute lower respiratory infections due to respiratory syncytial virus in children younger than 5 years in 2019: a systematic analysis. *Lancet* **399**, 2047–2064 (2022).
98. Munro, A. P. S., Martinón-Torres, F., Drysdale, S. B. & Faust, S. N. The disease burden of respiratory syncytial virus in Infants. *Current Opinion in Infectious Diseases* **36**, 379 (2023).
99. Kenmoe, S. & Nair, H. The disease burden of respiratory syncytial virus in older adults. *Current Opinion in Infectious Diseases* **37**, 129 (2024).

100. Falsey, A. R., Hennessey, P. A., Formica, M. A., Cox, C. & Walsh, E. E. Respiratory syncytial virus infection in elderly and high-risk adults. *N Engl J Med* **352**, 1749–1759 (2005).
101. Choi, Y. *et al.* Cost determinants among adults hospitalized with respiratory syncytial virus in the United States, 2017–2019. *Influenza Other Respir Viruses* **16**, 151–158 (2022).
102. Nguyen-Van-Tam, J. S. *et al.* Burden of respiratory syncytial virus infection in older and high-risk adults: a systematic review and meta-analysis of the evidence from developed countries. *Eur Respir Rev* **31**, 220105 (2022).
103. Thongpan, I., Vongpunsawad, S. & Poovorawan, Y. Respiratory syncytial virus infection trend is associated with meteorological factors. *Sci Rep* **10**, 10931 (2020).
104. Abu-Raya, B., Paramo, M. V., Reicherz, F. & Lavoie, P. M. Why has the epidemiology of RSV changed during the COVID-19 pandemic? *eClinicalMedicine* **61**, (2023).
105. Agha, R. & Avner, J. R. Delayed Seasonal RSV Surge Observed During the COVID-19 Pandemic. *Pediatrics* **148**, e2021052089 (2021).
106. Rice, E., Oakes, D. B., Holland, C., Moore, H. C. & Blyth, C. C. Respiratory syncytial virus in children: epidemiology and clinical impact post-COVID-19. *Curr Opin Infect Dis* **36**, 522–528 (2023).
107. Collins, P. L., Fearns, R. & Graham, B. S. Respiratory Syncytial Virus: Virology, Reverse Genetics, and Pathogenesis of Disease. *Current topics in microbiology and immunology* **372**, 3 (2013).
108. Nuttens, C. *et al.* Differences Between RSV A and RSV B Subgroups and Implications for Pharmaceutical Preventive Measures. *Infect Dis Ther* **13**, 1725–1742 (2024).
109. Kiss, G. *et al.* Structural Analysis of Respiratory Syncytial Virus Reveals the Position of M2-1 between the Matrix Protein and the Ribonucleoprotein Complex. *J Virol* **88**, 7602–7617 (2014).
110. Cao, D. *et al.* Structures of the promoter-bound respiratory syncytial virus polymerase. *Nature* **625**, 611–617 (2024).
111. Bakker, S. E. *et al.* The respiratory syncytial virus nucleoprotein–RNA complex forms a left-handed helical nucleocapsid. *J Gen Virol* **94**, 1734–1738 (2013).
112. Sibert, B. S. *et al.* Assembly of respiratory syncytial virus matrix protein lattice and its coordination with fusion glycoprotein trimers. *Nat Commun* **15**, 5923 (2024).
113. Braun, M. R. *et al.* Respiratory syncytial virus M2-1 protein associates non-specifically with viral messenger RNA and with specific cellular messenger RNA transcripts. *PLOS Pathogens* **17**, e1009589 (2021).
114. Bermingham, A. & Collins, P. L. The M2–2 protein of human respiratory syncytial virus is a regulatory factor involved in the balance between RNA replication and transcription. *Proc Natl Acad Sci U S A* **96**, 11259–11264 (1999).
115. Scudero, O. B., Santiago, V. F., Palmisano, G., Simabuco, F. M. & Ventura, A. M. The respiratory syncytial virus M2-2 protein is targeted for proteasome degradation and inhibits translation and stress granules assembly. *PLoS One* **18**, e0289100 (2023).
116. Gan, S.-W. *et al.* The small hydrophobic protein of the human respiratory syncytial virus forms pentameric ion channels. *J Biol Chem* **287**, 24671–24689 (2012).

117. Feldman, S. A., Audet, S. & Beeler, J. A. The Fusion Glycoprotein of Human Respiratory Syncytial Virus Facilitates Virus Attachment and Infectivity via an Interaction with Cellular Heparan Sulfate. *J Virol* **74**, 6442–6447 (2000).
118. Borochova, K. *et al.* Dissociation of the respiratory syncytial virus F protein-specific human IgG, IgA and IgM response. *Sci Rep* **11**, 3551 (2021).
119. McLellan, J. S., Ray, W. C. & Peeples, M. E. Structure and Function of Respiratory Syncytial Virus Surface Glycoproteins. in *Challenges and Opportunities for Respiratory Syncytial Virus Vaccines* (eds Anderson, L. J. & Graham, B. S.) 83–104 (Springer, Berlin, Heidelberg, 2013). doi:10.1007/978-3-642-38919-1_4.
120. Flynn, J. A. *et al.* Stability characterization of a vaccine antigen based on the respiratory syncytial virus fusion glycoprotein. *PLoS ONE* **11**, (2016).
121. Battles, M. B. *et al.* Molecular mechanism of respiratory syncytial virus fusion inhibitors. *Nat Chem Biol* **12**, 87–93 (2016).
122. Sun, Z., Pan, Y., Jiang, S. & Lu, L. Respiratory syncytial virus entry inhibitors targeting the F protein. *Viruses* **5**, 211–225 (2013).
123. Bergeron, H. C. & Tripp, R. A. RSV Replication, Transmission, and Disease Are Influenced by the RSV G Protein. *Viruses* **14**, 2396 (2022).
124. Feng, Z., Xu, L. & Xie, Z. Receptors for Respiratory Syncytial Virus Infection and Host Factors Regulating the Life Cycle of Respiratory Syncytial Virus. *Front Cell Infect Microbiol* **12**, 858629 (2022).
125. Roe, M. K. *et al.* An RSV Live-Attenuated Vaccine Candidate Lacking G Protein Mucin Domains Is Attenuated, Immunogenic, and Effective in Preventing RSV in BALB/c Mice. *J Infect Dis* **227**, 50–60 (2022).
126. Yang, P. *et al.* Respiratory syncytial virus nonstructural proteins 1 and 2 are crucial pathogenic factors that modulate interferon signaling and Treg cell distribution in mice. *Virology* **485**, 223–232 (2015).
127. Thornhill, E. M. & Verhoeven, D. Respiratory Syncytial Virus's Non-structural Proteins: Masters of Interference. *Front Cell Infect Microbiol* **10**, 225 (2020).
128. Shang, Z., Tan, S. & Ma, D. Respiratory syncytial virus: from pathogenesis to potential therapeutic strategies. *Int J Biol Sci* **17**, 4073–4091 (2021).
129. Lambert, L., Sagfors, A. M., Openshaw, P. J. M. & Culley, F. J. Immunity to RSV in Early-Life. *Front Immunol* **5**, 466 (2014).
130. Pickles, R. J. & DeVincenzo, J. P. Respiratory syncytial virus (RSV) and its propensity for causing bronchiolitis. *The Journal of Pathology* **235**, 266–276 (2015).
131. Lindemans, C. A. *et al.* Systemic eosinophil response induced by respiratory syncytial virus. *Clin Exp Immunol* **144**, 409–417 (2006).
132. Sigurs, N. *et al.* Severe respiratory syncytial virus bronchiolitis in infancy and asthma and allergy at age 13. *Am J Respir Crit Care Med* **171**, 137–141 (2005).
133. Fonseca, W., Lukacs, N. W. & Ptaschinski, C. Factors Affecting the Immunity to Respiratory Syncytial Virus: From Epigenetics to Microbiome. *Front. Immunol.* **9**, (2018).
134. Bont, L. *et al.* Natural Reinfection with Respiratory Syncytial Virus Does Not Boost Virus-Specific T-Cell Immunity. *Pediatr Res* **52**, 363–367 (2002).
135. Acosta, P. L., Caballero, M. T. & Polack, F. P. Brief History and Characterization of Enhanced Respiratory Syncytial Virus Disease. *Clin Vaccine Immunol* **23**, 189–195 (2016).

136. Polack, F. P. *et al.* Fatal enhanced respiratory syncytial virus disease in toddlers. *Sci Transl Med* **13**, eabj7843 (2021).
137. Derscheid, R. J. *et al.* Effects of formalin-inactivated respiratory syncytial virus (FI-RSV) in the perinatal lamb model of RSV. *PLoS One* **8**, e81472 (2013).
138. McLellan, J. S. *et al.* Structure-Based Design of a Fusion Glycoprotein Vaccine for Respiratory Syncytial Virus. *Science (New York, N.Y.)* **342**, 592 (2013).
139. Krarup, A. *et al.* A highly stable prefusion RSV F vaccine derived from structural analysis of the fusion mechanism. *Nat Commun* **6**, 8143 (2015).
140. Tregoning, J., Li, H., Thomas, C., Wang, Z. & Mosscrop, L. G. RSV vaccines: a new hope but the virus might strike back. https://www.insights.bio/vaccine-insights/journal/article/3145/RSV-vaccines-a-new-hope-but-the-virus-might-strike-back.
141. Respiratory syncytial virus (RSV) immunisation programme for infants and older adults: JCVI full statement, 11 September 2023. *GOV.UK* https://www.gov.uk/government/publications/rsv-immunisation-programme-jcvi-advice-7-june-2023/respiratory-syncytial-virus-rsv-immunisation-programme-for-infants-and-older-adults-jcvi-full-statement-11-september-2023.
142. Arexvy | European Medicines Agency (EMA). https://www.ema.europa.eu/en/medicines/human/EPAR/arexvy (2023).
143. Swathi, M. Arexvy: A Comprehensive Review of the Respiratory Syncytial Virus Vaccine for Revolutionary Protection. *Viral Immunology* **37**, 12–15 (2024).
144. Abrysvo | European Medicines Agency (EMA). https://www.ema.europa.eu/en/medicines/human/EPAR/abrysvo (2023).
145. Walsh, E. E. *et al.* Efficacy and Safety of a Bivalent RSV Prefusion F Vaccine in Older Adults. *New England Journal of Medicine* **388**, 1465–1477 (2023).
146. Kampmann, B. *et al.* Bivalent Prefusion F Vaccine in Pregnancy to Prevent RSV Illness in Infants. *New England Journal of Medicine* **388**, 1451–1464 (2023).
147. Moderna Receives U.S. FDA Approval for RSV Vaccine mRESVIA(R). https://investors.modernatx.com/news/news-details/2024/Moderna-Receives-U.S.-FDA-Approval-for-RSV-Vaccine-mRESVIAR/default.aspx.
148. Wilson, E. *et al.* Efficacy and Safety of an mRNA-Based RSV PreF Vaccine in Older Adults. *New England Journal of Medicine* **389**, 2233–2244 (2023).
149. Fenton, C., Scott, L. J. & Plosker, G. L. Palivizumab: a review of its use as prophylaxis for serious respiratory syncytial virus infection. *Paediatr Drugs* **6**, 177–197 (2004).
150. Ye, X. *et al.* Comparison of Palivizumab-Like Antibody Binding to Different Conformations of the RSV F Protein in RSV-Infected Adult Hematopoietic Cell Transplant Recipients. *The Journal of Infectious Diseases* **217**, 1247–1256 (2018).
151. Wilkins, D. *et al.* 1934. Nirsevimab is Associated with Higher and More Sustained RSV Neutralizing Antibody Responses Compared with Standard of Care Palivizumab: Observations from a 2:1 Randomized, Phase 2/3 Trial in Medically Vulnerable Children (MEDLEY). *Open Forum Infect Dis* **10**, ofad500.2465 (2023).
152. Hammitt, L. L. *et al.* Nirsevimab for Prevention of RSV in Healthy Late-Preterm and Term Infants. *New England Journal of Medicine* **386**, 837–846 (2022).
153. Spearman, P. *et al.* Intranasal parainfluenza virus type 5 (PIV5)–vectored RSV vaccine is safe and immunogenic in healthy adults in a phase 1 clinical study. *Sci Adv* **9**, eadj7611.

154. McFarland, E. J. *et al.* Live-Attenuated Respiratory Syncytial Virus Vaccine With M2-2 Deletion and With Small Hydrophobic Noncoding Region Is Highly Immunogenic in Children. *J Infect Dis* **221**, 2050–2059 (2020).
155. Influenza (Seasonal). https://www.who.int/news-room/fact-sheets/detail/influenza-(seasonal).
156. Romanelli, R. J. *et al.* The Societal and Indirect Economic Burden of Seasonal Influenza in the United Kingdom. *Rand Health Q* **10**, 2 (2023).
157. Clark, T. W. *et al.* Recent advances in the influenza virus vaccine landscape: a comprehensive overview of technologies and trials. *Clinical Microbiology Reviews* **0**, e00025-24 (2024).
158. Ryu, S. & Cowling, B. J. Human Influenza Epidemiology. *Cold Spring Harb Perspect Med* **11**, a038356 (2021).
159. Bouvier, N. M. & Palese, P. The biology of influenza viruses. *Vaccine* **26**, D49–D53 (2008).
160. Jang, Y. H. & Seong, B. L. The Quest for a Truly Universal Influenza Vaccine. *Front. Cell. Infect. Microbiol.* **9**, (2019).
161. Wang, Y. *et al.* Different Subtypes of Influenza Viruses Target Different Human Proteins and Pathways Leading to Different Pathogenic Phenotypes. *Biomed Res Int* **2019**, 4794910 (2019).
162. Kosik, I. & Yewdell, J. W. Influenza Hemagglutinin and Neuraminidase: Yin–Yang Proteins Coevolving to Thwart Immunity. *Viruses* **11**, 346 (2019).
163. Steinhauer, D. A. & Skehel, J. J. Genetics of influenza viruses. *Annu Rev Genet* **36**, 305–332 (2002).
164. Taubenberger, J. K. & Kash, J. C. Influenza Virus Evolution, Host Adaptation and Pandemic Formation. *Cell Host Microbe* **7**, 440–451 (2010).
165. Dhar, N. *et al.* Hemagglutinin Stalk Antibody Responses Following Trivalent Inactivated Influenza Vaccine Immunization of Pregnant Women and Association With Protection From Influenza Virus Illness. *Clin Infect Dis* **71**, 1072–1079 (2020).
166. Fukuyama, S. & Kawaoka, Y. The pathogenesis of influenza virus infections: the contributions of virus and host factors. *Curr Opin Immunol* **23**, 481–486 (2011).
167. Varki, A. & Schauer, R. Sialic Acids. in *Essentials of Glycobiology* (eds Varki, A. et al.) (Cold Spring Harbor Laboratory Press, Cold Spring Harbor (NY), 2009).
168. Kuiken, T., Riteau, B., Fouchier, R. & Rimmelzwaan, G. Pathogenesis of influenza virus infections: the good, the bad and the ugly. *Current Opinion in Virology* **2**, 276–286 (2012).
169. Gamblin, S. J. *et al.* Hemagglutinin Structure and Activities. *Cold Spring Harb Perspect Med* **11**, a038638 (2021).
170. Hu, Y., Sneyd, H., Dekant, R. & Wang, J. Influenza A virus nucleoprotein: a highly conserved multi-functional viral protein as a hot antiviral drug target. *Curr Top Med Chem* **17**, 2271–2285 (2017).
171. Matrosovich, M. N., Matrosovich, T. Y., Gray, T., Roberts, N. A. & Klenk, H.-D. Neuraminidase Is Important for the Initiation of Influenza Virus Infection in Human Airway Epithelium. *J Virol* **78**, 12665–12667 (2004).
172. Pielak, R. M. & Chou, J. J. Influenza M2 proton channels. *Biochim Biophys Acta* **1808**, 522–529 (2011).
173. Hao, W., Wang, L. & Li, S. Roles of the Non-Structural Proteins of Influenza A Virus. *Pathogens* **9**, 812 (2020).

174. Wang, R. *et al.* Examining the hemagglutinin subtype diversity among wild duck-origin influenza A viruses using ethanol-fixed cloacal swabs and a novel RT-PCR method. *Virology* **375**, 182–189 (2008).
175. Simonsen, L. *et al.* Global mortality estimates for the 2009 Influenza Pandemic from the GLaMOR project: a modeling study. *PLoS Med* **10**, e1001558 (2013).
176. Taubenberger, J. K. & Morens, D. M. 1918 Influenza: the Mother of All Pandemics. *Emerg Infect Dis* **12**, 15–22 (2006).
177. Viboud, C. *et al.* Global Mortality Impact of the 1957–1959 Influenza Pandemic. *J Infect Dis* **213**, 738–745 (2016).
178. Pr, S.-H. & D, K. Reviewing the History of Pandemic Influenza: Understanding Patterns of Emergence and Transmission. *Pathogens (Basel, Switzerland)* **5**, (2016).
179. Petersen, E. *et al.* Avian 'Bird' Flu – undue media panic or genuine concern for pandemic potential requiring global preparedness action? *International Journal of Infectious Diseases* **145**, (2024).
180. Qi, W. *et al.* Emergence and Adaptation of a Novel Highly Pathogenic H7N9 Influenza Virus in Birds and Humans from a 2013 Human-Infecting Low-Pathogenic Ancestor. *J Virol* **92**, e00921-17 (2018).
181. Cargnin Faccin, F. & Perez, D. R. Pandemic preparedness through vaccine development for avian influenza viruses. *Hum Vaccin Immunother* **20**, 2347019.
182. Avian influenza. https://www.who.int/westernpacific/wpro-emergencies/surveillance/avian-influenza.
183. Fouchier, R. A. M. *et al.* Avian influenza A virus (H7N7) associated with human conjunctivitis and a fatal case of acute respiratory distress syndrome. *Proceedings of the National Academy of Sciences* **101**, 1356–1361 (2004).
184. Hancock, K. *et al.* Cross-Reactive Antibody Responses to the 2009 Pandemic H1N1 Influenza Virus. *New England Journal of Medicine* **361**, 1945–1952 (2009).
185. McCullers, J. A. The co-pathogenesis of influenza viruses with bacteria in the lung. *Nat Rev Microbiol* **12**, 252–262 (2014).
186. The pathogenesis of influenza virus infections: the contributions of virus and host factors - ScienceDirect. https://www.sciencedirect.com/science/article/pii/S0952791511000896.
187. Kuiken, T. & Taubenberger, J. PATHOLOGY OF HUMAN INFLUENZA REVISITED. *Vaccine* **26**, D59–D66 (2008).
188. Recent advances in the influenza virus vaccine landscape: a comprehensive overview of technologies and trials. https://journals.asm.org/doi/epub/10.1128/cmr.00025-24 doi:10.1128/cmr.00025-24.
189. Koul, P. A. Influenza vaccination: A case for removal of B/Yamagata from the quadrivalent vaccine. *Lung India* **41**, 149–150 (2024).
190. Caini, S. *et al.* Probable extinction of influenza B/Yamagata and its public health implications: a systematic literature review and assessment of global surveillance databases. *The Lancet Microbe* **5**, (2024).
191. Trivalent Influenza Vaccines | CDC.
192. Flublok Influenza Vaccine | Sanofiflu.com. https://www.sanofiflu.com/flublok-influenza-vaccine/.
193. Krammer, F. The human antibody response to influenza A virus infection and vaccination. https://doi.org/10.1038/s41577-019-0143-6 doi:10.1038/s41577-019-0143-6.

194. Bissett, C. *et al.* Systemic prime mucosal boost significantly increases protective efficacy of bivalent RSV influenza viral vectored vaccine. *npj Vaccines* **9**, 1–14 (2024).
195. Rajão, D. S. & Pérez, D. R. Universal vaccines and vaccine platforms to protect against influenza viruses in humans and agriculture. *Frontiers in Microbiology* **9**, (2018).
196. Hu, L. *et al.* The race toward a universal influenza vaccine: Front runners and the future directions. *Antiviral Research* **210**, 105505 (2023).
197. Universal Influenza Vaccine Technology Landscape | CIDRAP. https://ivr.cidrap.umn.edu/universal-influenza-vaccine-technology-landscape (2022).
198. Casazza, J. P. *et al.* Phase 1 dose-escalation trial evaluating a group 2 influenza hemagglutinin stabilized stem nanoparticle vaccine. *npj Vaccines* **9**, 1–10 (2024).
199. Lim, C. M. L., Komarasamy, T. V., Adnan, N. A. A. B., Radhakrishnan, A. K. & Balasubramaniam, V. R. M. T. Recent Advances, Approaches and Challenges in the Development of Universal Influenza Vaccines. *Influenza and Other Respiratory Viruses* **18**, e13276 (2024).
200. Antrobus, R. D. *et al.* Clinical Assessment of a Novel Recombinant Simian Adenovirus ChAdOx1 as a Vectored Vaccine Expressing Conserved Influenza A Antigens. *Molecular Therapy* **22**, 668–674 (2014).
201. McMahon, M. *et al.* Vaccination with viral vectors expressing chimeric hemagglutinin, NP and M1 antigens protects ferrets against influenza virus challenge. *Frontiers in Immunology* **10**, 2005 (2019).
202. Puksuriwong, S. *et al.* MVA-NP+M1 vaccine activates mucosal M1-specific T cell immunity and tissue-resident memory T cells in human nasopharynx-associated lymphoid tissue. *The Journal of Infectious Diseases* https://doi.org/10.1093/infdis/jiz593 (2019) doi:10.1093/infdis/jiz593.
203. Nachbagauer, R. *et al.* A chimeric hemagglutinin-based universal influenza virus vaccine approach induces broad and long-lasting immunity in a randomized, placebo-controlled phase I trial. *Nature Medicine 2020 27:1* **27**, 106–114 (2020).
204. Alberts, B. *et al.* The Adaptive Immune System. in *Molecular Biology of the Cell. 4th edition* (Garland Science, 2002).
205. Charles A Janeway, J., Travers, P., Walport, M. & Shlomchik, M. J. B-cell activation by armed helper T cells. in *Immunobiology: The Immune System in Health and Disease. 5th edition* (Garland Science, 2001).
206. LeBien, T. W. & Tedder, T. F. B lymphocytes: how they develop and function. *Blood* **112**, 1570–1580 (2008).
207. Stebegg, M. *et al.* Regulation of the Germinal Center Response. *Front. Immunol.* **9**, (2018).
208. Hwang, J.-R., Byeon, Y., Kim, D. & Park, S.-G. Recent insights of T cell receptor-mediated signaling pathways for T cell activation and development. *Exp Mol Med* **52**, 750–761 (2020).
209. Golubovskaya, V. & Wu, L. Different Subsets of T Cells, Memory, Effector Functions, and CAR-T Immunotherapy. *Cancers (Basel)* **8**, 36 (2016).
210. Sun, L., Su, Y., Jiao, A., Wang, X. & Zhang, B. T cells in health and disease. *Sig Transduct Target Ther* **8**, 1–50 (2023).
211. Nutt, S. L., Hodgkin, P. D., Tarlinton, D. M. & Corcoran, L. M. The generation of antibody-secreting plasma cells. *Nat Rev Immunol* **15**, 160–171 (2015).

212. Gatto, D. & Brink, R. The germinal center reaction. *J Allergy Clin Immunol* **126**, 898–907; quiz 908–909 (2010).
213. Barinov, A. *et al.* Essential role of immobilized chemokine CXCL12 in the regulation of the humoral immune response. *Proc Natl Acad Sci U S A* **114**, 2319–2324 (2017).
214. De Silva, N. S. & Klein, U. Dynamics of B cells in germinal centres. *Nat Rev Immunol* **15**, 137–148 (2015).
215. Roco, J. A. *et al.* Class Switch Recombination Occurs Infrequently in Germinal Centers. *Immunity* **51**, 337-350.e7 (2019).
216. Liu, J.-C. *et al.* Immunoglobulin class-switch recombination: Mechanism, regulation, and related diseases. *MedComm* **5**, e662 (2024).
217. Charles A Janeway, J., Travers, P., Walport, M. & Shlomchik, M. J. T cell-mediated cytotoxicity. in *Immunobiology: The Immune System in Health and Disease. 5th edition* (Garland Science, 2001).
218. Mettelman, R. C., Allen, E. K. & Thomas, P. G. Mucosal immune responses to infection and vaccination in the respiratory tract. *Immunity* **55**, 749–780 (2022).
219. *Principles of Mucosal Immunology*. (Garland Science, New York, 2020). doi:10.1201/9781317212942.
220. Chakraborti, S., Sarkar, J., Pramanik, P. K. & Chakraborti, T. Role of Proteases in Lung Disease: A Brief Overview. *Proteases in Human Diseases* 333–374 (2017) doi:10.1007/978-981-10-3162-5_16.
221. Xu, D. & Lu, W. Defensins: A Double-Edged Sword in Host Immunity. *Front. Immunol.* **11**, (2020).
222. Allie, S. R. & Randall, T. D. Resident Memory B Cells. *Viral Immunol* **33**, 282–293 (2020).
223. Csencsits, K. L., Jutila, M. A. & Pascual, D. W. Nasal-Associated Lymphoid Tissue: Phenotypic and Functional Evidence for the Primary Role of Peripheral Node Addressin in Naive Lymphocyte Adhesion to High Endothelial Venules in a Mucosal Site1. *The Journal of Immunology* **163**, 1382–1389 (1999).
224. Randall, T. D. Bronchus-Associated Lymphoid Tissue (BALT). *Adv Immunol* **107**, 187–241 (2010).
225. Ding, Z. & Tarlinton, D. The case for BALT in human respiratory immunity. *Nat Immunol* **24**, 1220–1221 (2023).
226. Tang, J. & Sun, J. Lung tissue-resident memory T cells: the gatekeeper to respiratory viral (re)-infection. *Current Opinion in Immunology* **80**, 102278 (2023).
227. Carbone, F. R. Unique properties of tissue-resident memory T cells in the lungs: implications for COVID-19 and other respiratory diseases. *Nat Rev Immunol* **23**, 329–335 (2023).
228. Szabo, P. A., Miron, M. & Farber, D. L. Location, location, location: Tissue resident memory T cells in mice and humans. *Science Immunology* **4**, eaas9673 (2019).
229. Webb, J. R., Milne, K. & Nelson, B. H. PD-1 and CD103 Are Widely Coexpressed on Prognostically Favorable Intraepithelial CD8 T Cells in Human Ovarian Cancer. *Cancer Immunology Research* **3**, 926–935 (2015).
230. Pizzolla, A. *et al.* Resident memory CD8+ T cells in the upper respiratory tract prevent pulmonary influenza virus infection. *Science Immunology* **2**, eaam6970 (2017).
231. Allie, S. R. *et al.* The establishment of resident memory B cells in the lung requires local antigen encounter. *Nat Immunol* **20**, 97–108 (2019).

232. Anderson, K. G. *et al.* Cutting Edge: Intravascular Staining Redefines Lung CD8 T Cell Responses. *The Journal of Immunology* **189**, 2702–2706 (2012).
233. Anderson, K. G. *et al.* Intravascular staining for discrimination of vascular and tissue leukocytes. *Nat Protoc* **9**, 209–222 (2014).
234. Yuan, R. *et al.* The Roles of Tissue-Resident Memory T Cells in Lung Diseases. *Front Immunol* **12**, 710375 (2021).
235. Rosato, P. C. *et al.* Tissue-resident memory T cells trigger rapid exudation and local antibody accumulation. *Mucosal Immunol* **16**, 17–26 (2023).
236. Lee, S., Yeung, K. K. & Watts, T. H. Tissue-resident memory T cells in protective immunity to influenza virus. *Current Opinion in Virology* **65**, 101397 (2024).
237. Dynamics of influenza-induced lung-resident memory T cells underlie waning heterosubtypic immunity - PubMed. https://pubmed.ncbi.nlm.nih.gov/28783666/.
238. Turner, D. L. *et al.* Biased Generation and In Situ Activation of Lung Tissue-Resident Memory CD4 T Cells in the Pathogenesis of Allergic Asthma. *J Immunol* **200**, 1561–1569 (2018).
239. Turner, D. L. *et al.* Lung niches for the generation and maintenance of tissue-resident memory T cells. *Mucosal Immunol* **7**, 501–510 (2014).
240. Snyder, M. E. *et al.* Generation and persistence of human tissue-resident memory T cells in lung transplantation. *Sci Immunol* **4**, eaav5581 (2019).
241. Wu, T. *et al.* Lung-resident memory CD8 T cells (TRM) are indispensable for optimal cross-protection against pulmonary virus infection. *J Leukoc Biol* **95**, 215–224 (2014).
242. Allie, S. R. *et al.* The establishment of resident memory B cells in the lung requires local antigen encounter. *Nat Immunol* **20**, 97–108 (2019).
243. Horton, R. E. & Vidarsson, G. Antibodies and Their Receptors: Different Potential Roles in Mucosal Defense. *Front Immunol* **4**, 200 (2013).
244. Tissue-resident memory T cells trigger rapid exudation and local antibody accumulation - PMC. https://www.ncbi.nlm.nih.gov/pmc/articles/PMC10338064/.
245. Russell, M. W., Moldoveanu, Z., Ogra, P. L. & Mestecky, J. Mucosal Immunity in COVID-19: A Neglected but Critical Aspect of SARS-CoV-2 Infection. *Front. Immunol.* **11**, (2020).
246. Koutsakos, M. & Ellebedy, A. H. Immunological imprinting: Understanding COVID-19. *Immunity* **56**, 909–913 (2023).
247. Cox, R. M. *et al.* Therapeutic mitigation of measles-like immune amnesia and exacerbated disease after prior respiratory virus infections in ferrets. *Nat Commun* **15**, 1189 (2024).
248. Schiepers, A. *et al.* Molecular fate-mapping of serum antibody responses to repeat immunization. *Nature* **615**, 482–489 (2023).
249. Wang, L. *et al.* Antigenic distance between primary and secondary dengue infections correlates with disease risk. *Sci Transl Med* **16**, eadk3259 (2024).
250. Francis, M. E., King, M. L. & Kelvin, A. A. Back to the future for influenza preimmunity—Looking back at influenza virus history to infer the outcome of future infections. *Viruses* **11**, 122 (2019).
251. Dowell, A. C. *et al.* Immunological imprinting of humoral immunity to SARS-CoV-2 in children. *Nat Commun* **14**, 3845 (2023).

252. Chemaitelly, H. *et al.* Immune Imprinting and Protection against Repeat Reinfection with SARS-CoV-2. *N Engl J Med* NEJMc2211055 (2022) doi:10.1056/NEJMc2211055.
253. Pušnik, J. *et al.* Vaccination impairs de novo immune response to omicron breakthrough infection, a precondition for the original antigenic sin. *Nat Commun* **15**, 3102 (2024).
254. Wei, J. *et al.* Protection against SARS-CoV-2 Omicron BA.4/5 variant following booster vaccination or breakthrough infection in the UK. *Nat Commun* **14**, 2799 (2023).
255. Laghlali, G. *et al.* Enhanced mucosal B- and T-cell responses against SARS-CoV-2 after heterologous intramuscular mRNA prime/intranasal protein boost vaccination with a combination adjuvant. *bioRxiv* 2024.03.28.587260 (2024) doi:10.1101/2024.03.28.587260.
256. Liang, C.-Y. *et al.* Imprinting of serum neutralizing antibodies by Wuhan-1 mRNA vaccines. *Nature* 1–11 (2024) doi:10.1038/s41586-024-07539-1.
257. McNaughton, A. L. *et al.* Fatal COVID-19 outcomes are associated with an antibody response targeting epitopes shared with endemic coronaviruses. *JCI Insight* **7**, e156372.
258. Premazzi Papa, M. *et al.* Dengue NS1 Antibodies Are Associated With Clearance of Viral Nonstructural Protein-1. *J Infect Dis* **230**, e1226–e1234 (2024).
259. Wang, Q. *et al.* Deep immunological imprinting due to the ancestral spike in the current bivalent COVID-19 vaccine. *Cell Rep Med* **4**, 101258 (2023).
260. Francis, T. On the Doctrine of Original Antigenic Sin. *Proceedings of the American Philosophical Society* **104**, 572–578 (1960).
261. Xie, Y., Tian, X., Zhang, X., Yao, H. & Wu, N. Immune interference in effectiveness of influenza and COVID-19 vaccination. *Front. Immunol.* **14**, (2023).
262. Kandeil, W. *et al.* Immune interference (blunting) in the context of maternal immunization with Tdap-containing vaccines: is it a class effect? *Expert Rev Vaccines* **19**, 341–352 (2020).
263. King, S. M., Bryan, S. P., Hilchey, S. P., Wang, J. & Zand, M. S. First Impressions Matter: Immune Imprinting and Antibody Cross-Reactivity in Influenza and SARS-CoV-2. *Pathogens* **12**, 169 (2023).
264. Sangster, M. Y., Nguyen, P. Q. T. & Topham, D. J. Role of Memory B Cells in Hemagglutinin-Specific Antibody Production Following Human Influenza A Virus Infection. *Pathogens* **8**, 167 (2019).
265. Andrews, S. F. *et al.* Activation Dynamics and Immunoglobulin Evolution of Pre-existing and Newly Generated Human Memory B cell Responses to Influenza Hemagglutinin. *Immunity* **51**, 398-410.e5 (2019).
266. Dangi, T. *et al.* Pre-existing immunity modulates responses to mRNA boosters. *Cell Reports* **42**, (2023).
267. Schiepers, A., Wout, M. F. L. van't, Hobbs, A., Mesin, L. & Victora, G. D. Opposing effects of pre-existing antibody and memory T cell help on the dynamics of recall germinal centers. *Immunity* **57**, 1618-1628.e4 (2024).
268. Shinnakasu, R. *et al.* Regulated selection of germinal-center cells into the memory B cell compartment. *Nat Immunol* **17**, 861–869 (2016).
269. MacLean, A. J. *et al.* Secondary influenza challenge triggers resident memory B cell migration and rapid relocation to boost antibody secretion at infected sites. *Immunity* **55**, 718-733.e8 (2022).

270. Liang, C.-Y. *et al.* Imprinting of serum neutralizing antibodies by Wuhan-1 mRNA vaccines. *Nature* **630**, 950–960 (2024).
271. Wang, S. *et al.* Viral vectored vaccines: design, development, preventive and therapeutic applications in human diseases. *Sig Transduct Target Ther* **8**, 1–38 (2023).
272. Zhang, C., Berg, A., Joe, C. C. D., Dalby, P. A. & Douglas, A. D. Lyophilization to enable distribution of ChAdOx1 and ChAdOx2 adenovirus-vectored vaccines without refrigeration. *npj Vaccines* **8**, 1–9 (2023).
273. Saunders, J. E. *et al.* Adenoviral vectored vaccination protects against Crimean-Congo Haemorrhagic Fever disease in a lethal challenge model. *eBioMedicine* **90**, (2023).
274. Voysey, M. *et al.* Safety and efficacy of the ChAdOx1 nCoV-19 vaccine (AZD1222) against SARS-CoV-2: an interim analysis of four randomised controlled trials in Brazil, South Africa, and the UK. *Lancet* **397**, 99–111 (2021).
275. Bosaeed, M. *et al.* Safety and immunogenicity of ChAdOx1 MERS vaccine candidate in healthy Middle Eastern adults (MERS002): an open-label, non-randomised, dose-escalation, phase 1b trial. *The Lancet Microbe* **3**, e11–e20 (2022).
276. Jenkin, D. *et al.* Safety and immunogenicity of a ChAdOx1 vaccine against Rift Valley fever in UK adults: an open-label, non-randomised, first-in-human phase 1 clinical trial. *The Lancet Infectious Diseases* **23**, 956–964 (2023).
277. van Doremalen, N. *et al.* ChAdOx1 NiV vaccination protects against lethal Nipah Bangladesh virus infection in African green monkeys. *npj Vaccines* **7**, 1–8 (2022).
278. Cokarić Brdovčak, M. *et al.* ChAdOx1-S adenoviral vector vaccine applied intranasally elicits superior mucosal immunity compared to the intramuscular route of vaccination. *European Journal of Immunology* **52**, 936–945 (2022).
279. van Doremalen, N. *et al.* Intranasal ChAdOx1 nCoV-19/AZD1222 vaccination reduces viral shedding after SARS-CoV-2 D614G challenge in preclinical models. *Sci Transl Med* **13**, eabh0755 (2021).
280. Ewer, K. J. *et al.* Viral vectors as vaccine platforms: From immunogenicity to impact. *Current Opinion in Immunology* **41**, 47–54 (2016).
281. Coughlan, L. Factors Which Contribute to the Immunogenicity of Non-replicating Adenoviral Vectored Vaccines. *Front. Immunol.* **11**, (2020).
282. Tatsis, N. *et al.* Adenoviral vectors persist in vivo and maintain activated CD8+ T cells: implications for their use as vaccines. *Blood* **110**, 1916–1923 (2007).
283. Ewer, K. J. *et al.* Viral vectors as vaccine platforms: from immunogenicity to impact. *Current Opinion in Immunology* **41**, 47–54 (2016).
284. Zaiss, A. K., Machado, H. B. & Herschman, H. R. The influence of innate and pre-existing immunity on adenovirus therapy. *J Cell Biochem* **108**, 778–790 (2009).
285. Kim, J. *et al.* Immunogenicity Differences of the ChAdOx1 nCoV-19 Vaccine According to Pre-Existing Adenovirus Immunity. *Vaccines (Basel)* **11**, 784 (2023).
286. Zamai, L. & Rocchi, M. B. L. Hypothesis: Possible influence of antivector immunity and SARS-CoV-2 variants on efficacy of ChAdOx1 nCoV-19 vaccine. *Br J Pharmacol* **179**, 218–226 (2022).
287. Tang, J. *et al.* Respiratory mucosal immunity against SARS-CoV-2 after mRNA vaccination. *Science Immunology* **7**, eadd4853 (2022).
288. Sheikh-Mohamed, S. *et al.* Systemic and mucosal IgA responses are variably induced in response to SARS-CoV-2 mRNA vaccination and are associated with protection against subsequent infection. *Mucosal Immunol* **15**, 799–808 (2022).

289. SARS-CoV-2 pathogenesis | Nature Reviews Microbiology. https://www.nature.com/articles/s41579-022-00713-0#Sec10.
290. Winklmeier, S. *et al.* Intramuscular vaccination against SARS-CoV-2 transiently induces neutralizing IgG rather than IgA in the saliva. *Front Immunol* **15**, 1330864 (2024).
291. Shin, H. & Iwasaki, A. A vaccine strategy protects against genital herpes by establishing local memory T cells. *Nature* **491**, 463–467 (2012).
292. Singh, C. *et al.* Phase III Pivotal comparative clinical trial of intranasal (iNCOVACC) and intramuscular COVID 19 vaccine (Covaxin®). *NPJ Vaccines* **8**, 125 (2023).
293. Ye, T. *et al.* Inhaled SARS-CoV-2 vaccine for single-dose dry powder aerosol immunization. *Nature* **624**, 630–638 (2023).
294. Turner, P. V., Brabb, T., Pekow, C. & Vasbinder, M. A. Administration of Substances to Laboratory Animals: Routes of Administration and Factors to Consider. *Journal of the American Association for Laboratory Animal Science : JAALAS* **50**, 600 (2011).
295. Gao, J. Vaccination with CanSinoBIO's inhaled COVID-19 vaccine has begun in China. *J Biosaf Biosecur* **4**, 163 (2022).
296. Nasal Flu Vaccine FluMist Gets FDA Approval for At-Home Use. *Yale Medicine* https://www.yalemedicine.org/news/flumist-at-home.
297. Rathore, A. P. & John, A. L. S. Promises and challenges of mucosal COVID-19 vaccines. *Vaccine* **41**, 4042 (2023).
298. Gagne, M. *et al.* Mucosal adenovirus vaccine boosting elicits IgA and durably prevents XBB.1.16 infection in nonhuman primates. *Nat Immunol* 1–15 (2024) doi:10.1038/s41590-024-01951-5.
299. McMahan, K. *et al.* Mucosal boosting enhances vaccine protection against SARS-CoV-2 in macaques. *Nature* **626**, 385–391 (2024).
300. Lam, J.-Y. *et al.* A nasal omicron vaccine booster elicits potent neutralizing antibody response against emerging SARS-CoV-2 variants. *Emerg Microbes Infect* **11**, 964–967.
301. Wang, Q. *et al.* Intranasal booster using an Omicron vaccine confers broad mucosal and systemic immunity against SARS-CoV-2 variants. *Signal Transduct Target Ther* **8**, 167 (2023).
302. Cotter, C. A., Americo, J. L., Earl, P. L. & Moss, B. Protection from SARS-CoV-2 Variants by MVAs expressing matched or mismatched S administered intranasally to mice. *npj Vaccines* **8**, 1–12 (2023).
303. Mao, T. *et al.* Unadjuvanted intranasal spike vaccine elicits protective mucosal immunity against sarbecoviruses. *Science* **378**, eabo2523 (2022).
304. Lapuente, D. *et al.* Protective mucosal immunity against SARS-CoV-2 after heterologous systemic prime-mucosal boost immunization. *Nat Commun* **12**, 6871 (2021).
305. Li, X. *et al.* Combining intramuscular and intranasal homologous prime-boost with a chimpanzee adenovirus-based COVID-19 vaccine elicits potent humoral and cellular immune responses in mice. *Emerg Microbes Infect* **11**, 1890–1899.
306. Kiros, T. G. *et al.* The Importance of Animal Models in the Development of Vaccines. *Innovation in Vaccinology* 251–264 (2012) doi:10.1007/978-94-007-4543-8_11.

307. Dicks, M. D. J. *et al.* A Novel Chimpanzee Adenovirus Vector with Low Human Seroprevalence: Improved Systems for Vector Derivation and Comparative Immunogenicity. *PLoS One* **7**, e40385 (2012).
308. Cottingham, M. G. *et al.* Preventing Spontaneous Genetic Rearrangements in the Transgene Cassettes of Adenovirus Vectors. *Biotechnol Bioeng* **109**, 719–728 (2012).
309. van Doremalen, N. *et al.* ChAdOx1 nCoV-19 vaccine prevents SARS-CoV-2 pneumonia in rhesus macaques. *Nature* **586**, 578–582 (2020).
310. Cottingham, M. G. *et al.* Preventing spontaneous genetic rearrangements in the transgene cassettes of adenovirus vectors. *Biotechnology and Bioengineering* **109**, 719–728 (2012).
311. Cisney, E. D., Fernandez, S., Hall, S. I., Krietz, G. A. & Ulrich, R. G. Examining the Role of Nasopharyngeal-associated Lymphoreticular Tissue (NALT) in Mouse Responses to Vaccines. *JoVE (Journal of Visualized Experiments)* e3960 (2012) doi:10.3791/3960.
312. Miura, K. *et al.* Development and characterization of a standardized ELISA including a reference serum on each plate to detect antibodies induced by experimental malaria vaccines. *Vaccine* **26**, 193–200 (2008).
313. Sampson, A. T. *et al.* Coronavirus Pseudotypes for All Circulating Human Coronaviruses for Quantification of Cross-Neutralizing Antibody Responses. *Viruses* **13**, 1579 (2021).
314. Ferrara, F. & Temperton, N. Pseudotype Neutralization Assays: From Laboratory Bench to Data Analysis. *Methods and Protocols* **1**, 8 (2018).
315. Petrone, D. *et al.* Reduction of the risk of severe COVID-19 due to Omicron compared to Delta variant in Italy (November 2021 – February 2022). *Int J Infect Dis* **129**, 135–141 (2023).
316. Wolter, N. *et al.* Early assessment of the clinical severity of the SARS-CoV-2 omicron variant in South Africa: a data linkage study. *The Lancet* **399**, 437–446 (2022).
317. Halfmann, P. J. *et al.* SARS-CoV-2 Omicron virus causes attenuated disease in mice and hamsters. *Nature* **603**, 687–692 (2022).
318. Breznik, J. A. *et al.* Early Omicron infection is associated with increased reinfection risk in older adults in long-term care and retirement facilities. *eClinicalMedicine* **63**, (2023).
319. Evans, R. A. *et al.* Impact of COVID-19 on immunocompromised populations during the Omicron era: insights from the observational population-based INFORM study. *The Lancet Regional Health – Europe* **0**, (2023).
320. Kahn, F. *et al.* Risk of severe COVID-19 from the Delta and Omicron variants in relation to vaccination status, sex, age and comorbidities – surveillance results from southern Sweden, July 2021 to January 2022. *Euro Surveill* **27**, 2200121 (2022).
321. van Kessel, S. A. M., Olde Hartman, T. C., Lucassen, P. L. B. J. & van Jaarsveld, C. H. M. Post-acute and long-COVID-19 symptoms in patients with mild diseases: a systematic review. *Fam Pract* **39**, 159–167 (2022).
322. Paul, P. *et al.* Effectiveness of the pre-Omicron COVID-19 vaccines against Omicron in reducing infection, hospitalization, severity, and mortality compared to Delta and other variants: A systematic review. *Hum Vaccin Immunother* **19**, 2167410.
323. Buchan, S. A. *et al.* Estimated Effectiveness of COVID-19 Vaccines Against Omicron or Delta Symptomatic Infection and Severe Outcomes. *JAMA Network Open* **5**, e2232760 (2022).

324. Mykytyn, A. Z. *et al.* Antigenic cartography of SARS-CoV-2 reveals that Omicron BA.1 and BA.2 are antigenically distinct. *Science Immunology* **7**, eabq4450 (2022).
325. Mühlemann, B. *et al.* Antigenic cartography using variant-specific hamster sera reveals substantial antigenic variation among Omicron subvariants. *Proceedings of the National Academy of Sciences* **121**, e2310917121 (2024).
326. Zimmermann, P. *et al.* The Effect of Maternal Immunisation During Pregnancy on Infant Vaccine Responses. *EClinicalMedicine* **13**, 21–30 (2019).
327. McNaughton, A. L. *et al.* Fatal COVID-19 outcomes are associated with an antibody response targeting epitopes shared with endemic coronaviruses. *JCI Insight* **7**, e156372 (2022).
328. Hawman, D. W. *et al.* Replicating RNA platform enables rapid response to the SARS-CoV-2 Omicron variant and elicits enhanced protection in naïve hamsters compared to ancestral vaccine. 2022.01.31.478520 Preprint at https://doi.org/10.1101/2022.01.31.478520 (2022).
329. Costa Rocha, V. P. *et al.* A polyvalent RNA vaccine reduces the immune imprinting phenotype in mice and induces neutralizing antibodies against omicron SARS-CoV-2. *Heliyon* **10**, e25539 (2024).
330. Lin, D.-Y. *et al.* Durability of Bivalent Boosters against Omicron Subvariants. *N Engl J Med* NEJMc2302462 (2023) doi:10.1056/NEJMc2302462.
331. Holmgren, J. & Czerkinsky, C. Mucosal immunity and vaccines. *Nat Med* **11**, S45–S53 (2005).
332. Mitsi, E. *et al.* Respiratory mucosal immune memory to SARS-CoV-2 after infection and vaccination. *Nat Commun* **14**, 6815 (2023).
333. Lavelle, E. C. & Ward, R. W. Mucosal vaccines — fortifying the frontiers. *Nat Rev Immunol* **22**, 236–250 (2022).
334. Park, S.-C., Wiest, M. J., Yan, V., Wong, P. T. & Schotsaert, M. Induction of protective immune responses at respiratory mucosal sites. *Hum Vaccin Immunother* **20**, 2368288.
335. Jung, H. E. *et al.* Intranasal delivery of an adenovirus-vector vaccine co-expressing a modified spike protein and a genetic adjuvant confers lasting mucosal immunity against SARS-CoV-2. *Antiviral Res* **216**, 105656 (2023).
336. Tomayko, M. M., Steinel, N. C., Anderson, S. M. & Shlomchik, M. J. Cutting Edge: Hierarchy of Maturity of Murine Memory B Cell Subsets. *J Immunol* **185**, 7146–7150 (2010).
337. Horton, R. E. & Vidarsson, G. Antibodies and Their Receptors: Different Potential Roles in Mucosal Defense. *Frontiers in Immunology* **4**, 200 (2013).
338. Shamseldin, M. M. *et al.* Prime-Pull Immunization of Mice with a BcfA-Adjuvanted Vaccine Elicits Sustained Mucosal Immunity That Prevents SARS-CoV-2 Infection and Pathology. *J Immunol* **210**, 1257–1271 (2023).
339. Jacobsen, H. *et al.* Post-vaccination T cell immunity to omicron. *Front Immunol* **13**, 944713 (2022).
340. Jovicic, N. *et al.* Differential Immunometabolic Phenotype in Th1 and Th2 Dominant Mouse Strains in Response to High-Fat Feeding. *PLoS One* **10**, e0134089 (2015).
341. Lucas, E. D. *et al.* Circulating KLRG1+ long-lived effector memory T cells retain the flexibility to become tissue resident. *Science Immunology* **9**, eadj8356 (2024).

342. Flemming, A. Cross reactive T cells hold up against Omicron. *Nat Rev Immunol* **22**, 146–146 (2022).
343. Tang, J. *et al.* Respiratory mucosal immunity against SARS-CoV-2 after mRNA vaccination. *Science Immunology* **7**, eadd4853 (2022).
344. Hameed, S. A., Paul, S., Dellosa, G. K. Y., Jaraquemada, D. & Bello, M. B. Towards the future exploration of mucosal mRNA vaccines against emerging viral diseases; lessons from existing next-generation mucosal vaccine strategies. *npj Vaccines* **7**, 1–20 (2022).
345. Morgan, S. B. *et al.* Aerosol Delivery of a Candidate Universal Influenza Vaccine Reduces Viral Load in Pigs Challenged with Pandemic H1N1 Virus. *The Journal of Immunology* **196**, 5014–5023 (2016).
346. XS, H. *et al.* Cellular immune responses in children and adults receiving inactivated or live attenuated influenza vaccines. *Journal of virology* **80**, 11756–11766 (2006).
347. Mohn, K. G. I., Zhou, F., Brokstad, K. A., Sridhar, S. & Cox, R. J. Boosting of Cross-Reactive and Protection-Associated T Cells in Children After Live Attenuated Influenza Vaccination. *The Journal of Infectious Diseases* **215**, 1527 (2017).
348. Vlachantoni, I. *et al.* S68 Phase 1 trial of an intranasal respiratory syncytial virus (rsv) subunit candidate vaccine: safety results from the muc-syngem study. *Thorax* **72**, A43–A44 (2017).
349. Ivanov, V. *et al.* Intranasal and intrapulmonary vaccination with an M protein-deficient respiratory syncytial virus (RSV) vaccine improves clinical signs and reduces viral replication in infant baboons after an RSV challenge infection. *Vaccine* **39**, 4063–4071 (2021).
350. Study Record | Beta ClinicalTrials.gov. https://clinicaltrials.gov/study/NCT05655182.
351. Sridhar, S., Brokstad, K. A. & Cox, R. J. Influenza Vaccination Strategies: Comparing Inactivated and Live Attenuated Influenza Vaccines. *Vaccines* **3**, 373–389 (2015).
352. Oh, J. E. *et al.* Intranasal priming induces local lung-resident B cell populations that secrete protective mucosal antiviral IgA. *Science Immunology* **6**, eabj5129 (2021).
353. Fu, Y.-H. *et al.* Intranasal immunization with a helper-dependent adenoviral vector expressing the codon-optimized fusion glycoprotein of human respiratory syncytial virus elicits protective immunity in BALB/c mice. *Virology Journal* **10**, 183 (2013).
354. Khan, I. U., Huang, J., Li, X., Xie, J. & Zhu, N. Nasal immunization with RSV F and G protein fragments conjugated to an M cell-targeting ligand induces an enhanced immune response and protection against RSV infection. *Antiviral Res* **159**, 95–103 (2018).
355. Mossad, S. B. Demystifying FluMist, a new intranasal, live influenza vaccine. *Cleveland Clinic Journal of Medicine* **70**, 801–806 (2003).
356. Calzas, C. & Chevalier, C. Innovative Mucosal Vaccine Formulations Against Influenza A Virus Infections. *Frontiers in Immunology* **10**, (2019).
357. Shan, J., Britton, P. N., King, C. L. & Booy, R. The immunogenicity and safety of respiratory syncytial virus vaccines in development: A systematic review. *Influenza and other Respiratory Viruses* **15**, 539–551 (2021).
358. Soto, J. A. *et al.* Current Insights in the Development of Efficacious Vaccines Against RSV. *Frontiers in Immunology* **0**, 1507 (2020).

359. Firacative, C. *et al.* Identification of T helper (Th)1- and Th2-associated antigens of Cryptococcus neoformans in a murine model of pulmonary infection. *Sci Rep* **8**, 2681 (2018).
360. Van Erp, E. A., Luytjes, W., Ferwerda, G. & Van Kasteren, P. B. Fc-mediated antibody effector functions during respiratory syncytial virus infection and disease. *Frontiers in Immunology* **10**, 548 (2019).
361. Taylor, G. Animal models of respiratory syncytial virus infection. *Vaccine* **35**, 469–480 (2017).
362. Waris, M. E., Tsou, C., Erdman, D. D., Zaki, S. R. & Anderson, L. J. Respiratory synctial virus infection in BALB/c mice previously immunized with formalin-inactivated virus induces enhanced pulmonary inflammatory response with a predominant Th2-like cytokine pattern. *Journal of virology* **70**, 2852–2860 (1996).
363. Mytle, N. *et al.* Influenza Antigens NP and M2 Confer Cross Protection to BALB/c Mice against Lethal Challenge with H1N1, Pandemic H1N1 or H5N1 Influenza A Viruses. *Viruses* **13**, 1708 (2021).
364. Lin, H.-T., Chuang, C.-C., Wu, H.-L., Chu, D.-M. & Wang, Y.-C. Characterization of cross protection of Swine-Origin Influenza Virus (S-OIV) H1N1 and reassortant H5N1 influenza vaccine in BALB/c mice given a single-dose vaccination. *Journal of Biomedical Science* **20**, 19 (2013).
365. Balazs, A. B., Bloom, J. D., Hong, C. M., Rao, D. S. & Baltimore, D. Broad protection against influenza infection by vectored immunoprophylaxis in mice. *Nat Biotechnol* **31**, 647–652 (2013).
366. Rappazzo, C. G. *et al.* Recombinant M2e outer membrane vesicle vaccines protect against lethal influenza A challenge in BALB/c mice. *Vaccine* **34**, 1252–1258 (2016).
367. Lee, S. *et al.* Vaccine-Elicited CD8+ T Cells Protect against Respiratory Syncytial Virus Strain A2-Line19F-Induced Pathogenesis in BALB/c Mice. *J Virol* **86**, 13016–13024 (2012).
368. Stokes, K. L. *et al.* Differential pathogenesis of respiratory syncytial virus clinical isolates in BALB/c mice. *J Virol* **85**, 5782–5793 (2011).
369. Groves, H. T. *et al.* Mouse Models of Influenza Infection with Circulating Strains to Test Seasonal Vaccine Efficacy. *Front Immunol* **9**, 126 (2018).
370. Thwaites, R. S. *et al.* Early mucosal events promote distinct mucosal and systemic antibody responses to live attenuated influenza vaccine. *Nat Commun* **14**, 8053 (2023).
371. Baker, J. R., Farazuddin, M., Wong, P. T. & O'Konek, J. J. The unfulfilled potential of mucosal immunization. *Journal of Allergy and Clinical Immunology* **150**, 1–11 (2022).
372. Iwasaki, A. Exploiting Mucosal Immunity for Antiviral Vaccines. https://doi.org/10.1146/annurev-immunol-032414-112315 (2016) doi:10.1146/annurev-immunol-032414-112315.
373. Zens, K. D., Chen, J. K. & Farber, D. L. Vaccine-generated lung tissue–resident memory T cells provide heterosubtypic protection to influenza infection. *JCI Insight* **1**, (2016).
374. Li, Y., Li, Z., Zhao, Y. & Chen, X. Potentiation of Recombinant NP and M1-Induced Cellular Immune Responses and Protection by Physical Radiofrequency Adjuvant. *Vaccines (Basel)* **9**, 1382 (2021).
375. Vatzia, E. *et al.* Respiratory and Intramuscular Immunization With ChAdOx2-NPM1-NA Induces Distinct Immune Responses in H1N1pdm09 Pre-Exposed Pigs. *Front Immunol* **12**, 763912 (2021).

376. Rowell, J. *et al.* The effect of respiratory viruses on immunogenicity and protection induced by a candidate universal influenza vaccine in mice. *PLoS One* **14**, e0215321 (2019).
377. Evans, T. G. *et al.* Efficacy and safety of a universal influenza A vaccine (MVA-NP+M1) in adults when given after seasonal quadrivalent influenza vaccine immunisation (FLU009): a phase 2b, randomised, double-blind trial. *Lancet Infect Dis* **22**, 857–866 (2022).
378. Vanderven, H. A. *et al.* What Lies Beneath: Antibody Dependent Natural Killer Cell Activation by Antibodies to Internal Influenza Virus Proteins. *EBioMedicine* **8**, 277–290 (2016).
379. Rijnink, W. F. *et al.* Characterization of non-neutralizing human monoclonal antibodies that target the M1 and NP of influenza A viruses. *J Virol* **97**, e01646-22.
380. LaMere, M. W. *et al.* Contributions of Antinucleoprotein IgG to Heterosubtypic Immunity against Influenza Virus. *The Journal of Immunology* **186**, 4331–4339 (2011).
381. Fujimoto, Y. *et al.* Cross-protective potential of anti-nucleoprotein human monoclonal antibodies against lethal influenza A virus infection. *Journal of General Virology* **97**, 2104–2116 (2016).
382. Vanderven, H. A. *et al.* Poor protective potential of influenza nucleoprotein antibodies despite wide prevalence. *Immunol Cell Biol* **100**, 49–60 (2022).
383. Vanderven, H. A. *et al.* Poor protective potential of influenza nucleoprotein antibodies despite wide prevalence. *Immunol Cell Biol* **100**, 49–60 (2022).
384. Collins, A. M. IgG subclass co-expression brings harmony to the quartet model of murine IgG function. *Immunology & Cell Biology* **94**, 949–954 (2016).
385. Geevarghese, B. & Weinberg, A. Cell-mediated immune responses to respiratory syncytial virus infection. *Hum Vaccin Immunother* **10**, 1047–1056 (2014).
386. Prince, G. A., Horswood, R. L., Camargo, E., Koenig, D. & Chanock, R. M. Mechanisms of immunity to respiratory syncytial virus in cotton rats. *Infect Immun* **42**, 81–87 (1983).
387. Walsh, E. E., Schlesinger, J. J. & Brandriss, M. W. Protection from respiratory syncytial virus infection in cotton rats by passive transfer of monoclonal antibodies. *Infect Immun* **43**, 756–758 (1984).
388. Fong, Y. *et al.* Antibody Correlates of Protection From Severe Respiratory Syncytial Virus Disease in a Vaccine Efficacy Trial. *Open Forum Infectious Diseases* **10**, ofac693 (2023).
389. Joyce, M. G. *et al.* Iterative structure-based improvement of a fusion-glycoprotein vaccine against RSV. *Nature Structural and Molecular Biology* **23**, 811–820 (2016).
390. Mclellan, J. S. *et al.* Structure of RSV Fusion Glycoprotein Trimer Bound to a Prefusion-Specific Neutralizing Antibody. https://doi.org/10.1126/science.1234914 doi:10.1126/science.1234914.
391. Zhang, B. *et al.* Protection of calves by a prefusion-stabilized bovine RSV F vaccine. *NPJ Vaccines* **2**, (2017).
392. Endt, K. *et al.* A Recombinant MVA-Based RSV Vaccine Induces T-Cell and Antibody Responses That Cooperate in the Protection Against RSV Infection. *Front. Immunol.* **13**, (2022).
393. De, C. *et al.* Human T cells efficiently control RSV infection. *JCI Insight* **8**, e168110.

394. Luangrath, M. A., Schmidt, M. E., Hartwig, S. M. & Varga, S. M. Tissue-Resident Memory T Cells in the Lungs Protect against Acute Respiratory Syncytial Virus Infection. *Immunohorizons* **5**, 59–69 (2021).
395. Jozwik, A. *et al.* RSV-specific airway resident memory CD8+ T cells and differential disease severity after experimental human infection. *Nat Commun* **6**, 10224 (2015).
396. Lindell, D. M. *et al.* A novel inactivated intranasal respiratory syncytial virus vaccine promotes viral clearance without TH2 associated Vaccine-Enhanced disease. *PLoS ONE* **6**, (2011).
397. Boyce, T. G. *et al.* Mucosal immune response to trivalent live attenuated intranasal influenza vaccine in children. *Vaccine* **18**, 82–88 (1999).
398. Takamura, S. *et al.* The route of priming influences the ability of respiratory virus-specific memory CD8+ T cells to be activated by residual antigen. *Journal of Experimental Medicine* **207**, 1153–1160 (2010).
399. Price, G. E. *et al.* Single-dose mucosal immunization with a candidate universal influenza vaccine provides rapid protection from virulent H5N1, H3N2 and H1N1 viruses. *PLoS ONE* **5**, (2010).
400. Pierantoni, A. *et al.* Mucosal delivery of a vectored RSV vaccine is safe and elicits protective immunity in rodents and nonhuman primates. *Molecular Therapy - Methods and Clinical Development* **2**, 15018 (2015).
401. Li, H., Ren, H., Zhang, Y., Cao, L. & Xu, W. Intranasal vaccination with a recombinant protein CTA1-DD-RBF protects mice against hRSV infection. *Sci Rep* **11**, 18641 (2021).
402. Etchart, N. *et al.* Intranasal immunisation with inactivated RSV and bacterial adjuvants induces mucosal protection and abrogates eosinophilia upon challenge. *European Journal of Immunology* **36**, 1136–1144 (2006).
403. Verdijk, P. *et al.* First-in-human administration of a live-attenuated RSV vaccine lacking the G-protein assessing safety, tolerability, shedding and immunogenicity: a randomized controlled trial. *Vaccine* **38**, 6088–6095 (2020).
404. Karron, R. A. *et al.* Evaluation of the live-attenuated intranasal respiratory syncytial virus (RSV) vaccine RSV/6120/ΔNS2/1030s in RSV-seronegative young children. *The Journal of Infectious Diseases* jiad281 (2023) doi:10.1093/infdis/jiad281.
405. Lorenzen, E. *et al.* Intramuscular Priming and Intranasal Boosting Induce Strong Genital Immunity Through Secretory IgA in Minipigs Infected with Chlamydia trachomatis. *Front Immunol* **6**, 628 (2015).
406. Sullivan, S. G., Price, O. H. & Regan, A. K. Burden, effectiveness and safety of influenza vaccines in elderly, paediatric and pregnant populations. *Ther Adv Vaccines Immunother* **7**, 2515135519826481 (2019).
407. The top 10 causes of death. https://www.who.int/news-room/fact-sheets/detail/the-top-10-causes-of-death.
408. Liang, B., Hyland, L. & Hou, S. Nasal-Associated Lymphoid Tissue Is a Site of Long-Term Virus-Specific Antibody Production following Respiratory Virus Infection of Mice. *JOURNAL OF VIROLOGY* **75**, 5416–5420 (2001).
409. Universal Influenza Vaccine Technology Landscape | CIDRAP. https://ivr.cidrap.umn.edu/universal-influenza-vaccine-technology-landscape (2022).

Appendix

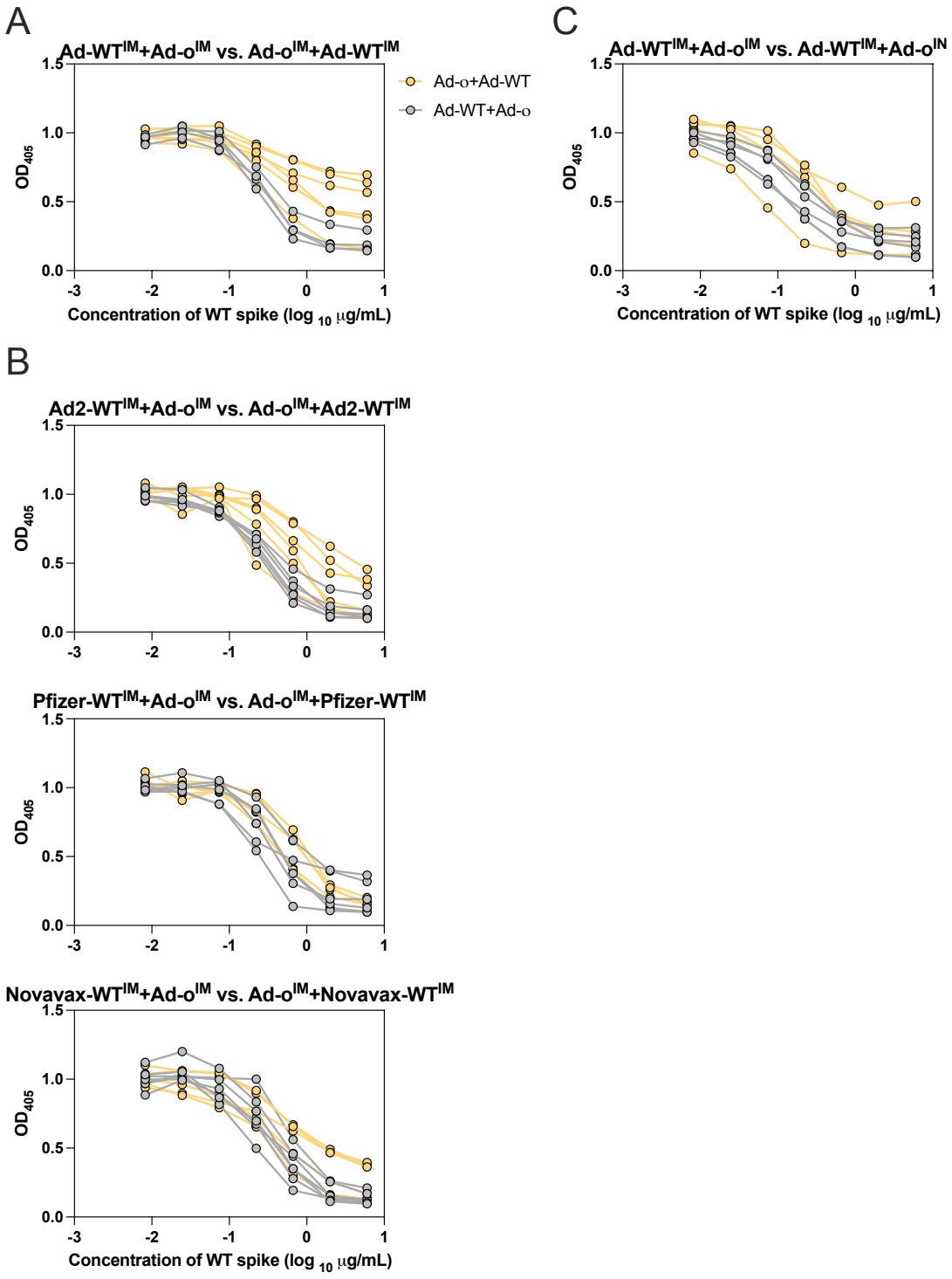

Supplemental Figure 1: Raw WT spike pre-absorption assay data

Levels of anti-o-RBD IgG in serum samples from Ad-WT^{IM}+Ad-o^{IM}- and Ad-WT^{IM}+Ad-o^{IN}-vaccinated mice, that were pre-incubated with increasing concentrations of WT spike. (A) Data featured in Figure 3.9. (B) Data featured in Figure 3.14. (C) Data featured in Figure 4.7.

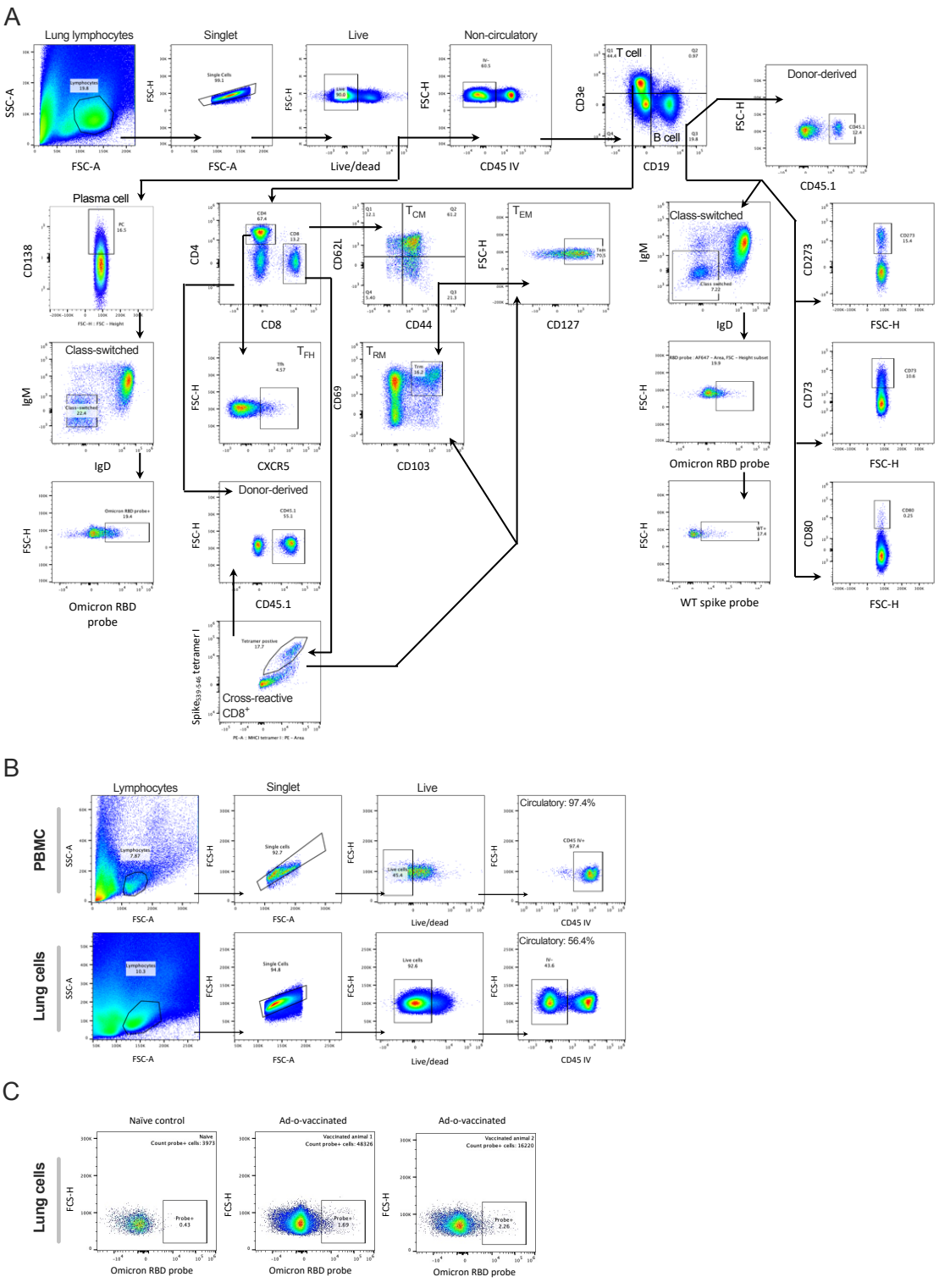

Supplemental Figure 2: Flow cytometry gating strategies

(A) Gating strategy for experiments featured in Figure 4.11, Figure 4.12, Figure 5.8 and Figure 5.9. The use of CD45.1 antibody was only used for the adoptive cell transfer experiment featured in Figure 5.8 and Figure 5.9. (B) Staining of circulatory leukocytes through intravenous injection of anti-CD45 antibody. Example comparison of the relative frequencies of circulatory leukocytes in a peripheral blood mononuclear cell (PBMC) sample and lung sample. (C) Example plots from the experiment in Figure 4.11 of the staining of B cells using an o-RBD probe. Comparison of naïve (negative control) and two positive, vaccinated lung samples.

A

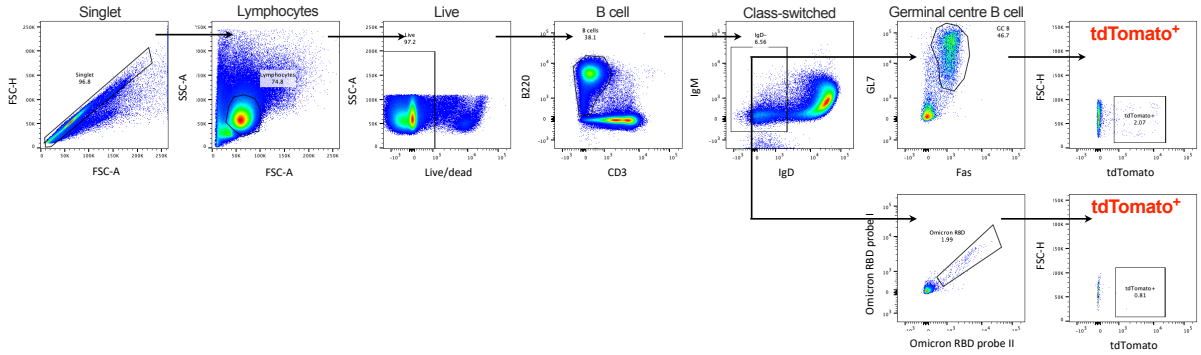

Supplemental Figure 3: Flow cytometry gating strategy for the transgenic S1pr2-Cre tdTomato mouse experiment

(A) Gating strategy for the experiment featured in Figure 5.2 and Figure 5.3

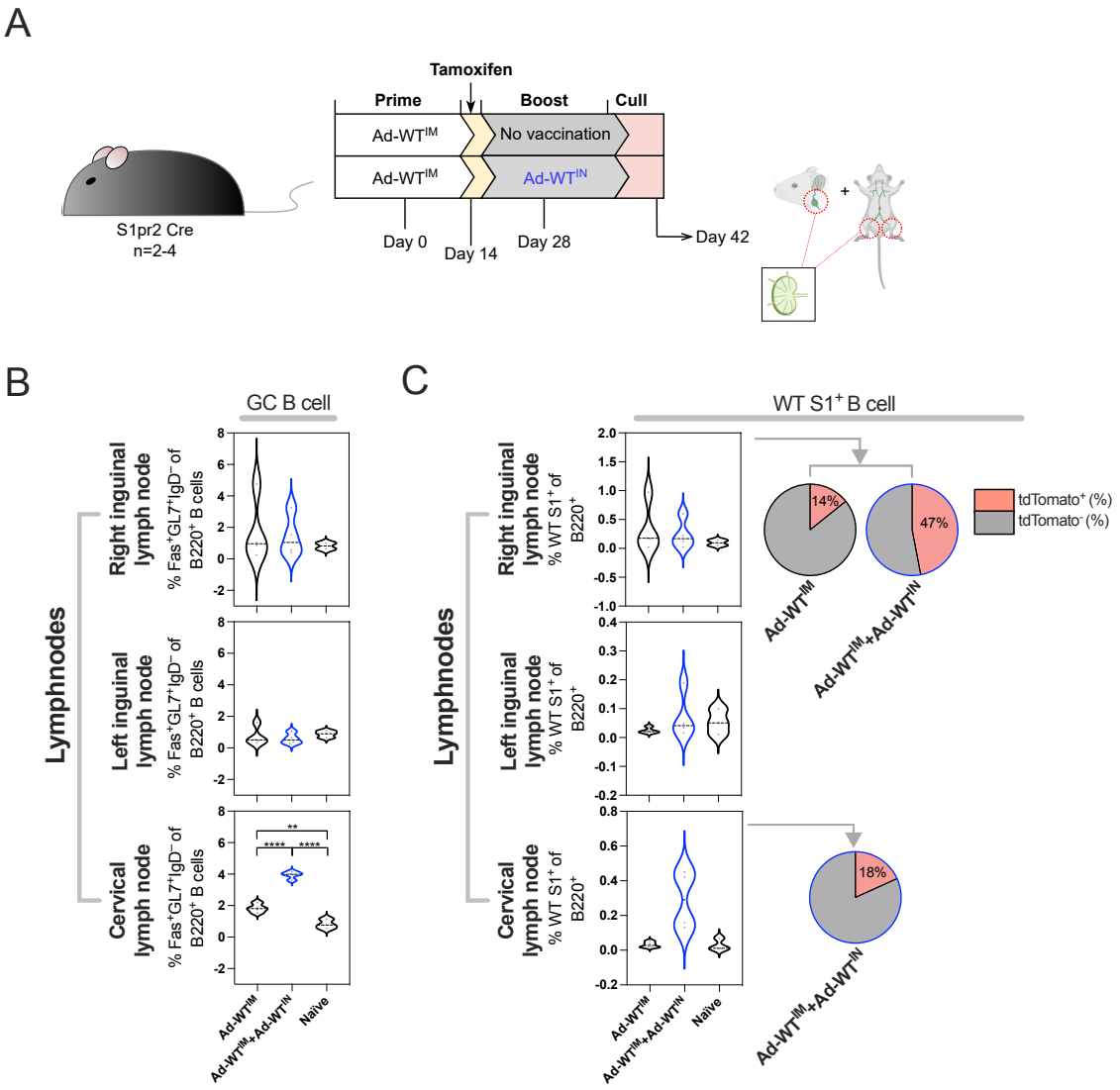

Supplemental Figure 4: Ad-WT^{IM} vs. Ad-WT^{IM}+Ad-WT^{IN} vaccination of S1pr2-Cre tdTomato mice

Residual GCs persist in the right leg 42 days post-prime. (A) Vaccination schedule using transgenic "S1pr2-Cre tdTomato" fate tracking mice (n=2-4), experiment repeated once. Tamoxifen was administered in mice 14 days post-prime at time of optimal germinal centre (GC) B cell production. Mice were culled two weeks post-boost, with left and right inguinal lymph nodes (LILN and RILN, respectively) and cervical lymph nodes (CLN) removed for analysis. (B) Frequencies of GC B cells (Fas$^+$GL7$^+$IgD$^-$B220$^+$) in LILN, RILN and CLN as measured by cell staining and flow cytometry. (C) Frequencies of WT-S1$^+$ B cells (B220$^+$) in LILN, RILN and CLN. The proportion of WT-S1$^+$ B cells that were Ad-WT^{IM} prime-derived (tdTomato$^+$) (median group response) were indicated in pie charts. Data were subset to only include samples that had detectable WT-S1$^+$ B cells. Data in (B) and (C) were normally distributed, and parametric one-way ANOVA tests were completed to test for statistically significant differences between groups (**=P<0.01, ****=P≤0.0001).

A

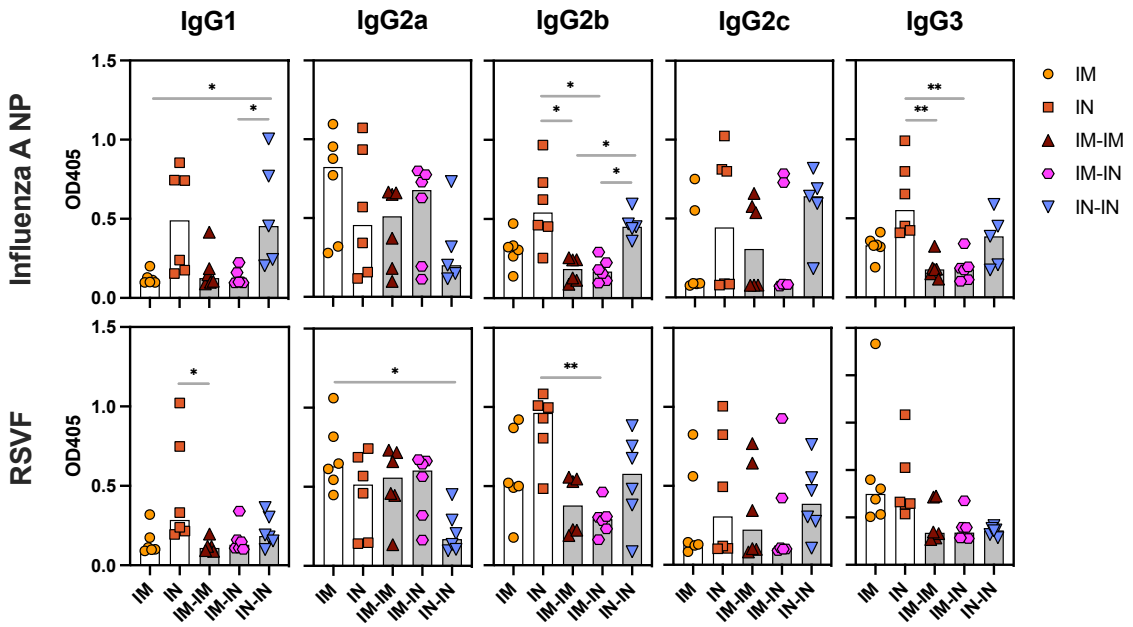

Supplemental Figure 5: Relative levels of IgG subclasses between regimens

(A) The raw values (OD405) for the normalised IgG subclass data presented in Figure 6.4A.

A

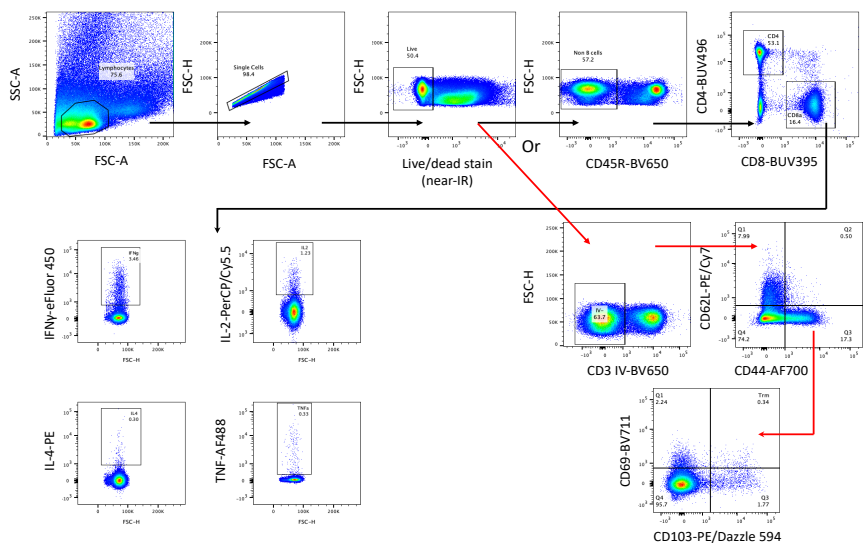

B

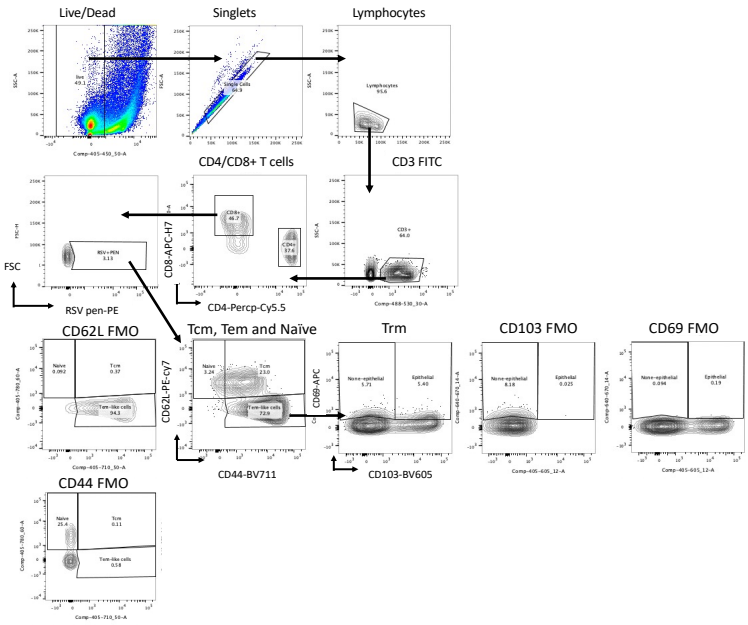

Supplemental Figure 6: Flow cytometry gating strategies for experiments in Chapter 6

(A) Gating strategy for the assessment of the cellular immunogenicity of ChAdOx1-NP+M1-RSVF. For the assessment of cytokine expression, CD45R was stained to exclude B cells from the T cell gating (Figure 6.5). For the assessment of lung T_{RM} populations, CD45R was not included in staining, and alternatively, CD3 antibody was injected into mice prior to cull to stain circulatory T cells that were excluded from the T_{RM} definition (Figure 6.6). (B) Flow gating strategy for infection studies (Figure 6.8, Figure 6.10 and Figure 6.12)

Supplemental Table 1: Peptide pool for omicron S1 IFNγ ELISpots completed in Figure 4.12 and Figure 5.5

Omicron S1 spike-specific peptides used	WT equivalent S1 spike-peptides for reference
14 : : DLFLPFFSNVTWFHV	14 : : DLFLPFFSNVTWFHA
15 : : PFFSNVTWFHVISGT	15 : : PFFSNVTWFHAIHVS
16 : : NVTWFHVISGTNGTK	16 : : NVTWFHAIHVSGTNG
17 : : FHVISGTNGTKRFDN	17 : : FHAIHVSGTNGTKRF
18 : : SGTNGTKRFDNPVLP	18 : : HVSGTNGTKRFDNPV
33 : : KVCEFQFCNDPFLDH	33 : : KVCEFQFCNDPFLGV
34 : : FQFCNDPFLDHKNNK	34 : : FQFCNDPFLGVYYHK
35 : : NDPFLDHKNNKSWME	35 : : NDPFLGVYYHKNNKS
36 : : LDHKNNKSWMESEFR	36 : : LGVYYHKNNKSWMES
37 : : NNKSWMESEFRVYSS	37 : : YHKNNKSWMESEFRV
51 : : FKIYSKHTPINIVEP	51 : : FKIYSKHTPINLVRD
52 : : SKHTPINIVEPERDL	52 : : SKHTPINLVRDLPQG
53 : : PINIVEPERDLPQGF	53 : : PINLVRDLPQGFSAL
54 : : VEPERDLPQGFSALE	54 : : VRDLPQGFSALEPLV
55 : : RDLPQGFSALEPLVD	55 : : PQGFSALEPLVDLPI
82 : : SIVRFPNITNLCPFD	82 : : SIVRFPNITNLCPFG
83 : : FPNITNLCPFDEVFN	83 : : FPNITNLCPFGEVFN
84 : : TNLCPFDEVFNATRF	84 : : TNLCPFGEVFNATRF
85 : : PFDEVFNATRFASVY	85 : : PFGEVFNATRFASVY
91 : : CVADYSVLYNLAPFF	91 : : CVADYSVLYNSASFS
92 : : YSVLYNLAPFFTFKC	92 : : YSVLYNSASFSTFKC
93 : : YNLAPFFTFKCYGVS	93 : : YNSASFSTFKCYGVS
94 : : PFFTFKCYGVSPTKL	94 : : SFSTFKCYGVSPTKL
102 : : DEVRQIAPGQTGNIA	102 : : DEVRQIAPGQTGKIA
103 : : QIAPGQTGNIADYNY	103 : : QIAPGQTGKIADYNY
104 : : GQTGNIADYNYKLPD	104 : : GQTGKIADYNYKLPD
105 : : NIADYNYKLPDDFTG	105 : : KIADYNYKLPDDFTG
108 : : FTGCVIAWNSNKLDS	108 : : FTGCVIAWNSNNLDS
109 : : VIAWNSNKLDSKVSG	109 : : VIAWNSNNLDSKVGG
110 : : NSNKLDSKVSGNYNY	110 : : NSNNLDSKVGGNYNY
111 : : LDSKVSGNYNYLYRL	111 : : LDSKVGGNYNYLYRL
112 : : VSGNYNYLYRLFRKS	112 : : VGGNYNYLYRLFRKS
117 : : ERDISTEIYQAGNKP	117 : : ERDISTEIYQAGSTP
118 : : STEIYQAGNKPCNGV	118 : : STEIYQAGSTPCNGV
119 : : YQAGNKPCNGVAGFN	119 : : YQAGSTPCNGVEGFN
120 : : NKPCNGVAGFNCYFP	120 : : STPCNGVEGFNCYFP
121 : : NGVAGFNCYFPLRSY	121 : : NGVEGFNCYFPLQSY
122 : : GFNCYFPLRSYSFRP	122 : : GFNCYFPLQSYGFQP
123 : : YFPLRSYSFRPTYGV	123 : : YFPLQSYGFQPTNGV
124 : : RSYSFRPTYGVGHQP	124 : : QSYGFQPTNGVGYQP
125 : : FRPTYGVGHQPYRVV	125 : : FQPTNGVGYQPYRVV
126 : : YGVGHQPYRVVVLSF	126 : : NGVGYQPYRVVVLSF
127 : : HQPYRVVVLSFELLH	127 : : YQPYRVVVLSFELLH
134 : : LVKNKCVNFNFNGLK	134 : : LVKNKCVNFNFNGLT
135 : : KCVNFNFNGLKGTGV	135 : : KCVNFNFNGLTGTGV
136 : : FNFNGLKGTGVLTES	136 : : FNFNGLTGTGVLTES
137 : : GLKGTGVLTESNKKF	137 : : GLTGTGVLTESNKKF
161 : : NVFQTRAGCLIGAEY	161 : : NVFQTRAGCLIGAEH
162 : : TRAGCLIGAEYVNNS	162 : : TRAGCLIGAEHVNNS
163 : : CLIGAEYVNNSYECD	163 : : CLIGAEHVNNSYECD
164 : : AEYVNNSYECDIPIG	164 : : AEHVNNSYECDIPIG
167 : : PIGAGICASYQTQTK	167 : : PIGAGICASYQTQTN
168 : : GICASYQTQTKSHRR	168 : : GICASYQTQTNSPRR
169 : : SYQTQTKSHRRARSV	169 : : SYQTQTNSPRRARSV

170 : : QTKSHRRARSVASQS	170 : : QTNSPRRARSVASQS
171 : : HRRARSVASQSIIAY	171 : : PRRARSVASQSIIAY

Supplemental Table 2: P values calculated using Dunn's multiple comparisons test on data presented in Figure 3.1

	IgG							
Regimen	**Ad-α^{IM}**		**Ad-β^{IM}**		**Ad-γ^{IM}**		**Ad-δ^{IM}**	
	Comparison	P value	Comparison	P value	Comparison	P value	Comparison	P value
	α>β	0.0058			γ>α	0.0002	δ>ε	0.0108
	α>γ	0.0002			γ>δ	0.0032		
	α>ε	0.0304			γ>ε	0.0304		
Regimen	**Ad-α^{IM}+Ad-α^{IM}**		**Ad-β^{IM}+Ad-β^{IM}**		**Ad-γ^{IM}+Ad-γ^{IM}**		**Ad-δ^{IM}+Ad-δ^{IM}**	
	Comparison	P value	Comparison	P value	Comparison	P value	Comparison	P value
	α>β	0.0017	β>B.1	0.0032	γ>B.1	0.0009	δ>γ	0.0005
	α>γ	0.0179			δ>B.1	0.0179	δ>α	0.0179
	ε>β	0.0304					ε>γ	0.0304
							B.1>γ	0.0179

Supplemental Table 3: P values calculated using Dunn's multiple comparisons tests on data presented in Figure 3.2

	ACE-2-competition							
Regimen	**Ad-α^{IM}**		**Ad-β^{IM}**		**Ad-γ^{IM}**		**Ad-δ^{IM}**	
	Comparison	P value	Comparison	P value	Comparison	P value	Comparison	P value
	α>β	0.0175	γ>δ	0.0175	γ>α	0.0026		
					γ>δ	0.0102		
Regimen	**Ad-α^{IM}+Ad-α^{IM}**		**Ad-β^{IM}+Ad-β^{IM}**		**Ad-γ^{IM}+Ad-γ^{IM}**		**Ad-δ^{IM}+Ad-δ^{IM}**	
	Comparison	P value	Comparison	P value	Comparison	P value	Comparison	P value
	α>β	0.0102	WT>α	0.0191	γ>α	0.0013	δ>WT	0.0349
	α>δ	0.0052	WT>δ	0.0349	γ>δ	0.0026	γ>WT	0.0349
	WT>β	0.0349	γ>α	0.0102				
	WT>δ	0.0191	γ>δ	0.0191				

Supplemental Table 4: P values calculated using Dunn's multiple comparisons tests on data in Figure 3.4 and Figure 3.5

	IgG							
Regimen	**Ad-α^{IM}+Ad-β^{IM}**		**Ad-β^{IM}+Ad-α^{IM}**		**Ad-α^{IM}+Ad-γ^{IM}**		**Ad-γ^{IM}+Ad-α^{IM}**	
	Comparison	P value	Comparison	P value	Comparison	P value	Comparison	P value
	α>γ	0.0001	β>γ	0.0103	α>β	0.0032	γ>B.1	0.0017
			β>B.1	0.0005	α>γ	0.0005	γ>β	0.0304
	ACE-2-competition							
Regimen	**Ad-α^{IM}+Ad-β^{IM}**		**Ad-β^{IM}+Ad-α^{IM}**		**Ad-α^{IM}+Ad-γ^{IM}**		**Ad-γ^{IM}+Ad-α^{IM}**	
	Comparison	P value	Comparison	P value	Comparison	P value	Comparison	P value
	α>β	0.0349	α>γ	0.0102	γ>δ	0.0102	γ>δ	0.0102
	α>δ	0.0013	α>δ	0.0013	WT>δ	0.0191	WT>δ	0.0102
	WT>δ	0.0191	WT>δ	0.0191				

Supplemental Table 5: P values for plots in Figure 6.2

	Kruskal-Wallis test significant P values					
	Serum IgG			Serum IgA		
	RSV A2-F	H1N1-NP	H1N1-M1	RSV A2-F	H1N1-NP	H1N1-M1
IM-IN>IM	0.0089	0.0017	0.0021	0.0013	0.0013	0.0029
IN-IN>IM	0.0049	0.0019	0.00323	0.0034	0.0061	0.0082
IM-IN>IN	0.0228	0.0128	0.0027			
IN-IN>IN	0.0126	0.0131	0.0401			
IM-IN>IM-IM				0.044	0.0489	

Supplemental Table 6: P values for plots in Figure 6.3

	Kruskal-Wallis test significant P values					
	H1N1-NP			RSV A2-F		
	NALT	BALF	LHS	NALT	BALF	LHS
IM-IN>IM-IM	0.0197		0.0255			0.0285
IN-IN>IM-IM	0.0134	0.032	0.0427	0.0433	0.0254	0.0102
IN>IM		0.0427		0.0184		
IN-IN>IM		0.0094	0.0093	0.0005	0.0094	0.0081
IM-IN>IM			0.0048	0.0051		0.0228

Supplemental Table 7: P values for plots in Figure 6.8 and Figure 6.10

	Kruskal-Wallis test significant P values			
	Days post-RSV A2 challenge			
	Day 4	Day 5	Day 6	Day 7
IM-IN>Control	0.0416	0.0327	0.0046	0.0067
IM-IM>Control				0.0385
	Days post-X-31 (H3N2) challenge			
	Day 3	Day 4	Day 5	Day 6
IM-IN>Control	0.0385	0.0031	0.0067	0.0066
IM-IN>IM-IM	0.0116			
IN-IN>Control		0.0234	0.0234	0.0233

Supplemental Table 8: Peptides used to make RSVF and NP+M1 peptide pools for IFNγ ELISpots completed in Figure 4.12 and Figure 5.5

Pool	RSV(F) peptide pools	Pool	NP+M1 peptide pools
Pool I	1 : MELLILKANAITTIL	Pool I	1 : MASQGTKRSYEQMETDGDR
	2 : ILKANAITTILTAVT		2 : YEQMETDGDRQNATEIRASV
	3 : NAITTILTAVTFCFA		3 : RQNATEIRASVGKMIDGIGR
	4 : TILTAVTFCFASGQN		4 : VGKMIDGIGRFYIQMCTELK
	5 : AVTFCFASGQNITEE		5 : FYIQMCTELKLSDYEGRLI
	6 : CFASGQNITEEFYQS		6 : KLSDYEGRLIQNSLTIEKMV
Pool II	7 : GQNITEEFYQSTCSA		7 : IQNSLTIEKMVLSAFDERR
	8 : TEEFYQSTCSAVSKG		8 : MVLSAFDERRNRYLEEHPSA
	9 : YQSTCSAVSKGYLSA		9 : NRYLEEHPSAGKDPKKTGG
	10 : CSAVSKGYLSALRTG		10 : AGKDPKKTGGPIYRRVDGKW
	11 : SKGYLSALRTGWYTS		11 : PIYRRVDGKWMRELVLYDK
	12 : LSALRTGWYTSVITI		12 : WMRELVLYDKEEIRRIWRQA
	13 : RTGWYTSVITIELSN		13 : EEIRRIWRQANNGEDATAGL
	14 : YTSVITIELSNIKEN		14 : NNGEDATAGLTHMMIWHSNL
	15 : ITIELSNIKENKCNG		15 : THMMIWHSNLNDTTYQRTRA
	16 : LSNIKENKCNGTDAK		16 : NDTTYQRTRALVRTGMDPRM
	17 : KENKCNGTDAKVKLI		17 : LVRTGMDPRMCSLMQGSTL
	18 : CNGTDAKVKLIKQEL		18 : MCSLMQGSTLPRRSGAAGAA
	19 : DAKVKLIKQELDKYK		19 : PRRSGAAGAAVKGIGTMVM
	20 : KLIKQELDKYKNAVT		20 : AVKGIGTMVMELIRMVKRGI
	21 : QELDKYKNAVTELQL	Pool II	21 : ELIRMVKRGINDRNFWRG
	22 : KYKNAVTELQLLMQS		22 : GINDRNFWRGENGRKTRSAY
	23 : AVTELQLLMQSTPAT		23 : ENGRKTRSAYERMCNILKGK
	24 : LQLLMQSTPATNNRA		24 : ERMCNILKGKFQTAAQRAMV
	25 : MQSTPATNNRARREL		25 : FQTAAQRAMVDQVRESRNPG
	26 : PATNNRARRELPRFM		26 : DQVRESRNPGNAEIEDLIFL
	27 : NRARRELPRFMNYTL		27 : NAEIEDLIFLARSALILRG
	28 : RELPRFMNYTLNNAK		28 : LARSALILRGSVAHKSCLPA
	29 : RFMNYTLNNAKKTNV		29 : SVAHKSCLPACVYGPAVSSG
	30 : YTLNNAKKTNVTLSK		30 : CVYGPAVSSGYDFEKEGYSL
	31 : NAKKTNVTLSKKRKR		31 : YDFEKEGYSLVGIDPFKLL
	32 : TNVTLSKKRKRRFLG		32 : LVGIDPFKLLQNSQVYSLIR
	33 : LSKKRKRRFLGFLLG		33 : LQNSQVYSLIRPNENPAHK
	34 : RKRRFLGFLLGVGSA		34 : IRPNENPAHKSQLVWMACH
	35 : FLGFLLGVGSAIASG		35 : KSQLVWMACHSAAFEDLRLL
	36 : LLGVGSAIASGVAVC		36 : SAAFEDLRLLSFIRGTKV
	37 : GSAIASGVAVCKVLH		37 : LLSFIRGTKVSPRGKLSTRG
	38 : ASGVAVCKVLHLEGE		38 : SPRGKLSTRGVQIASNENM
	39 : AVCKVLHLEGEVNKI		39 : GVQIASNENMDNMGSSTLEL
	40 : VLHLEGEVNKIKSAL		40 : DNMGSSTLELRSGYWAIRTR
	41 : EGEVNKIKSALLSTN	Pool III	41 : RSGYWAIRTRSGGNTNQQRA
	42 : NKIKSALLSTNKAVV		42 : SGGNTNQQRASAGQISV
	43 : SALLSTNKAVVSLSN		43 : NQQRASAGQISVQPTFSVQR
	44 : STNKAVVSLSNGVSV		44 : SVQPTFSVQRNLPFEKSTVM
	45 : AVVSLSNGVSVLTFK		45 : NLPFEKSTVMAAFTGNTEGR
	46 : LSNGVSVLTFKVLDL		46 : AAFTGNTEGRTSDMRAEIIR
	47 : VSVLTFKVLDLKNYI		47 : TSDMRAEIIRMMEGAKPEEV
	48 : TFKVLDLKNYIDKQL		48 : MMEGAKPEEVSFRGRGVFEL
	49 : LDLKNYIDKQLLPIL		49 : SFRGRGVFELSDEKATNPIV
	50 : NYIDKQLLPILNKQS		50 : SDEKATNPIVPSFEMSNEG
	51 : KQLLPILNKQSCSIS		51 : VPSFEMSNEGSYFFGDNA

	52 : PILNKQSCSISNIET		52 : EGSYFFGDNAEEYDNGGGPG
	53 : KQSCSISNIETVIEF		53 : EEYDNGGGPGGGMSLLTEV
	54 : SISNIETVIEFQQKN		54 : GGGMSLLTEVETYVLSIV
	55 : IETVIEFQQKNNRLL		55 : EVETYVLSIVPSGPLKAEIA
	56 : IEFQQKNNRLLEITR		56 : PSGPLKAEIAQRLEDVFAGK
	57 : QKNNRLLEITREFSV		57 : AQRLEDVFAGKNTDLEALM
	58 : RLLEITREFSVNAGV		58 : GKNTDLEALMEWLKTRPIL
	59 : ITREFSVNAGVTTPV		59 : MEWLKTRPILSPLTKGILGF
	60 : FSVNAGVTTPVSTYM		60 : SPLTKGILGFVFTLTVPSER
	61 : AGVTTPVSTYMLTNS	Pool IV	61 : VFTLTVPSERGLQRRRFV
	62 : TPVSTYMLTNSELLS		62 : ERGLQRRRFVQNALNGNG
	63 : TYMLTNSELLSLIND		63 : FVQNALNGNGDPNNMDKAVK
	64 : TNSELLSLINDMPIT		64 : DPNNMDKAVKLYRKLKREI
	65 : LLSLINDMPITNDQK		65 : KLYRKLKREITFHGAKEIAL
	66 : INDMPITNDQKKLMS		66 : TFHGAKEIALSYSAGALA
Pool III	67 : PITNDQKKLMSNNVQ		67 : ALSYSAGALASCMGLIYNRM
	68 : DQKKLMSNNVQIVRQ		68 : SCMGLIYNRMGAVTTEVAFG
	69 : LMSNNVQIVRQQSYS		69 : GAVTTEVAFGLVCATCEQIA
	70 : NVQIVRQQSYSIMCI		70 : LVCATCEQIADSQHRSHRQM
	71 : VRQQSYSIMCIIKEE		71 : DSQHRSHRQMVATTNPLIKH
	72 : SYSIMCIIKEEVLAY		72 : VATTNPLIKHENRMVLA
	73 : MCIIKEEVLAYVVQL		73 : IKHENRMVLASTTAKAMEQM
	74 : KEEVLAYVVQLPLYG		74 : STTAKAMEQMAGSSEQAAEA
	75 : LAYVVQLPLYGVIDT		75 : AGSSEQAAEAMEIASQARQM
	76 : VQLPLYGVIDTPCWK		76 : MEIASQARQMVQAMRTVGTH
	77 : LYGVIDTPCWKLHTS		77 : VQAMRTVGTHPSSSTGLR
	78 : IDTPCWKLHTSPLCT		78 : THPSSSTGLRDDLLENLQTY
	79 : CWKLHTSPLCTTNTK		79 : DDLLENLQTYQKRMGVQMQR
	80 : HTSPLCTTNTKEGSN		80 : QKRMGVQMQRFK
	81 : LCTTNTKEGSNICLT		
	82 : NTKEGSNICLTRTDR		
	83 : GSNICLTRTDRGWYC		
	84 : CLTRTDRGWYCDNAG		
	85 : TDRGWYCDNAGSVSF		
	86 : WYCDNAGSVSFFPQA		
	87 : NAGSVSFFPQAETCK		
	88 : VSFFPQAETCKVQSN		
	89 : PQAETCKVQSNRVFC		
	90 : TCKVQSNRVFCDTMN		
	91 : QSNRVFCDTMNSLTL		
	92 : VFCDTMNSLTLPSEV		
	93 : TMNSLTLPSEVNLCN		
	94 : LTLPSEVNLCNVDIF		
	95 : SEVNLCNVDIFNPKY		
	96 : LCNVDIFNPKYDCKI		
	97 : DIFNPKYDCKIMTSK		
	98 : PKYDCKIMTSKTDVS		
	99 : CKIMTSKTDVSSSVI		
	100 : TSKTDVSSSVITSLG		
	101 : DVSSSVITSLGAIVS		
	102 : SVITSLGAIVSCYGK		
	103 : SLGAIVSCYGKTKCT		
	104 : IVSCYGKTKCTASNK		
	105 : YGKTKCTASNKNRGI		
	106 : KCTASNKNRGIIKTF		

	107 : SNKNRGIIKTFSNGC
	108 : RGIIKTFSNGCDYVS
	109 : KTFSNGCDYVSNKGV
	110 : NGCDYVSNKGVDTVS
	111 : YVSNKGVDTVSVGNT
	112 : KGVDTVSVGNTLYYV
	113 : TVSVGNTLYYVNKQE
	114 : GNTLYYVNKQEGKSL
	115 : YYVNKQEGKSLYVKG
	116 : KQEGKSLYVKGEPII
	117 : KSLYVKGEPIINFYD
	118 : VKGEPIINFYDPLVF
	119 : PIINFYDPLVFPSDE
	120 : FYDPLVFPSDEFDAS
	121 : LVFPSDEFDASISQV
	122 : SDEFDASISQVNEKI
	123 : DASISQVNEKINQSL
	124 : SQVNEKINQSLAFIR
	125 : EKINQSLAFIRKSDE
	126 : INQSLAFIRKSDELL
Pool IV	127 : SAIGGYIPEAPRDGQ
	128 : GYIPEAPRDGQAYVR
	129 : EAPRDGQAYVRKDGE
	130 : DGQAYVRKDGEWVLL
	131 : YVRKDGEWVLLSTFL
	132 : DGEWVLLSTFLGGLV
	133 : VLLSTFLGGLVPRGS
	134 : TFLGGLVPRGSHHHH
	135 : GLVPRGSHHHHHHSA
	136 : RGSHHHHHHSAWSHP
	137 : HHHHHSAWSHPQFEK
Pool V	138 : HNVNTGKSTTNIMIT
	139 : TGKSTTNIMITTIII
	140 : TTNIMITTIIIVIIV
	141 : MITTIIIVIIVVLLS
	142 : IIIVIIVVLLSLIAI
	143 : IIVVLLSLIAIGLLL
	144 : LLSLIAIGLLLYCKA
	145 : IAIGLLLYCKAKNTP
	146 : LLLYCKAKNTPVTLS
	147 : CKAKNTPVTLSKDQL
	148 : NTPVTLSKDQLSGIN
	149 : TLSKDQLSGINNIAF
	150 SKDQLSGINNIAFSK